THE BEHAVIOUR AND CHARACTERISTICS OF A VORTEX DIODE IN STEAM FLOWS

by

AMIR MOTAMED-AMINI,
B.Sc.(Hons.), M.Eng., A.M.I.Mech.E.

Thesis submitted in accordance with the requirements of The University of Liverpool for the Degree of Doctor of Philosophy.

Heat and Mass Transfer Laboratory,
Department of Mechanical Engineering,
The University of Liverpool.

October 1987.

SUMMARY

The forward and reverse flow characteristics have been measured for Zobel type vortex diode with 19 mm throat diameter using superheated stea with inlet pressures up to 12 bar absolute, and exhausting into a sub-atmospheric condenser to achieve inlet to outlet pressure ratios up to 30 A discharge factor, Cf, which relates the measured mass flow rate to the theoretical mass flow rate of a critical flow through a comparable isentropic nozzle, has been used to describe the resistance of the diode. In the choked region of the forward and reverse flow, Cf has a constant value of 0.95 and 0.38 respectively. The critical pressure ratios in the forward and reverse flow are approximately 2 and 4.

Repeating the tests using wet steam with known dryness fractions, ha shown separately the effects of wetness on the diode performance. The forward flow discharge factor in the choked condition is seen to be independent of dryness fraction, and found to lie between 0.9 and 1.0, which is similar to that found with superheated steam. The reverse flow discharge factor in the choked condition varied from about 0.4 for a dryness fraction of 0.98, to 0.48 for a dryness fraction of 0.92. Excessive steam wetness (quality less than 0.93) in the reverse flow direction led to a build-up of water and when this was eventually swept through to the diode, the resistance was seen to fall substantially as th strong internal vortex was destroyed. This problem can be overcome in practice, however, by installing a water separator before the diode.

Reverse flow characteristics of four 10 mm throat diameter Zobel typ vortex diodes have been measured using air with inlet pressure up to 31 bar absolute, and exhausting into atmosphere. The characteristics are seen to be similar to those found with superheated steam, with a value of Cf of 0.38. The effect of installing the four diodes in series was investigated. It was shown that by sharing the pressure drop between the diodes and moving the operating point into the incompressible regime, som of the high resistance performance could be recovered.

A detailed study of vortex flow was carried out using a large vortex throttle with superheated steam as the working fluid. The static pressur distribution has been determined experimentally both across the vortex an along the axis of the chamber exit duct. The chamber internal wall temperatures have been obtained using insulated, flush-mounted thermocouples. The measurements enabled the velocity field to be calculated. The bulk of the internal vortex was found to have an exponen of 0.69. It was found that the vortex throttle choked at an upstream to downstream pressure ratio of about 6 with corresponding Cf value of 0.28.

The resistance of vortex chambers is known to be strongly influenced by the presence of reversed flow in the exit, due to vortex breakdown. Schlieren photography of the swirling exhaust flow was used to show that whilst vortex breakdown does occur, it can only do so after the flow has become subsonic downstream of the exit and cannot therefore influence the vortex chamber resistance.

ACKNOWLEDGEMENTS

The author's special gratitude goes to Dr. I. Owen for his valuable advice and encouragement throughout the course of the research.

The financial support of the United Kingdom Atomic Energy Authority is gratefully acknowledged.

The author wishes to thank members of the Mechanical Engineering Workshop for their practical assistance. Particular thanks are due to Mr E. Hughes for assembly of the experimental rigs and for patiently carrying out the inevitable modifications, and to Mr. G. Williams for manufacturing various components. Thanks are also extended to Mrs. M. Hemingway for typing this thesis.

Finally, thanks to my wife Nahid for all her support and encouragement throughout my study.

NOTATION

A_a cross-sectional area at outlet of axial diffuser

A_e cross-sectional area at throat of axial diffuser

A_t cross-sectional area at throat of tangential diffuser

a distance betwen axial diffuser and deswirling chamber

$a_a = \frac{A_a}{A_e}$ dimensionless cross-sectional area at outlet from axial diffuser

$a_t = \frac{A_t}{A_e}$ dimensionless cross-sectional area at throat at outlet of tangential diffuser.

a_o speed of sound

a_u^* upstream speed of sound

BL boundary layer interaction parameter

BLC boundary layer coefficient

BLC* modified boundary layer coefficient

Cd discharge coefficient

Cm non-dimensional mass flow rate

Cf discharge factor

C_p specific heat at constant pressure

D diameter of pipe

D_a diameter at exit of axial diffuser

D_e diameter at throat of axial diffuser

D_i diodicity

D_o diameter of vortex chamber

D_t diameter at throat of tangential diffuser

$d_a = \frac{D_a}{D_o}$ dimensionless diameter at exit of axial diffuser

$d_t = \frac{D_t}{D_o}$ dimensionless diameter at throat of tangential diffuser

d_o diameter of connecting pipe

d_p droplet diameter

E total energy

e distance between ribs in deswirling chamber

F frequency

f fraction coefficient

f_2 end wall fraction coefficient

f_m minimum mass flow to the outer region

G viscous torque

g gravitational acceleration

H vortex chamber height

$h = \frac{H}{D_o}$ dimensionless vortex chamber height

h' specific enthalpy

h_u upstream specific enthalpy

K thermal conductivity

k constant value

k_d dissipation defined in section 2.1.2

L length of the deswirling chamber

l_a length of axial diffuser

l_t length of tangential diffuser

M Mach number

M_t tangential Mach number

$\dot{m}_{act}$ measured mass flow rate

$\dot{m}_{cr}$ ideal critical mass flow rate

$\dot{m}_m$ mixture mass flow rate

$\dot{m}_{th}$ theoretical mass flow rate

N number of droplets

n vortex exponent

n_1 polytropic exponent

P absolute pressure

P* pressure at critical condition

P_a atmospheric pressure

P_c absolute pressure at control port

P_o total pressure and pressure at outlet

Pr Prandtl number

P_R absolute pressure at outer radius

P_s absolute supply pressure

P_u absolute upstream pressure

P_{u1} absolute upstream pressure of first diode

P_v vapour pressure

Q heat transfer

Q_C control flow rate

Q_o total flow rate

Q_S supply flow rate

R specific gas constant

Re Reynolds Number, $Re = \frac{v_e D_e}{\nu}$

Re_r radial Reynolds number $= \frac{v_r r}{\nu}$

Re_p pipe Reynolds number

$R_{r\theta}$ ratio of radial to tangential velocity

r radius

r_o chamber radius

r_e exit radius

T temperature

T^* temperature at critical condition

T_c temperature of cold fluid

T_h temperature of hot fluid

T_o total temperature

T_r recorded temperature

T_s temperature of injected fluid

T_u upstream temperature

T_∞ free stream temperature

$T_{o\infty}$ total temperature at outer radius

TD turndown ratio $TD = \frac{(Q_s)_{max}}{(Q_c)_{max}}$

t width of annular inlets

U internal energy

v velocity

v_e velocity at throat of axial diffuser

v_{fu} upstream specific volume (saturated liquid)

v_{gu} upstream specific volume (saturated vapour)

v_m specific volume of mixture

v_o velocity at connecting pipe

v_r component of velocity in radial direction

v_z component of velocity in axial direction

v_θ component of velocity in tangential direction

w width of the control port

w_a axial velocity at the axis of vortex core

w_R axial velocity at the boundary of vortex core

x axial direction

x_u upstream dryness fraction

$\tilde{z}$ non-dimensional axial position

Greek

α recovery factor

β angle of tangential diffuser

Γ circulation

γ ratio of specific heats

Δ_{hw} difference between pressure differential across the deswirling chamber with and without the swirl at the same flow rate

ΔP pressure differential

ε critical pressure ratio

θ angle of axial diffuser

λ swirl ratio, $\lambda = \frac{v_\theta}{v_r}$

μ viscosity

μ' performance ratio

ν kinematic viscosity

ζ_F forward flow Euler number

ζ_R reverse flow Euler number, $\zeta = \frac{\Delta P}{\frac{1}{2}\rho v^2}$

π constant

ρ density

ρ_a density at axis of vortex core

ρ_R density at boundary of vortex core

σ cavitation coefficient

τ shear stress

Ω vorticity

Ω_c circulation No , $\Omega_c = \frac{\Gamma}{W_a D_e}$

ω angular velocity

CONTENTS

CHAPTER 1

INTRODUCTION

The purpose of the study described in this thesis was to fully characterise the performance of a fluidic vortex diode operating on compressible wet steam and to understand the complex three-dimensional, two-phase, compressible fluid mechanics which are involved.

A vortex is formed by the rotating motion of a multitude of material particles around a common centre, [1]. This motion was studied by Leonardo da Vinci (1510-15), [2]. As a foundation for his studies, he outlined a basic classification of natural spirals, three of which were variations on the basic schema illustrated in Fig. 1.1. Altogether, there were four varieties, namely convex, planar, concave and columnar spirals. Each of these possessed its own dynamic properties and reacted to opposing forces in a different way. The peculiar form resulting from the circulatory force in a vortex comes from what da Vinci called 'a circumstance worthy of note'.

> "The spiral or rotary movement of every fluid is so much the faster as it nears the centre of its revolution, unlike a wheel in which the movement is so much slower as it nears the centre."

The above classification of vortices is perhaps inadequate for modern engineers and scientists, but it is an indication of how vortex flow has long held a fascination for man. Studies of unbounded rotating fluids, such as a vortex ring in water, a vortex

pair behind an aircraft or the generation of a vortex behind a stationary object, have been made by numerous researchers. Confined vortex flow is a kind of flow in which the fluid is enclosed within a body, the walls of the container have a very strong influence on the vortex formed within it.

The concept of generating a vortex within a container has been used in the technology of Power Fluidics to produce flow control valves which have no moving parts, inferring high reliability and long life. These devices are usually simple and have operating lifetimes limited only by the durability of the material from which they are manufactured. Numerous types of vortex devices have been designed up to this time and these have been geometrically optimised and extensively characterised. One of the simplest configurations of vortex device is a vortex diode which was first investigated by Zobel [3] in the 1920's. Vortex diodes are passive elements which offer different resistances to fluid flow in the two directions of flow. Thus a vortex diode is a non-moving part element which offers little resistance to fluid in one direction of flow, but imposes a high resistance when the flow is reversed. This characteristic has made vortex diodes very attractive to the nuclear industry where such devices can safely be placed behind biological shielding without the need for provision for regular maintenance. Vortex diodes are extremely useful in the nuclear reprocessing industry in fluidic pumping systems where they are used as rectifying elements; they have also been installed in the coolant systems of advanced gas cooled

reactors to prevent rapid depressurisation of the reactor in the event of a pipe fracture.

Beyond the nuclear industry, however, the diode has the potential to handle highly corrosive and erosive fluids in the chemical industry and other difficult fluids in, for example, the oil industry. Apart from erosion, there are many other problems encountered in these industries which are related to the control of multi-phase fluids. The simplest and most common case of multi-phase flow is two-phase flow. The term two-component is sometimes used to describe flows in which the phases do not consist of the same chemical substance. For example, steam-water flows are single component and two-phase, while air-water flows are two component and two-phase. All such flows can cause serious damage to conventional control valves which suggests that Power Fluidics has considerable potential outside the nuclear industry.

In the present work, the flow of wet steam has been considered. This constitutes a relatively high quality single component, two-phase flow. In order to understand the behaviour of vortex valves operating with saturated steam, a Zobel type vortex diode was selected. The Zobel diode is a standard fluidic component with relatively good performance. A vortex diode operating with steam at, or near, saturation conditions is likely to experience both phase change and compressibility effects when subjected to such pressure differentials as those found between a steam main and the atmosphere. It is reasonable to expect, therefore, that the characteristics of a

vortex diode with steam will reflect these complications. With this in mind, it was decided that the diode should be first characterised using superheated steam and that following this, the degree of superheat be lowered towards the saturation line and ultimately the steam condition be taken into the wet region. This approach would enable the effects of compressibility and steam wetness to be observed separately.

The research work reported in the following Chapters consists of an experimental and theoretical study of the vortex diode. Chapter 2 gives a review of confined vortex devices. Chapter 3 deals with vortex flow regimes; governing differential equations; velocity, pressure and temperature distributions; and also problems associated with this type of fluid motion, such as vortex breakdown, choking, and compressibility effects.

Chapter 4 covers the experimental investigation of the diode in the reverse and forward flow directions for superheated steam and also the reverse flow characteristic of the diode using air as a working fluid. The performance of a number of diodes cascaded together was investigated, again using air. A description of the experimental apparatus, together with a presentation of the data and experimental results obtained are presented and discussed.

In Chapter 5, two-phase, wet steam characteristics are presented and compared with the superheated steam data. Results are given for the reverse and forward flow directions. Flow visualisation of the wet steam expansion within the body of the vortex diode revealed an

insight to the internal two-phase flow and its influence on the diode (and rig) behaviour.

The internal flow structure of a simplified diode (vortex throttle) is the main subject of Chapter 6. In this Chapter the measurement of pressure and temperature distribution, calculation of tangential velocity and the determination of the vortex exponent are given. In order to cover the whole vortex flow, Schlieren photography has been used to study the vortex core exhausting into the atmosphere from a vortex valve for a range of upstream pressures, covering sub- to supersonic flow.

Finally, in Chapter 7, the main conclusions from the investigation are drawn together. On the basis of these the present state of knowledge can be assessed and suggestions for future work are made thereon.

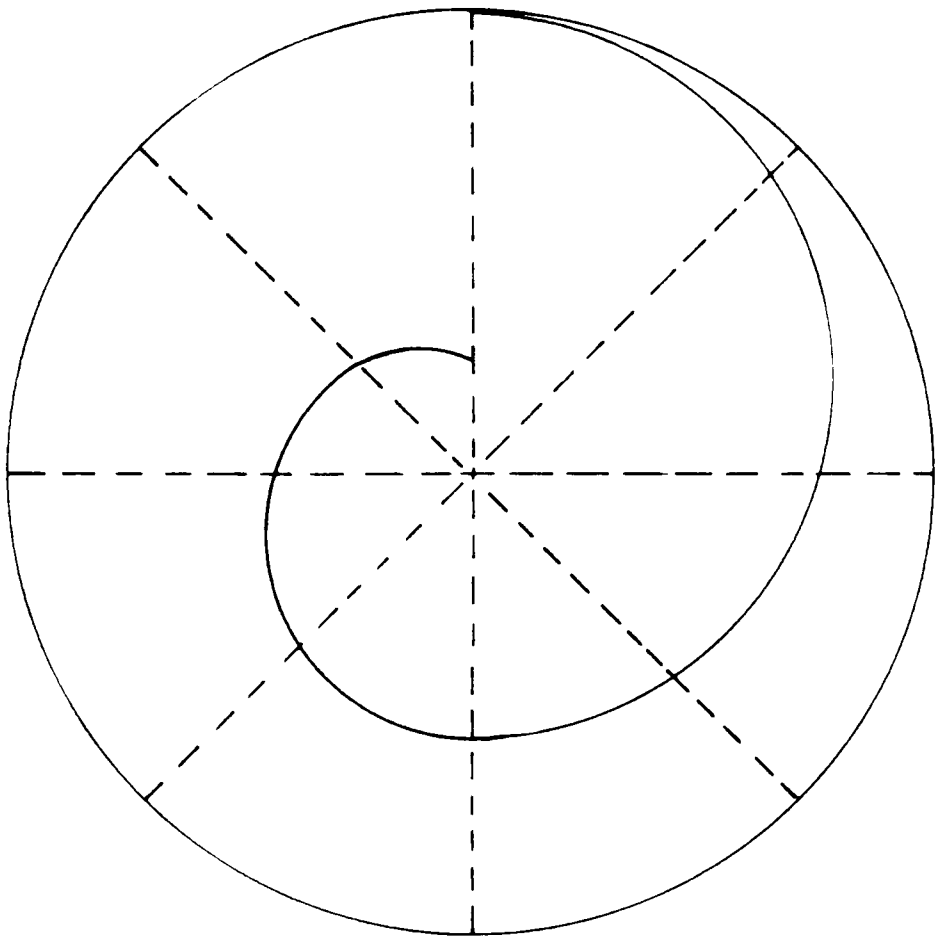

Fig. 1.1 Construction of a Spiral

CHAPTER 2

VORTEX DEVICES

Confined vortex flows are found in a variety of engineering applications. Devices to generate the vortex generally consist of a cylindrical wall coaxial with the vortex axis, and two end walls which are necessarily surfaces of revolution and generally either plane, e.g. vortex diode or conical, e.g. spray nozzle chambers. One or more tangential nozzles inject the fluid into the chamber to generate the vortex. The fluid moves towards the centre and leaves the chamber through one or two central holes. Vortex flows within such containers exhibit a number of important phenomena such as vortex breakdown, temperature and pressure gradient, cavitation, recirculation, boundary layer growth, etc. These effects will be discussed in Chapter 3.

A number of devices have been designed for a variety of applications, such as a vortex valve as a pseudo non-return valve, a vortex amplifier as a flow controller, a vortex tube as a cooling device, a vortex whistle to produce sound, and a "cyclone" as a dust separator. Such applications will be discussed in the following sections.

2.1 Vortex Diode

A vortex diode is a fluidic valve which was invented by Thoma (1928). The device was developed by Zobel in 1930 [3]. The basic design of the Zobel diode is shown in Fig. 2.1, which shows the

device has a tangential inlet and an axial outlet. The fluid enters through a tangential port forming a vortex within the chamber which increases the fluid residence time in the chamber, since the helical path from entrance to outlet is much longer than the straight distance between them. Generation of this vortex causes a pressure gradient which consequently reduces the mass flow rate through the diode since much of the pressure head is consumed in generating the vortex. This orientation is the high resistance direction and is called the reverse flow direction. However, when the flow is in the opposite direction, entering the diode through the axial port at the centre of the vortex chamber and exiting through the tangential port, the flow experiences a much lower resistance such as it might encounter when flowing through a right angled bend. This orientation is called the forward flow direction, (Fig. 2.2). The vortex diode can be considered as a pseudo non-return valve without any moving parts, since it had a high resistance in reverse flow and a low resistance in forward flow.

Vortex diodes have been installed to prevent rapid depressurisation of the advanced gas cooled reactors, such as those at Hartlepool and Heysham. In the event of a pipe fracture in the auxiliary circuits, (Fig. 2.3), they can reduce the outflow of gas between 10 and 20 times, [4]. The diodes are installed in the bypass circuits which comprise 125 mm diameter pipes. On each reactor, eight ducts have been fitted with a fluidic diode by the designers, the National Nuclear Corporation, [5].

Vortex diodes have very high mechanical reliability because they have no moving parts, and consequently no maintenance. They can handle highly active liquor in the nuclear industry and have the ability of handling corrosive fluids in chemical plant.

2.1.1 Performance of vortex diodes

The measure of resistance to flow can be defined as the ratio of the pressure forces on the system to the inertia forces,

$$\xi = \frac{\Delta P}{\frac{1}{2} \rho v_e^2} \qquad (2.1)$$

This coefficient is known as the Euler number, $\frac{1}{2}$ being inserted so that the denominator represents the kinetic energy per unit volume. Euler numbers have been used to characterise vortex diodes in reverse and forward flow directions. The ratio of reverse flow to forward flow Euler number for the same pressure drop is known as diodicity. Zobel reported a diodicity of 93 for a pressure drop of 3 m of water and 122 at 14 m of water. He found that ξ_R, ξ_F varied with Reynolds number measured at the tangential port and also showed the effect of cavitation on diode performance, (Fig. 2.4).

Cavitation can be looked upon as a local boiling of liquid which occurs where its pressure is sufficiently low. This will happen where the local velocity is high. Thoma, [6], derived a cavitation coefficient, σ, for turbines and later defined for the vortex diode as:

$$\sigma = \frac{P_d + P_a - P_v}{\Delta P} \qquad (2.2)$$

where P_v = vapour pressure, ΔP = differential pressure, P_a the atmospheric pressure and P_d the downstream gauge pressure.

Syred and Roberts, [4], obtained a similar performance for a cathe-rine wheel vortex diode with Reynolds number ($Re = \frac{v_e D_e \rho}{\mu}$) based on axial throat, which is shown in Fig. 2.5.

Compressible flow characteristics of a Zobel diode were first presented by Zobel, [3], using superheated steam as the working fluid. Figures 2.6(a) and (b) shows reverse and forward flow characteristics in terms of Euler and Reynolds number based on the condition of steam at the supply pipe with 80 mm internal diameter. He concluded that the characteristics for water and superheated steam exhibit a similar trend in forward flow direction up to certain velocities, above that there is an increase in the Euler number for steam due to choking, and for water due to cavitation. Similar effects were reported by Kumar, [7], in the forward flow direction using air as a working fluid. It was also shown that the use of Euler number to characterise vortex diodes was misleading, especially if it is based on the axial throat. The use of Euler number and its validity as a parameter to characterise vortex diodes, which has been used by most workers for incompressible fluids, will be discussed in more detail for compressible fluids in Chapter 4, section 4.4.

2.1.2 Zobel type vortex diode

The optimum design of the Zobel diode is the result of extensive experiments on geometrical changes and was carried out by Zobel in 1930. Since this design has been used in this work, it is necessary to discuss it in more detail.

To achieve the optimum design, Zobel decided to alter the vortex chamber, tangential connection and axial port (inclusive of the deswirling chamber). By doing this, a large number of vortex diodes were manufactured from bronze (in order to obtain a better surface finish, especially in the nozzles) and tested. The performance of the diodes were obtained by calculating the resistance in the reverse and forward flow directions and diodicity of the diode. The resistance of the deswirling chamber with regard to diodicity of the devices was also measured.

The deswirling chamber in the axial port was the first component tested and the optimum design took account of simple fabrication, Fig. 2.7. Typical experimental results for one of the deswirling chambers in terms of Euler numbers, $\frac{L}{d_o}$ ratio, diodicity, $\frac{e}{d_o}$ ratio and dissipation of the vortex $\left(K_d = \frac{\Delta_{hw}}{v_o^2/2g}\right)$ are shown in Fig. 2.8. L is the length of chamber, d_o is the diameter of the deswirling chamber. The value of $\frac{L}{d_o} = 1$ was selected according to the obtained diodicity, other ratios like $\frac{e}{d_o} = 0.5$ and $\frac{a}{d_o} = 0.5$ were obtained in a similar way, a is the distance between outlet nozzle and deswirling chamber.

He noticed that a had no effect on the quality of the deswirling chamber but produces a higher diodicity at a = 19 mm if the ribs were thin, but if the thickness of the ribs were increased, the value of a has an optimum value of 38 mm.

The tangential port geometry was investigated firstly by considering that the smaller curvature at the inlet to the chamber gives a higher resistance in the forward flow through cavitation and less retardation in the subsequent enlarged portion. On the other hand, greater curvature prevents the formation of the eddy in the reverse flow direction and reduces the Euler number. Secondly, the shape of the nozzle in the tangential port should be chosen to provide optimum possible resistance in the forward flow between the minimum cross section, D_t, and the exit of the nozzle, see Fig. 2.9. This figure also includes the notation which will be included in the discussion.

In this investigation, Zobel used two different vortex chambers (logarithmic spiral and circular cylinder). The spiral vortex chamber with α = 0 to 37.5^{o}, was used to optimise the geometry of the tangential port fittings. He noticed that the performance of the diode increased as the angle, α, reached the maximum of 37.5^{o} which was obtainable for the spiral chamber. To investigate the effect of angle, α, he constructed a cylindrical chamber which allowed him to increase the angle up to 80^{o}. With this chamber he tested 35 combinations of the five tangential connections with 7 different axial nozzles (especially the effect of angle, θ), with the

deswirling chamber, (Fig. 2.7), and concluded that the most efficient combination to achieve higher performances was the one which gave $\frac{d_o^2}{D_t^2} = 2.5$ and $\frac{d_o^2}{D_e^2} = 4$ at $\Delta P = 5$ m WG with angle $\theta = 7^o$.

The spiral form chamber was difficult to manufacture and also the relative wall roughness exerted an appreciable influence on the performance of the diode. He therefore designed a cylindrical chamber for further investigation which was easy to machine. By changing the internal design and dimensions of the chamber, it was found that a simple version of this chamber with a height of 25 mm was the most efficient, Fig. 2.10a.

By keeping all the internal dimensions constant, with the exception of the chamber diameter, Zobel assumed that the forward flow resistance would remain constant (i.e. wall friction was assumed to be negligible). By investigating the higher resistance performance with increasing chamber size the effect on the diodicity was directly implied. It was noticed that in practice, however, the frictional effects did have some influence on the diodicity. The general conclusion was that larger diameter chambers produced a better diodicity at higher values of Reynolds numbers.

The effect of increasing the chamber diameter was also reported by Jacobs, [8]. Results showed a substantial reduction of reverse flow Euler number and a slight change in forward flow Euler number (as assumed by Zobel). This was accounted for by the wall friction which reduces the value of the vortex diodicity as a function of

Reynolds number, as shown for three different chamber sizes in Fig. 2.11. Baker, [9], characterised a Zobel type vortex diode and obtained a poor performance (diodicity of 50). This was blamed on the vortex chamber to axial port diameter ratio which was 50% of Zobel's optimum design and limited maximum velocity through the diode (12 m/sec), to avoid cavitation there was also a right angled bend close to the axial port. The diode had a spiral form chamber which was previously investigated by Zobel.

More recently, Markland, [10], tested a series of single inlet, single outlet diodes and found empirical expressions for forward and reverse flow Euler number in terms of various geometrical parameters as follows:

$$\xi_F = 0.12 + 0.23/a_a^2 + 0.16/a_t^2 \qquad (2.3)$$

$$\xi_R = 3.1\ d_t^{-1.5}\ (1 - 2.33\ d_a)(1 - 0.6\ h) \qquad (2.4)$$

He suggested a form of design chart in terms of diodicity, throat and pipe diameters and loss coefficients of connections in the associated pipelines with a fixed diameter of cross section of connections. The effect of cavitation and Reynolds number in the case of incompressible fluid and compressibility and choking in compressible fluids were not considered and could be considered for future work.

2.1.3 Diode pumps

Zobel type vortex diodes have been used as a non-moving-part rectifier in a fluidic two diode pump for pumping highly radioactive liquors in reprocessing plant, [11]. A schematic diagram of such a pump is shown in Fig. 2.12. The pump consists of two diodes (supply diode and delivery diode), supply tank, displacement vessel and delivery pipe. In conventional reciprocating pumps, mechanical valves are used to rectify the reciprocating action to produce the suction and power strokes. Compressed air is alternately vented and supplied to provide a reciprocating action. During the suction period liquid is drawn from the supply tank, passes through the axial port of the supply diode (forward flow, low resistance) into the displacement vessel. At the same time, only a fraction of the liquid will be drawn from the delivery pipe since the delivery diode provides a high resistance to the flow (reverse flow direction). During the power stroke, liquid passes through the axial port of the delivery diode (forward flow direction) and is delivered to the delivery pipe. In this period only a fraction of the liquid passes through the tangential port of the suction diode to return to the supply tank, (reverse flow direction).

In comparison with mechanical pumps, the pumping rate is low and the delivery pressure is limited by the supply of the compressed air. If the pump is submerged below the tank level, which is usually the case, no suction is needed for the intake stroke. Average delivery rate depends largely upon the time taken to fill the displacement vessel. When the liquid becomes hot and enters the vessel too quickly, it will cavitate in the source diode, and this is where the

limit on the delivery rate would be expected. This limit was reported by Roberts and Syred, [12]. They used two 10 mm throat diameter diodes with a pump cylinder 20 cm diameter x 90 cm high and showed that the rectifying efficiency of two diode pumps can be as high as 75% for water (30°C - 90°C), whilst the performance reduced by 40 - 50% at 95°C.

Cavitation is especially important in forward flow direction in a typical high performance diode which necessarily depends on diffuser-aided pressure recovery. The forward flow Euler number may increase by a factor of four in going from non-cavitating to cavitating flow, [13]. This effect of cavitation in forward flow is clearly shown in Figs. 2.4(b) and 2.5(b), and is reflected in a reduction in the performance of diode pumps, particularly during the suction stroke. The cavitation in reverse flow state is significant, but is not as severe as in the forward flow.

2.1.4 Vortex throttle

The principle operation of this vortex device is the same as that of a vortex diode, but they are used solely for their high resistance to flow and no attempt is made to reduce the resistance in the forward flow direction. This results in a device with a simple geometry which consists of a vortex chamber, larger than Zobel's optimum design, with a straight tangential port, a central exit hole, followed by a sudden expansion diffuser. Throttles usually have a higher resistance compared with vortex diodes in reverse flow, where

the main objective is to achieve a higher pressure drop for a given minimum flow area.

Brombach, [14], has developed and tested a conical type of vortex throttle for use in sewer systems. Fig. 2.13 shows a typical combined sewer system. Sewage flow rate to the treatment plant must be regulated according to the capacity of the plant. Conventional flow controllers can experience blockage and consequently cause some damage to the system. In dry seasons, when there is no rain, the water flow rate through the system is low, thus most of the contaminants remain in the duct. In rainy conditions, the flow through the sewer increases to a very large volume and sweeps the sewerage through the duct into the storm water overflow tank. The contaminants are collected in the bottom of the tank and pass through the flow controller into the treatment plant, and overflow which is relatively clean can be directed into the river. The capacity of the flow controller depends on the capacity of the treatment plant. Typical flow is of the order of 25 to 50 ℓ/sec with a head of 2.5 m across the controller, an orifice with a diameter of about 100 mm is required to regulate the flow rate, which is small and could be easily blocked. A conical vortex throttle, Fig. 2.14, with a considerably bigger nozzle diameter and a single tangential port, can be used instead of the conventional controller to regulate the flow rate and also to eliminate the possible blockage of the system. A typical installation is shown in Fig. 2.15. The tangential port is connected to the lowest possible point of the storm tank. The gate

valve is fully open during operation and the outlet port of the vortex throttle is connected to the supply pipe of the treatment plant.

If there is no rain, i.e. water level is low, the pressure at the tangential port is low; a free water level is formed in the chamber and the pattern is not axially symmetrical, thus preventing the generation of a vortex. As the head of water rises, the water level inside the chamber also rises and air is vented from the chamber through air vents and a vortex can be formed. The vortex generation is initiated entirely by the tangential nozzle.

Another application of vortex throttle is in the sampling of highly corrosive fluid in a chemical plant, where the use of conventional valves for bleeding a small flow from a high pressure main stream could present corrosion or blockage problems. Thus the valve, or bleed nozzle, can be replaced by a vortex throttle with a larger minimum area.

Fluid resistors such as orifices and capillary tubes always exhibit a positive temperature sensitivity, Fig. 2.16. The steady state characteristic of these resistors depend on the geometrical parameter of the devices, and fluid properties such as density and temperature or viscosity. Investigation by Hamid, [15], showed that the vortex throttles could be designed and used with capillary tubes and orifices to obtain temperature or viscosity compensation. This is because the vortex chamber and central hole (orifice) contributes

a negative temperature sensitivity and the tangential inlet and sudden expansion diffuser contributes a positive temperature sensitivity. These effects tend to cancel each other.

The temperature sensitivity of a fluid resistor is defined as the change in the steady-state flow rate through the resistor as a function of the temperature variation for a constant pressure drop across the resistor.

2.1.5 Single inlet double outlet diode

Figure 2.17 shows a typical vortex diode with two exhausts. The principle operation of this diode is similar to single inlet, single outlet diodes. In the forward flow direction, fluid enters the exhausts and leaves tangentially. In the reverse flow direction, fluid enters tangentially and leaves through two axial ports. The performance of this type of diode, using air as a working fluid, was reported by Dilley et al [16] where they obtained reverse flow Euler numbers up to 56.5 at Reynolds numbers of 13,500 and forward flow Euler numbers of 0.4 at Reynolds numbers of 70,000. In water, reverse flow Euler numbers of 63 at Reynolds numbers of 20,000 and forward flow Euler numbers of 0.3 at Reynolds numbers of 200,000.

The purpose of the double outlet was to reduce the forward flow resistance by increasing the flow area whilst in the reverse flow direction it was believed that the pressure drop would remain much the same as for a single outlet. The latter assumption presumes that the pressure drop is achieved across the vortex only and is not

influenced significantly by the flow through the exit ports. This assumption is not consistent with the findings of the present work.

2.1.6 Cathrine Wheel vortex diode

This type of diode was developed at Cardiff University by Syred, Roberts, and Sidhu, [17]. The device has a thin chamber to produce a stronger vortex and 8 tangential inlets to reduce the forward flow resistance because of the flow symmetry within the chamber, and to achieve higher reverse flow resistance because of a more symmetrical vortex, i.e. a greater conservation of the angular momentum. Characteristics of this diode were reported by Dilley et al, [16], where it was shown to have a better performance compared with a Zobel type diode. Fig. 2.18 shows a Cathrine Wheel vortex diode. Increasing the number of tangential inlets from 8 to 16, [18], reduced both the forward and reverse flow Euler number and led to a poorer performance. Comparison of reverse and forward flow Euler number for diodes are given in Fig. 2.19, although it should be pointed out that the diodes with 8 inlets had a smaller diameter vortex chamber.

2.1.7 Scroll diode

A scroll diode such as that shown in Fig. 2.20 is a device which allows the fluid to pass through the chamber smoothly in forward flow. In the reverse flow direction, the fluid undergoes pressure losses because of the rapid separation of the fluid behind the sharp edge and also the formation of a vortex. This device was developed to

prevent backflow in a crankcase scavenged two-stroke engine, [19]. The diode was connected to the engine as shown in Fig. 2.21(a), and produced a considerable effect on delivery ratio at low speeds. The delivery ratio is defined as the ratio of the mass charge delivered to the displaced volume at ambient density. Fig. 2.21(b) shows the variation of delivery ratio with engine speed. This figure also shows the effect of increasing the width, h, of the entrance to the vortex chamber. These effects are caused by the changes in forward and reverse flow losses. Sher, [20], also used the scroll diode at the scavenge port as well as at the inlet port of a two-stroke crank case-scavenged engine, and reported that because of the diode's presence, backflows are prevented, the delivery ratio improved, and the scavenging mechanism is changed.

2.2 **Vortex Amplifier**

Fig. 2.22 shows a simple vortex amplifier with a radial supply port, tangential control port and axial exhaust port. With no control flow, the supply flow enters radially and passes through the axial exhaust with a minimum of losses. If a secondary flow is introduced into the chamber through the tangential port, the two flows will combine to produce a spiral vortex. This produces a pressure gradient within the chamber, thus increasing resistance to the flow. As the control pressure is increased, the supply flow is further restricted until the supply flow is reduced to zero. This effect is shown in Fig. 2.23. For a constant pressure drop across the device, the supply flow may be totally restricted by increasing

the control flow, i.e. zero supply flow and maximum control flow, (Q_S = 0, Q_C = max). If the control pressure is not sufficiently large it will have no effect on the supply flow, i.e. it can be considered that Q_S = max, Q_C = 0. The turn down ratio is defined as the ratio of maximum supply flow to the maximum control flow, TD = $\frac{(Q_S)_{max}}{(Q_C)_{max}}$, turndown ratios of of 6.5 and 11.5 have been reported by [21] and [22], respectively. A typical value for a conventional vortex amplifier is 10. Chow, [23], constructed a plexi glass vortex amplifier with chamber diameter of approximately 203 mm. It had 4 control flow ports, two exhaust holes, 12 annular supply flow inlets, 6 to each side of the vortex chamber. The valve was designed so that the exhaust hole diameter, D_e, the width of the annular inlets, t, the width of the control flow ports, w, and the depth of the vortex chamber, H, were changeable, Fig. 2.24. Experimental results showed that higher turndown ratios were achieved by fixing the ratio w/D_o and increasing, D_o/D_e. Fig. 2.25 shows the relation between turndown ratio and control to supply pressure ratio. It can be seen that by reducing the ratio, w/D_o, that although the turndown ratio increases, the control to supply pressure also increased which limits the possible applications of the valve.

It is possible to achieve a very wide range of operating pressures for a variety of applications. The U.K.A.E.A. have long been using radial vortex amplifiers as a pressure controller on glove boxes, where the duty of the valve is to maintain a steady depression during normal operation and also to prevent the leak of radioactive material in the case of emergency, such as a torn glove, by extracting

sufficient flow through the glove box to maintain the depression within it, Fig. 2.26(a). The supply port of the vortex amplifier is connected to the glove box and its control port is open to the atmosphere. The outlet of the amplifier is connected to the purge duct. Under normal operating conditions, the extract system draws air from the atmosphere through the vortex amplifier, thus the flow rate is small because of the vortex motion which effectively increases the pressure drop across the amplifier. In the event of emergency, since the glove box is maintained at sub-atmospheric pressure, the air passing through the supply port will prevent the generation of vortex within the chamber, i.e. connecting the glove box into the extract duct. This type of controller is very effective and more reliable than conventional methods, Fig. 2.26(b), since there is no moving parts and the response is very quick. In a conventional system, the pressure sensor actuates a solonoid valve in the event of any depression loss to ensure a high purge flow.

Large vortex amplifiers of 0.6 to 1.3 m have been constructed, [24], and installed for building ventilation systems in an active chemical plant. Fig. 2.27 shows a typical reprocessing plant ventilation system with vortex amplifiers as controllers for controlling a common extract duct from several glove boxes, extracting fumes from a vessel, ventilating a cell and two caves.

A simplified model of the ventilation system was tested at Sheffield University where the main objective was to hold the depressions and flows within certain limits; in the case of

emergencies, such as gradual blockage of the main filter, torn glove, fan failure, occasional opening of hatches in the cell and variable permeability of the walls of the room-sized regions.

Very large vortex amplifiers have been designed to prevent flooding, [25], with a chamber diameter of 19.0 m, an exit diameter of 1.69 m and a chamber height of 2 m. Supply and control nozzles are 2.0 m square. Data from a non-controllable flood retention basin already in operation in the southern part of Germany, were used for the purpose of this design. The principle of using a series of vortex amplifiers to control the reservoir outflow is shown in Fig. 2.28. The supply and control ports are connected to the retention basin as shown. As the water level in the basin increases, the outflow will increase until the maximum allowable is reached. At this stage, the first vortex amplifier will be regulated by the action of the control port, thus controlling the outflow. The other vortex amplifiers will be activated in sequence as the water level increases.

Vortex amplifiers have also been tested in order to control fuel flow into aircraft engines, [26]. The system is shown in Fig. 2.29. As the pressure before the heat exchanger increases, i.e. high engine demand, the tangential control flow increases to generate the vortex within the chamber, thus ensuring sufficient fuel reaches the engine by reducing return flow to the tank. The return flow could be further reduced as the radial flow becomes negative. At low engine demand, most of the fuel can be returned through the radial port into

the chamber, and since the tangential control pressure is at a minimum, the fuel will pass through the axial outlet of the valve and returned to the tank. The purpose of the vortex amplifier was to increase the reliability, reduce the cost and also to maintain at least a given minimum fuel flow through the heat exchanger, even when the engine demand falls below that minimum.

2.3 **Vortex Tube**

This device was originally designed by Ranque in 1931 and investigated by Hilsch [27] in 1947. The device is very simple and consists of a long tube with tangential inlet nozzles, an orifice in one end and a centre body in the other end, Fig. 2.30. When fluid is injected into the tube, a vortex is formed which has a cooler fluid at the core and hotter fluid at the outer radius. The cold fluid escapes from the orifice and the hot fluid from the control valve. The amount of cold and hot fluid can be regulated for different applications. This physical property of the device has been the subject of many published papers and also has been useful in the commercial field. Presently, a vortex tube using compressed air as a working fluid is being used as a cooling device, [28], for protective clothing and helmets for such jobs as sand blasting, welding, painting, and handling toxic materials. This clothing can be simply cooled by connecting the vortex tube to a compressed air supply. Smaller types of device with smaller volume flow rate have found applications in cooling machining operations such as drilling, milling, turning, and reaming.

The principles of operation within the vortex tube have been described as follows, [29]: As the axial pressure gradient is created in the central portion of the chamber by a radial drop in pressure that is inversely proportional to the decay of the swirl velocity, a back flow is generated and flows out through the cold end orifice as a cold air stream. On the other hand, the annular flow, which follows along the chamber wall, passes out through the cone-shaped valve regulating the rate of flow as a hot air stream.

The temperature difference has been defined by many authors, [30]. The fluid in the core of the vortex is cooled as a result of an adiabatic expansion ($Q = 0$) and it is heated at the outer radius of the vortex because of the centrifugal pressure. The performance of the vortex tube is described by the degree of heating and cooling of the air leaving each end of the tube. It is commonly described in terms of the parameter, μ', which is the ratio of cold mass flow rate to total mass flow rate. A typical performance curve is shown in Fig. 2.31.

Takahama et al, [31], experimentally investigated the performance of a steam operated vortex tube and concluded that provided the steam is in the superheated condition at the outlet nozzle of the vortex tube, the energy separation performance is the same as that for air, and it is independent of the degree of superheat, total mass flow rate and discharge resistance. When the steam condition at the outlet nozzle is wet, even if steam at the inlet nozzle is super-heated, the performance decreases, and for dryness fraction

less than 0.98, the energy separation cannot take place since the droplets are separated from the annular flow region by centrifugal force, and because of the latent heat of droplet vaporisation, all the available energy cannot be separated and also some of the steam condenses by the effect of the vortex tube.

2.4 Vortex Oscillator

Sarpkaya, [32], described the forced and periodic instabilities resulting from two vortex motions rotating in opposite directions in a device consisting of 2 vortex chambers with a central connecting pipe, as shown in Fig. 2.32. In order to achieve the forced instability, the surge chamber was firstly taken out of the system. The upstream tangential port was opened and the downstream was kept closed. By increasing the upstream flow to a maximum, the vortex was fully formed. At this point, the downstream port was opened and the flow increased gradually. This caused a variation in the discharge of the flow through the exit port, which is shown in terms of discharge coefficient and downstream to upstream pressure ratio, in Fig. 2.33. The minimum discharge coefficient is the indication of the intensity of the vortex downstream of the device. Upstream and downstream pressures and flow rates were recorded during the experiment and it was observed that as the value of $\frac{Q_C}{Q_S}$ increased the ratio, $\frac{P_C}{P_S}$ decreased slowly at first, and then suddenly when the vortex in the downstream chamber collapsed and the emergent jet became turbulent. It was also shown that the value of $\frac{P_C}{P_S}$ remains constant for $\frac{Q_C}{Q_S}$ between 0.16 and 0.4.

Similar experiments were made by adding the surge chamber into the system and it was concluded that only the unique combination of pressure at the two vortex chambers produced periodic oscillations of constant amplitude. This amplitude is large in magnitude at the downstream, and small in the upstream, and independent of the frequency of oscillation. The frequency depended on the inertance and capacitance characteristics of the unit, and of the external conduit-resonator system; the vortex device requires a capacitance provided by the surge chamber or possibly by either the compressibility of the fluid or by the elasticity of the conduit walls.

By ignoring viscous effects and keeping total temperature constant, the frequency of oscillation is seen to be, [33]:

$$F = \frac{1}{2\pi}\left(\frac{1}{CI}\right)^{1/2} \tag{2.5}$$

where C and I are capacitance and inertance given by:

$$C = \frac{1}{\rho_{air} a_o^2} \sum^{k} (L_K\ A_K) \tag{2.6}$$

and

$$I = \rho \sum^{k} L_K/A_K \tag{2.7}$$

A comparison between theoretical values and those which were obtained by the use of an oscillograph are shown in Fig. 2.34 for both air and water.

The theoretical and experimental investigation of a thin chamber vortex oscillator was carried out later by Sarpkaya et al [34], where it was shown that a vortex chamber coupled with two resonators, works like a hydrodynamic oscillator. A maximum discharge coefficient of about 0.3 at $\frac{Q_C}{Q_s}$ equal to 1 was obtained, (exit throat diameter of 12.7 mm). The variation of discharge coefficient with $\frac{Q_C}{Q_s}$ is shown in Fig. 2.35. Oscillations were noticed at $0.83 < \frac{Q_C}{Q_s} < 1.2$. The theoretical frequency was calculated by use of equation (2.5) and found to be three times higher than the measured value, and was accounted for by the contribution of the fluid within the vortex chamber to the capacitance and inertance of the system (which was difficult to predict) and furthermore, the viscous and form resistances in the fluid lines were completely ignored. The frequency characteristics obtained for the thin chamber vortex oscillator is the same as the vortex chamber with a connecting pipe.

2.5 **Cyclonic Chambers**

A funnel-shaped vortex device which has been used for removing particles from air or other fluids by centrifugal means, is known as a cyclone separator. This is perhaps the oldest type of vortex device and has been in operation for over 100 years. Many types of cyclone device, such as a cyclone dust separator and cyclone furnace, are widely used in industry. Fig. 2.36 shows the most simple and common form of cyclone separator with a typical performance curve and also a cyclone furnace.

2.5.1 Cyclone furnace

The crushed coal is introduced tangentially into the cyclone furnace chamber at the front end of the device. The strength of the vortex is further increased by the tangential admission of high velocity secondary air into the cyclone, [35].

The combustible material is burned from the fuel in the cyclone furnace, and the resulting high temperature gases melt the ash into liquid slag, a thin layer of which adheres to the walls of the cyclone. The incoming fuel particles, except those fines burned in suspension, are thrown to the walls by centrifugal force and caught in the running slag.

The secondary air sweeps past the coal particles embedded in the slag surface at high speed. Thus, the air required to burn the coal is quickly supplied and the products of combustion are rapidly removed. The products of combustion are discharged from the cyclone into the boiler furnace. The part of the molten slag that does not adhere to the cyclone walls also flows toward the rear and is discharged through a taphole in the boiler furnace. Fuel, gas and oil can also be burned in cyclone furnaces. When oil is the fuel, it is injected adjacent to the secondary air ports and directed downward into the secondary airstream which produces further atomisation.

2.5.2 Cyclone dust separator

For collection of particles greater than 10 microns, cyclones

have a relatively high efficiency (more than 90%), Fig. 2.36. Cyclones are useful devices to clean up dirty gases before they are discharged to the atmosphere. They can be used in series in order to separate particles into two or more size classes. High temperature and high pressure flue gases from pressurised, fluidised bed combustion (PFBC) can be used, after removing particles, to drive a gas turbine. The use of both a steam and gas turbines in a combined power cycle results in a significant increase in efficiency. The collecting of the particles which cause damage to the gas turbine by erosion, corrosion or deposition of solids on the turbine blades, could be carried out by the use of high efficiency cyclone separators.

Three conventional cyclones have been used successfully at high temperature and pressure to clean up flue gases from a PFBC, [36]. Ernest M. et al, [37], reported the use of a three stage cyclone at temperatures up to 900^{o}C and pressures up to 9 bar for removing particles from exhaust gases of a PFBC with 95% overall efficiency. However, the efficiency could reduce for full scale plant operation since the efficiency of a cyclone decreases as its diameter is increased, [38]. At higher temperatures, the selection of material should be considered carefully since the corrosive nature of the gases could cause problems.

The use of various stainless steels or other alloys will increase the cost of the cyclone. If smaller cyclones are banked together, plugging becomes a major problem and will decrease the

efficiency of the cyclones, [39].

2.6 **Vortex Whistle**

Vonnegut, [40], designed whistles which operated by discharging vortex flow through an axial port. The device was tested on air and water. The vortex produced a note having a frequency that was continuously variable with inlet pressure. Fig. 2.37 shows frequency against the quantity, $[\frac{P_u - P_d}{P_u}]^{1/2}$ for two types of whistle, where P_u is the inlet pressure and P_d is the downstream pressure. It was found that the frequency decreased as the length of the outlet tube was increased. It was therefore concluded that the frequency is the result of the rotation of the fluid at the point where it leaves the whistle and that as the rotating air proceeds down the outlet tube, its angular velocity is reduced by viscous forces.

On the basis of the above test, Michelson, [41], described the theory of vortex whistle and derived a formula for frequency as:

$$F = \frac{a^*_u}{\pi D_e} \left[\frac{2}{\gamma}\right]^{1/2} \left[\frac{P_u - P_d}{P_d}\right] \qquad (2.8)$$

where a^*_u is the upstream speed of sound, D_e is the exit diameter, P_u and P_d are upstream and downstream pressure.

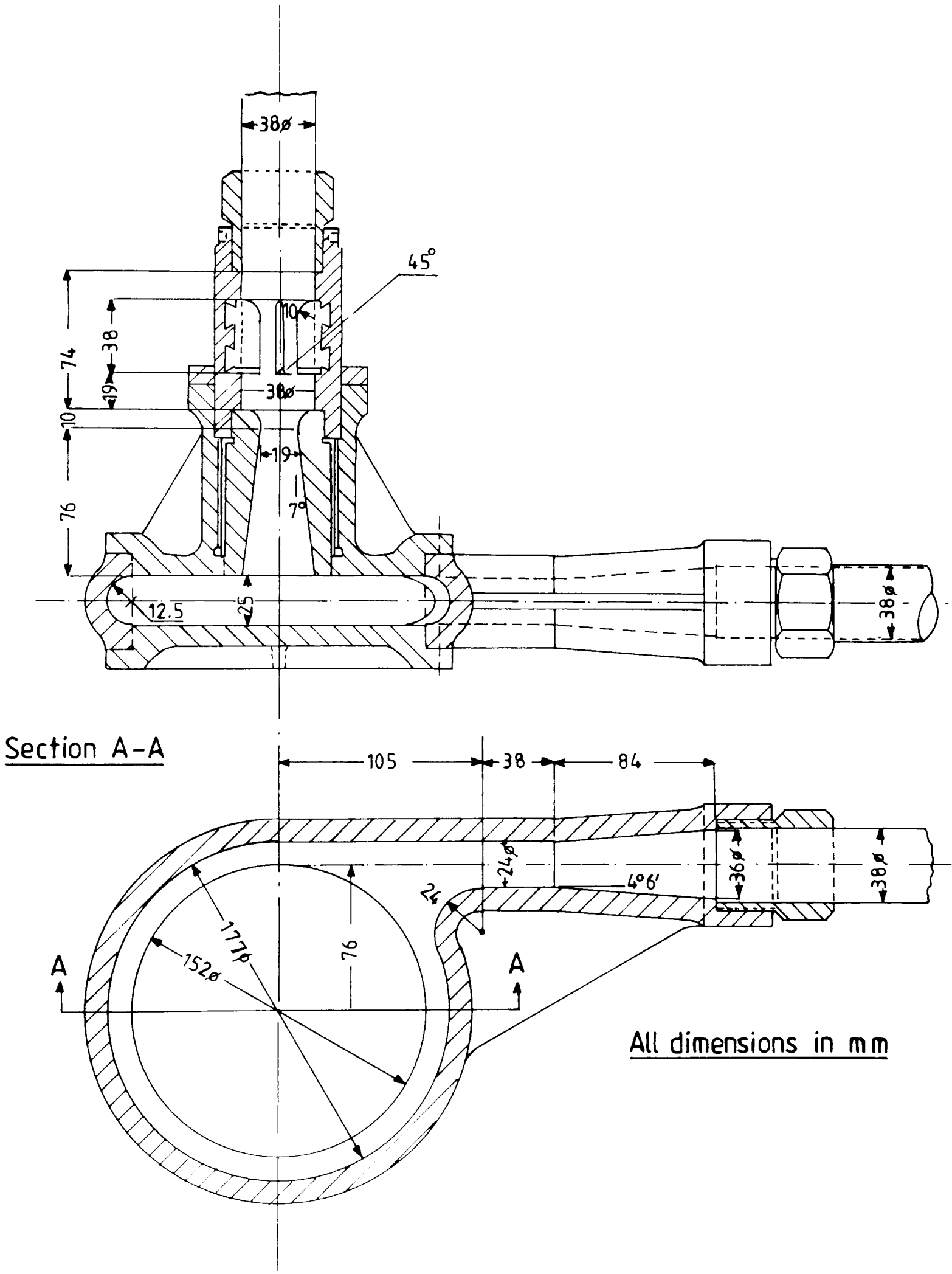

~~Fig. 2.1~~ Zobel Diode

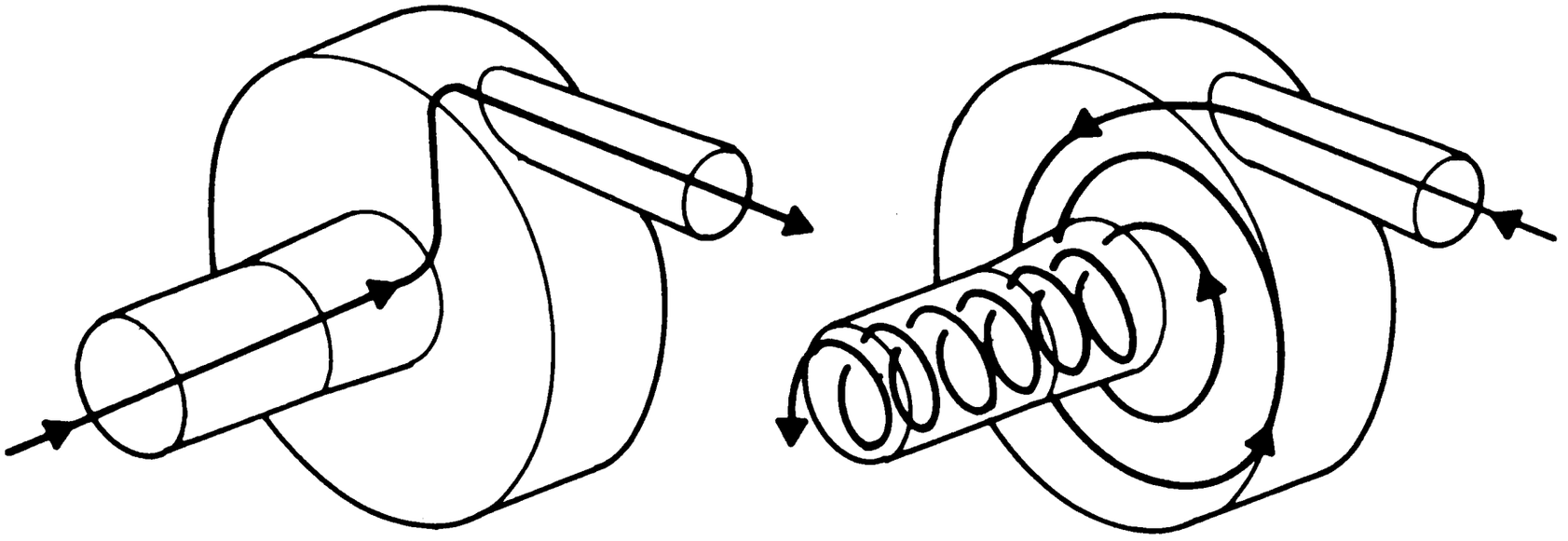

Forward flow - low resistance

Reverse flow - high resistance

Fig. 2.2 Flow Through Vortex Diode

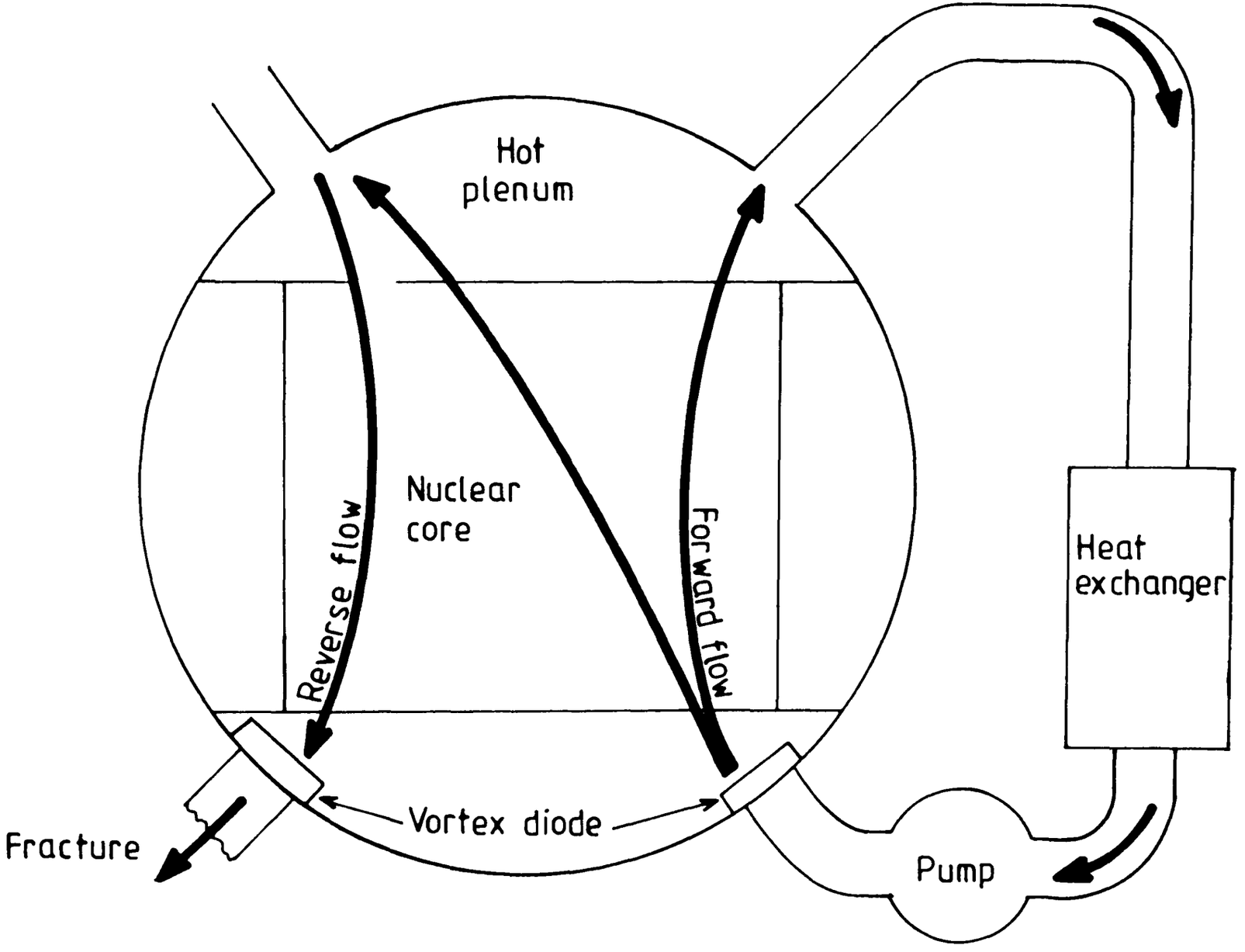

Fig. 2.3 Model for Reactor Containment Breach

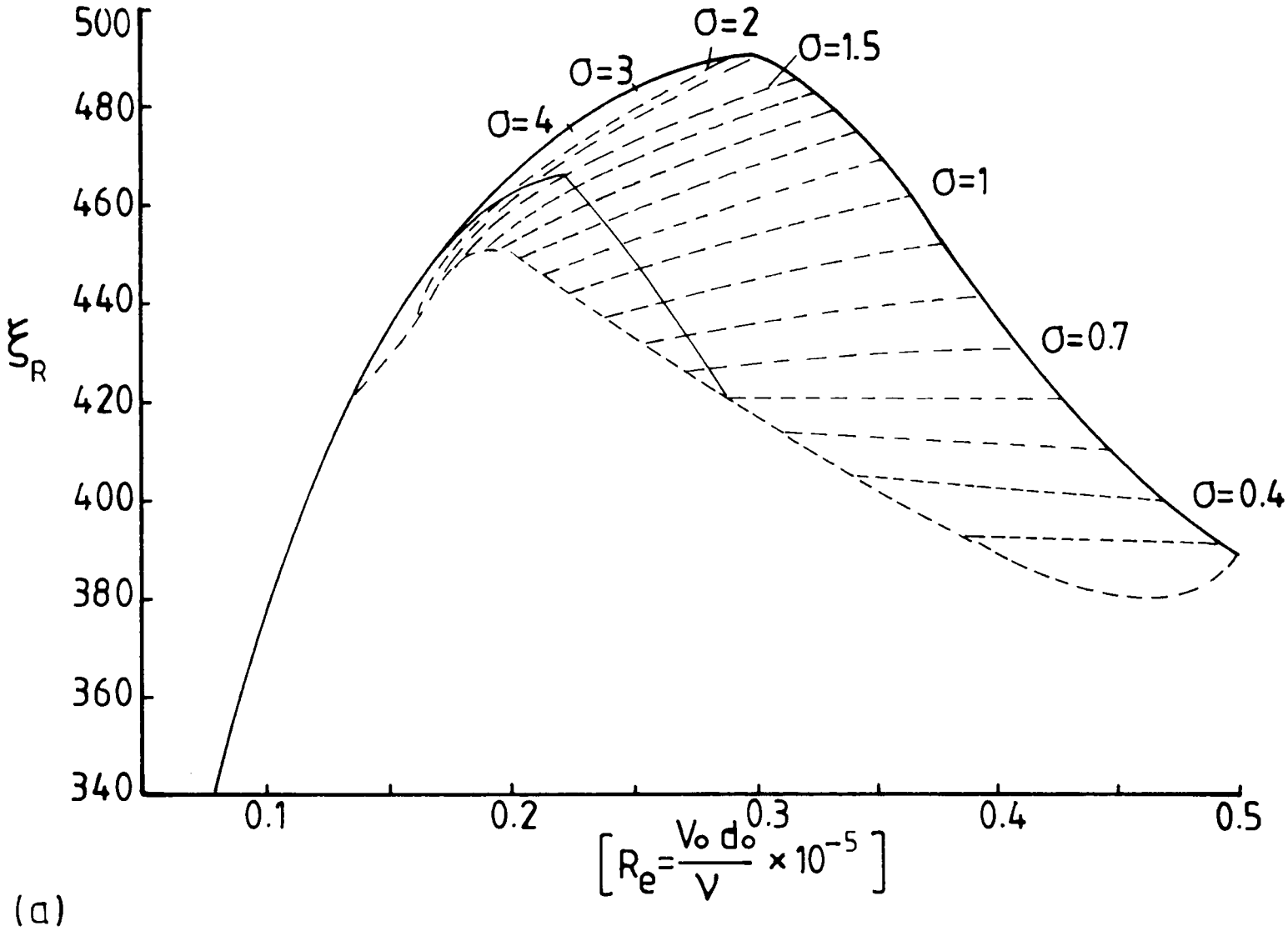

(a)

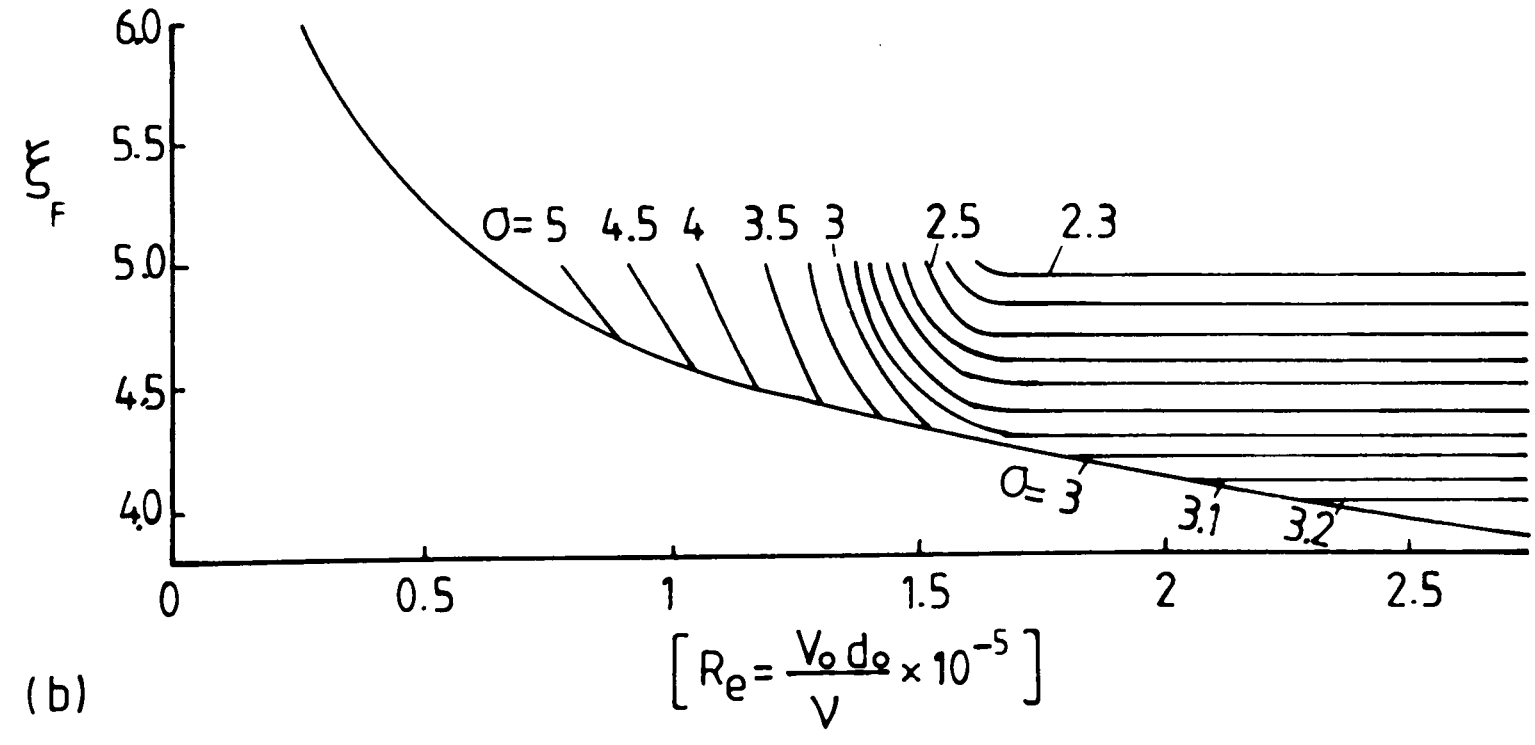

(b)

Fig. 2.4 Flow Characteristics of Zobel's Diode (a) Reverse (b) Forward

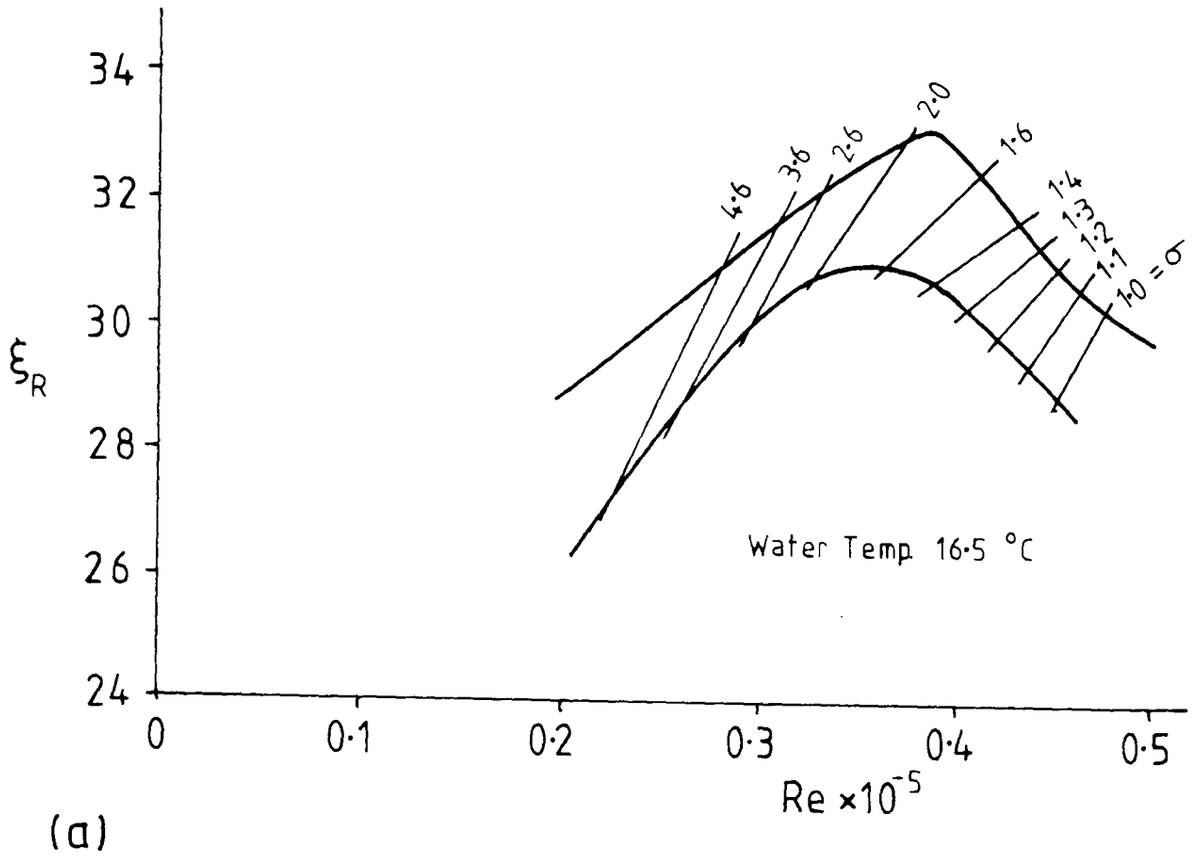

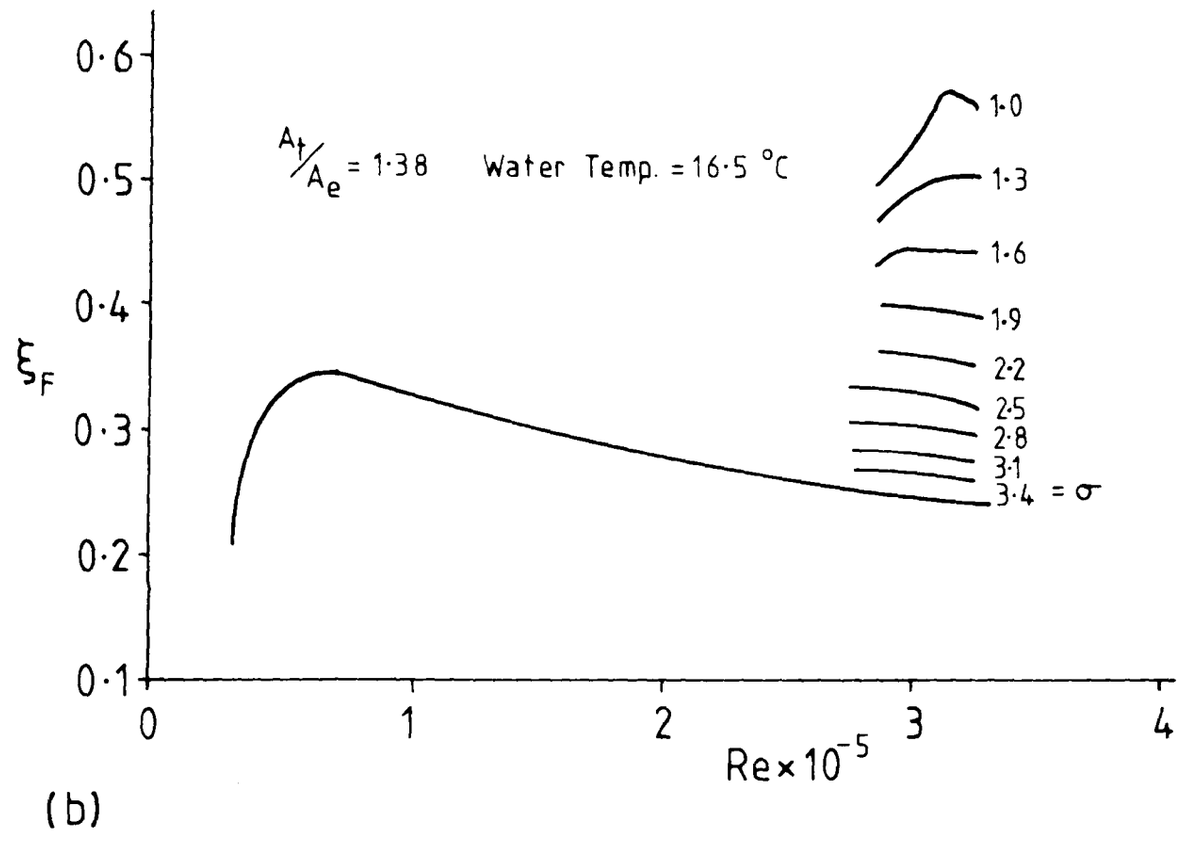

Fig. 2.5 **High Performance** catherine wheel vortex diode **Characteristics**

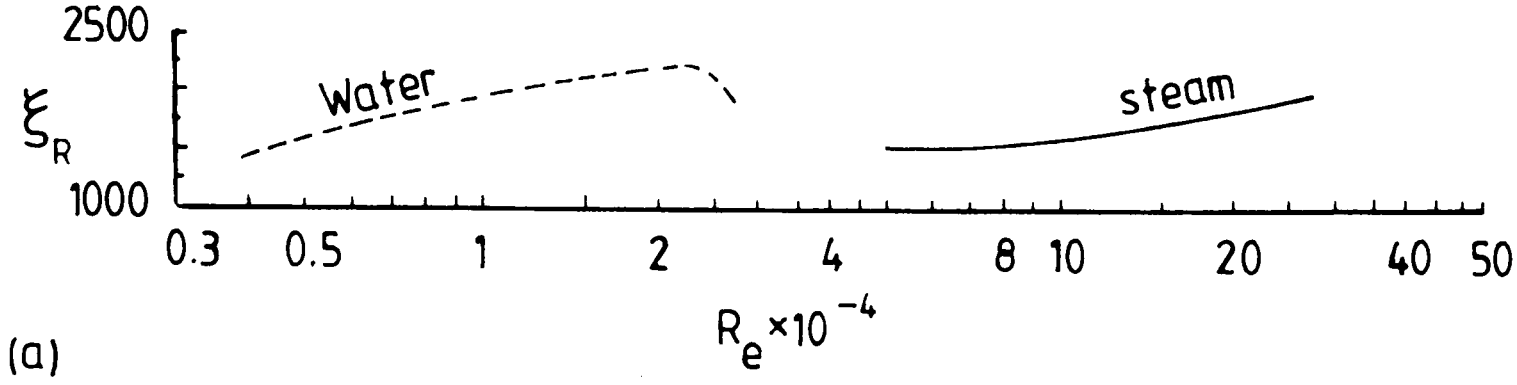

(a)

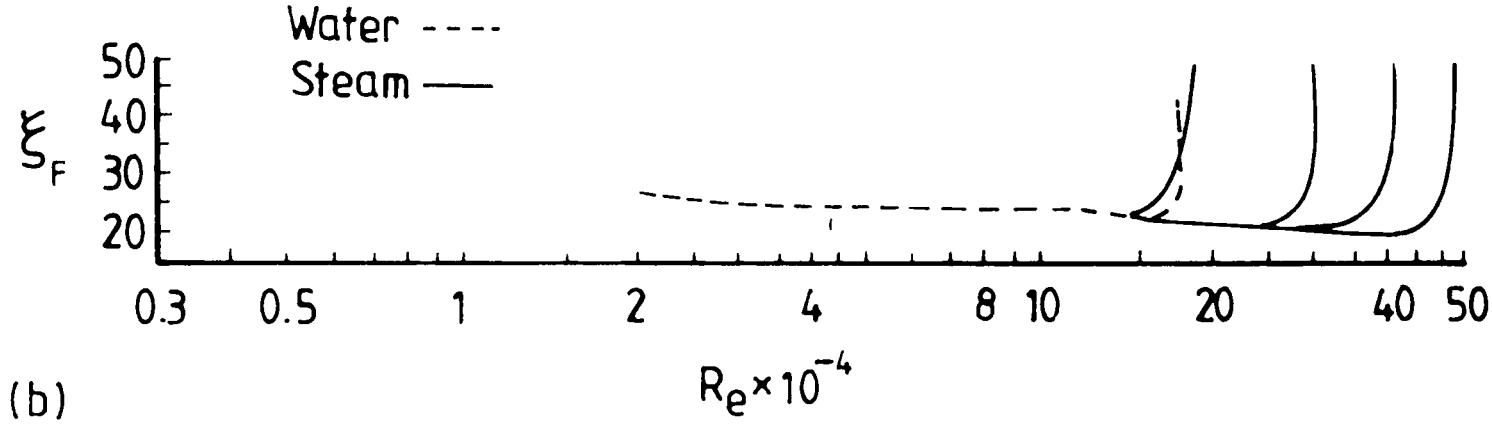

(b)

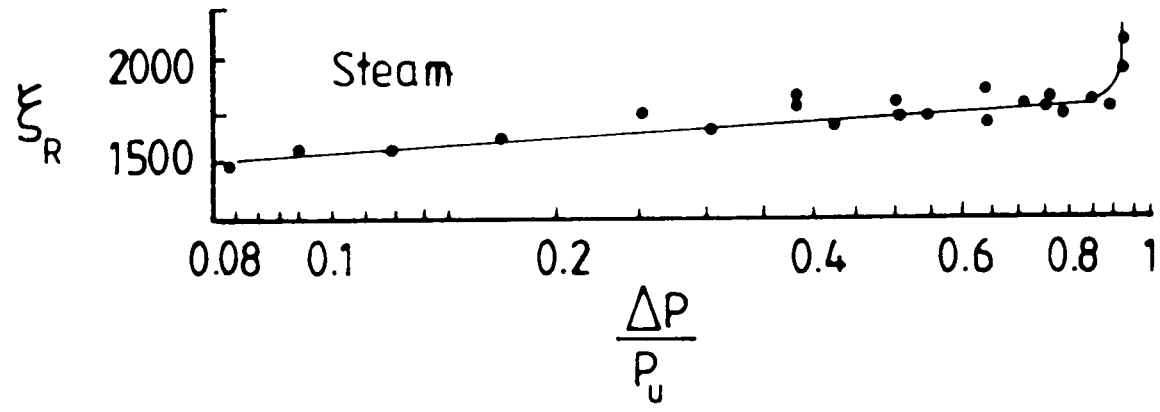

(c)

Fig. 2.6 Zobel Diode Steam and Water Characteristics

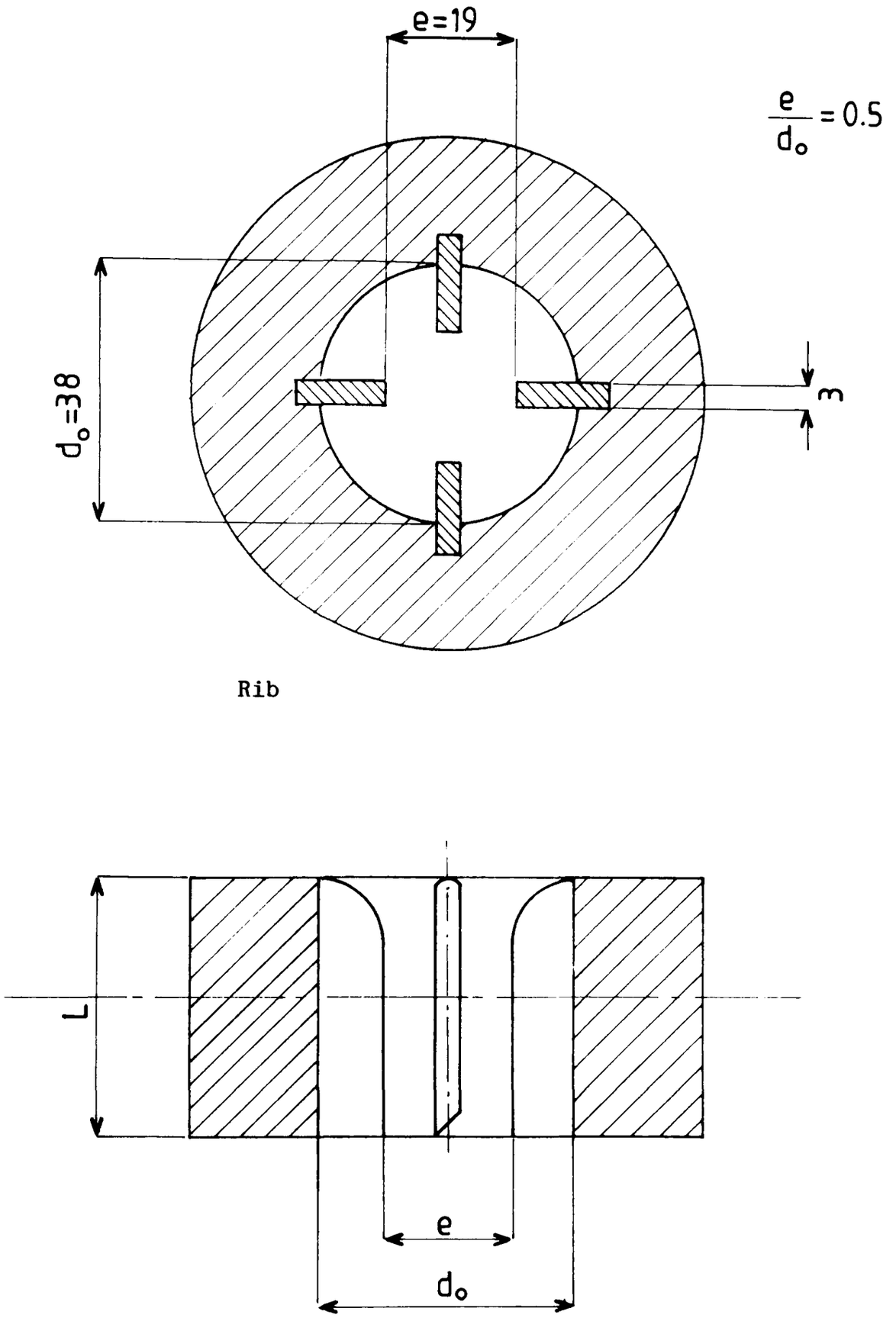

Fig. 2.7 Optimum Design of De-swirling Chamber

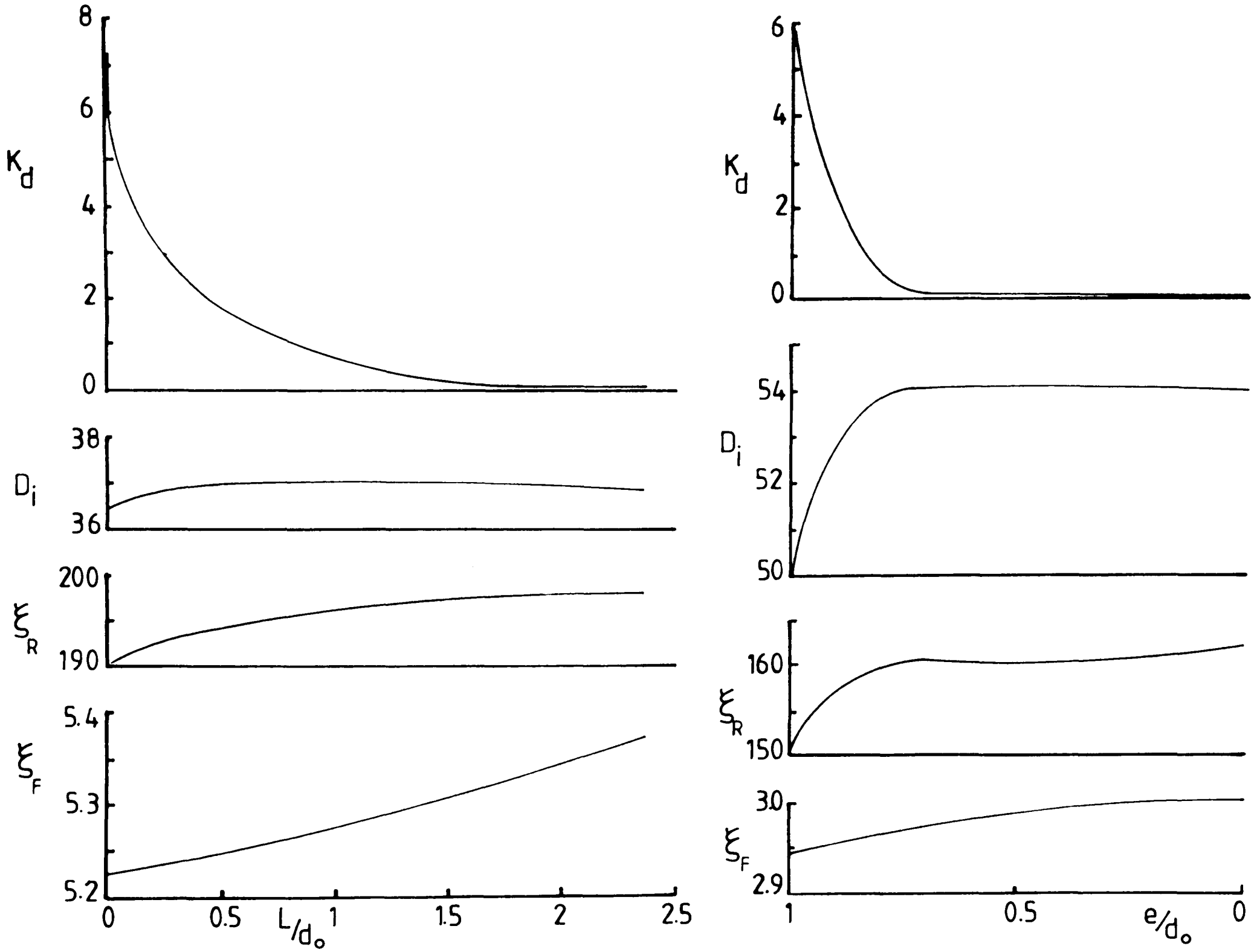

Fig. 2.8 Typical Optimisation Results for De-swirling Chamber

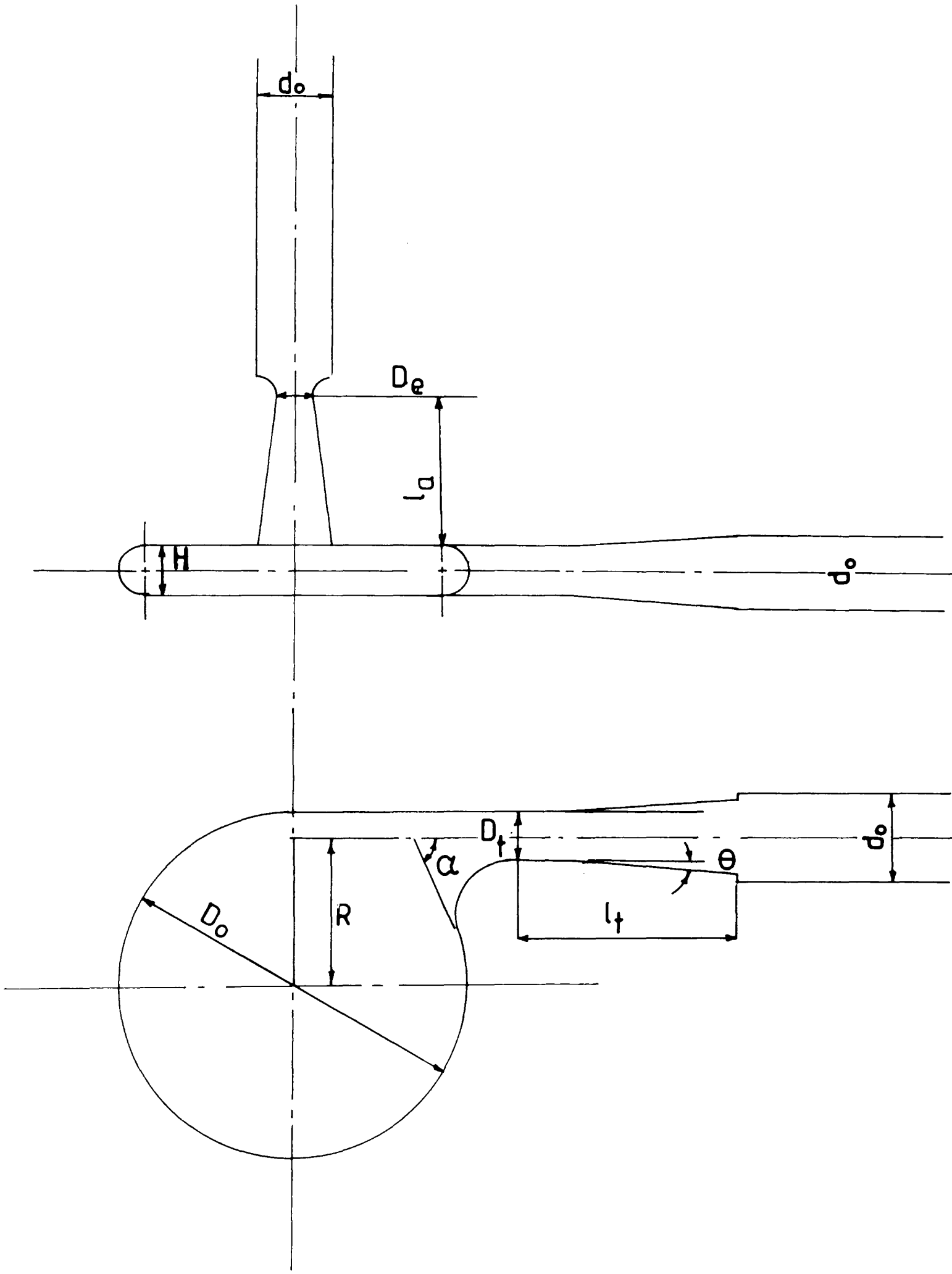

Fig. 2.9 Internal Detail of the Zobel Diode

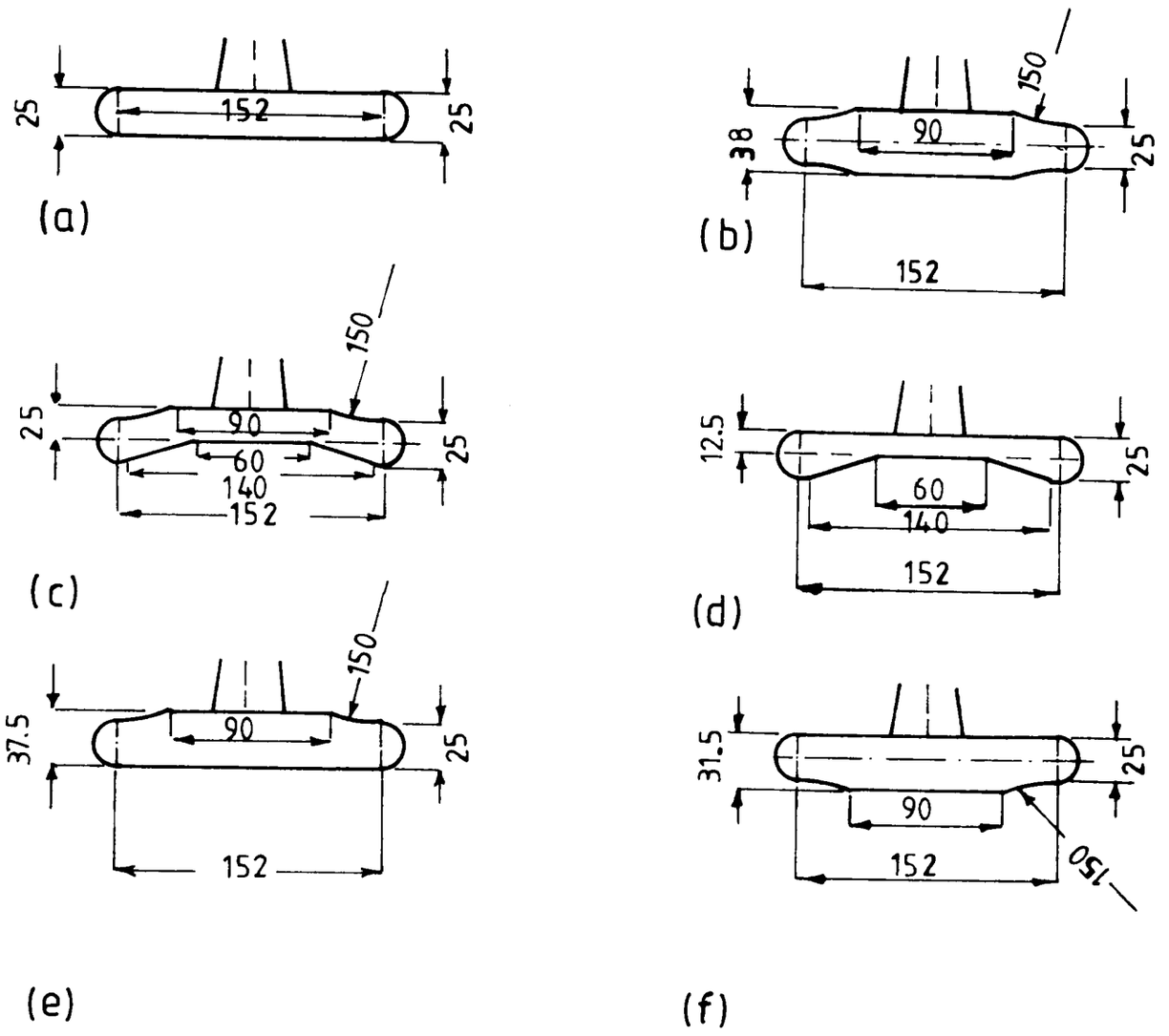

Fig. 2.10 Internal Detail of Vortex Chambers used by Zobel

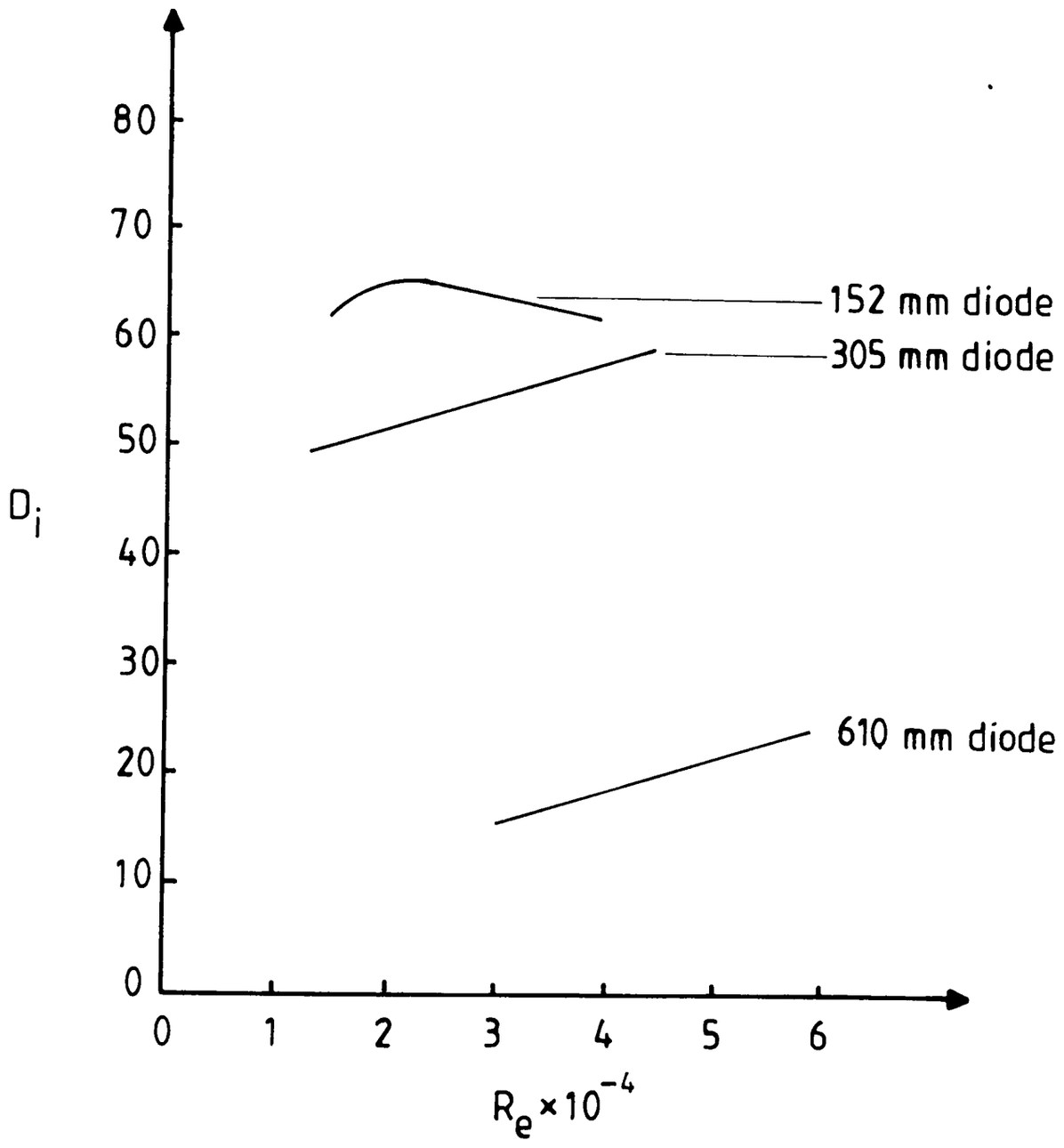

Fig. 2.11 Effect of Increasing Chamber's Diameter on Performance of the Diode

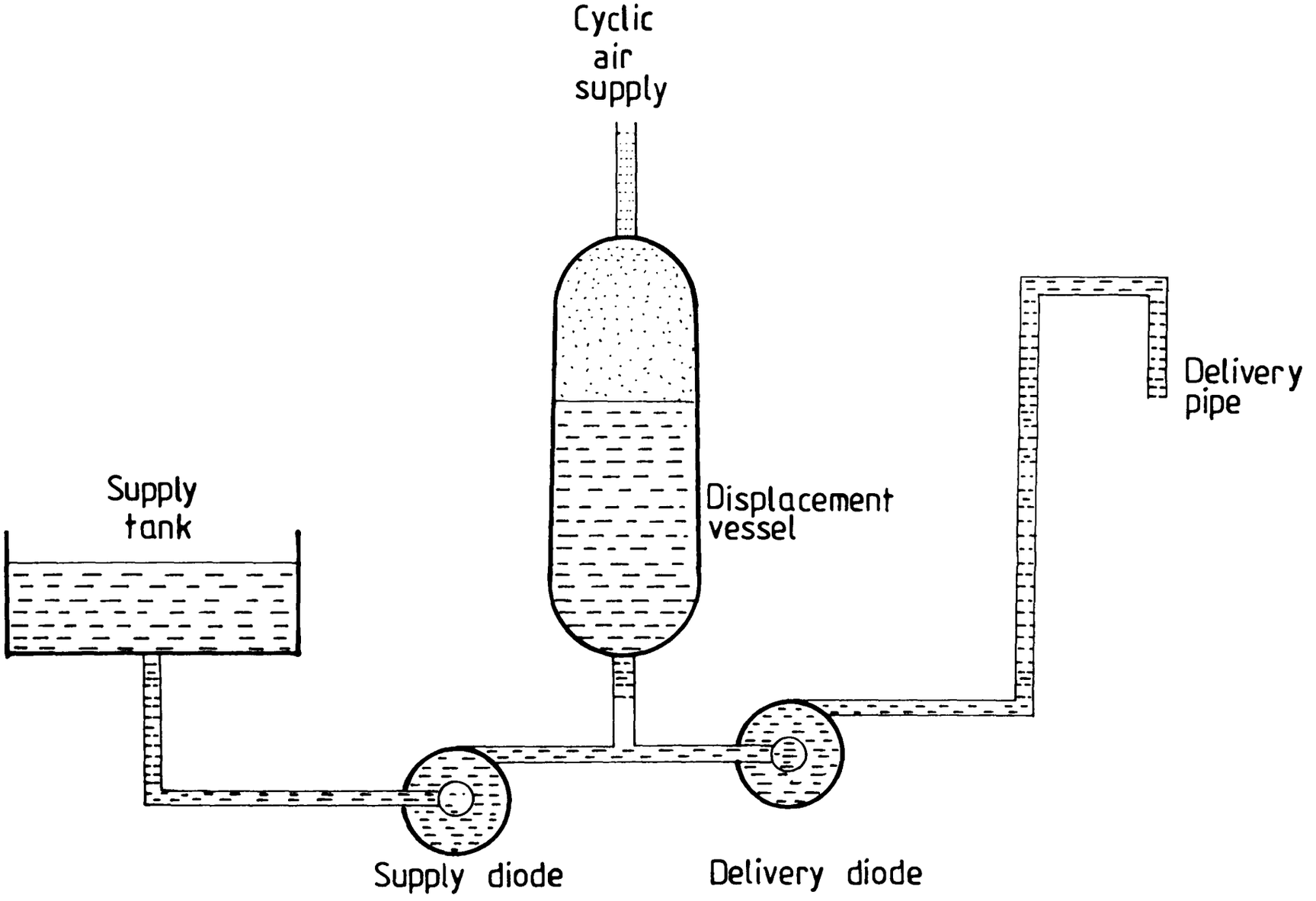

Fig. 2.12 Single Acting Diode Pump

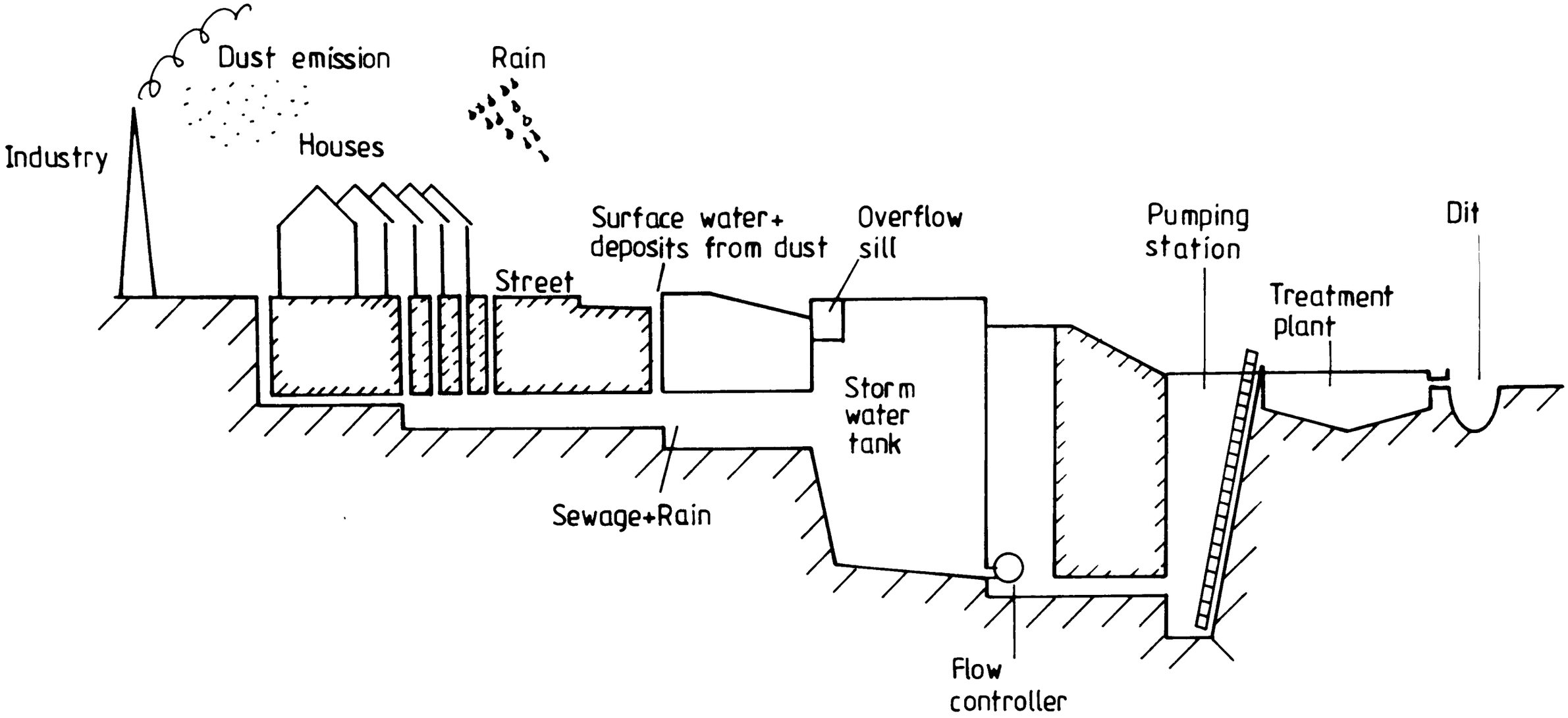

Fig. 2.13 Combined Sewer System

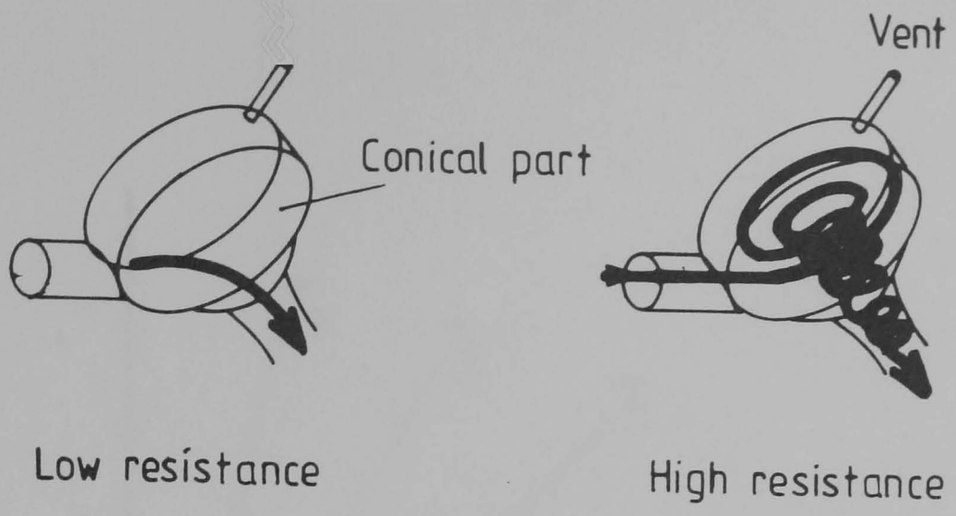

Fig. 2.14 Conical Vortex Throttle

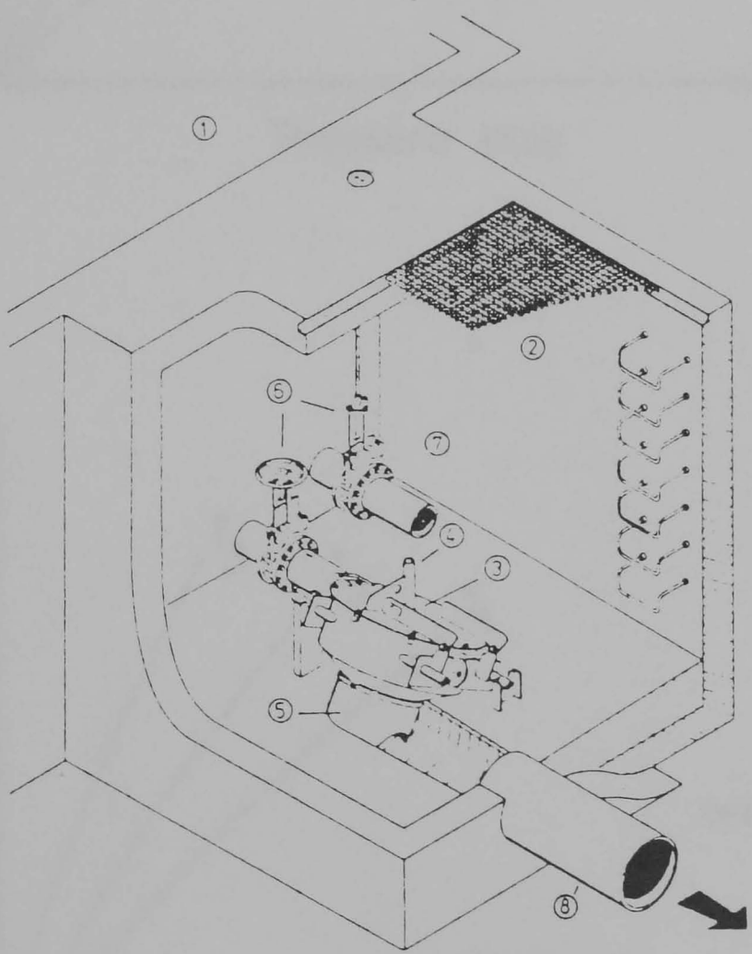

(1) Storm water tank
(2) Control shaft
(3) Vortex flow controller
(4) Vent
(5) Splash protection
(6) Slide valves
(7) Bypass
(8) Pipe to sewage treatment plant

Fig. 2.15 Typical Installation of a Conical Single Inlet Vortex Throttle

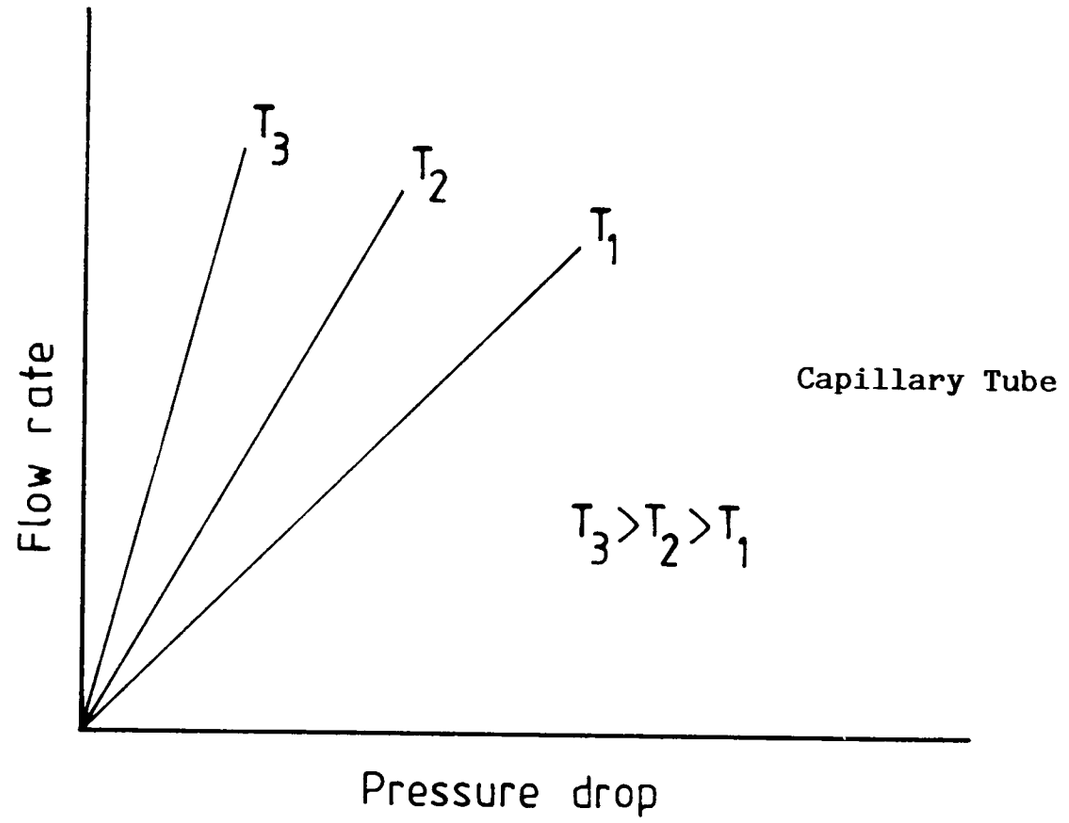

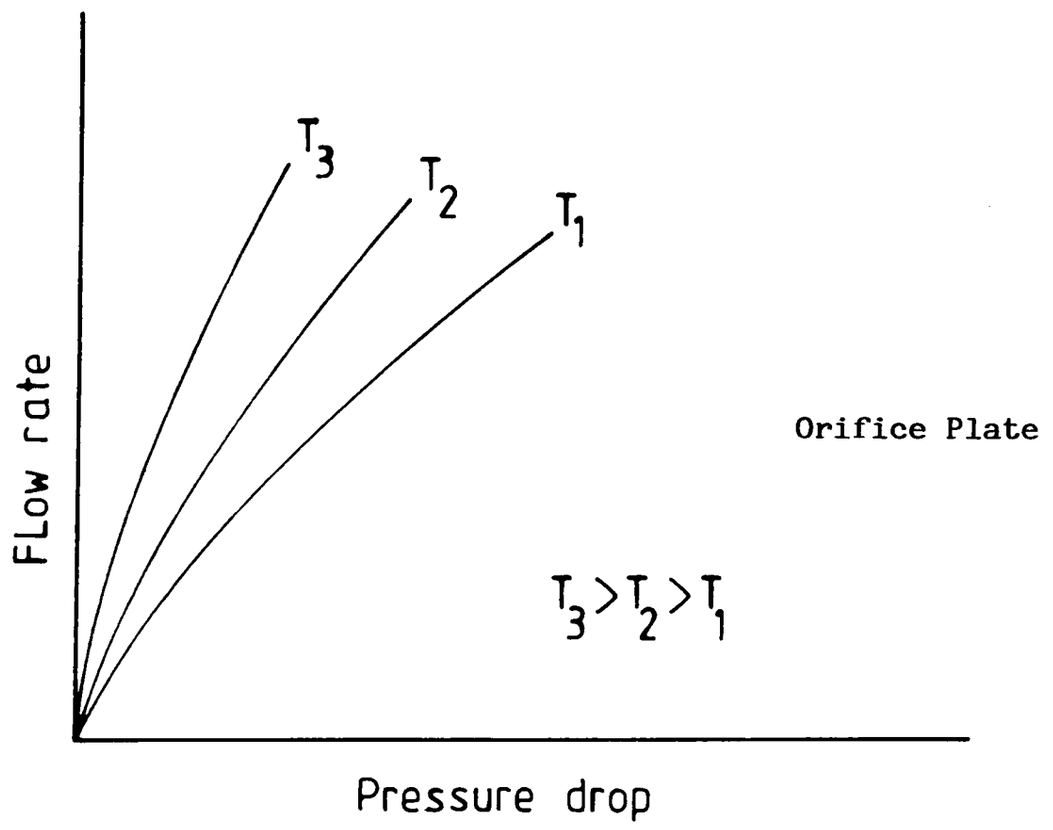

Fig. 2.16 Steady-State Characteristics of Capillary Tube and Sharp-Edged Orifice Plate

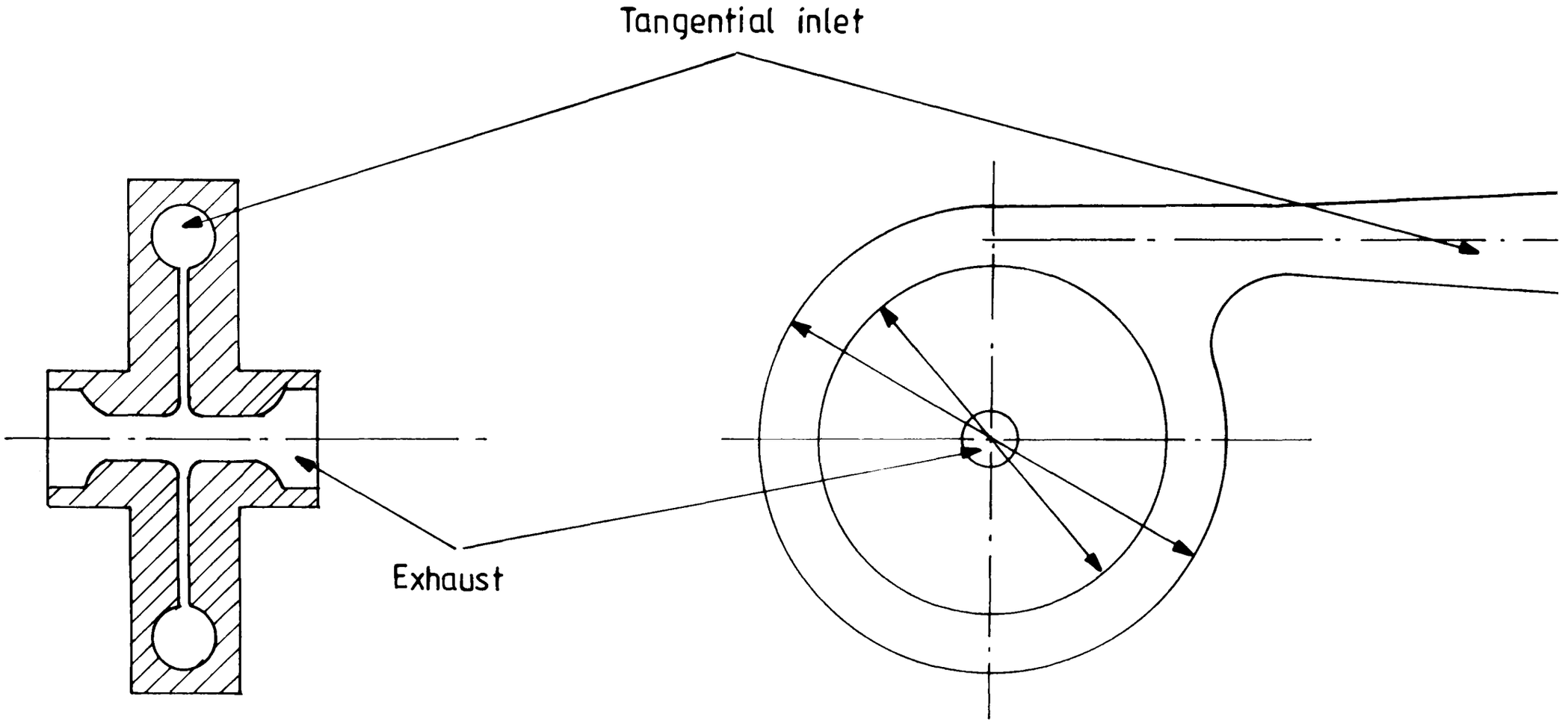

Fig. 2.17 Single Inlet Double Outlet Diode

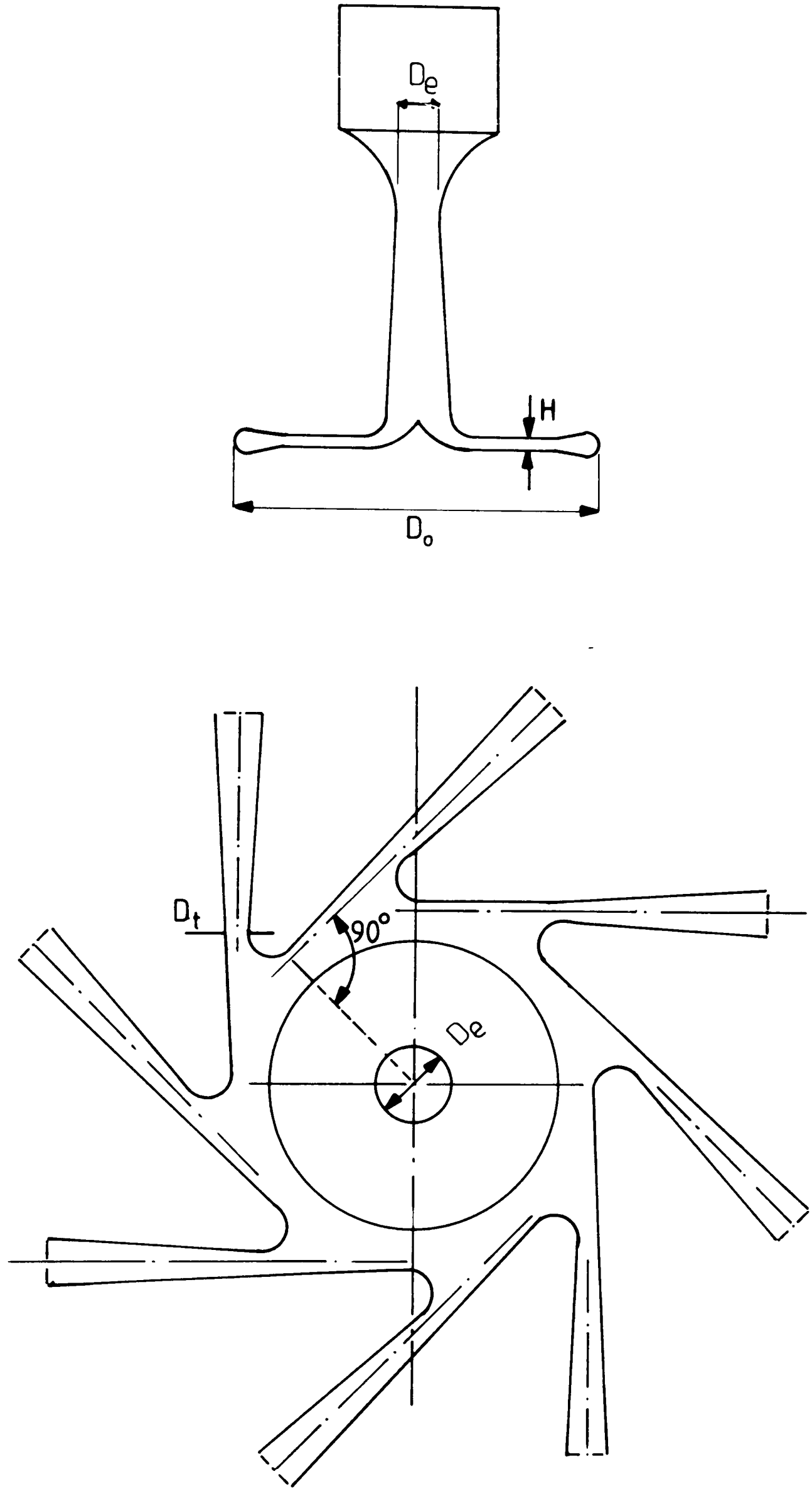

Fig. 2.18 Cathrine Wheel Vortex Diode

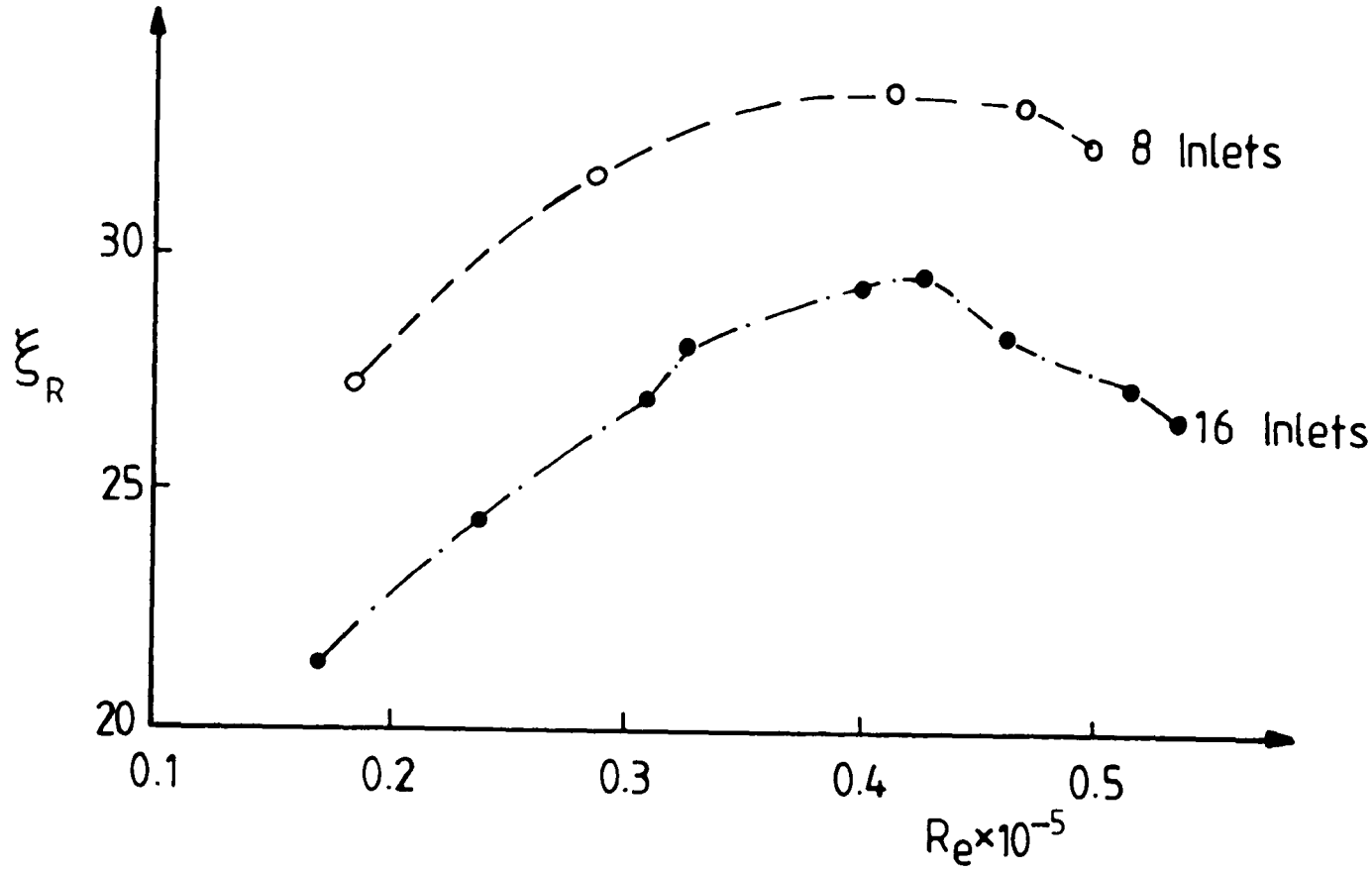

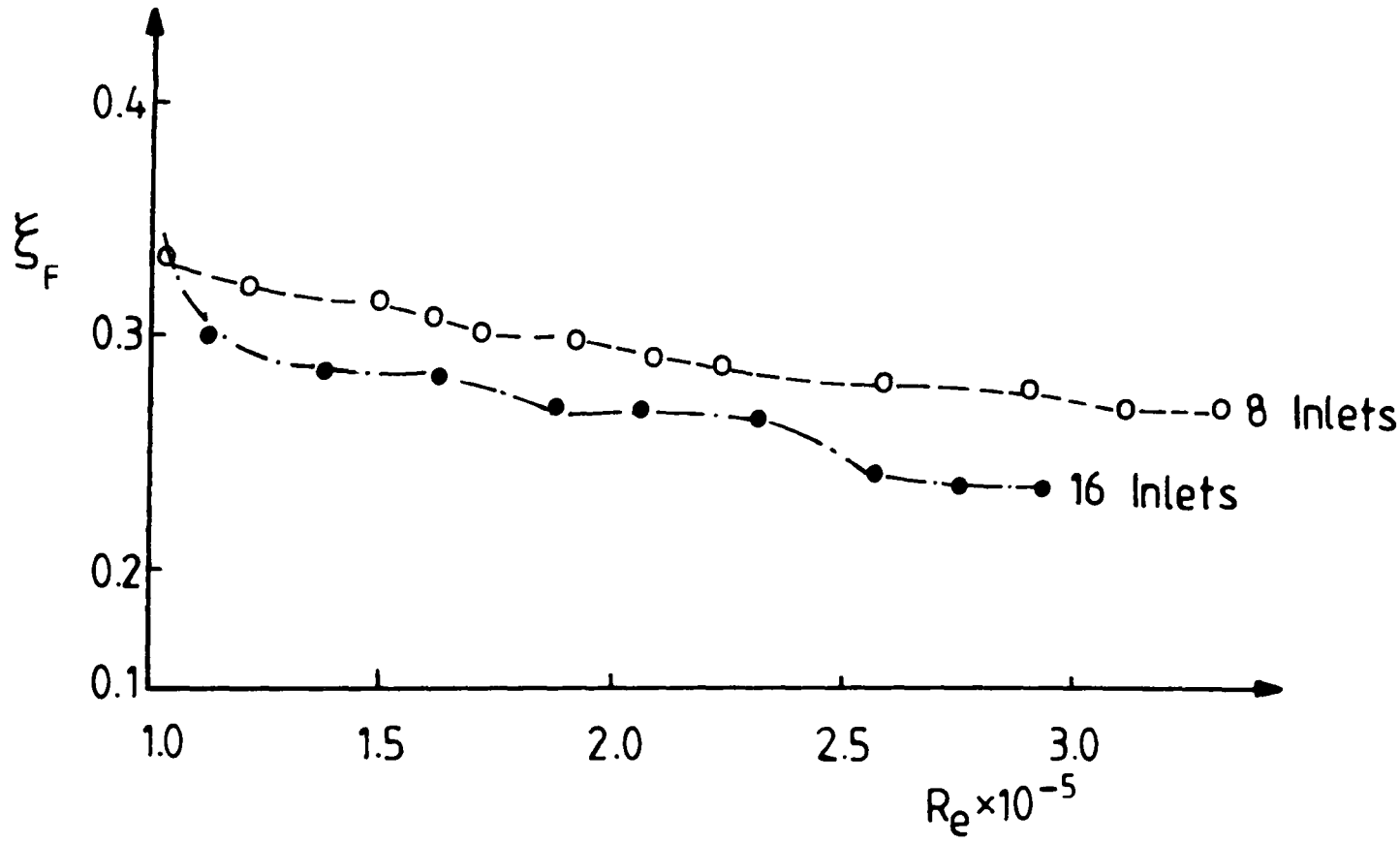

Fig. 2.19 Comparison of Reverse and Forward Flow Characteristics of Cathrine Wheel Vortex Diode with 8 and 16 Inlets

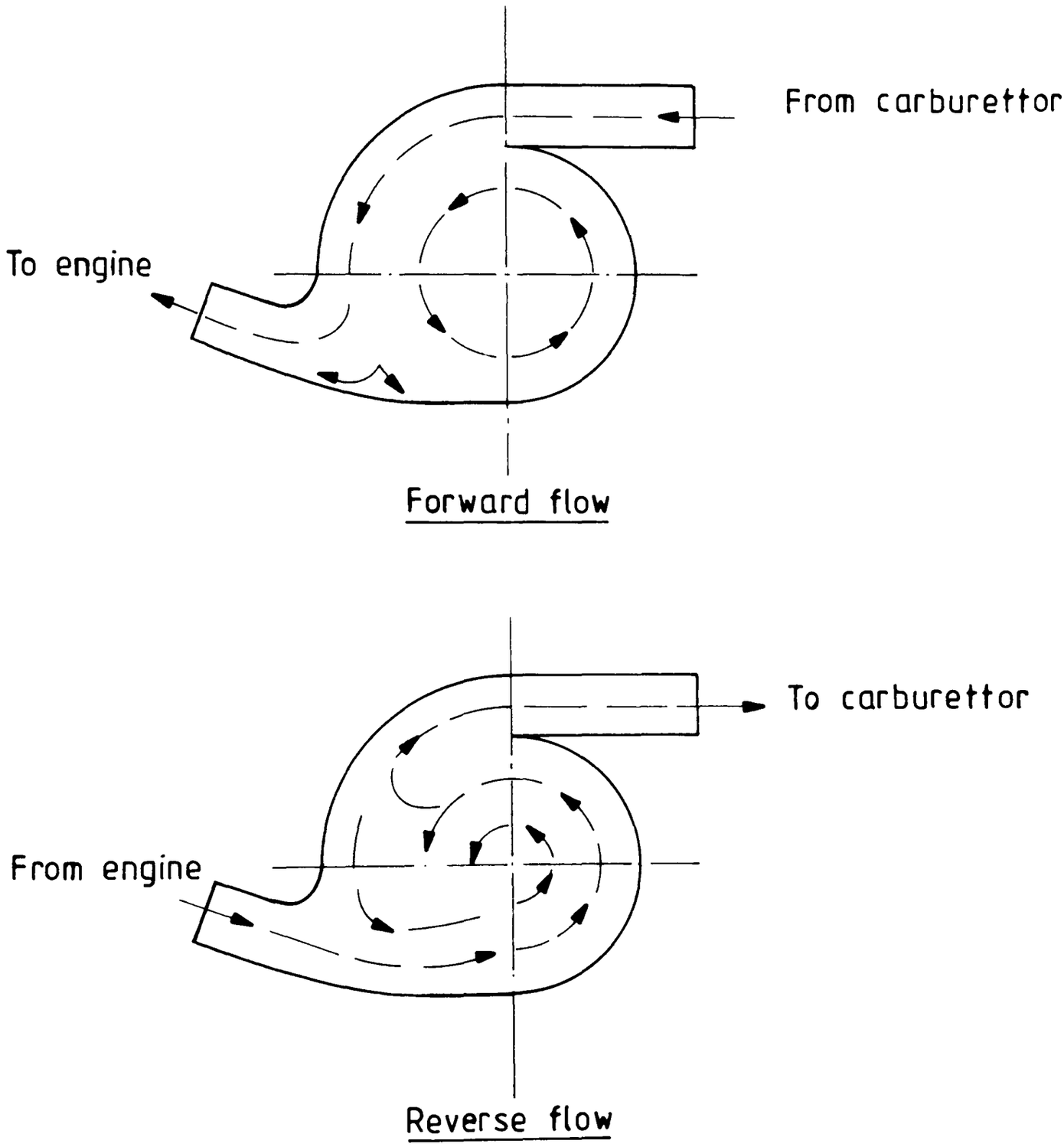

Fig. 2.20 Scroll Diode

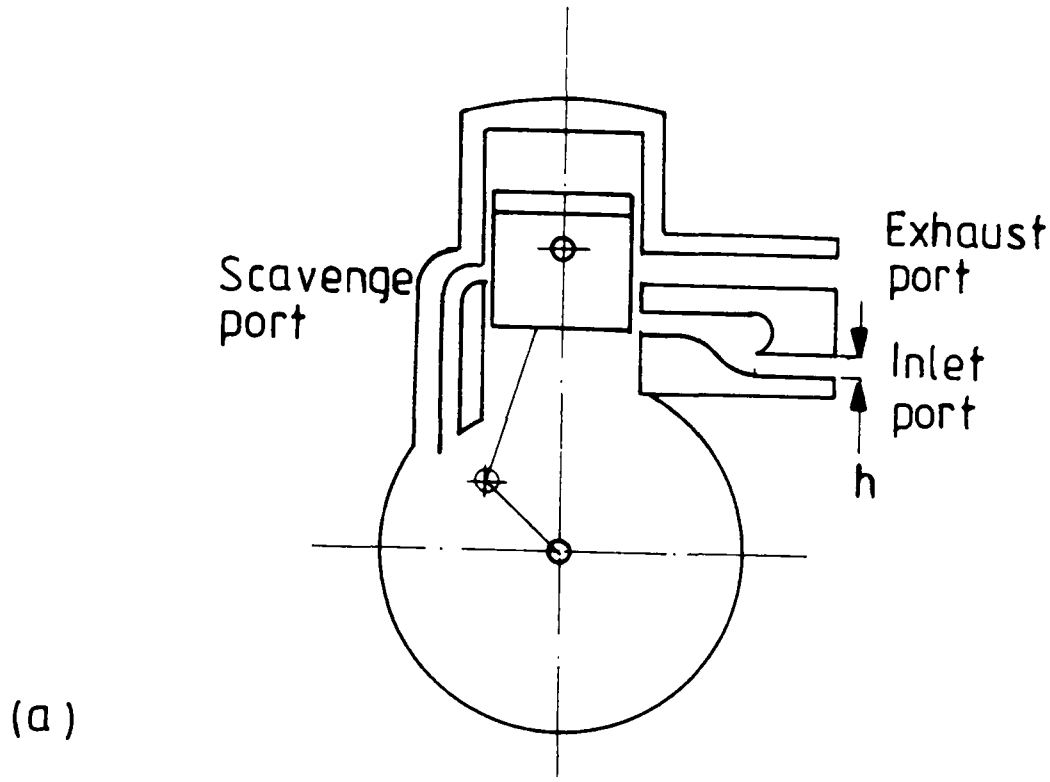

(a)

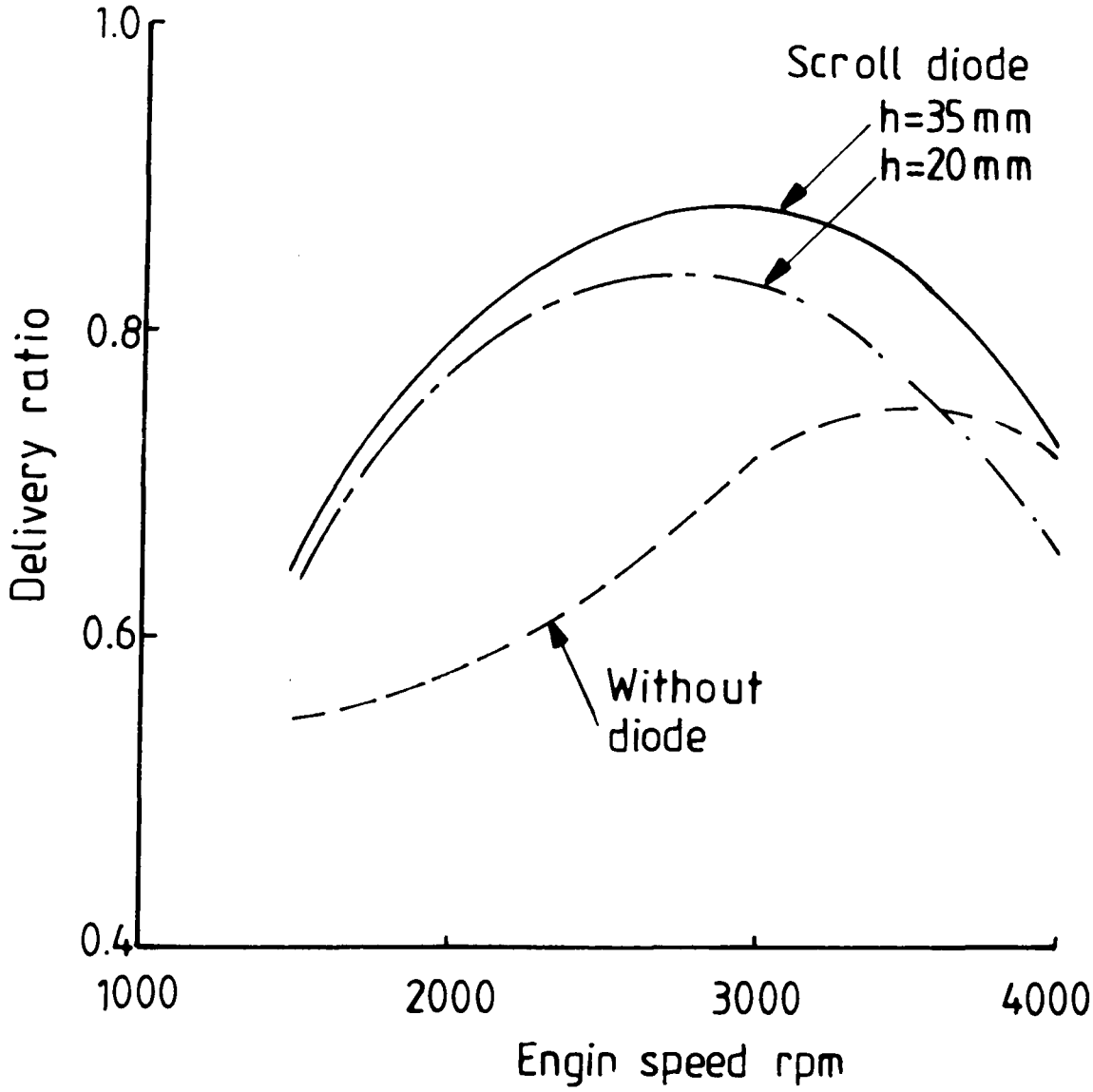

(b)

Fig. 2.21 (a) Scroll Diode Installation

(b) Effect of Scroll Diode on Delivery Ratio

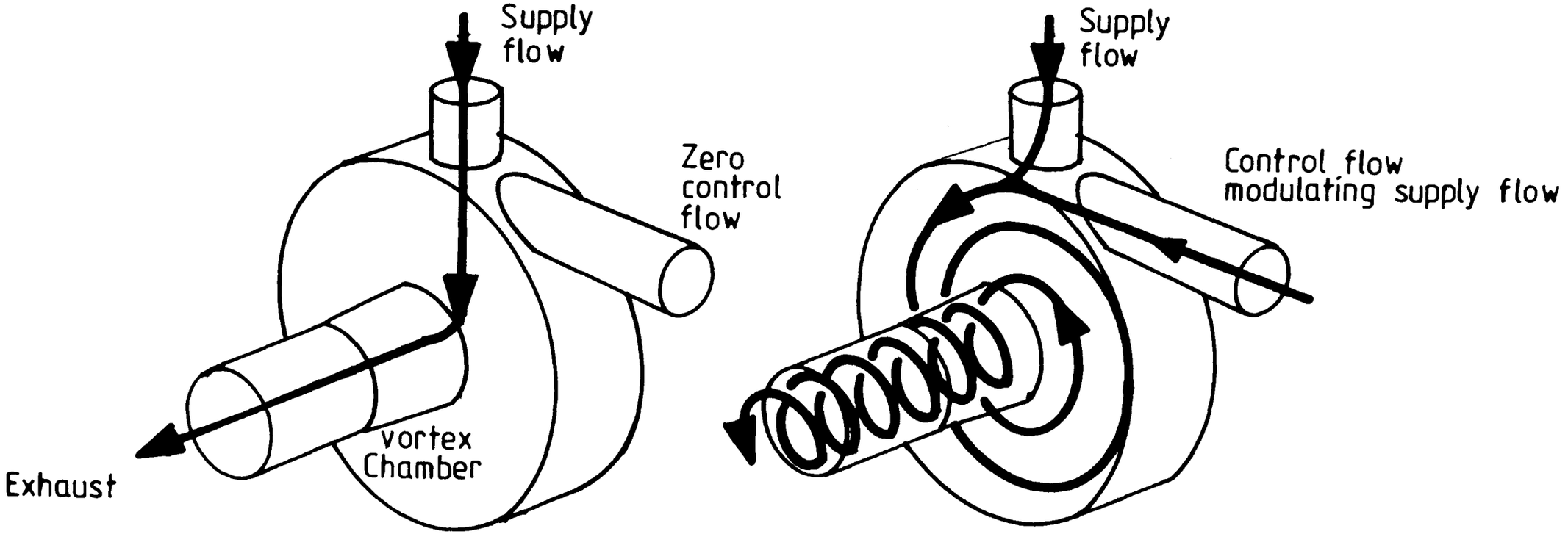

Fig. 2.22 Flow Through a Vortex Amplifier

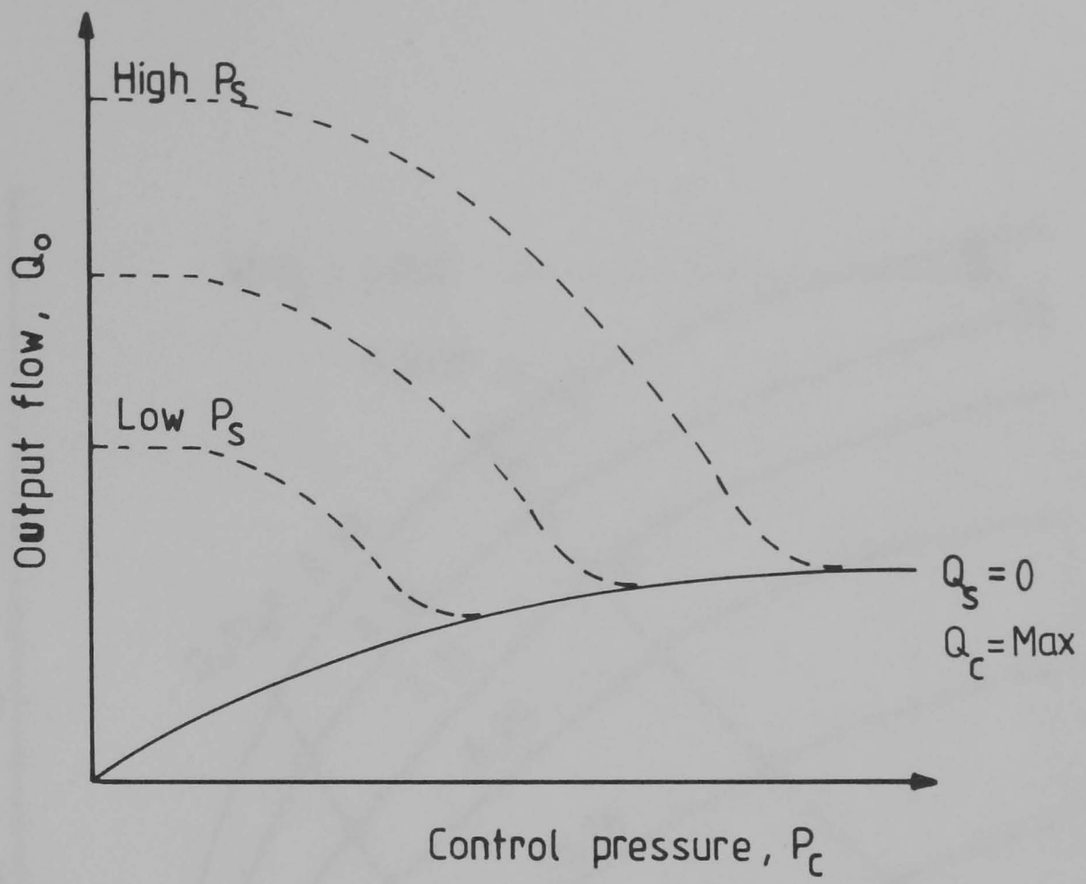

Fig. 2.23 Typical Performance of Vortex Amplifier

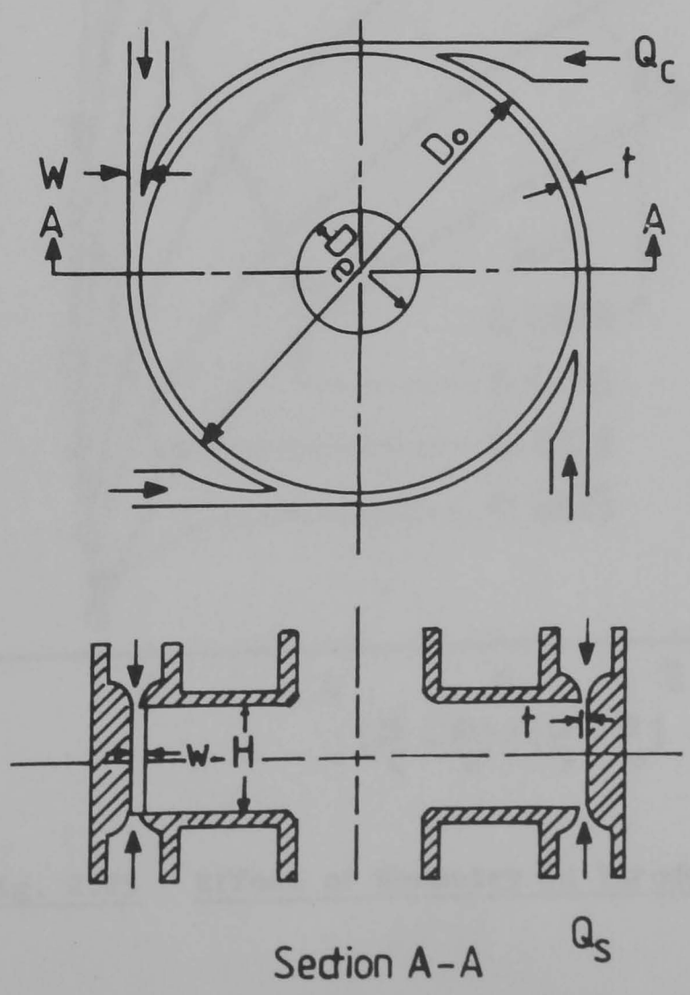

Fig. 2.24 High Turndown Ratio Vortex Amplifier

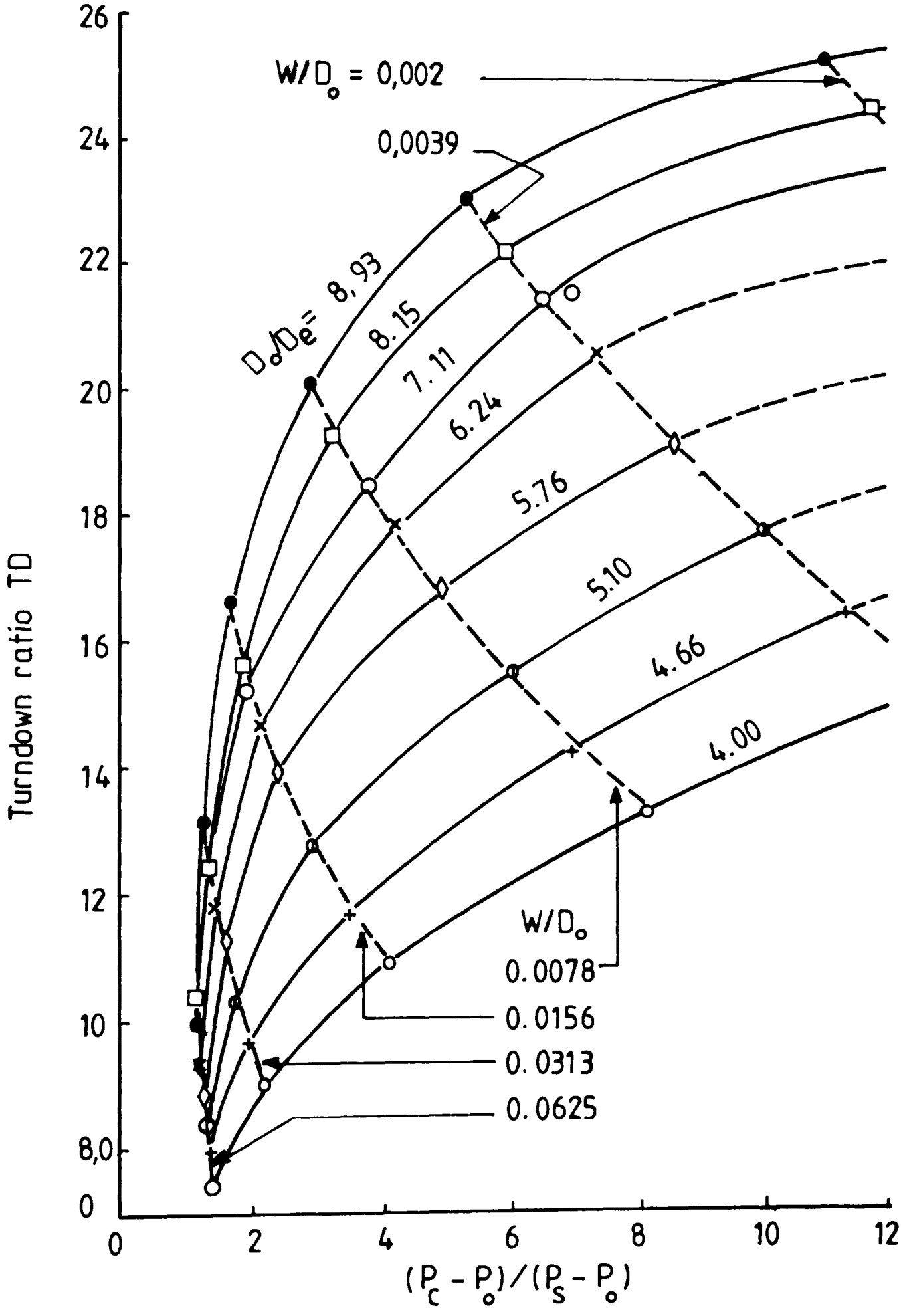

Fig. 2.25 Effect of Geometry on Turndown Ratio

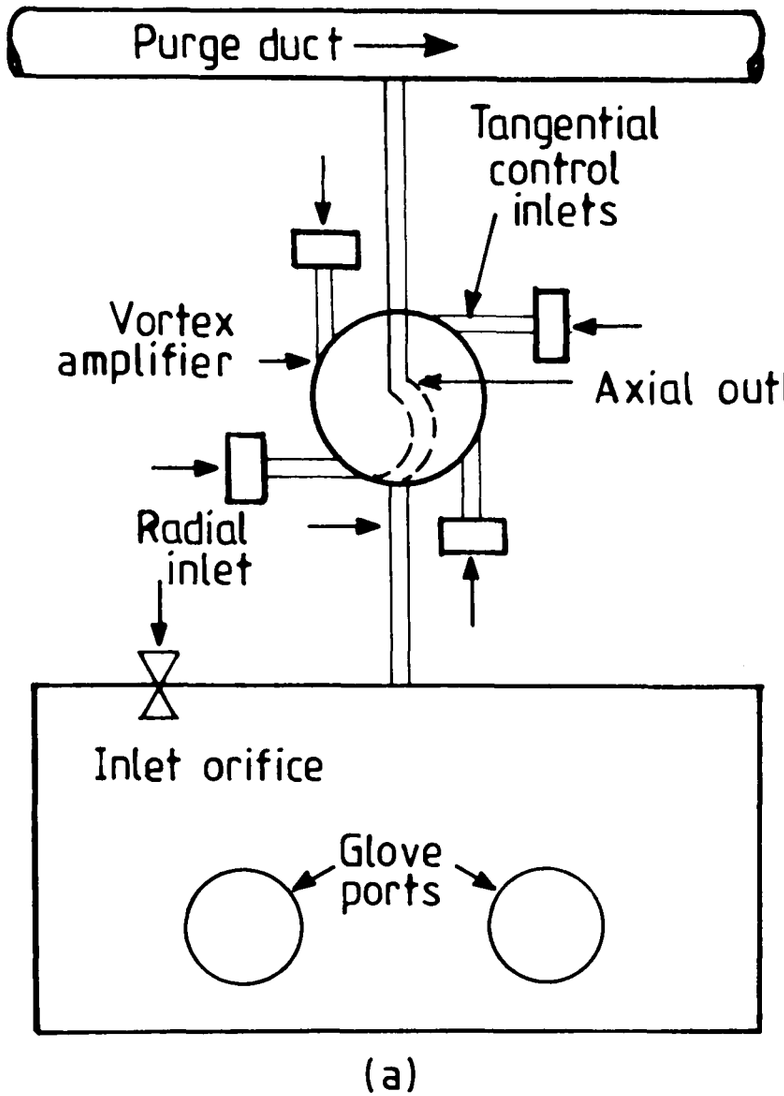

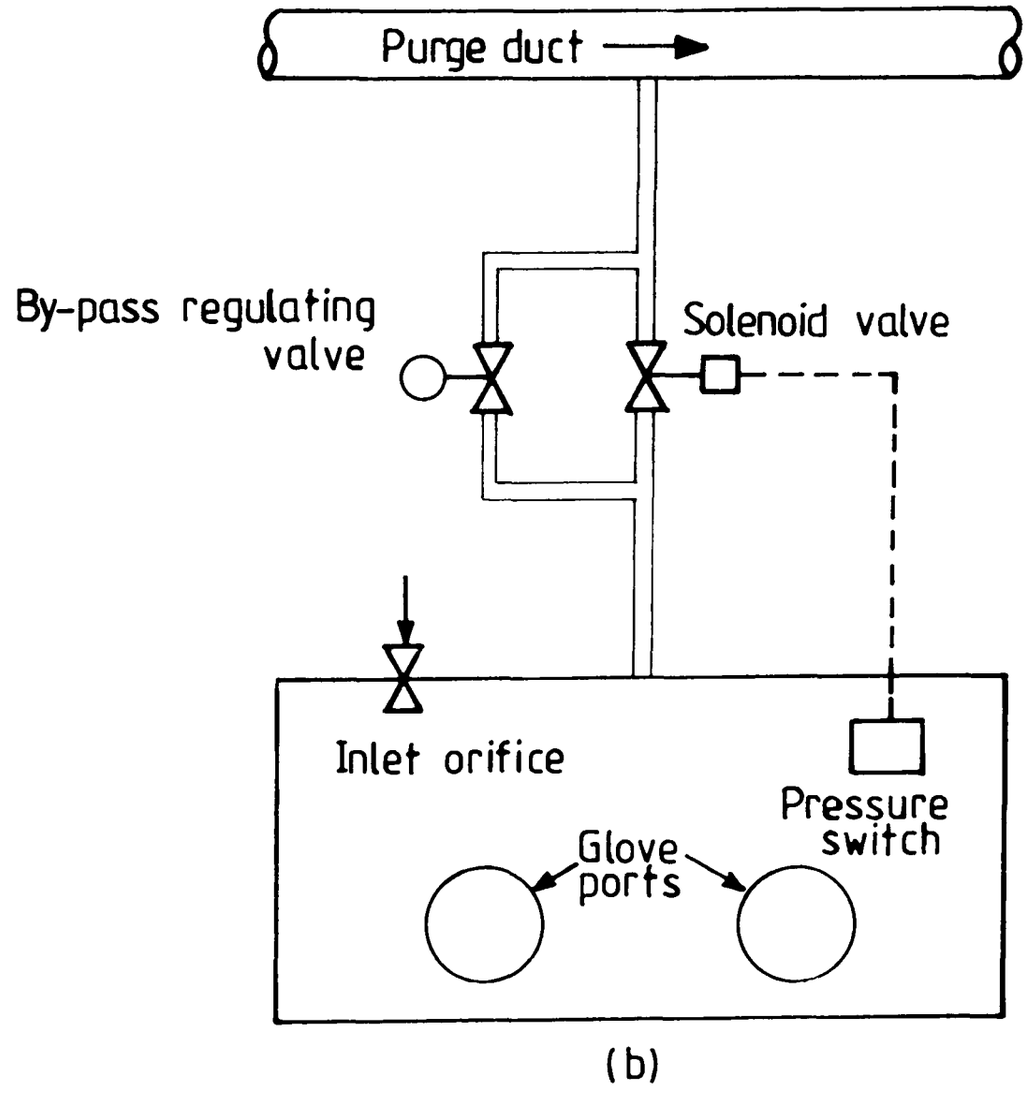

Fig. 2.26 (a) Fluidic Glove-box Regulator

(b) Conventional Glove-box Regulator

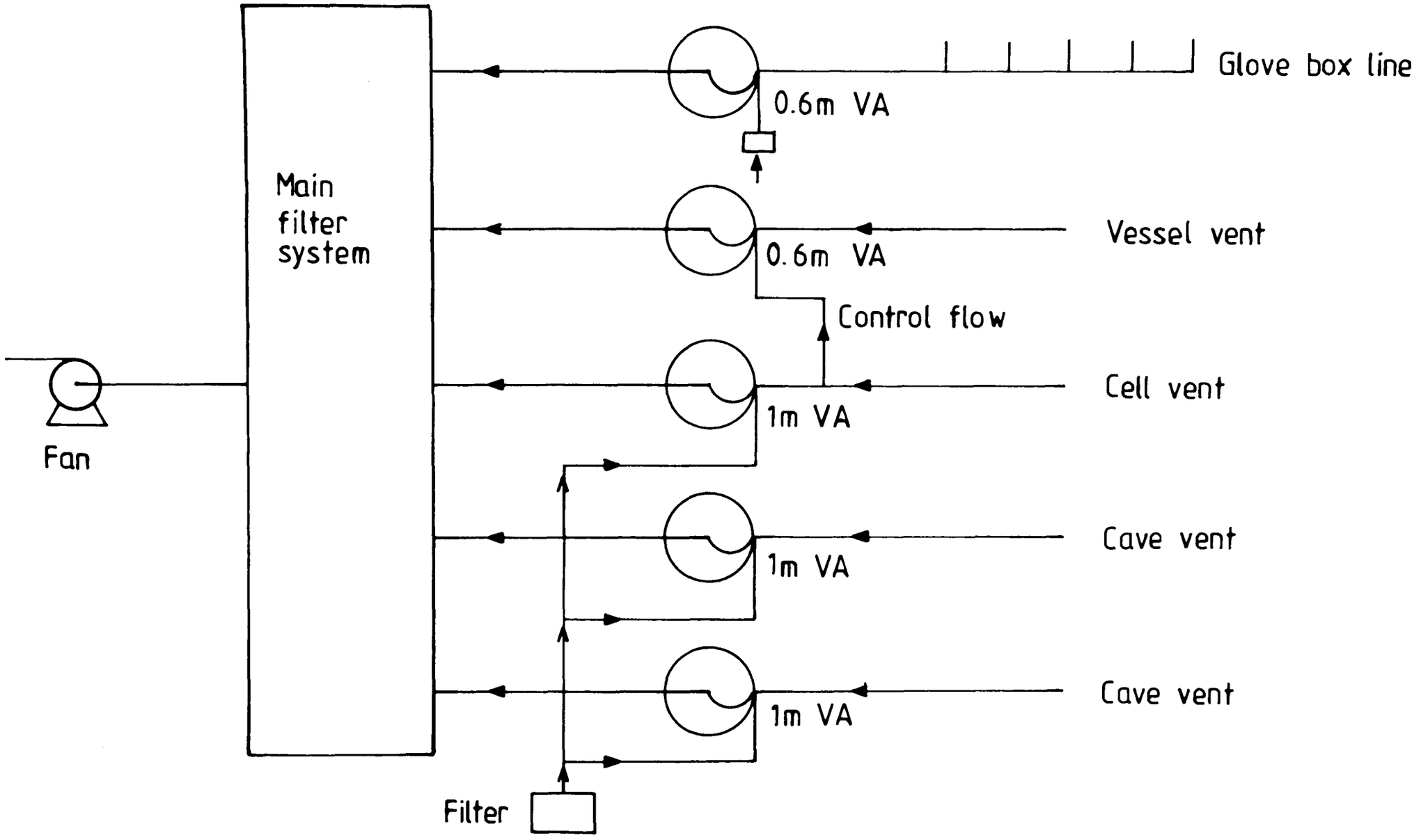

Fig. 2.27 Reprocessing Plant Ventilation System

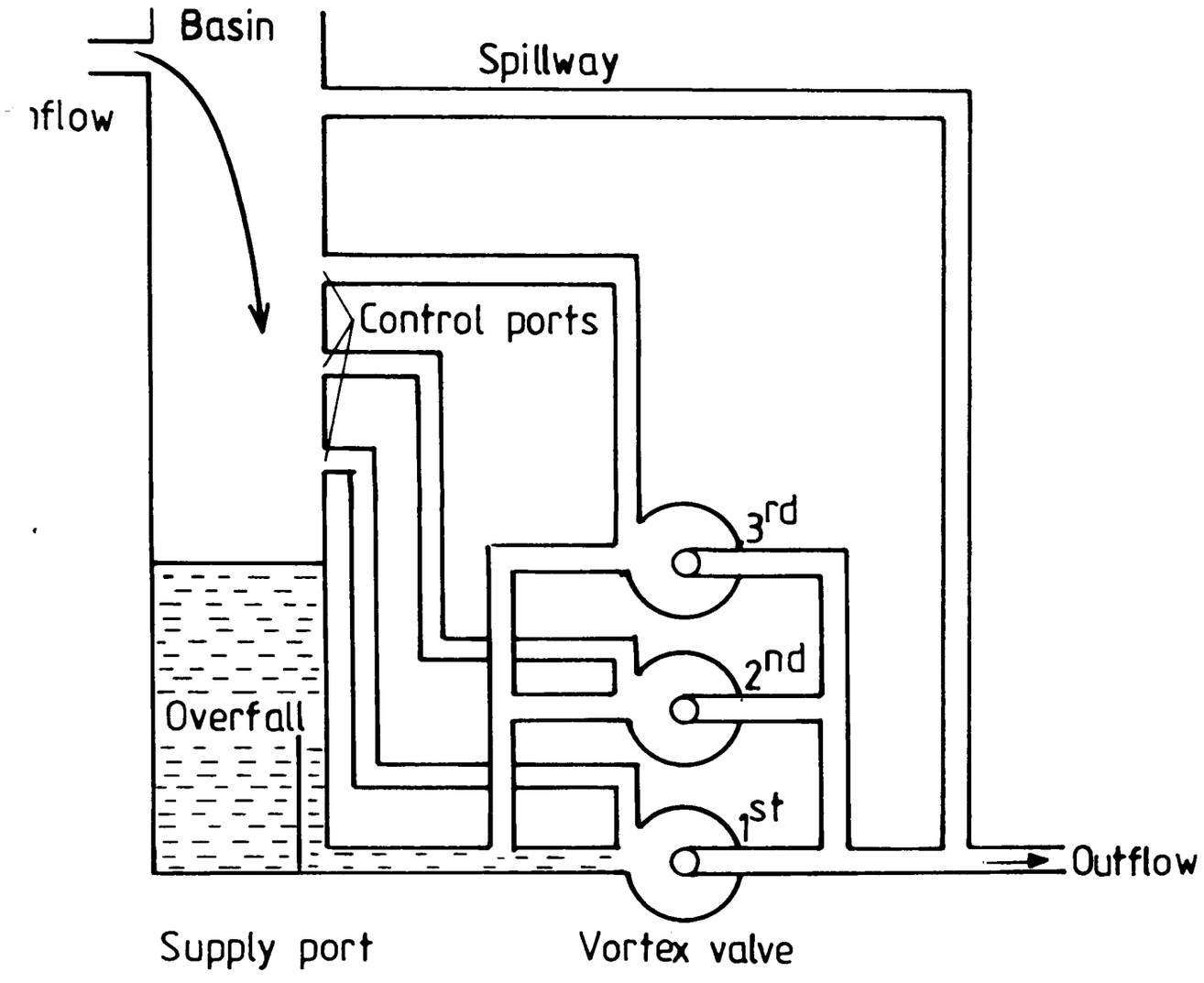

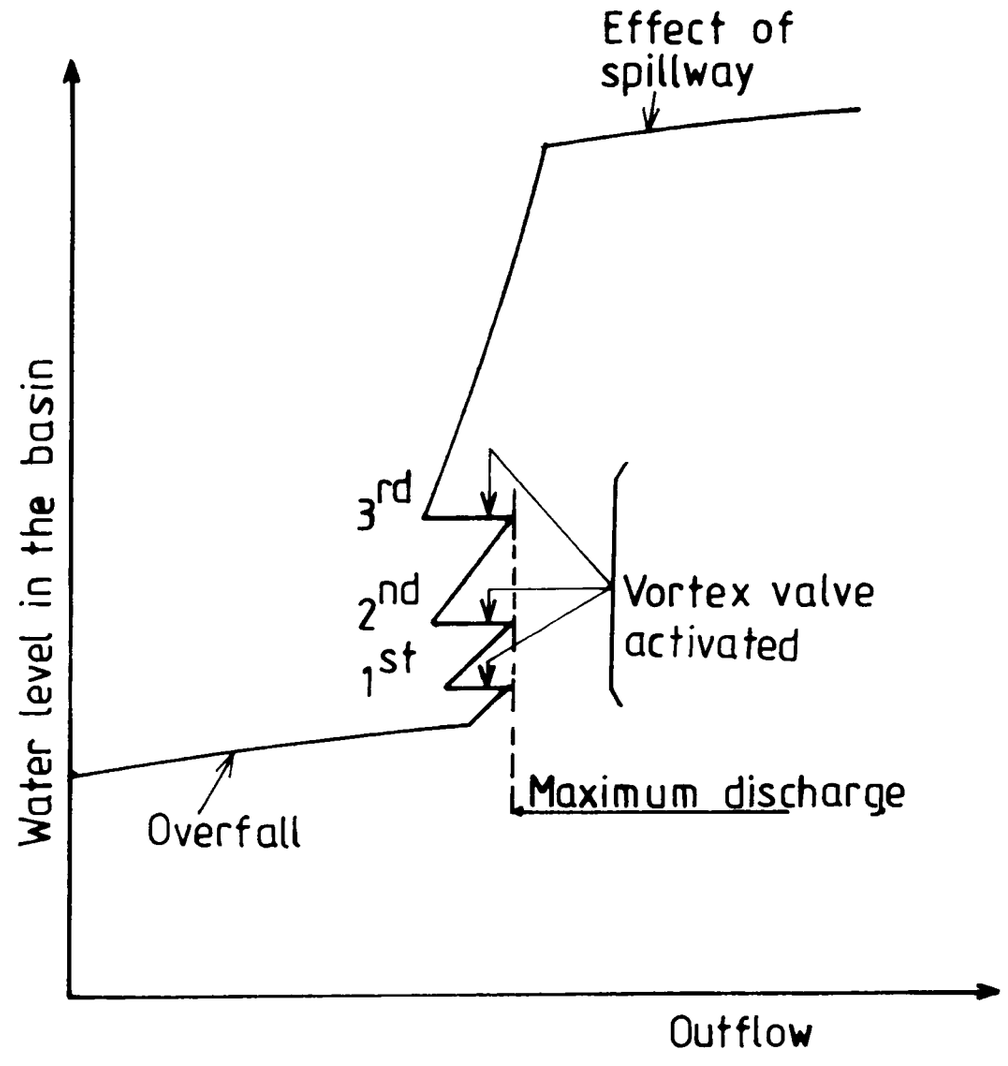

Fig. 2.28 Flood Retention Basin Drainage Control

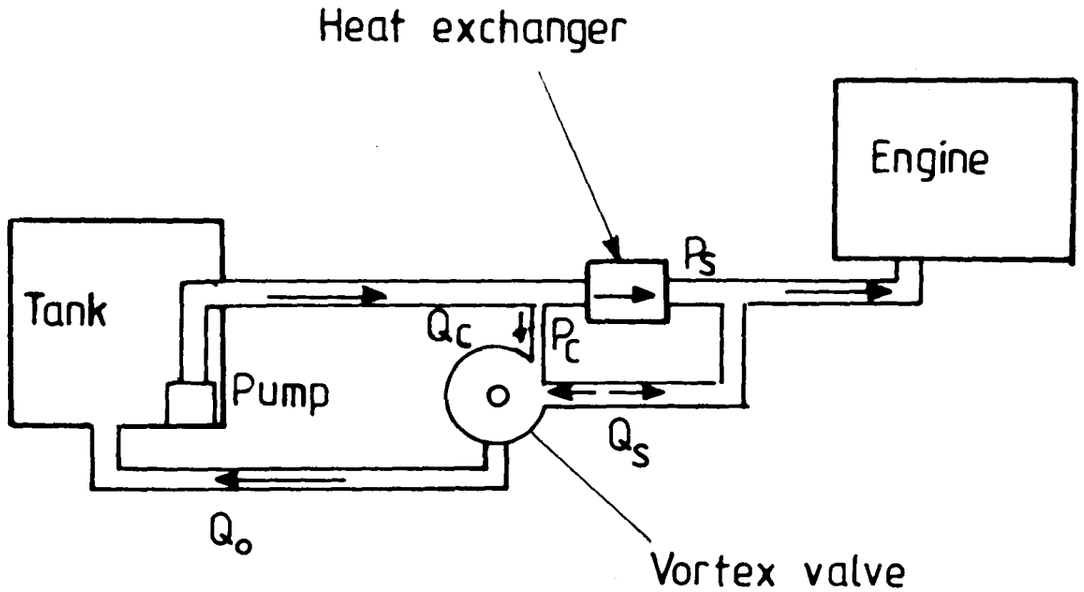

Fig. 2.29 Aircraft Engine Fuel System

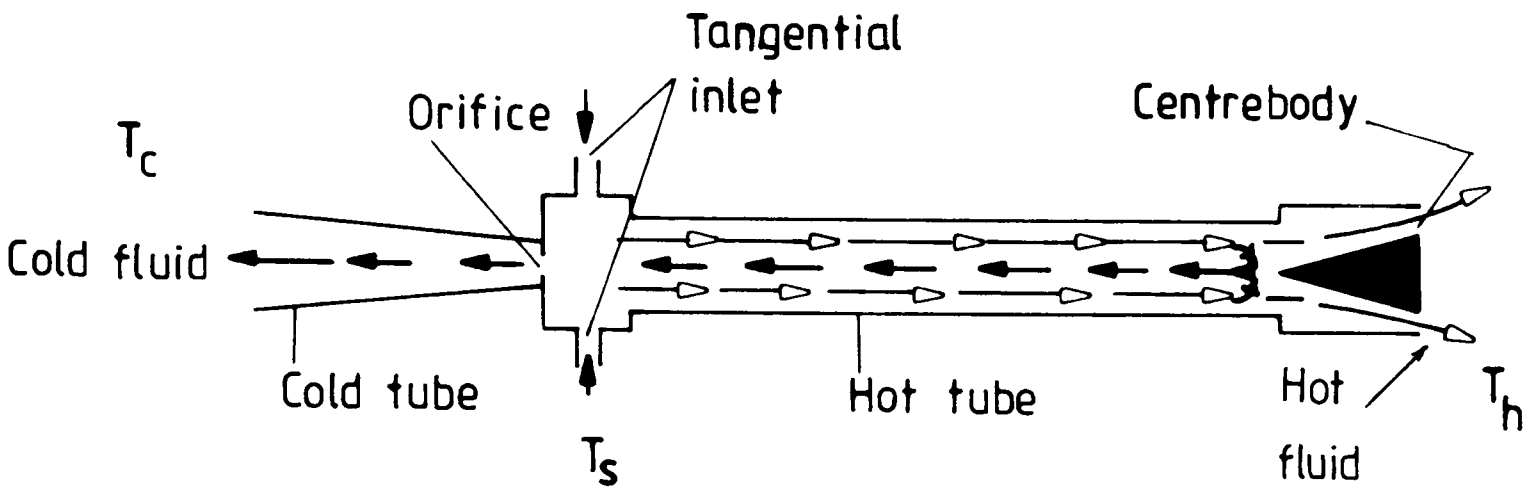

Fig. 2.30 Schematic of the Ranque-Hilsch Vortex Tube

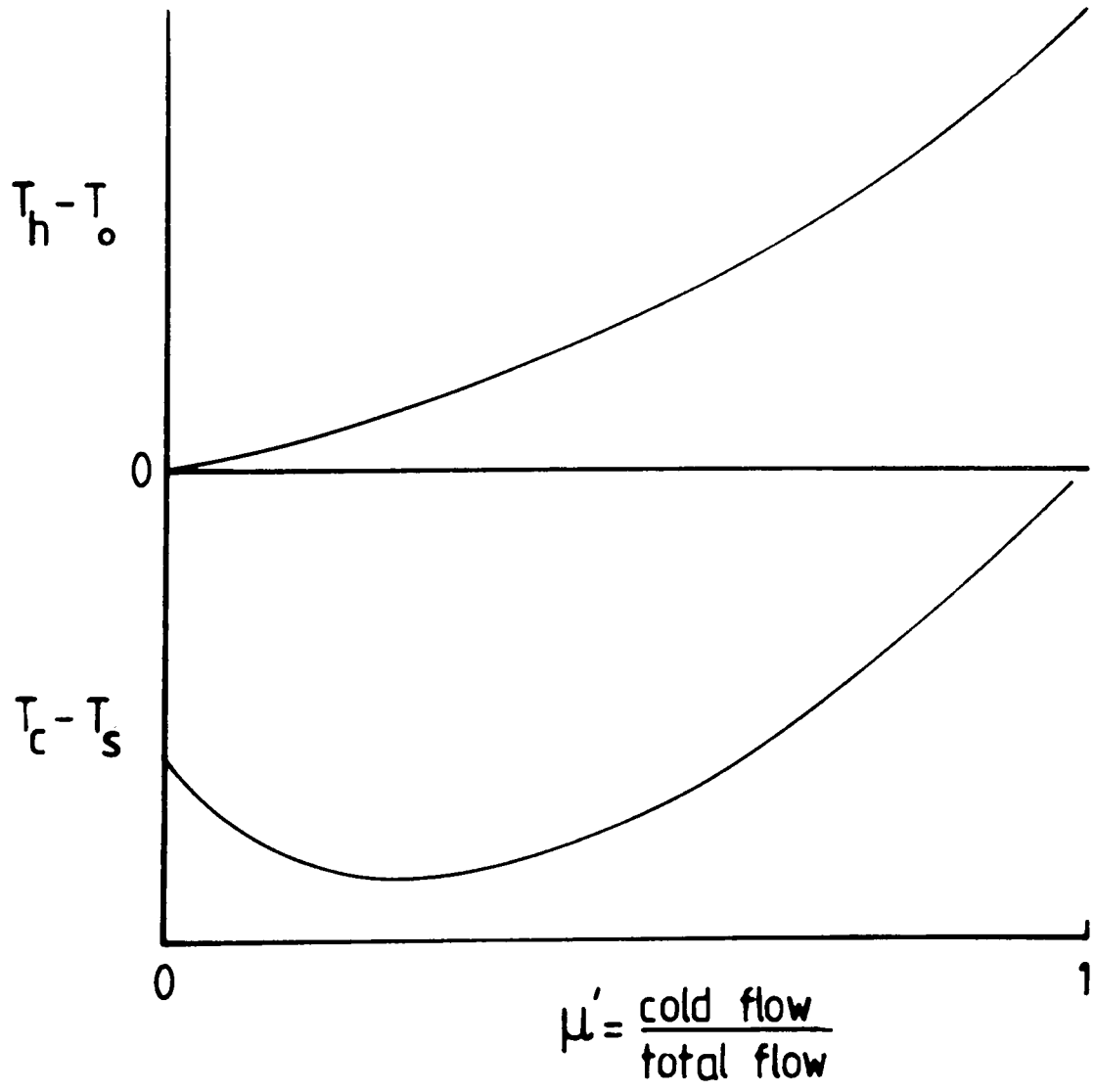

Fig. 2.31 Typical Performance Characteristics of Vortex Tubes

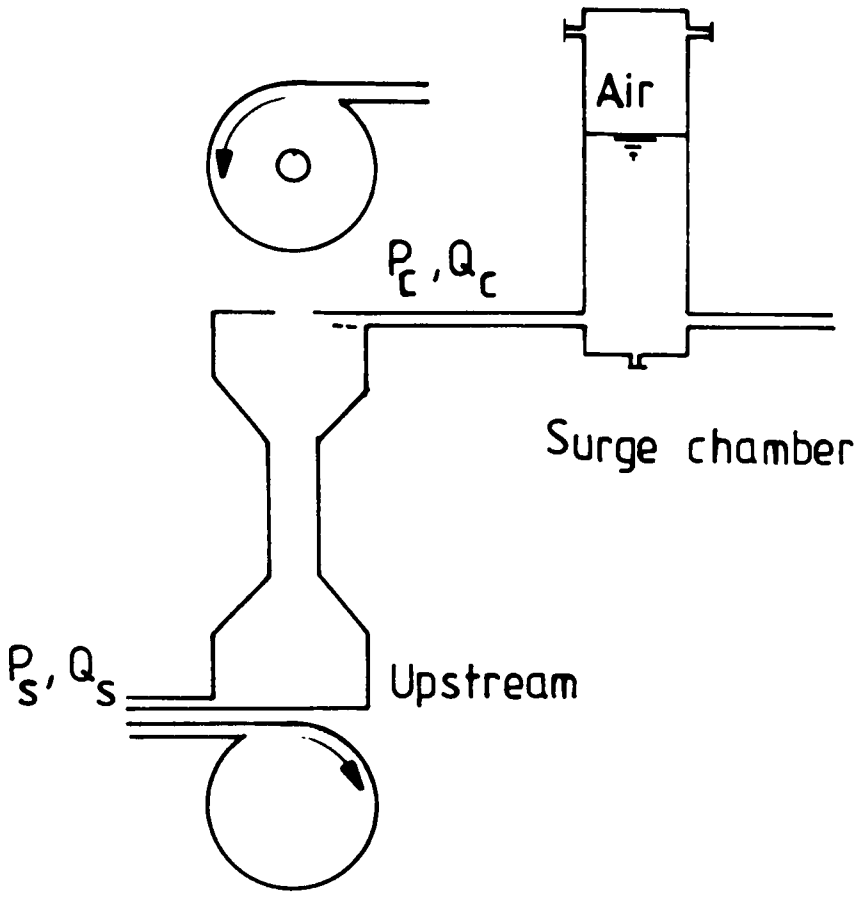

Fig. 2.32 Confined Vortex Oscillator

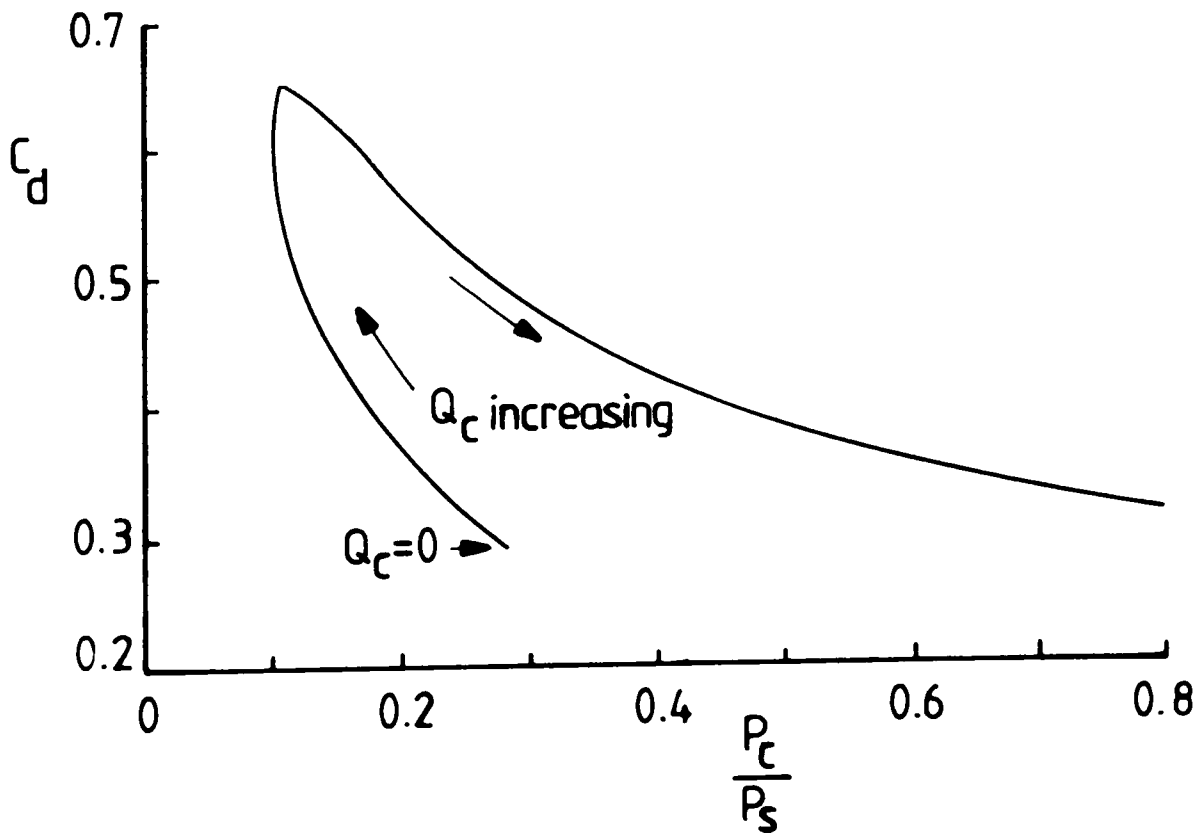

Fig. 2.33 Variation of Discharge Coefficient with Pressure Ratio

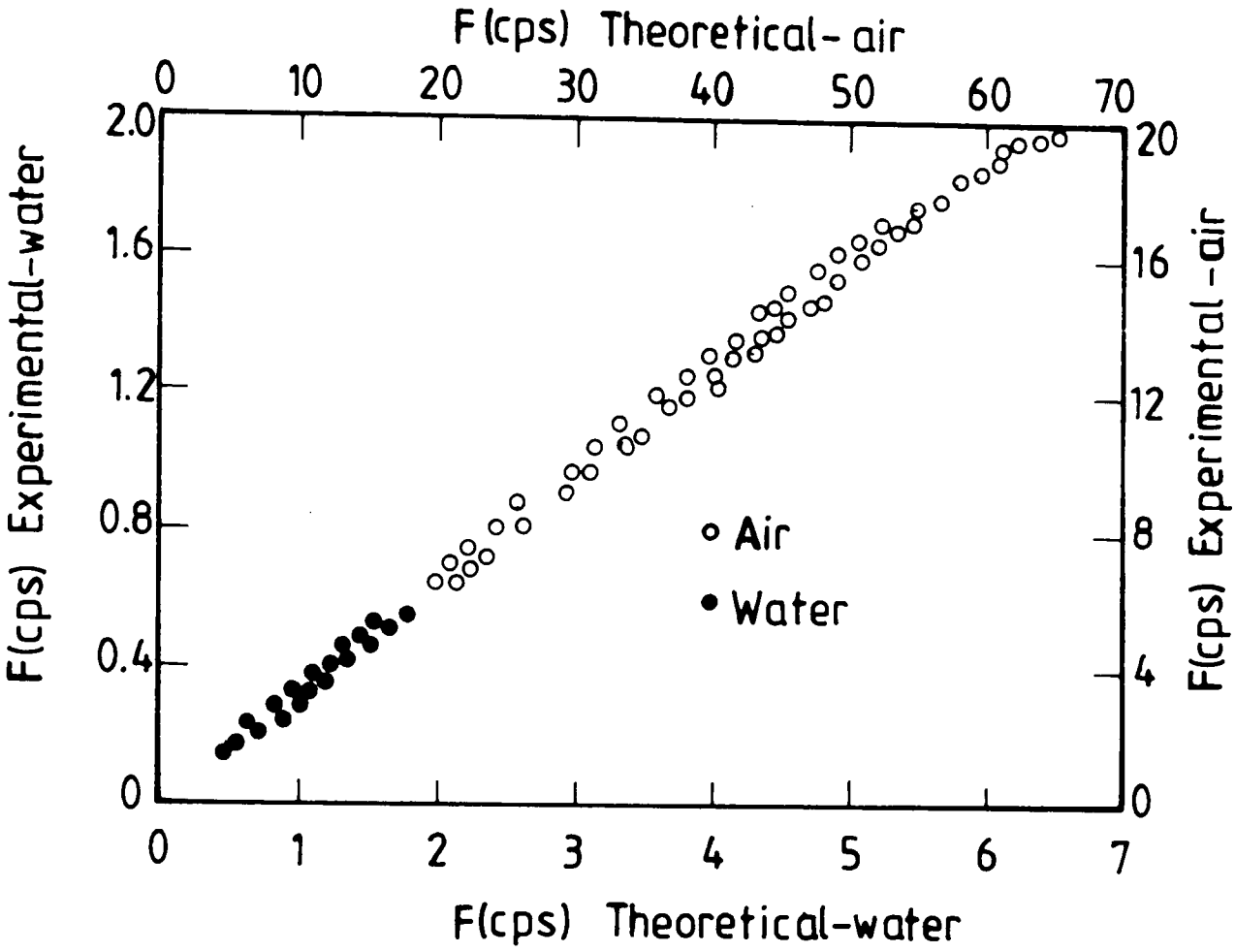

Fig. 2.34 Frequency Characteristics of the Vortex Oscillator

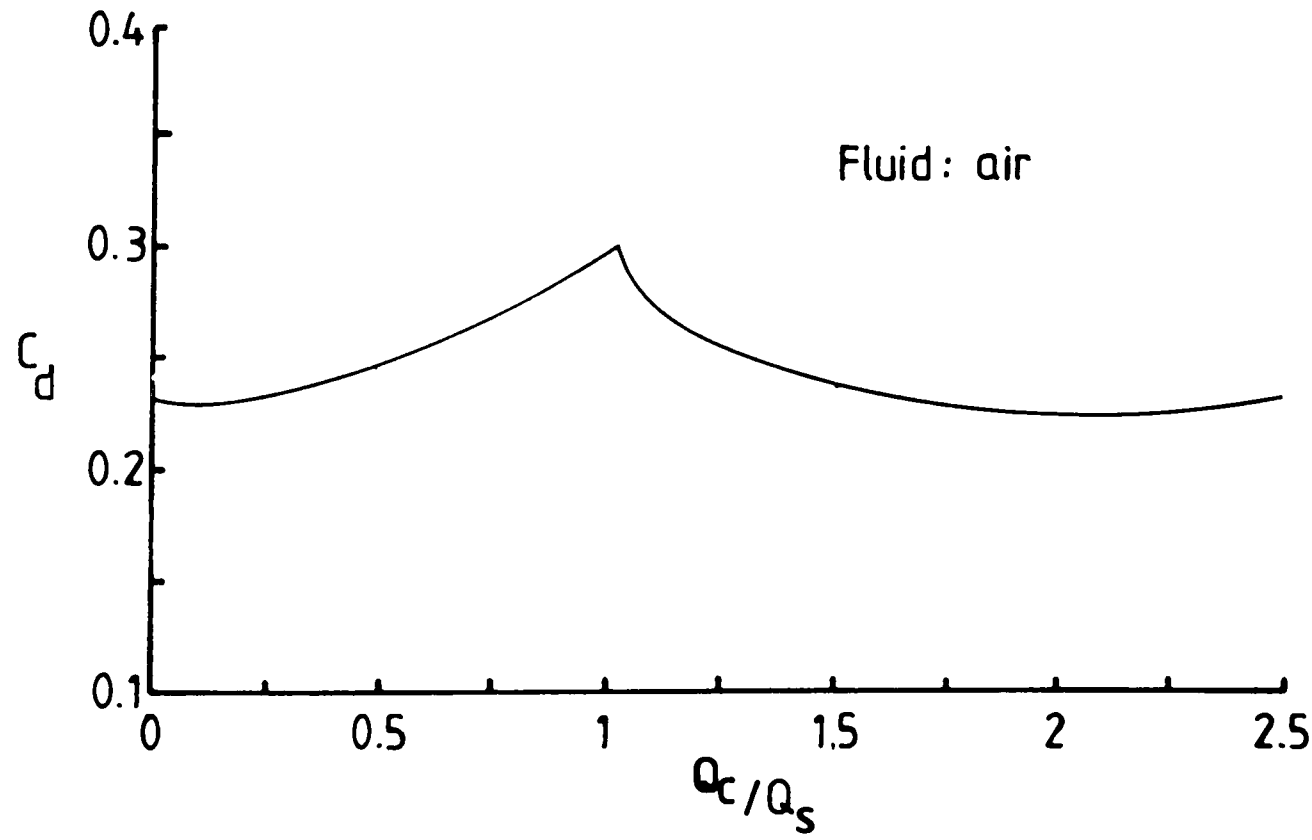

Fig. 2.35 Variation of Discharge Coefficient with Q_c/Q_s

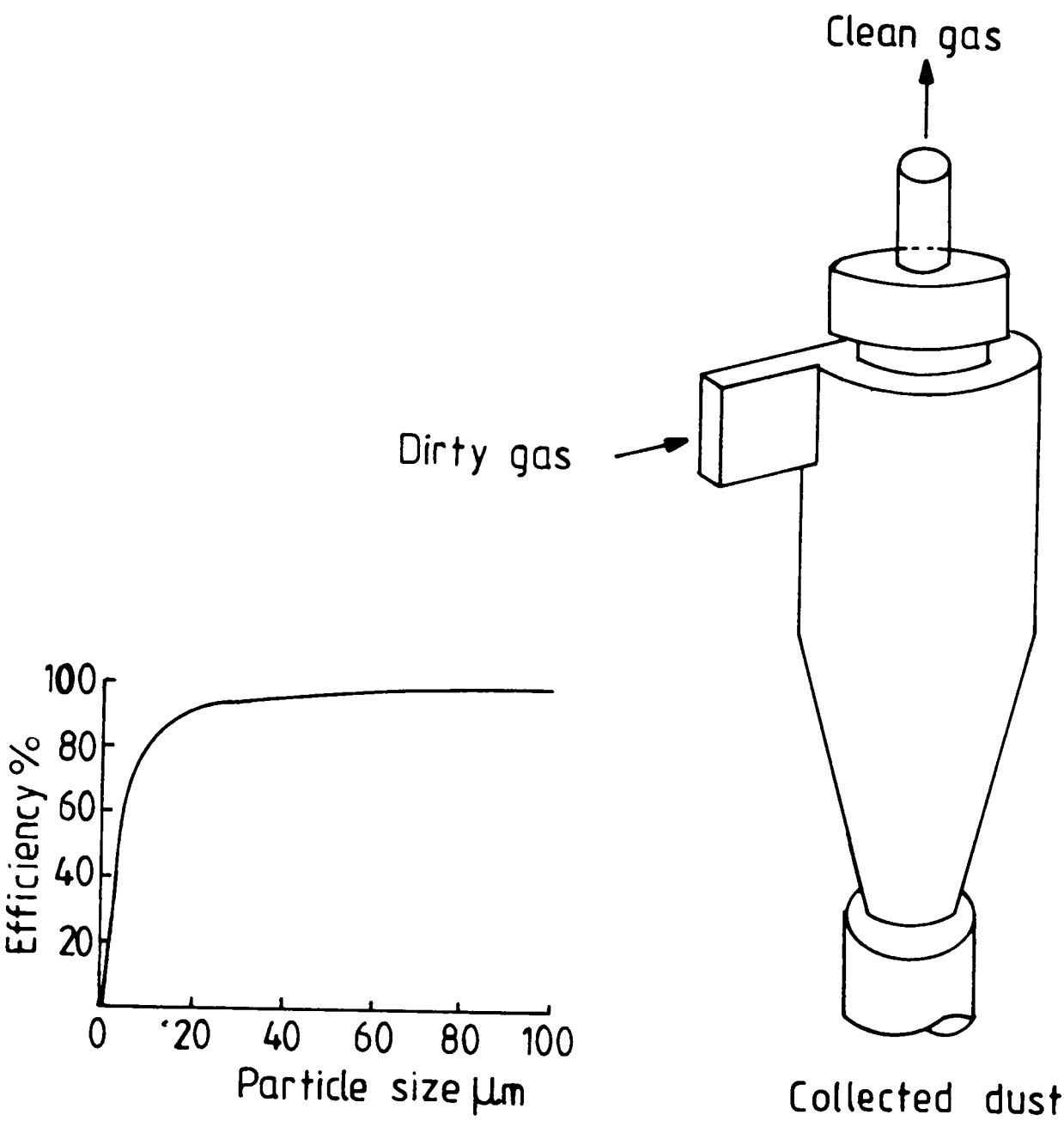

(a)

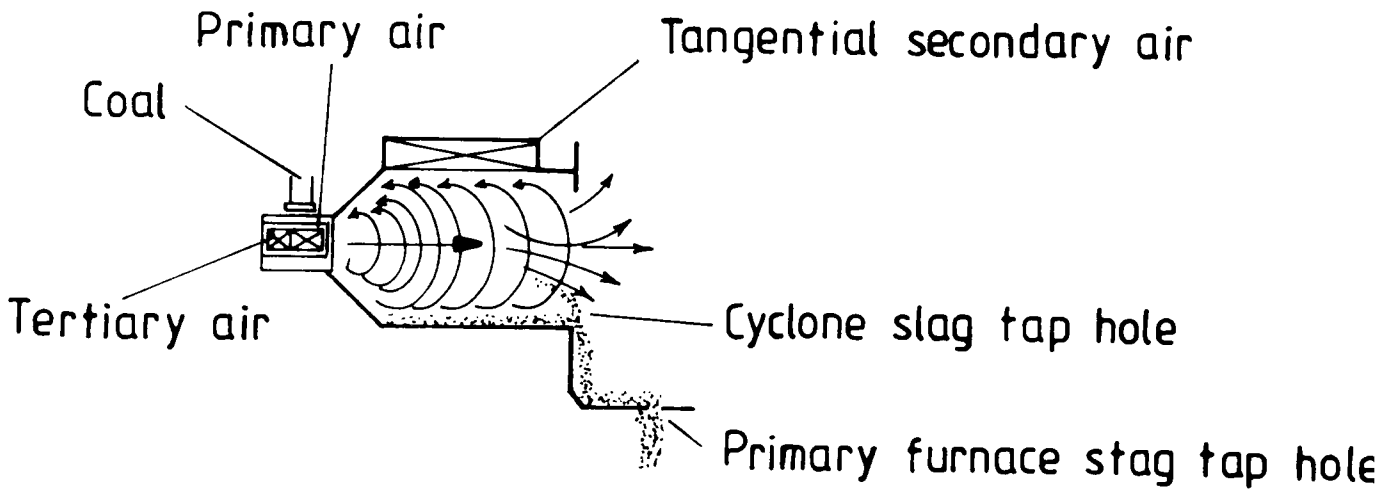

(b)

Fig. 2.36 Schematic Diagram of (a) Cyclone Separator (b) Cyclone Furnace

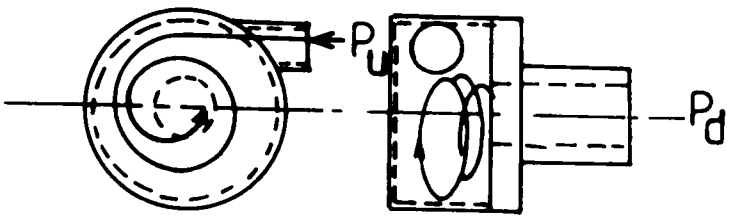

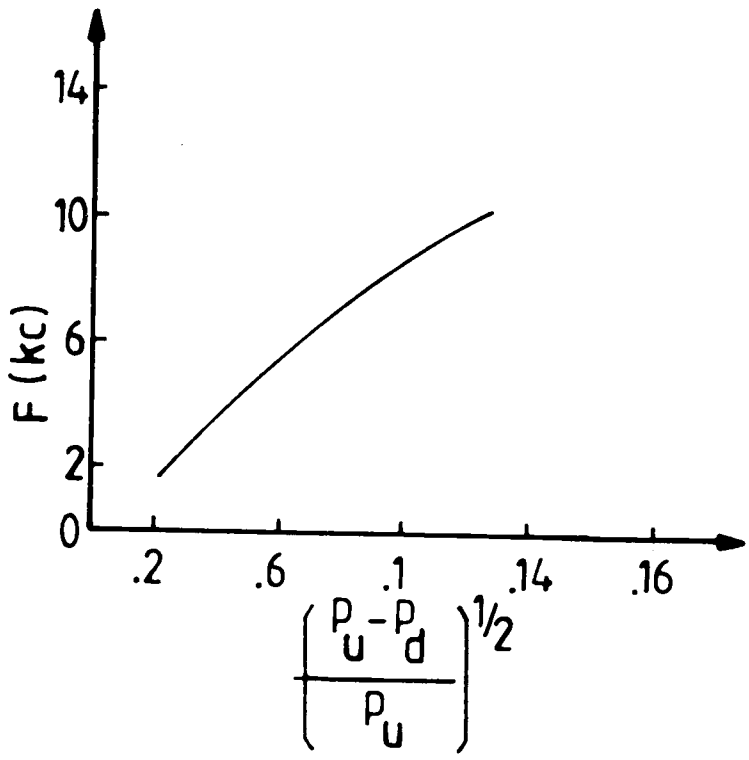

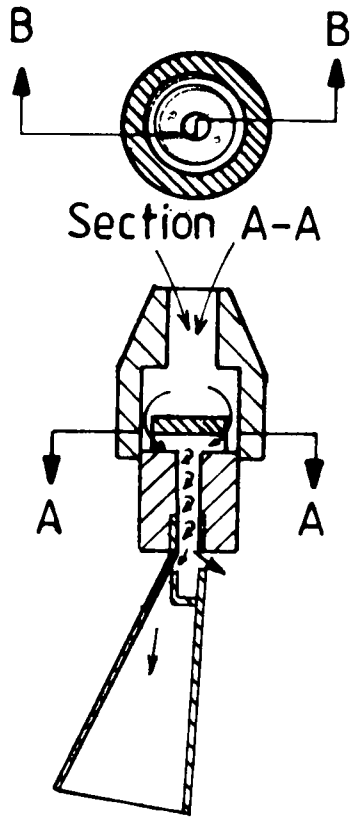

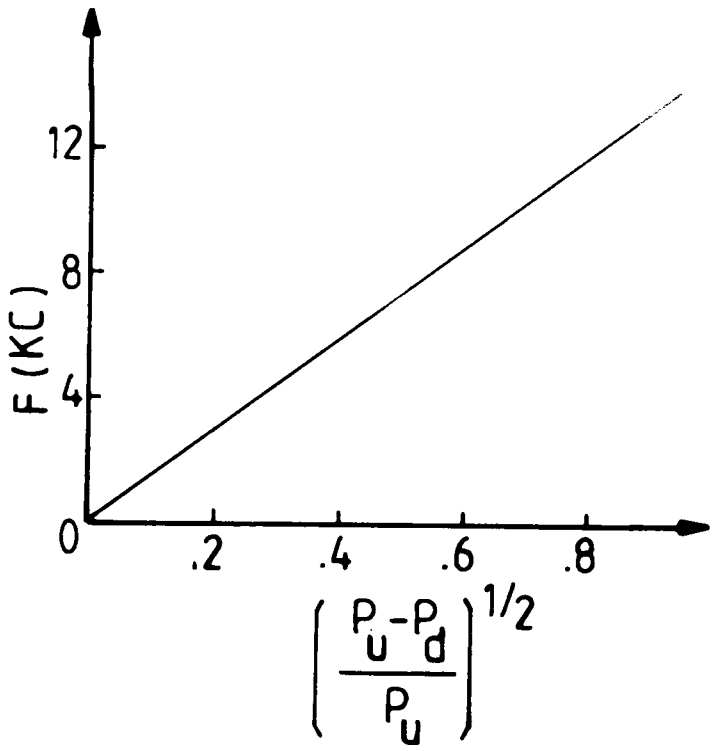

Fig. 2.37 Frequency as a Function of Inlet and Outlet Air for Two Different Designs of Vortex Whistle

CHAPTER 3

STRUCTURE OF VORTEX FLOW

Confined vortex flow is a type of fluid motion which is classified under the specialist topic of rotating fluid mechanics. The purpose of this Chapter is to describe the swirling fluid motion and also, by review of the published material relevant to the confined vortex chamber, to identify the mathematical relations, the problems and instabilities associated with this type of complex flow, and thus to set the scene for the experimental work carried out and reported in Chapters 4, 5 and 6.

3.1 Types of Vortex

3.1.1 Forced vortex

A simple example of rotational action in a fluid is the solid body type of angular motion about an axis. In this case the fluid behaves like a solid body rotating steadily around an axis through its centre. The velocity of the fluid increases linearly with the distance from the centre of rotation. The angular velocity is constant, this only occurring if the fluid motion is steady. The stream lines are concentric circles and the tangential velocity along a stream line can be written as:

$$v_\theta = \omega r \qquad (3.1)$$

This is derived from the general vortex flow equation which is in the form of

$$v_\theta r^n = \text{const} = k \tag{3.2}$$

where n is the vortex exponent and in this case is equal to -1 and k $= \omega$.

The circulation can be evaluated along any circular streamline of radius r,

$$\Gamma = \int_o^{2\Pi} v_\theta r \, d\theta = 2\Pi\omega r^2 \tag{3.3}$$

where Γ is the circulation of any closed circuit enclosing the origin.

(For definition of mathematical symbols, see Appendix A.)

The vorticity vector is defined by:

$$\Omega = \text{curl } v_\theta \tag{3.4}$$

$$\text{curl } v_\theta = \nabla x v_\theta = \nabla x(\omega r)$$

$$= \nabla x \begin{vmatrix} i & j & k \\ \omega_1 & \omega_2 & \omega_3 \\ x & y & z \end{vmatrix}$$

$$= \nabla x \left[(\omega_2 z - \omega_3 y)i + (\omega_3 x - \omega_1 z)j + (\omega_1 y - \omega_2 x)k\right]$$

$$= \begin{vmatrix} i & j & k \\ \frac{\partial}{\partial x} & \frac{\partial}{\partial y} & \frac{\partial}{\partial z} \\ (\omega_2 z - \omega_3 y) & (\omega_3 x - \omega_1 z) & (\omega_1 y - \omega_2 x) \end{vmatrix}$$

$$= 2(\omega_1 i + \omega_2 j + \omega_3 k) = 2\omega \qquad (3.5)$$

Therefore for a solid body rotation the vorticity is

$$\Omega = \text{curl } (\omega r) = 2\omega \qquad (3.6)$$

this gives a measure of the angular velocity at the centre of rotation.

3.1.2 Potential vortex (free vortex)

The potential vortex is a type of irrotational fluid motion. In this type of vortex the stream lines again form concentric circles and the tangential velocity along any stream line is inversely proportional to the radius of the stream line ($v_\theta \alpha \frac{1}{r}$). Thus when $n = 1$ the equation (3.2) becomes

$$v_\theta r = k \qquad (3.7)$$

where k is a constant.

The circulation can be obtained by:

$$\Gamma = \int_0^{2\Pi} v_\theta r \, d\theta = 2\Pi k \qquad (3.8)$$

The circulation of any region not enclosing the origin of the vortex is zero. For a potential vortex (irrotational fluid) the vorticity vector Ω is equal to zero except at $r = 0$, i.e. curl $v_\theta = 0$, (vorticity defined as the angular velocity of a fluid at a point in space, i.e. for irrotational fluid vorticity is zero in the whole fluid, except for singular points). A potential vortex does not have vorticity outside the core.

3.1.3 Rankine vortex

A fluid motion formed of a solid body rotation surrounded by a potential vortex is known as a Rankine vortex. The outer flow in a Rankine vortex is irrotational while giving a rigid rotation at the centre. In this type of vortex the core diameter can be exactly determined since the maximum tangential velocity occurs in the transition region. A typical velocity distribution of a Rankine vortex is shown in Fig. 3.1a. It can be seen that there is an almost uniform angular velocity at the vortex core ($v \alpha r$) and almost a constant circulation at the larger radii ($v \alpha \frac{1}{r}$). Fig. 3.1b shows the vorticity distribution.

3.2 **Equations of Compressible Vortex Flow**

In analysing compressible fluids, six equations are required for the solution of the problem. These are governed by the law of conservation of mass (continuity equation); the law of conservation of momentum (momentum equation); the law of conservation of energy or the first law of thermodynamics (energy equation) and the equation of

state.

The momentum equation is actually three equations, since there are three velocity components u, v, w. The other unknown properties are pressure, P, density, ρ and temperature T. The above equations can be listed as follows:

3.2.1 Continuity Equation

For compressible fluid the continuity equation is in the form of:

$$\frac{\partial \rho}{\partial t} + \rho \nabla . V = 0 \qquad (3.9)$$

In rectangular co-ordinates the continuity equation is:

$$\frac{\partial \rho}{\partial t} + \frac{\partial \rho u}{\partial x} + \frac{\partial \rho v}{\partial y} + \frac{\partial \rho w}{\partial z} = 0 \qquad (3.10)$$

and in cylindrical co-ordinates:

$$\frac{\partial \rho}{\partial t} + \frac{1}{r} \frac{\partial (\rho v_r r)}{\partial r} + \frac{1}{r} \frac{\partial (\rho v_\theta)}{\partial \theta} + \frac{\partial (\rho v_z)}{\partial z} \qquad (3.11)$$

where v_r, v_θ, v_z are the velocity components in the radial, tangential and axial directions respectively.

3.2.2 Navier-Stokes equations (momentum equations)

The general momentum equation in vector notation is in the form of:

$$\rho \frac{dV}{dt} = \rho g - \nabla P + \frac{1}{3} \nabla (\mu \nabla . V) + (\nabla . \mu \nabla) V + (\nabla x . \mu \nabla) x V \qquad (3.12a)$$

or

$$\frac{dV}{dt} = g - \frac{1}{\rho} \text{ grad } P + \nu \nabla^2 V + \frac{\nu}{3} \text{ grad div } V \qquad (3.12b)$$

where V is the velocity vector, μ is the viscosity and ρ is the density. The above equation (3.12b) is known as the Navier-Stokes equation, to which there is no general solution. This equation, in rectangular co-ordinates is:

$$\rho \frac{du}{dt} = \rho g - \frac{\partial P}{\partial x} + \frac{\partial}{\partial x}\left[2\mu \frac{\partial u}{\partial x} - \frac{2}{3}\mu\left(\frac{\partial u}{\partial u} + \frac{\partial v}{\partial y} + \frac{\partial w}{\partial z}\right)\right]$$

$$+ \frac{\partial}{\partial y}\left[\mu\left(\frac{\partial v}{\partial x} + \frac{\partial u}{\partial y}\right)\right] + \frac{\partial}{\partial y}\left[\mu\left(\frac{\partial w}{\partial x} + \frac{\partial u}{\partial z}\right)\right] \qquad (3.13)$$

$$\rho \frac{dv}{dt} = \rho g - \frac{\partial P}{\partial y} + \frac{\partial}{\partial y}\left[2\mu \frac{\partial v}{\partial y} - \frac{2}{3}\mu\left(\frac{\partial u}{\partial x} + \frac{\partial w}{\partial z} + \frac{\partial v}{\partial y}\right)\right]$$

$$+ \frac{\partial}{\partial x}\left[\mu\left(\frac{\partial v}{\partial x} + \frac{\partial u}{\partial y}\right)\right] + \frac{\partial}{\partial z}\left[\mu\left(\frac{\partial w}{\partial y} + \frac{\partial v}{\partial z}\right)\right] \qquad (3.14)$$

$$\rho \frac{dw}{dt} = \rho g - \frac{\partial P}{\partial z} + \frac{\partial}{\partial z}\left[2\mu \frac{\partial w}{\partial z} - \frac{2}{3}\mu\left(\frac{\partial u}{\partial x} + \frac{\partial v}{\partial y} + \frac{\partial w}{\partial z}\right)\right]$$

$$+ \frac{\partial}{\partial x}\left[\mu\left(\frac{\partial w}{\partial x} + \frac{\partial u}{\partial z}\right)\right] + \frac{\partial}{\partial y}\left[\mu\left(\frac{\partial w}{\partial y} + \frac{\partial v}{\partial z}\right)\right] \qquad (3.15)$$

where

$$\frac{d}{dt} = \frac{\partial}{\partial t} + u\frac{\partial}{\partial x} + v\frac{\partial}{\partial y} + w\frac{\partial}{\partial z}$$

and in cylindrical co-ordinates the equations are as follows:

Radial Momentum:

$$\rho\left(\frac{\partial v_r}{\partial t} + v_r\frac{\partial v_r}{\partial r} + \frac{v_\theta}{r}\frac{\partial v_r}{\partial \theta} - \frac{v_\theta^2}{r} + v_z\frac{\partial v_r}{\partial z}\right)$$

$$= \rho g - \frac{\partial P}{\partial r} + \frac{\partial}{\partial r}\left[\mu\left(2\frac{\partial v_r}{\partial r} - \frac{2}{3}\nabla.V\right)\right] + \frac{1}{r}\frac{\partial}{\partial \theta}\left[\mu\left(\frac{1}{r}\frac{\partial v_r}{\partial \theta} + \frac{\partial v_\theta}{\partial r}\frac{v_\theta}{r}\right)\right]$$

$$+\frac{\partial}{\partial z}\left[\mu\left(\frac{\partial v_r}{\partial z}+\frac{\partial v_z}{\partial r}\right)\right]+2\frac{\mu}{r}\left(\frac{\partial v_r}{\partial r}-\frac{1}{r}\frac{\partial v_\theta}{\partial \theta}-\frac{v_r}{r}\right) \tag{3.16}$$

Tangential Momentum:

$$\rho\left(\frac{\partial v_\theta}{\partial t}+v_r\frac{\partial v_\theta}{\partial r}+\frac{v_\theta}{r}\frac{\partial v_\theta}{\partial \theta}+\frac{v_r v_\theta}{r}+v_z\frac{\partial v_\theta}{\partial z}\right)$$

$$=\rho g-\frac{1}{r}\frac{\partial P}{\partial \theta}+\frac{1}{r}\left[\mu\left(\frac{2}{r}\frac{\partial v_\theta}{\partial \theta}-\frac{2}{3}\nabla.V\right)\right]+\frac{\partial}{\partial z}\left[\mu\left(\frac{1}{r}\frac{\partial v_z}{\partial \theta}+\frac{\partial v_\theta}{\partial v}\right)\right]$$

$$+\frac{\partial}{\partial r}\left[\mu\left(\frac{1}{r}\frac{\partial v_r}{\partial \theta}+\frac{\partial v_\theta}{\partial r}-\frac{v_\theta}{r}\right)\right]+2\frac{\mu}{r}\left(\frac{2}{r}\frac{\partial v_r}{\partial \theta}+\frac{\partial v_\theta}{r}-\frac{v_\theta}{r}\right) \tag{3.17}$$

Axial Momentum:

$$\rho\left(\frac{\partial v_z}{\partial t}+v_r\frac{\partial v_z}{\partial r}+\frac{v_\theta}{r}\frac{\partial v_z}{\partial \theta}+v_z\frac{\partial v_z}{\partial z}\right)=\rho g-\frac{\partial P}{\partial z}$$

$$+\frac{\partial}{\partial z}\left[\mu\left(2\frac{\partial v_z}{\partial z}-\frac{2}{3}\nabla.V\right)\right]+\frac{1}{r}\frac{\partial}{\partial r}\left[\mu r\left(\frac{\partial v_r}{\partial z}+\frac{\partial v_r}{\partial r}\right)\right]$$

$$+\frac{1}{r}\frac{\partial}{\partial \theta}\left[\mu\left(\frac{1}{r}\frac{\partial v_z}{\partial \theta}+\frac{\partial v_\theta}{\partial z}\right)\right] \tag{3.18}$$

Each term in the general equation (equation 3.12b) can be expressed by a variable or combination of variables. Each term also has physical significance. The physical meaning and expression of each term are as follows: [43]

$\frac{dV}{dt}$	rate of change of momentum force (acceleration or inertia force)
g	gravity force

$\frac{\nabla P}{\rho}$ pressure force

$\nu\nabla V + \frac{\nu}{3}$ grad div V viscous force (force resulting from the action of viscosity)

each of the terms has dimensions of $\frac{L}{T^2}$ so the ratio of any two of them will produce a dimensionless group. Dividing each of the terms on the right hand side of equation (3.12b) by the inertia forces, ($\rho\ L^2\ v^2$), produces the following dimensionless groups:

$$\frac{\text{Gravitational force}}{\text{inertia force}} = \frac{\rho L^3 g}{\rho L^2 v^2} = \frac{gL}{v^2} \quad \text{or} \quad \frac{v}{\sqrt{gL}} = \text{Froude No.}$$

$$\frac{\text{pressure force}}{\text{inertia force}} = \frac{\nabla P L^2}{\rho L^2 v^2} = \frac{\nabla P}{\rho v^2} \quad \text{or} \quad \frac{\Delta P}{\frac{1}{2}\rho v^2} = \text{Euler No.}$$

(N.B. see 4.1.4 for factor 1/2)

$$\frac{\text{viscous force}}{\text{inertia force}} = \frac{\mu v L}{\rho L^2 v^2} = \frac{\mu}{\rho L v} \quad \text{or} \quad \frac{\rho L v}{\mu} = \text{Reynolds No.}$$

The Froude No. is a measure of gravity effect and is usually applied in the case of hydraulic systems.

3.2.3 Energy equation

The energy equation can be derived in the following general terms:

$$\rho \frac{dE}{dt} = \nabla.(K\nabla T) + \rho g.V - \nabla.(PV) + \psi \qquad (3.19)$$

where $-\nabla.(PV) + \psi$ is the total rate of work per unit volume due to

shear stress and normal stress, and

$$\psi = 2\mu \left[\left(\frac{\partial u}{\partial x}\right)^2 + \left(\frac{\partial v}{\partial y}\right)^2 + \left(\frac{\partial w}{\partial z}\right)^2\right] - \frac{2}{3}\mu\,(\nabla.V)^2$$

$$+ \mu\left(\frac{\partial v}{\partial x} + \frac{\partial u}{\partial y}\right)^2 + \mu\left(\frac{\partial v}{\partial x} + \frac{\partial u}{\partial z}\right)^2 + \mu\left(\frac{\partial w}{\partial y} + \frac{\partial v}{\partial z}\right)^2$$

E is the energy and consists of both internal and kinetic energy. The term $K\nabla T$ is the thermal conductivity. The enthalpy h' is related to the internal energy by:

$$h' = U + \frac{P}{\rho} \tag{3.21}$$

where U is the internal energy

or

$$\frac{dh'}{dt} = \frac{dU}{dt} + \frac{d}{dt}\left(\frac{P}{\rho}\right) \tag{3.22}$$

$$\frac{dU}{dt} = \frac{dh'}{dt} - \frac{1}{\rho}\frac{dP}{dt} + \frac{P}{\rho^2}\frac{d\rho}{dt} \tag{3.23}$$

$$\frac{dU}{dt} = \frac{dh'}{dt} - \frac{1}{\rho}\frac{dP}{dt} + \frac{P}{\rho^2}\frac{d\rho}{dt} + \frac{P}{\rho^2}(\rho\nabla.V) - \frac{P}{\rho^2}(\rho\nabla.V) \tag{3.24}$$

i.e. $$\frac{dU}{dt} = \frac{dh'}{dt} - \frac{1}{\rho}\frac{dP}{dt} + \frac{P}{\rho^2}\left(\frac{d\rho}{dt} + \rho\nabla.V\right) - \frac{P}{\rho^2}(\rho\nabla.V) \tag{3.25}$$

multiply both sides of equation (3.25) by ρ

$$\rho\frac{dU}{dt} = \rho\frac{dh'}{dt} - \frac{dP}{dt} + \frac{P}{\rho}\left(\frac{dP}{dt} + \rho\nabla.V\right) - P\,(\nabla.V) \tag{3.26}$$

$\frac{d\rho}{dt} + \rho\nabla.V = 0$ since it is the continuity equation

Therefore,

$$\rho \frac{dU}{dt} = \rho \frac{dh'}{dt} - \left(\frac{dP}{dt} + P\nabla.V\right) \qquad (3.27)$$

since E = internal energy + kinematic energy.

Substitution of equation (3.27) into equation (3.19) gives, after rearranging, the energy equation in vector notation:

$$\rho \frac{dh'}{dt} - \frac{dP}{dt} + \rho \frac{d}{dt}\left(\frac{1}{2} V.V\right) = \nabla.(K\nabla T) + \rho gV - V\nabla P + \psi \qquad (3.28)$$

in rectangular Cartesian co-ordinates:

$$\rho \frac{dh'}{dt} - \frac{dP}{dt} + \frac{\rho}{2} \frac{d}{dt}\left(u^2 + v^2 + w^2\right)$$

$$= \left[\frac{\partial}{\partial x}\left(K \frac{\partial T}{\partial x}\right) + \frac{\partial}{\partial y}\left(K \frac{\partial T}{\partial y}\right) + \frac{\partial}{\partial z}\left(K \frac{\partial T}{\partial z}\right)\right]$$

$$+ \rho \left(ug_x + vg_y + wg_z\right) + \psi - \left(u \frac{\partial P}{\partial x} + v \frac{\partial P}{\partial y} + w \frac{\partial P}{\partial z}\right) \qquad (3.29)$$

In cylindrical co-ordinates:

$$\rho \frac{dh'}{dt} - \frac{dP}{dt} + \frac{\rho}{2} \frac{d}{dt}\left(v_r^2 + v_\theta^2 + v_z^2\right)$$

$$= \left[\frac{1}{r} \frac{\partial}{\partial r}\left(rk \frac{\partial T}{\partial r}\right) - \frac{1}{r^2} \frac{\partial}{\partial \theta}\left(k \frac{\partial T}{\partial \theta}\right) - \frac{\partial}{\partial z}\left(k \frac{\partial T}{\partial z}\right)\right]$$

$$+ \rho \left(v_r g_r + v_\theta g_\theta + v_z g_z\right) + \psi_c - \left(v_r \frac{\partial P}{\partial \theta} + \frac{v_\theta}{r} + v_z \frac{\partial P}{\partial z}\right) \qquad (3.30)$$

where

$$\psi_c = 2\mu \left[\left(\frac{\partial v_\theta}{\partial r}\right)^2 + \left(\frac{1}{r}\frac{\partial v_\theta}{\partial_\theta} + \frac{v_r}{r}\right)^2 + \left(\frac{\partial v_z}{\partial z}\right)^2\right]$$

$$+ \mu \left(\frac{1}{r}\frac{\partial v_z}{\partial \theta} + \frac{\partial v_\theta}{\partial z}\right)^2 + \mu \left(\frac{\partial v_r}{\partial z} + \frac{\partial v_z}{\partial r}\right)^2$$

$$+ \mu \left(\frac{1}{r}\frac{\partial v_r}{\partial \theta} + \frac{\partial v_\theta}{\partial r}\right)^2 + \mu \left(\frac{\partial v_r}{\partial z} + \frac{\partial v_z}{\partial r}\right)^2$$

$$+ \mu \left(\frac{1}{r}\frac{\partial v_r}{\partial \theta} + \frac{\partial v_\theta}{\partial r} - \frac{v_\theta}{r}\right)^2 \qquad (3.31)$$

3.2.4 The equation of state

$$P = \rho RT \qquad (3.32)$$

3.3 **Temperature and Viscosity Effects**

Mack [44] simplified the tangential momentum equation by considering an axisymmetric vortex flow with no radial or axial component of velocity, i.e. the tangential velocity is a function of r only. In this case the momentum equation reduces to:

$$\frac{d}{dr}\left[r^3 \mu \frac{d}{dr}\left(\frac{v_\theta}{r}\right)\right] = 0 \qquad (3.33)$$

where μ is the viscosity coefficient, a function of temperature. The shear stress is:

$$\tau = \mu r \frac{d}{dr}\left(\frac{v_\theta}{r}\right) \qquad (3.34)$$

the first integral of equation (3.34) can be written as:

$$G = 2\Pi r^2 \tau = \text{const.} \qquad (3.35)$$

where G is the viscous torque for unit length normal to the plane of flow. For a potential vortex flow, it is required that μ be constant, i.e. the irrotational velocity distribution $\left(v \alpha \frac{1}{r}\right)$.

The energy equation was simplified by neglecting the convection terms, therefore, in terms of the shear stress and the heat transferred by conduction, the energy equation becomes:

$$\frac{d}{dr}\left[Kr \frac{dT}{dr} + \mu r^2 v_\theta \frac{d}{dr}\left(\frac{v_\theta}{r}\right)\right] = 0 \qquad (3.36)$$

The radial momentum equation reduces to:

$$\frac{dP}{dr} = \frac{\rho v_\theta^2}{r} \qquad (3.37)$$

When the above equations are combined for a perfect gas, Mack shows that even for the potential velocity distribution there is a gradient in total temperature across the vortex.

$$\frac{T_o}{T_{o\infty}} = \frac{1 + \frac{1}{2}(\gamma - 1) M^2}{1 + (\gamma - 1) P_r M^2} \qquad (3.38)$$

The subscript ∞ refers to conditions at the outer edge of the vortex ($r = \infty$). T_o is the total temperature. The pressure in terms of temperature, Prandtl number and γ was also shown by Mack to be:

$$\frac{P_o}{P_{o\infty}} = \left(\frac{T_o}{T_{o\infty}}\right)^{\frac{\gamma}{\gamma-1}} \left(\frac{T_\infty}{T}\right)^{\left[\frac{\gamma}{\gamma-1}\right]\left[1 - \frac{2}{Pr}\right]} \qquad (3.39)$$

if Pr = 0.5 the equation (3.38) is an isentropic relation. As long as Pr = $\frac{C_p \mu}{K}$ exceeds 0.5 there is a decrease in total temperature with decreasing radius.

The above solution can be expected to be accurate only for low Mach numbers where the temperature variation across the vortex is small. Mack also obtained an exact solution for the rotational vortex which is suitable for numerical evaluation. The distribution of velocity, temperature, pressure, density and stagnation temperature through the rotational vortex for a given case were evaluated. Fig. 3.2 shows the temperature and velocity distribution for the rotational and irrotational case. Although for $r/r_s < 0.8$ (Fig. 3.2), the two curves for temperature diverge considerably, at the same Mach number, the temperature is roughly the same. The minimum radius obtained from the rotational solution is larger than obtained from the irrotational solution. In the case of velocity distribution, the rotational distribution gave a steeper slope than the irrotational distribution, which is necessary to maintain constant torque even though the viscosity coefficient decreases with decreasing radius. Ultimately at the minimum radius where $\mu = 0$, the velocity slope is infinite.

A study relating to the effect of temperature on the tangential velocity distribution across a cyclone, [45], has shown that higher temperatures reduce the maximum tangential velocity due to increased viscosity, Fig. 3.3.

In a Rankine vortex, the velocity in the central region of the vortex is linear (solid body rotation) hence the shear stress reduces. For larger radii, the vortex is potential ($v_\theta \alpha \frac{1}{r}$) i.e. it can be said that the value of vorticity decreases with some power of radius, r. This means that work done by shear stress is a maximum at the maximum tangential velocity, i.e. in the transition region. This feature possibly relates also to the location of the maximum temperature which occurs at about the same radius.

3.4 **Pressure Distribution**

The pressure distribution across a vortex is not uniform. In a solid body rotation it has the form of a parabola, Fig. 3.4a. This is because of centrifugal forces which increase towards the outer radius. This centrifugal force is balanced by a centripetal force which is acting towards the centre and maintaining the equilibrium. In confined rotating fluid, equilibrium exists for constant density fluids. The pressure distribution across a potential vortex is shown in Fig. 3.4b and it also increases with radius. The increase is larger near the centre. A combination of the pressure distributions of solid body and potential vortices gives the Rankine vortex pressure distribution which is shown in Fig. 3.4c.

A typical experimental pressure distribution of hydrogen gas through a vortex device is shown in Fig. 3.5, [46]. Also, a comparison between water and nitrogen gas was obtained. It was seen that there was a difference in the shape of the pressure

distributions and the nitrogen yielded a lower centreline pressure, Fig. 3.6. This difference between a gas and a liquid vortex for a constant inlet pressure was examined by changing the aspect ratio $(\frac{H}{D_o})$ of the vortex chamber. It was reported that the water vortex became stronger with increasing aspect ratio, up to a value at which the cavitation (which occurs due to too low fluid pressure) diminished in size, or disappeared completely. After this point, the vortex strength rapidly decreased. The nitrogen vortex exhibited a general decrease in strength with increasing aspect ratio. It was thus concluded that the aspect ratio exerts a strong influence on the shapes of the pressure distribution, especially at low values. Differences in vortex flow field structures in liquids and gases, secondary flows, are probably more pronounced at low $(\frac{H}{D_o})$ than at high $(\frac{H}{D_o})$.

In general, solution of the basic equations of motion to obtain an expression for the pressure distribution is only possible by numerical integration, with the aid of a computer. However, it is possible to find a simplified solution by neglecting some of the variables in the general equations as described in section 3.2.

For vortex flow, the radial momentum equation (3.16) can be simplified by assuming steady flow, symmetry about the axis, and by neglecting the body forces and the radial velocity (which is much smaller than the tangential velocity). Thus, it is still appropriate to assume that the pressure gradient, $\frac{dP}{dr}$ is the only term

in the radial momentum equation which provides the necessary centripetal force, and to use this equation for analysing the experimental data, (i.e. the relation is in the form of equation 3.37):

$$\frac{dP}{dr} = \rho \frac{v_\theta^2}{r}$$

Substituting $v_\theta^2 = K^2 r^{-2n}$ from (3.2) gives

$$\frac{dP}{dr} = \rho K^2 r^{-(2n+1)} \qquad (3.40)$$

For a compressible fluid ρ is not constant and can be calculated from the equation of state for a perfect gas, (equation 3.31), i.e.

$$\frac{dP}{dr} = \frac{P}{RT} \cdot K^2 r^{-(2n+1)} \qquad (3.41)$$

From the energy equation the following relation can be derived Appendix B:

$$T_\infty = T_o - \frac{v_\theta^2}{2C_p} \qquad (3.42)$$

(T_o is the total temperature).

This is a theoretical relationship which cannot be applied in the experimental situation. For experimental work, the temperature measuring probe does not always give the stagnation value, thus the relation can be written as:

$$T_\infty = T_o - \alpha \frac{v_\theta^2}{2C_p} \qquad (3.43)$$

where α is known as the recovery factor (Appendix B) $\alpha = Pr^{1/2}$ for laminar air flow and $\alpha = Pr^{1/3}$ for turbulent air flow, [47].

Substituting equation (3.2) into equation (3.43) gives:

$$T_\infty = T_o - \alpha \frac{k^2}{2C_p r^{2n}} \tag{3.44}$$

Integrating equation (3.41) and employing the boundary condition $P = P_R$ at $r = R$

$$P = P_R - \frac{k^2}{2^n R T_o} \left[\frac{1}{r^{2n}} - \frac{1}{R^{2n}}\right] \tag{3.45}$$

Substituting (3.44) into (3.45) and rearranging, gives:

$$P_R - P = \frac{K^2}{nRT_o \left[2 - \frac{\alpha K^2}{Cpr^{2n}T_o}\right]} \left[\frac{1}{r^{2n}} - \frac{1}{R^{2n}}\right] \tag{3.46}$$

where α can be written in terms of Pr.

3.5 **Boundary Layers in Vortex Flow**

Analysing the flow of real fluids, where viscosity and thermal conductivity are neither zero nor infinite, is extremely difficult. This means that the terms involving these effects in the Navier-Stokes equations are never wholly negligible and therefore to completely solve any such problem, the full equations must be considered. In a real fluid shear stresses cause an adhesion of the fluid to a wall wetted by it, that is, the velocity components are uniformly zero at a boundary.

From the theoretical viewpoint, the inclusion of frictional forces causes great difficulty, hence, ideal fluid theory has been developed by neglecting the viscous effects. In the case of real fluids, one must rely on experimental results to a greater extent than for ideal fluids.

In compressible fluids, the effect of compressibility, which depends on heat transfer across the wall, and Mach number, have to be considered. A characteristic of every compressible flow is that thermodynamic processes occur simultaneously. For supersonic velocities there is a generation of heat by friction in the boundary layer. The heating of the flowing medium by the frictional effects is confined essentially to the same thin boundary layer in which viscosity noticeably affects the flows. A thermal boundary layer is then formed along the immersed wall with the velocity boundary layer. (The relation for temperature increase due to frictional heating is given in Appendix B under recovery factor.)

The presence of pressure gradients in vortex flows makes it even more difficult to solve the equations for a real fluid. Thus, most of the published papers containing theoretical investigations are for ideal fluid flows. On the other hand, it is difficult to obtain reliable experimental data inside a vortex chamber owing to the very disturbing effect which probes have on this type of flow. Savino et al [48] used a vortex chamber, 11.72 inches in diameter and 1.25 inches in height, to investigate experimentally the velocity and pressure distribution. They noticed that the insertion of the probe

into the vortex chamber produced a shift in the radial distribution of static pressure, which indicated an overall reduction in tangential velocities. The same effect was noted by Owen and Motamed-Amini [49] and also Holman and Moore [50], who reported changes in static pressure of the order of 50%.

Taylor [51] obtained a solution for the laminar boundary layer generated inside a cone by a constant circulation vortex flow, and concluded that even when the fluid concerned was water with low values of kinematic viscosity, and when it was injected through a small diameter inlet orifice with a high pressure, a large part of the flow exhausting through the exit hole was boundary layer flow. By assuming that the flow is steady and axisymmetric, Rosenzweig et al [52] used Navier-Stokes' equations for an incompressible fluid with constant viscosity and presented equations governing the interaction between primary flow and end-wall boundary layer in a vortex tube, and obtained a solution by a numerical method. The controlling parameters included a boundary layer interaction parameter (BL) representing a measure of the mass fraction diverted to the boundary layers, the radial Reynolds number, and a parameter ζ representing the boundary layer mass ejection occurring as a result of the geometrical discontinuity existing at the exhaust hole radius. A typical result is shown in Fig. 3.7 for $\zeta = 0$ and $\zeta = 1$ where it can be seen that when BL ≤ 1 the effect of the boundary layer interaction on circulation ratio $\frac{\Gamma_e}{\Gamma_o}$ is relatively small; the

influence of ζ is also small. As the value of BL increases, the boundary layer interaction exerts a considerable influence, especially at higher values of radial Reynolds number. The effect of ζ also becomes more pronounced. The results were also characterised by the minimum mass flow, f_m, in the outer flow region, and the effect of increasing value of BL, Fig. 3.8. The negative values are accounted for by reverse flow regions in the outer flow. In the above calculation, the recirculation of fluid originating downstream of the exhaust hole, which is known as vortex breakdown, was neglected. Vortex breakdown will be discussed in more detail in the next section. Experimental work by Savino et al [48] has shown that when viscous effects are considered, the tangential and radial velocity distributions at various radial positions in a short vortex chamber, are strongly influenced by the end wall shear at high swirl ratios. Fig. 3.9 shows that it is possible for all the radial flow through the chamber to occur in the end wall boundary layers, and the radial velocity at the middle of the chamber (axial distance) may be zero, or at some positions, even negative. In this situation, circulation decreases due to end wall shear.

The influence on tangential velocity is shown in Fig. 3.10, [48]. It can be seen that the tangential velocity in the end wall boundary layers is reduced by the shear stress, and approaches zero. Thus in the boundary layer, the centrifugal force is reduced by the shear, while the pressure force persists resulting in an acceleration of the radial flow in the boundary layer. The above discussion can be summarised as follows.

When the swirl is low, the radial inflow will have enough inward momentum to penetrate the centrifugal field, and inflow will exist at all axial and radial positions away from the walls. When the swirl is high, the radial inflow is diverted axially , and if two stationary end walls are present, all the fluid leaves the chamber by way of the boundary regions adjacent to these end walls. Because the centrifugal force field near the walls is reduced due to no-slip conditions ($u = v = w = 0$ at $z = 0$ & 1) on the surface, in this near wall region, inward radial velocities exist. Therefore, the presence of a negative radial velocity in viscous and turbulent vortices interacts with the tangential velocity causing the motion to depart from solid body rotation, and to tend towards the inviscid vortex ($v \alpha \frac{1}{r}$) as negative radial velocity becomes larger. This was also reported by Wormley [53] who obtained the circulation distribution as a function of swirl, λ,, and the modified boundary layer coefficient $BLC^* = (BLC)(\lambda)$, where

$$BLC = \frac{2r_o f}{H} \quad \text{with } f = f_2/\left(\frac{\rho u_o H}{2\mu}\right)$$

where f_2 is the end wall fraction coefficient. Fig. 3.11 shows that for $BLC^* < 0.25$ the circulation distribution is almost constant and the vortex is potential. As BLC^* increases due to increased swirl, the circulation distribution decays and a potential vortex is obtained over only a portion of the chamber. Using a vortex chamber 114 mm in diameter and 152.4 mm in height, Kotas [54] reported the results of an experimental investigation of radial and tangential velocity distributions, and confirmed the existence of a reversed

radial flow due to flow recirculation between the boundary layers and the main flow. He discussed how the end wall boundary layers can be regarded as leakage routes through which the fluid injected into the vortex chamber may bypass the central region, and flow out of the chamber without entering the main part of the vortex. Thus this boundary layer flow plays a very important part in determining the flow regime in the rest of the vortex chambers.

3.6 **Vortex Breakdown**

Vortex breakdown phenomena, which can occur at any station along the axis of a swirling flow, was observed by Peckham & Atkinson [55] in tip vortices of delta wings. This breakdown can be defined in general as the stagnation of the axial flow and the occurrence of a reversed axial flow region. It is generally believed that this phenomenon is the result of substantial swirl velocities which increases the pressure along the axis of a swirling flow. This development of reversed axial flow is beyond the state of equilibrium between centrifugal acceleration and pressure gradient. Leibovich [56] described two types of vortex breakdown: the "bubble" and the "spiral" breakdown. In either form, a stagnation point appears on the vortex axis, followed by a limited region of reversed axial flow near the vortex centreline. In both forms the upstream approach flow has a jet-like axial velocity component with a centreline speed exceeding the axial velocity outside the jet core by a factor ranging up to three or even more. Deceleration of this strong axial jet to rest at an internal stagnation point is accomplished in an axial distance of one or two diameters of the upstream vortex core. The

flow downstream of the breakdown is turbulent, and has periodic oscillations. Fig. 3.12 shows an axisymmetric bubble followed by spiral breakdown, [57].

It has been reported that the vortex breakdown phenomenon is governed by two basic and conceptually different mechanisms. According to Jones [58], the breakdown ultimately exhibits the spiral form rather than the axisymmetric configuration. Benjamin [59] considered vortex breakdown as the finite-transition between two dynamically conjugate states of axisymmetric flow analogous to the hydraulic jump in open channel flow. Each of these mechanisms can change the structure of a vortex core. Experimental investigations by Sarpkaya [57] support the above mechanisms and reported that the occurrence of these mechanisms depends on the particular combination of the Reynolds and circulation numbers of the flow. Hydrodynamic instability manifests itself more emphatically at low Reynolds and high circulation numbers. The finite transition type of behaviour of the axisymmetric breakdown is brought out more clearly in an unsteady swirling flow than in a swirling steady flow. Sarpkaya [60] identified four states of swirling flow which are shown in Fig. 3.13. It can be seen that there is a region fairly well defined by certain values of Reynolds and circulation number in which only spiral types of breakdown occur, (A), below that is region (B) where the swirling flow is highly unstable to spiral disturbances. In region (C) the flow is stable regardless of magnitude of circulation. Region (D), with high Reynolds number and high circulation, is the region where axisymmetric vortex breakdown occurs.

Flow visualisation experiments by Escudier and Zehnder [61] provided a simple criterion in terms of pipe Reynolds number Re_p at which vortex breakdown occurs, circulation number Ω_c and the ratio of the radial to tangential velocities in the inflow region $\frac{v_r}{v_{\theta o}}$. The correlation is based on experimental work for a range of Reynolds numbers ($5 \times 10^2 - 10^5$), circulation number (0.66 - 46.4) and ratio of radial to tangential velocities (0.012 - 0.058) and is in the form of $Re_p \sim \Omega_c^{-3} R_{r\theta}^{-1}$, and is practically independent of the type of vortex breakdown. Their general observation revealed that as the circulation number decreases with increasing Reynolds numbers, the structure of the vortex breakdown becomes less distinct and complex, although the bubble and spiral forms are still identifiable, at even higher Reynolds number, Fig. 3.14.

The flow downstream of the breakdown zone is wake-like and invariably turbulent with coherent periodic oscillations. Garg & Leibovich [62] experimentally provided a detailed axial and tangential velocity fluctuation at different stations in a vortex core, and showed that the coherent fluctuations were more energetic for the axisymmetric form of breakdown than for the spiral form. Also in the near wake region of vortex breakdown, only a single dominant frequency was observed in the case of spiral breakdown, as opposed to two at nearly equal frequencies which was generally observed. Spectral analysis of his data indicates prominent oscillation in the wakes at less than 10 Hz.

3.7 Precessing Vortex Core (P.V.C.)

Considerable effort has been expended to understand the mechanism which produces the flow reversal and also the conditions under which it occurs. The occurrence of the breakdown can lead to the development of other complex phenomena such as the precessing vortex core (P.V.C.). A type of P.V.C. reported by Boucher et al [63] showed that the central region of the vortex becomes unstable and begins to precess about the axis of symmetry. A P.V.C. was reported by Syred et al [64] to be formed in the exit of a swirl combustor with very weak fuel/air mixtures, the P.V.C. was visible since the combustion was more intense in that region. Syred and Beer [65] showed that the P.V.C. lies on the boundary of the recirculation zone and that the diameter of the P.V.C. is about 0.15 times the diameter of the exit throat of the swirl combustor, and about 80% of the exit diameter is occupied by a recirculation zone.

In general, the complex phenomena described above were studied in free swirling flows, such as vortices over delta wings and also in confined vortex chambers where the flows had little turbulence. In these cases, no account was taken of the problems associated with highly turbulent flow. Theoretical analysis of turbulent flow in the exit region of a vortex chamber is very difficult to perform due to the complex interactions of the boundary layers, reverse flow and the P.V.C. The situation is even more complex when compressibility effects and choking are considered.

3.8 Compressibility Effects in Vortex Flow

The density of gas can vary for different reasons, for example, a system may undergo drastic temperature changes or it may undergo appreciable pressure changes, or both. In the vortex core, the existence of a three-dimensional complex structure which results from the changes in axial and rotary motion, will be significantly influenced by compressibility. This will add an extra problem to the highly complex nature of this type of flow, especially at higher pressure and temperature, where compressibility effects depend on heat transfer and Mach number.

There are few published papers available on compressible vortex flows and this is an area which could be looked at more closely.

Hall [66] discussed two physical effects of compressibility. First, he integrated the simplified radial momentum equation (equation (3.37)) and obtained an equation relating the change of axial velocity along the axis of an incompressible and a compressible core to a change in the axial velocity along the boundary of the core. Thus integrating the radial momentum equation yields:

$$\frac{P_R - P_a}{\rho} = \int_o^R \frac{C^2}{r^3}\, dr \qquad (3.47)$$

where $C \equiv rv_\theta$ is a circulation function. As $r \to R$ value of C varies (R is outer radius of the core), in the case of incompressible flow:

$$\frac{P_R - P_a}{\rho} = \frac{C^2}{2R^2} \qquad (3.48)$$

Thus the pressure in the core increases if the core diameter increases with distance downstream, leading to an axial deceleration (expanding tube). The rate of change of equation (3.48) as it proceeds downstream is:

$$\frac{d}{dz}\left(\frac{P_R - P_a}{\rho}\right) = \int_o^R \frac{1}{r^3}\frac{\partial C^2}{\partial z}\,dr + \frac{C_R{}^2\,dR}{R^3 dz} \qquad (3.49)$$

Combining Bernoulli's theorem with Kelvin's theorem, yields:

$$\frac{d}{dz}\left(\frac{P_R - P_a}{\rho}\right) = \frac{1}{2}\frac{d}{dz}\left(w_a{}^2 - w_R{}^2\right) + \frac{C_R{}^2}{R^3}\frac{dR}{dz} \qquad (3.50)$$

thus

$$\rho\frac{dw_a{}^2}{dz} - \rho\frac{dw_R{}^2}{dz} = 2\rho\int_o^R \frac{1}{r^3}\frac{\partial C^2}{\partial z}\,dr = -2\rho\int_o^R \frac{1}{r^3}\frac{u}{w}\frac{\partial C^2}{\partial r}\,dr \qquad (3.51)$$

$\frac{dC^2}{dr}$ is positive (Rayleigh criterion),

i.e. the integral is positive.

The value of $\frac{dw_R{}^2}{dz}$ is negative for an expanding stream. Therefore, the gradient $\frac{dw^2}{dz}$ would be more pronounced on the axis than at the outside. The effect of swirl is to reduce the value of $\frac{dw_a{}^2}{dz}$ to below a value of $\frac{dw_R{}^2}{dz}$ as it proceeds downstream, i.e.

$\left|\ \rho\left(\frac{dw_a{}^2}{dz} - \frac{dw_R{}^2}{dz}\right)\ \right|$ is increasing (amplification).

For compressible flow (inviscid and non-conducting) he derived equation:

$$\rho_a \frac{dw_a^2}{dz} - \rho_R \frac{dw_R^2}{dz} = 2\int_o^R \frac{1}{r^3} \frac{\partial(\rho_C^2)}{\partial z} dr \qquad (3.52)$$

For a supersonic flow (expanding stream) velocity increases, therefore, a value of $\frac{dw^2}{dz}$ is positive and hence, a value of $\rho_a \frac{dw_a^2}{dz}$ is positive and smaller than $\rho_R \frac{dw_R^2}{dz}$ i.e. $\left| \rho_a \frac{dw_a^2}{dz} - \rho_a \frac{dw_R^2}{dz} \right|$ for supersonic flow is decreasing as it proceeds downstream. It is evident from this that the structure of the flow within the core is different in the sub- and supersonic cores. The physical meaning of these expressions will be discussed further in Chapter 6.

The second effect discussed by Hall was a tendency for exceedingly low densities approaching a vacuum, to occur near the axis of the core. Measurement by Gaudet & Winter [67] in the leading edge vortex over a slender delta wing in supersonic flow, showed a region of such low pressure and density that it was impossible to define a core structure.

3.9 **Choking in a Swirling Nozzle**

Nozzles are often used in vortex devices to exhaust the swirling flow which is generated within the vortex chamber. Mechanisms of swirling flow, as described previously, are very complex and are not clearly understood, especially with respect to the passage of flow through a nozzle. Available one-dimensional theory which is usually

applicable to nozzles with no swirl gives good results when the area change is gradual, and the nozzle wall curvature is small. For non-swirling nozzles, the acceleration in a converging nozzle is limited by the requirement that the velocity in the throat does not exceed the local speed of sound. When the flow at the throat is sonic or critical, the nozzle is said to be choked.

In the case of swirling nozzle flow, choking criterion are not simple to analyse because the flow varies radially as well as axially. Lewellen et al [68] obtained a one-dimensional equation for flow varying only in the radial direction, i.e. in a constant area region and showed that for a choked condition, both axial and tangential Mach number for a relatively large value of swirl increases within the vortex, as Reynolds number increases.

In general, the critical pressure ratio decreases with increase in either value of swirl or Reynolds number. At the point of maximum flow, the pressure ratio required to choke the flow is approximately 0.1 (outlet to inlet pressure ratio), which is considerably lower than the 0.528 for a non-swirling nozzle flow using air. An experimental investigation by Norton and Hoffman [69] to determine the effect of choking in a set of converging nozzles, indicated that vortex choking is influenced by the type of vortex (free or forced) initially generated in the chamber, the nozzle contraction ratio ($\frac{A}{A_e}$, extent of reduction in flow area) and the vortex strength. Fig. 3.15 shows the effect of contraction ratio on free and forced vortex choking. It can be seen that for different contraction ratios, there is a continuous decrease in the flow rate parameter $(\frac{\dot{m}\, a_o}{P_o\, A_e})$ as

the swirl parameter $(\frac{r_R\omega}{a_o})$ increases from zero. Their data also showed that the actual mass flow rate has, at most, a secondary effect on the mass flow rate reduction.

A theoretical investigation by Hsu & DeJoode [70] showed that the axial Mach numbers in swirling nozzle flows are usually smaller than the corresponding value of one-dimensional nozzles in the convergent portion, but they are larger in the divergent portion. This was accounted for in the presence of a void region which gradually grows as the axial Mach number is increased. The decrease in mass flow rate was also attributed to the decrease in the gas density in the void region at the throat, through which little mass flows. Binnie [71] showed that the effective area of a nozzle throat is reduced by the spinning gases of a free vortex. Carpenter [71] presented an approximate analytical method for determining the swirling compressible flow through a nozzle and reported that the choking pressure ratio decreases as swirl intensity increased, and also the axial Mach number at the throat is always less than unity.

From this review of published papers on compressible swirling flow through nozzles, it is seen that the mechanisms controlling this type of flow are not simple, and require further investigation. In particular, there is a lack of experimental data to complement the available theories which, at present, are unable to adequately describe the complex fluid mechanics.

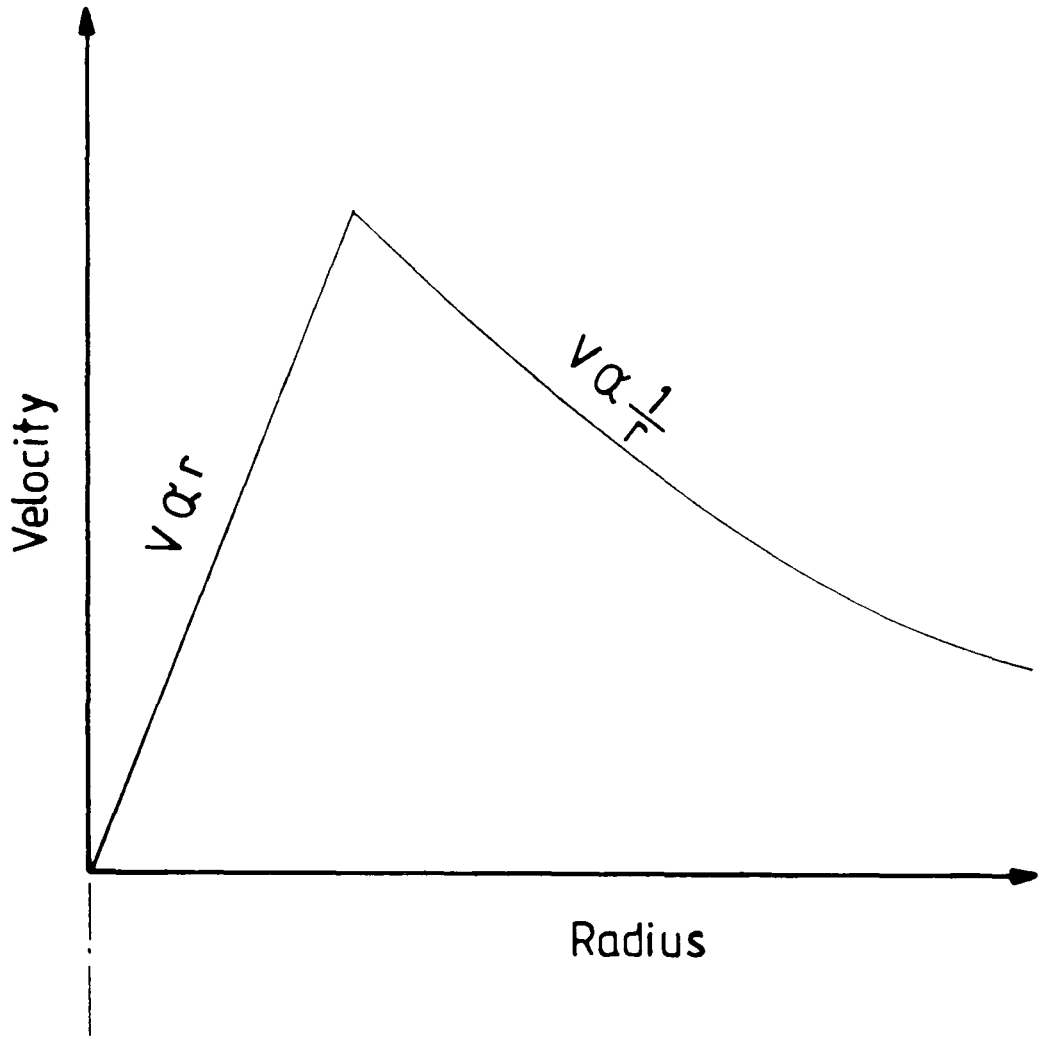

Fig. 3.1 Rankine Vortex: (a) Velocity Distribution;

`` Vorticity Distribution

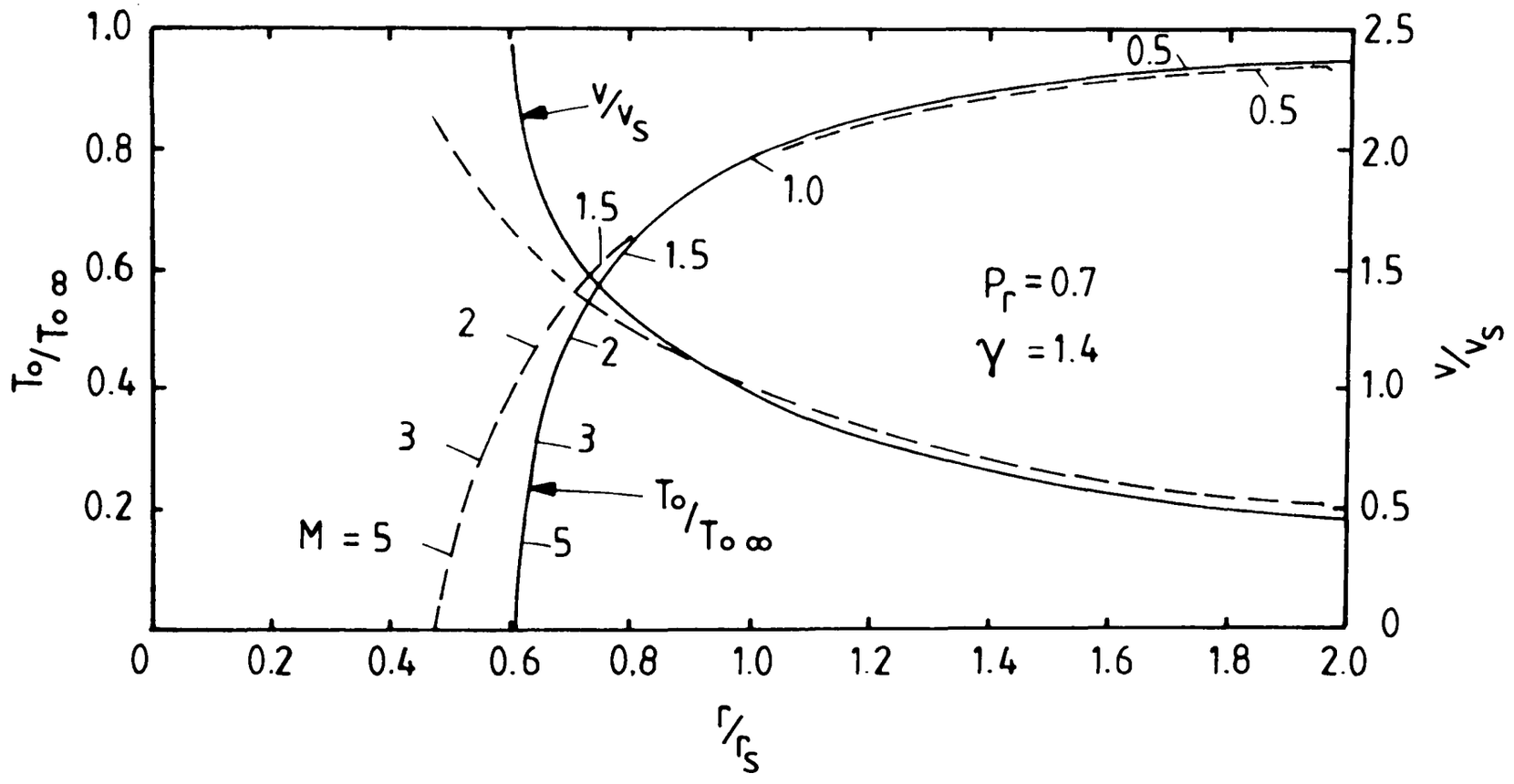

Fig. 3.2 Velocity and Temperature Distribution for Rotational ——— and Irrotational ---- Solution [44]

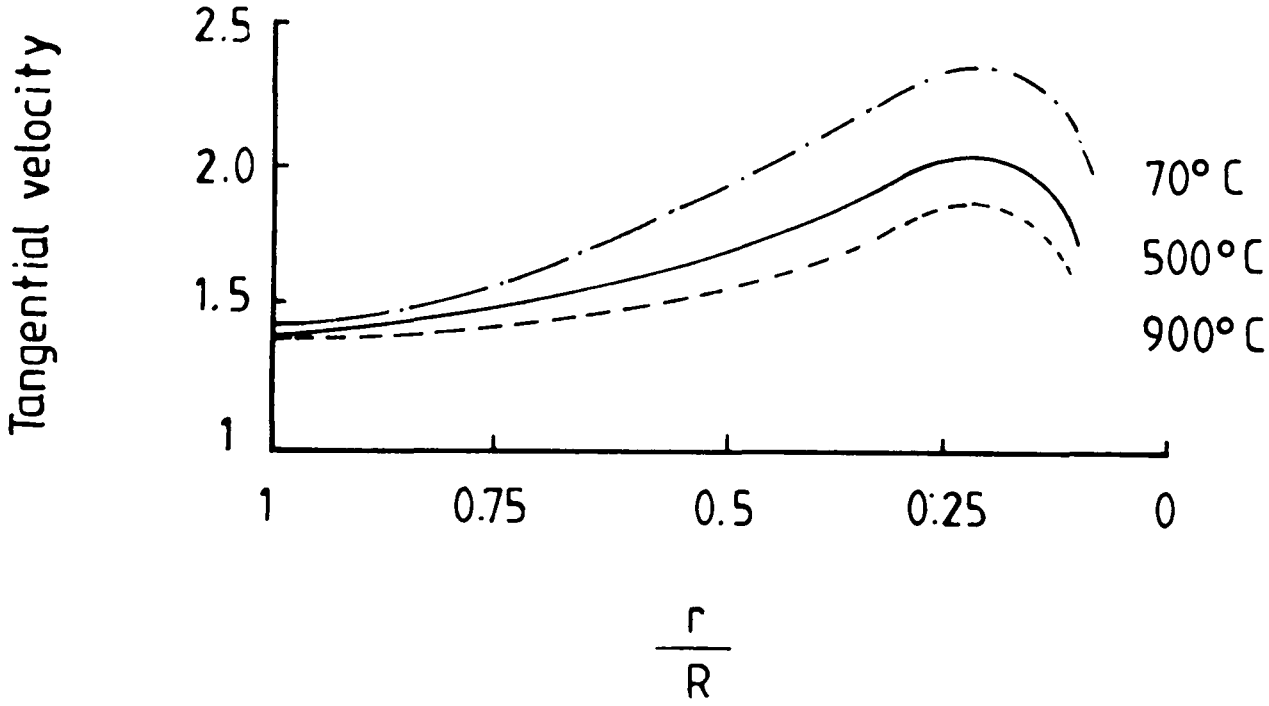

Fig. 3.3 Effect of Temperature on the Tangential Velocity Distribution Across a Cyclone.

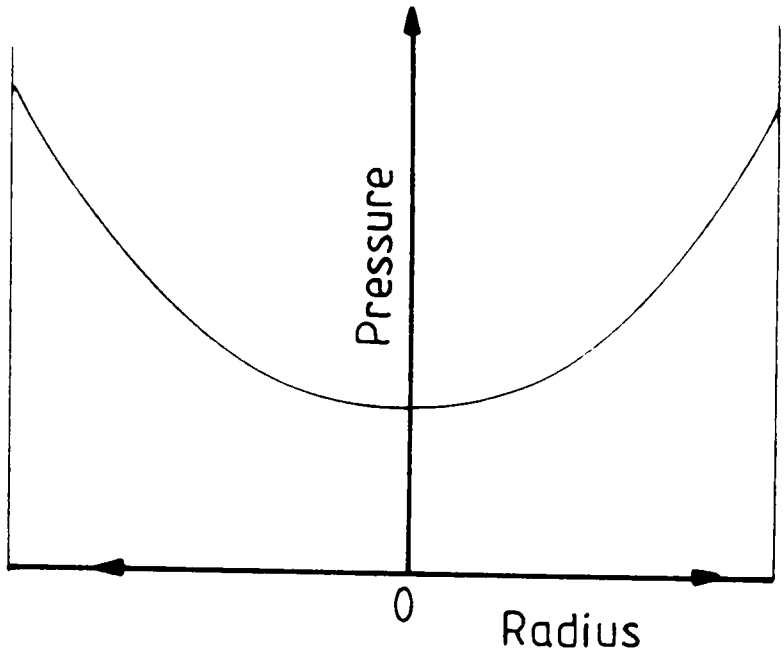

(a)

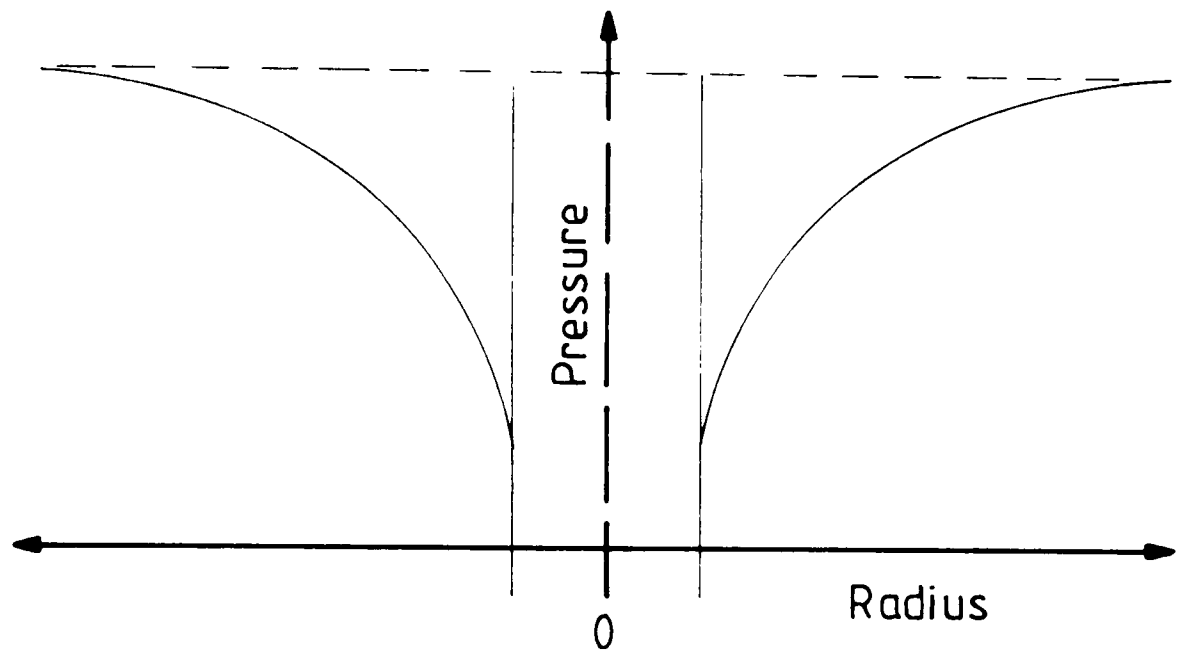

(b)

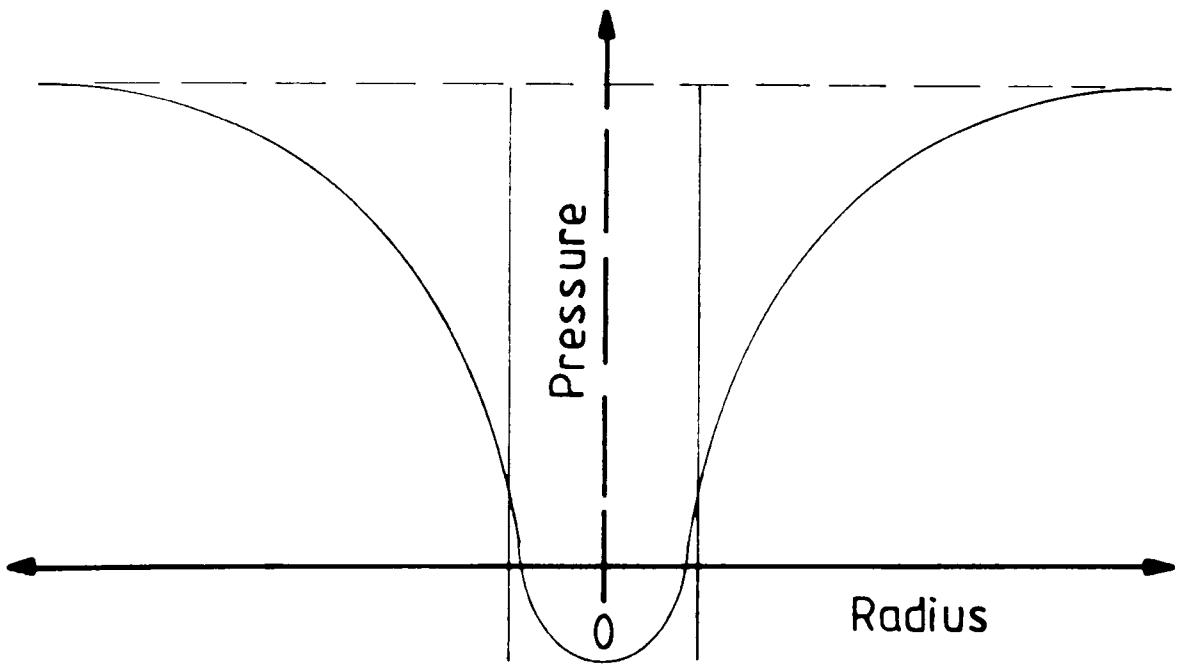

(c)

Fig. 3.4 Pressure Distribution Across a Vortex: (a) Solid Body, (b) Potential, (c) Rankine.

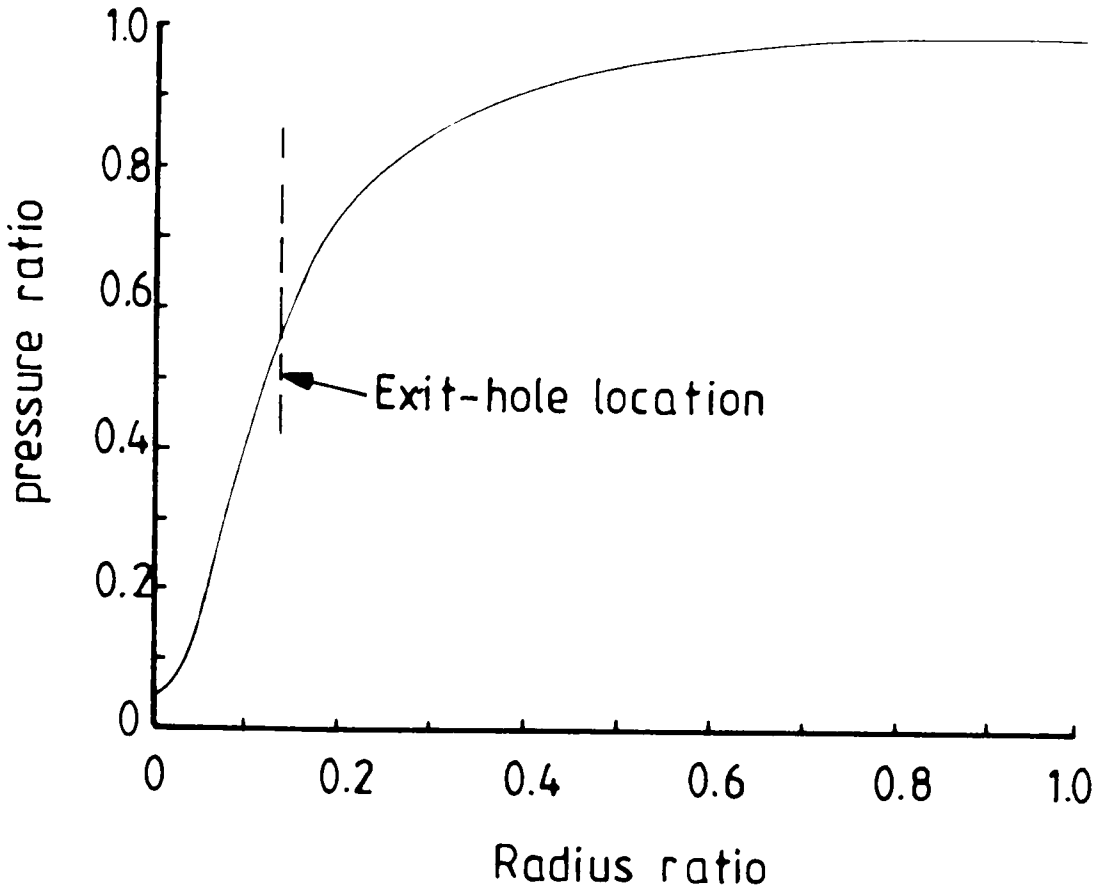

Fig. 3.5 A Typical Experimental Pressure Distribution

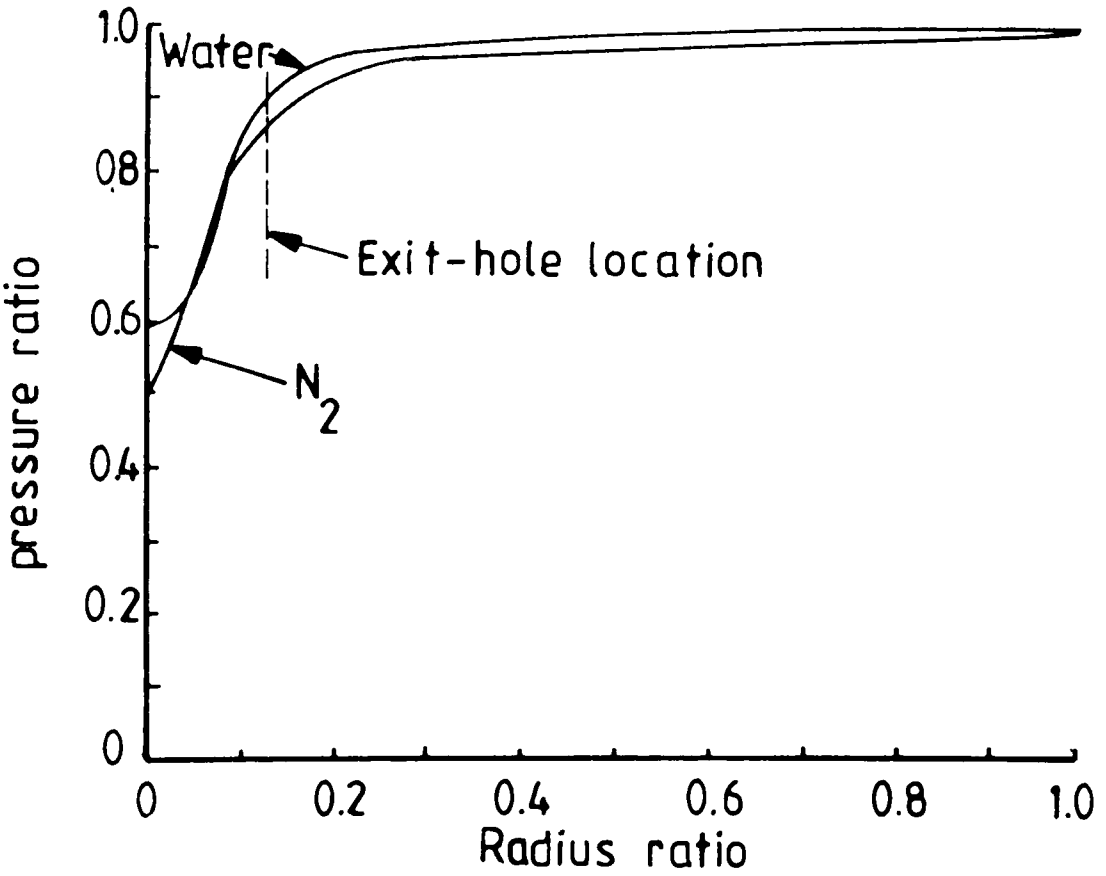

Fig. 3.6 Comparison Between Pressure Distribution of Water and Nitrogen Gas for a Constant Inlet Pressure

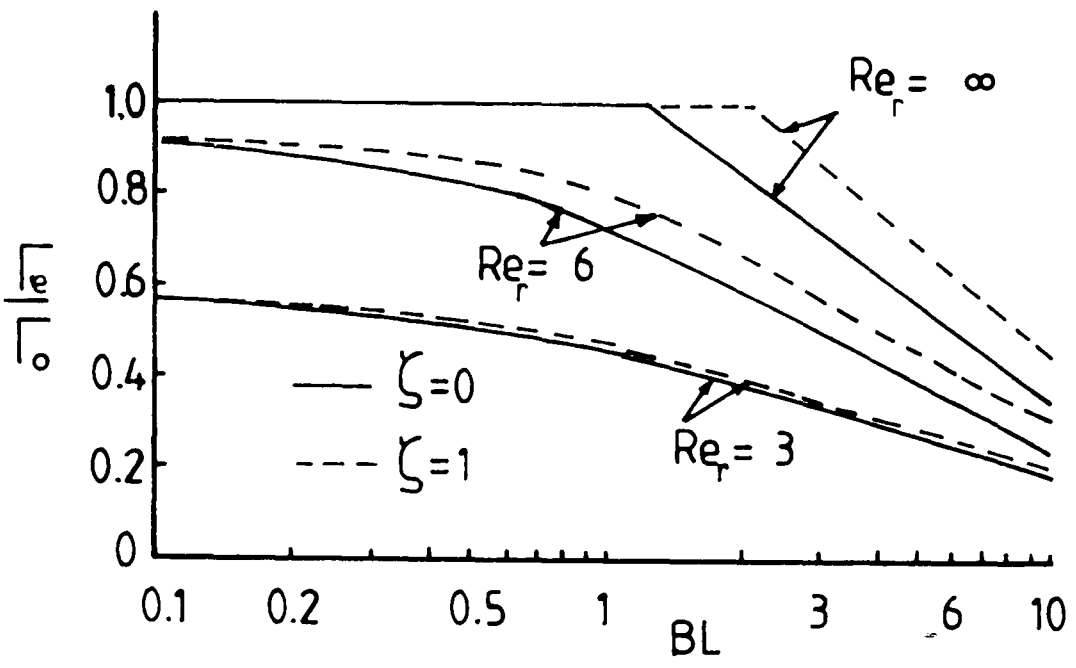

Fig. 3.7 Circulation at the Edge of the Exhaust Hole as a Function of BL for Constant Re_r [52].

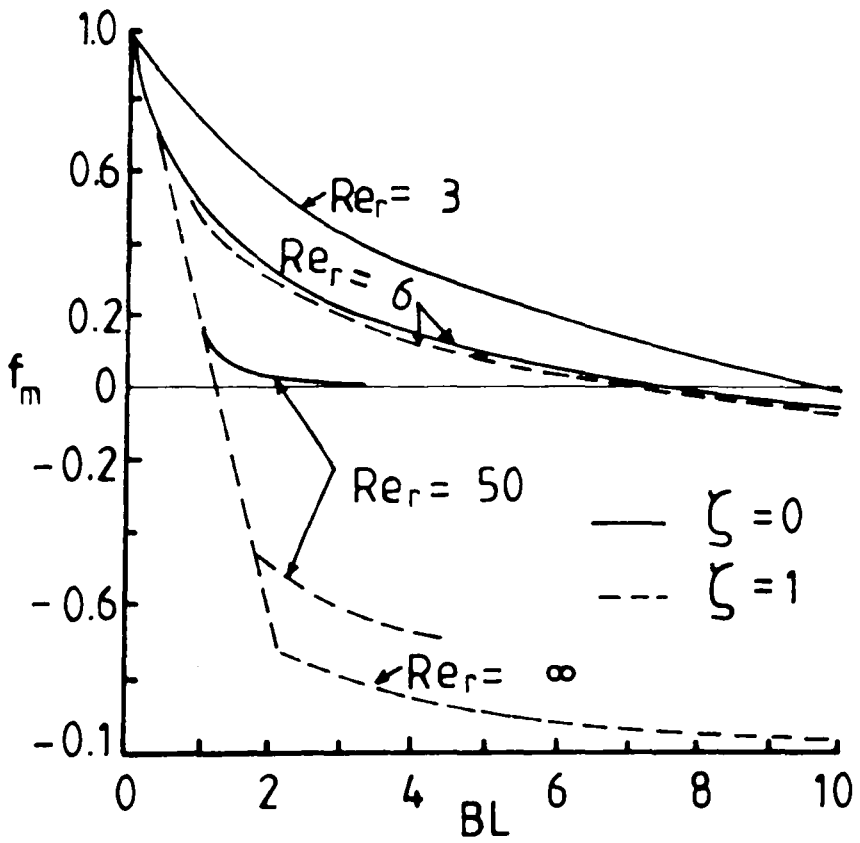

Fig. 3.8 Minimum Mass Flow in the Outer Flow Region as a Function of BL for Constant Re_r [58]

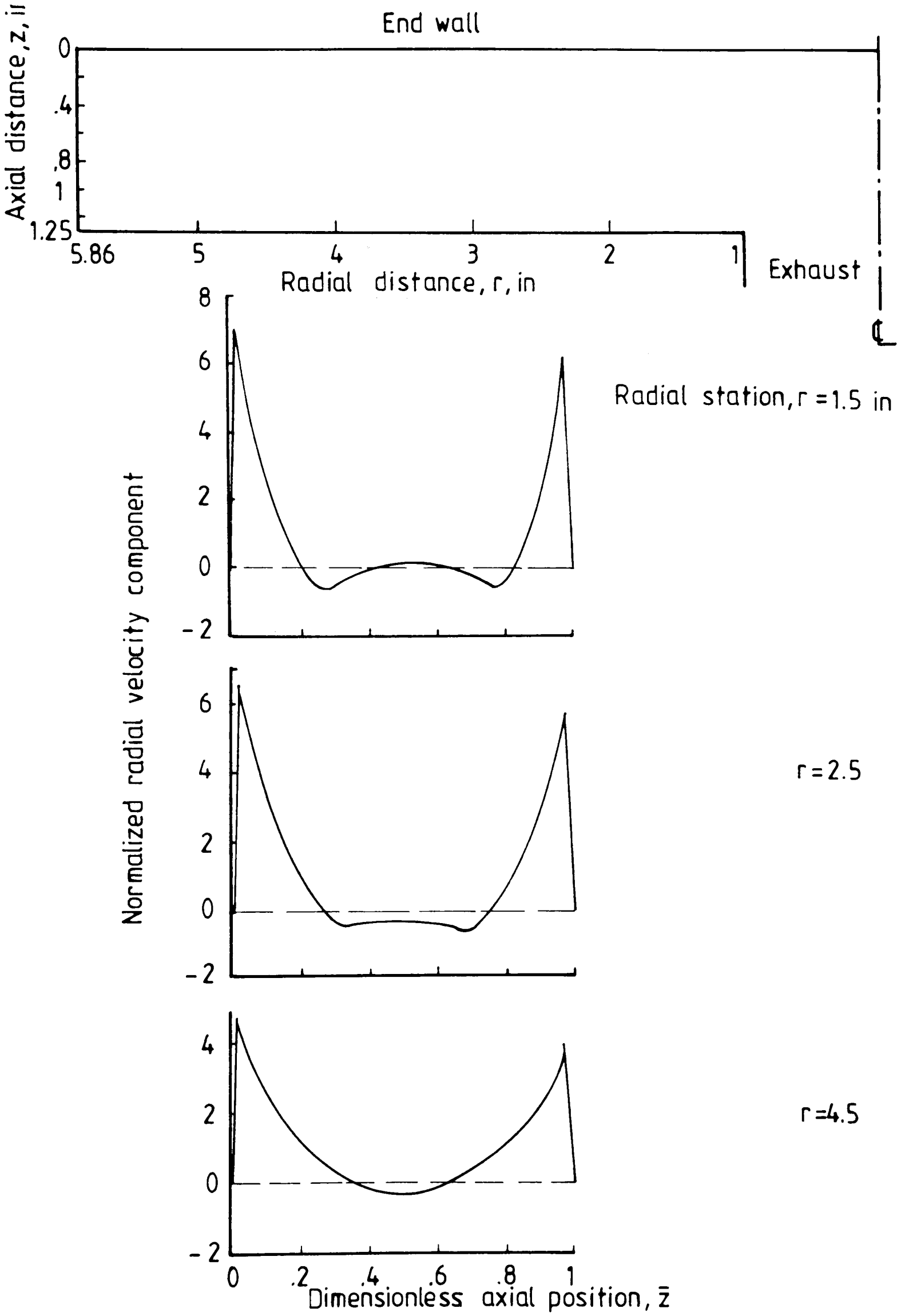

Fig. 3.9 Radial Velocity Distribution at Various Radial Positions [48]

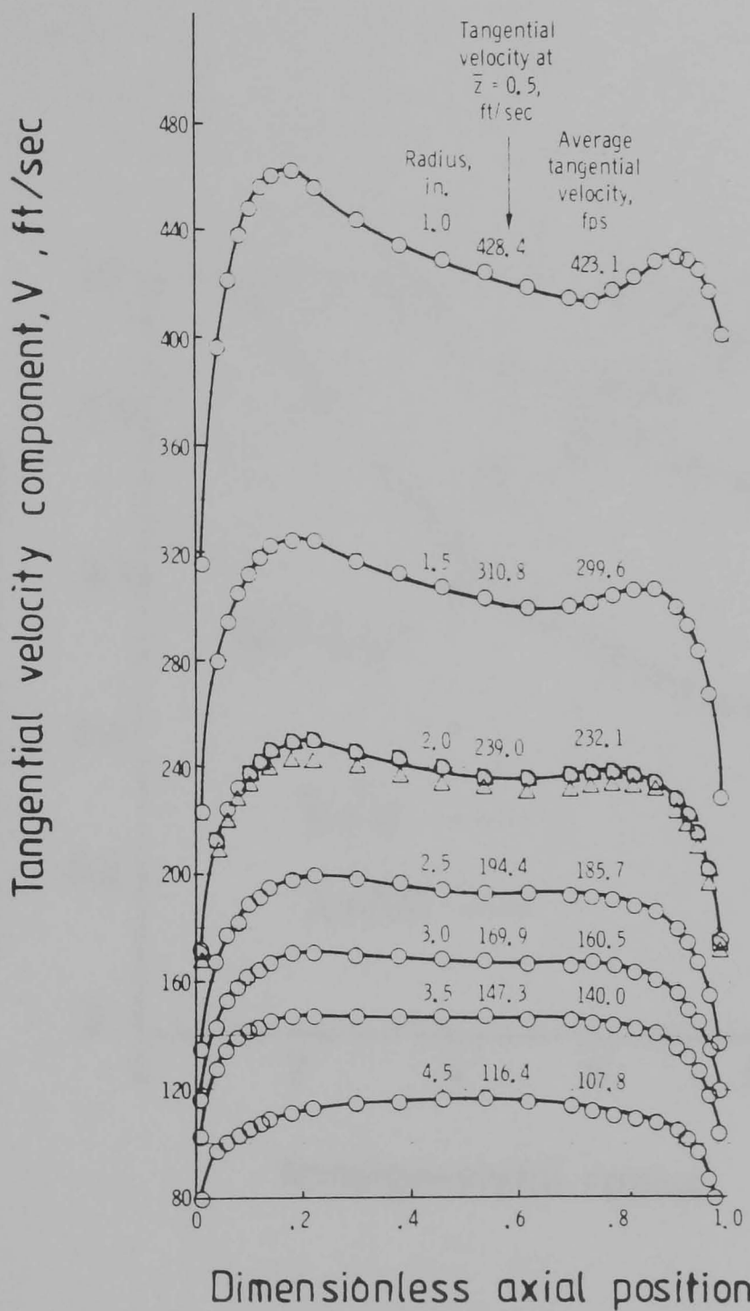

Fig. 3.10 Tangential Velocity Distributions at Various Radial Positions [48]

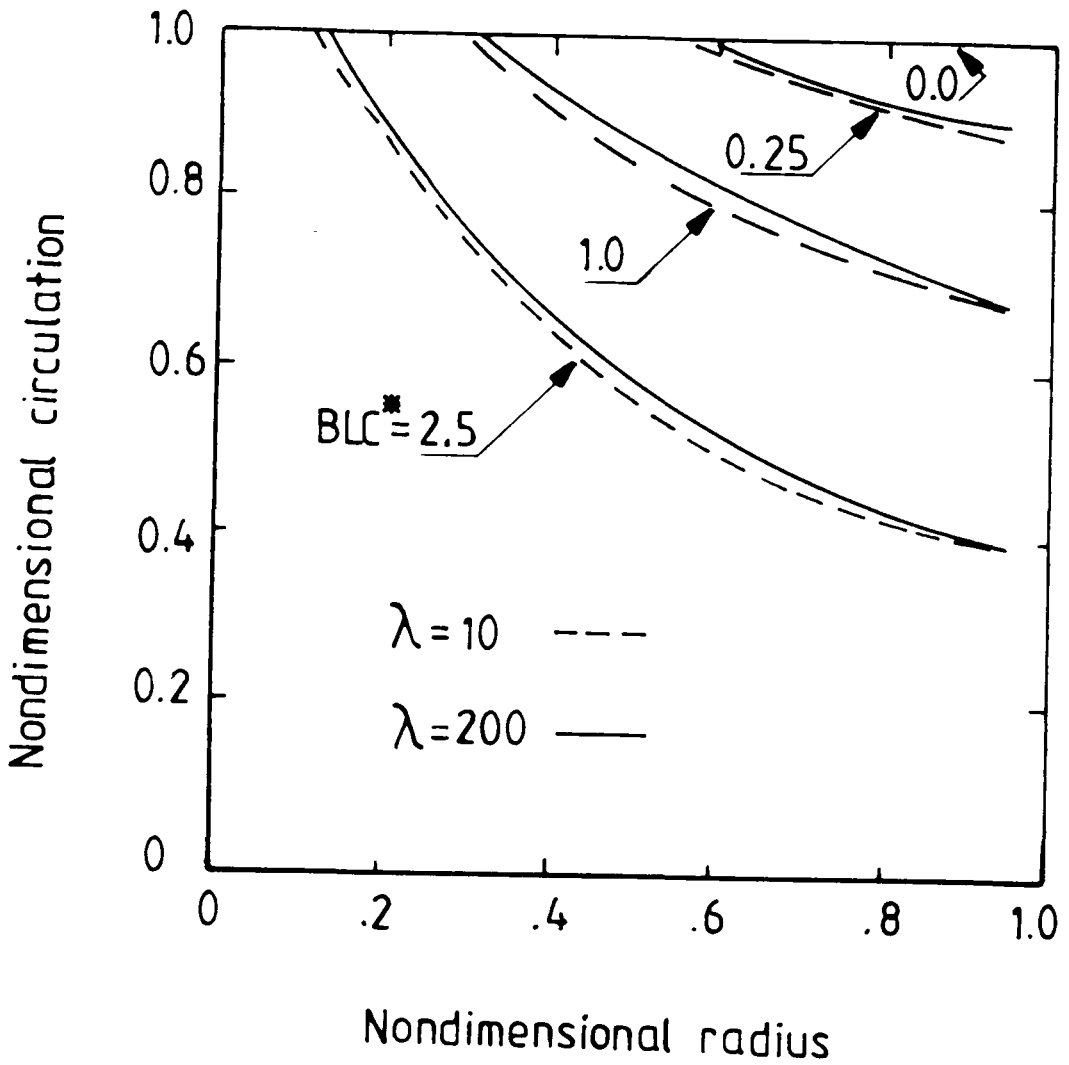

Fig. 3.11 Circulation Distribution in a Vortex Chamber [53]

Fig. 3.12 A Typical Axisymmetric Bubble Followed by Spiral Vortex Breakdown [57]

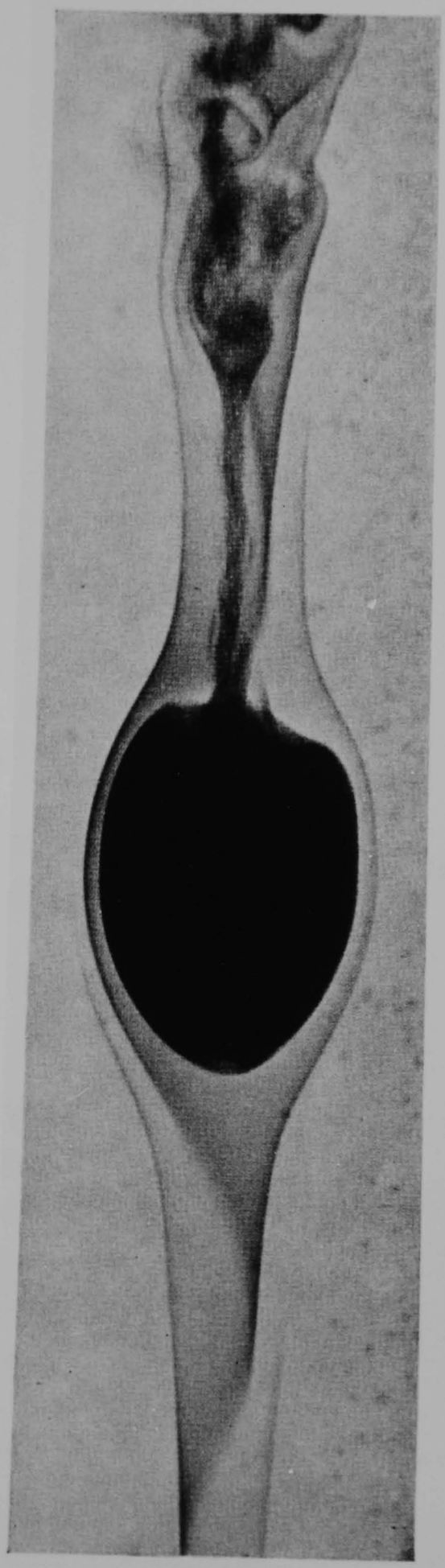

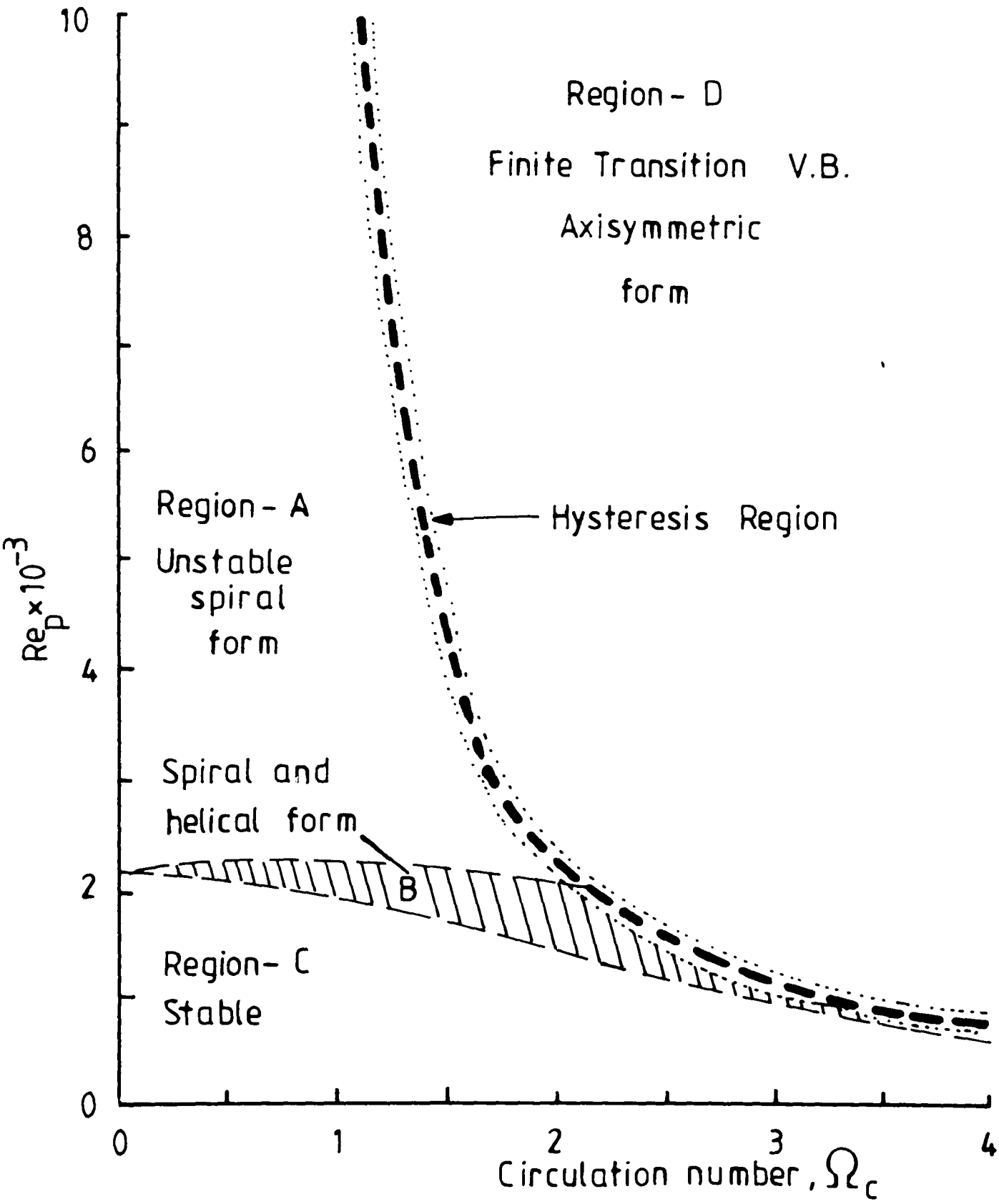

Fig. 3.13 The Four States of Swirling Flow [60]

Fig. 3.14 **Incompressible Vortex Breakdown at Higher Reynolds Number** [61]

(a) Circulation No. = 1.46, Re No. = 3300
(b) Circulation No. = 1.46, Re No. = 15000
(c) Circulation No. = 1.46, Re No. 15000

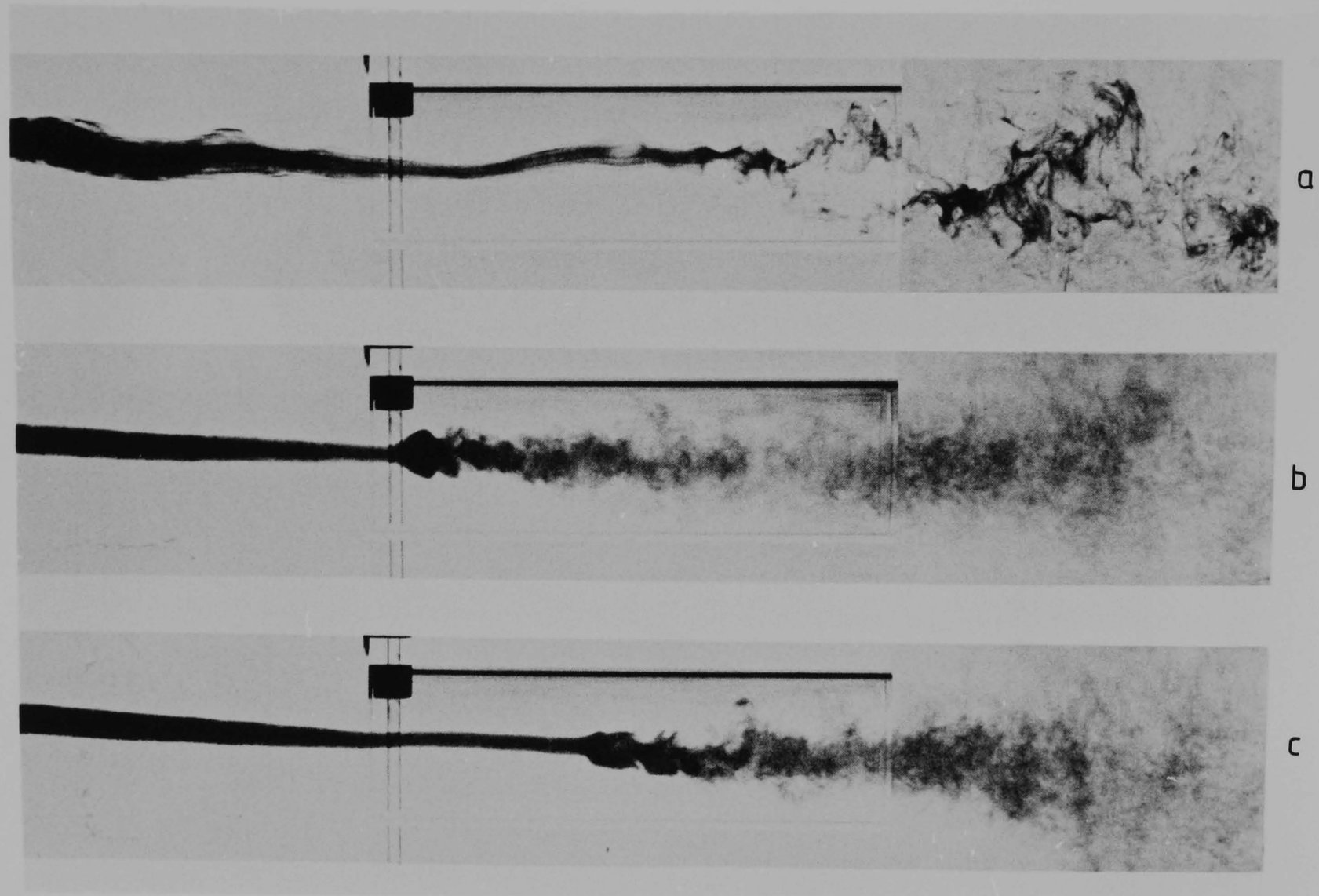
a
b
c

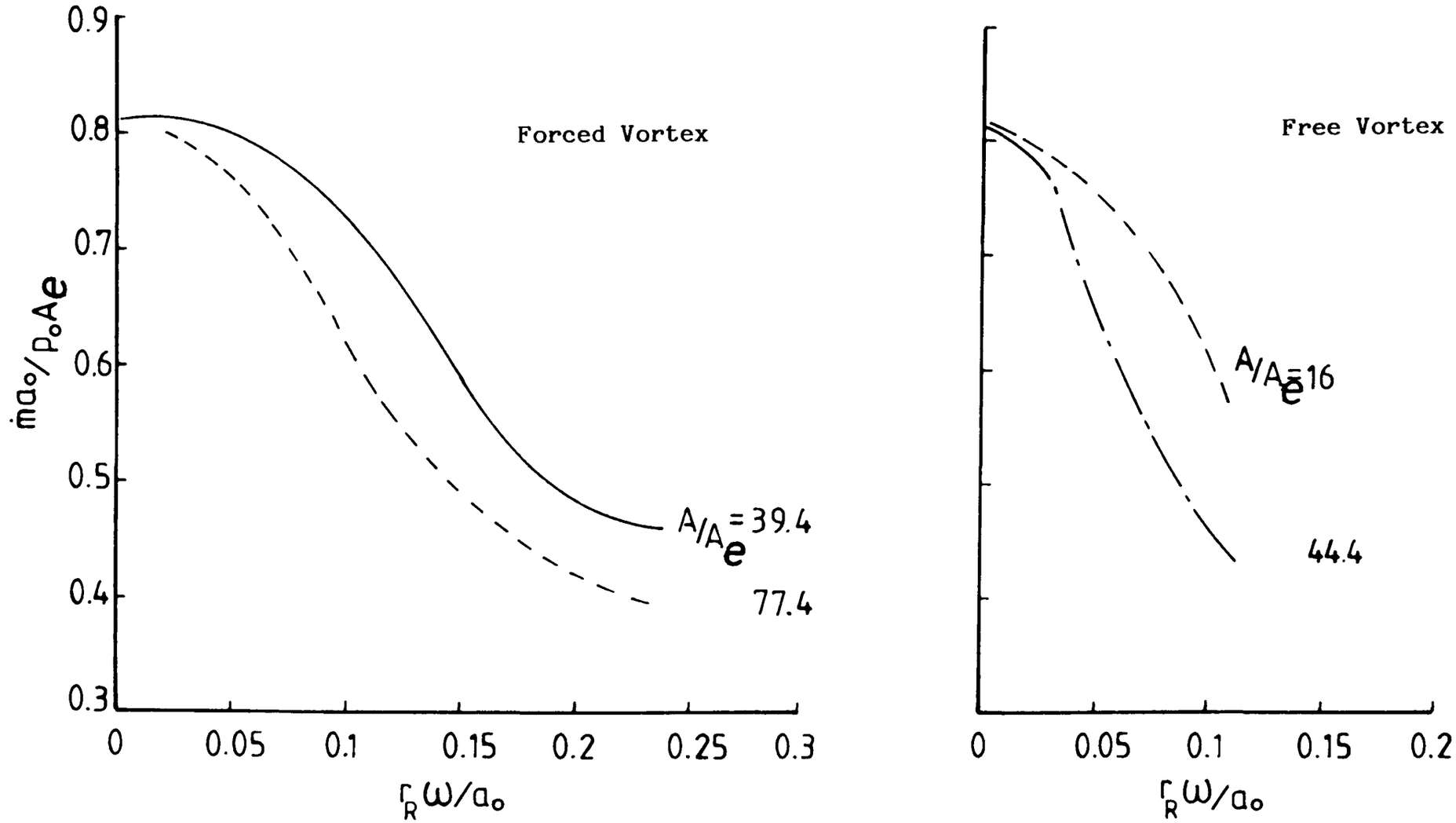

Fig. 3.15 Effect of Contraction Ratio on Vortex Choking [69]

CHAPTER 4

THE MEASUREMENT OF COMPRESSIBLE FLOW CHARACTERISTICS OF VORTEX DIODES

As a result of the efforts of a number of researchers, over the last decade in particular, the performance characteristics are now available for numerous designs of vortex diodes operating with a variety of fluids over a wide range of operating conditions. Much of the data is for air with moderately incompressible flow, and for water. As the pressure drop and hence the flow rate through the diode is increased so the characteristics become complicated; by the onset of cavitation in the case of liquids, and by the effects of choking and compressibility in the case of gases. An important process fluid which, until now, has not been investigated in this context is steam. A vortex diode operating with steam at or near saturation conditions is likely to experience both phase-change and compressibility effects when subjected to such pressure differentials as those found between a steam main and the atmosphere. It is reasonable to expect, therefore, that the characteristics of a vortex diode with steam will reflect these complications.

Anticipating these complications, the characterising of a vortex diode was firstly carried out using superheated steam. The results are presented in the first part of this chapter. There were two reasons for this approach, firstly this established a benchmark

against which to compare the wet steam characteristics which are given in the following chapter. Secondly, an equally important reason for using superheated steam is that it was realised early in the study that it behaves as an ideal gas. It has therefore been possible to obtain extensive forward and reverse flow characteristics over a greater range of inlet to outlet pressure ratios than might naturally be possible with a compressed air rig. The only detailed published data concerning vortex diode behaviour with high pressure ratios is that of George, Ward and Mitchell [73] who used the blowdown from a pressure vessel and a vortex diode in reverse flow. They obtained their steady state characteristics by taking an instantaneous operating point during the dynamic process. This data compared well with some limited characteristics presented by Syred and Roberts [4].

In the first part of this Chapter, forward and reverse flow characteristics of a Zobel type vortex diode operating with superheated steam are presented. The diode is similar to that used by Syred and Roberts with a 19 mm axial throat diameter. The full description of the diode is given in Section 4.1.1. The reverse flow characteristics were measured for pressure ratios up to thirty whilst, due to the very high flow rates involved, the forward flow was limited to a pressure ratio of about eight. Inlet pressures from 3 to 12 bar absolute were used.

Smaller vortex diodes have also been constructed with 10 mm axial throat diameters. The experimental investigation of these,

operating with air, are given in Section 4.2 of this chapter. Reverse flow characteristics were measured for pressure ratios up to thirty. Inlet pressures for these tests were varied between 2.76 bar (40 psi) and 28.6 bar (415 psi) absolute, the flow was exhausted to the atmosphere. In this investigation the effect of installing vortex diodes in series was also examined.

The extensive data from the above experimental work shows clearly the choking effect in both directions and shows how compressibility affects the diode performance. The method of presenting the data is discussed in some detail.

The range of experimental error in the basic data has been calculated in accordance with [74] and reflects the reliability of the instrumentation and the accuracy with which it could be read. The calculation of errors are presented in Appendix C.

4.1 Superheated Steam Characteristics of the Vortex Diode

4.1.1 Experimental Apparatus and Instrumentation

Figure 4.1 shows a schematic of the vortex diode characterisation rig. The steam generator produces saturated steam which is passed through the superheater and then delivered to the manifold in a superheated condition; from there it is supplied to the vortex diode through a 77 mm pipe. The superheated steam mass flow rate was measured by an orifice plate with D and $^{D}/_{2}$ pressure tapping (B.S. 1042 [75]). Two throttle valves, one either side of the diode, were used to regulate the upstream and downstream

pressures. The temperature and pressure were measured in the 77 mm pipe and were essentially stagnation values. Pressure gauges were used to measure the pressures upstream of the diode and at the orifice. Half-shielded thermocouple temperature probes were constructed and used to measure the stagnation temperatures before and after the diode and also downstream of the orifice plate. Figure 4.2 shows in detail the construction of the temperature probe. This type of probe is least sensitive to radiation and to Mach and Reynolds number effects [76]. It should be noted that real probes do not always stagnate a moving fluid effectively. This is important when the fluid is compressible; that is, although there will be stagnation at a point, most temperature-sensing probes indicate a mean temperature and the effect of the entire probe geometry must be considered. Thus an insulating material was used for the main body of the probe in order to reduce the heat conduction to the pipe walls. The shield stagnates the moving steam and the measured temperatures are close to the stagnation value. In addition, a calculation of dynamic temperature, which is the thermal equivalent of the directed kinetic energy of the steam, has shown that for the maximum velocity available when the diode was installed in the reverse flow direction this value will not exceed 0.62°C, Fig. 4.3, and most of this will be recovered by the half-shielded probe. In other words, the measured temperatures are, for all practical purposes, stagnation values.

After passing through the diode, the steam is condensed into a sub-atmospheric condenser which enables high pressure ratios,

especially in reverse flow, to be achieved - a feature which is not possible on non-condensing high pressure compressible flow rigs.

The diode is of a Zobel design and is illustrated in Figs. 4.4 and 4.5. The geometric values are as follows (see Fig. 2.9):

Inlet nozzle throat diameter	D_t = 23.8 mm
Axial throat diameter	D_e = 19 mm
Chamber height	H = 25 mm
Chamber outer diameter	D_o = 177 mm
Length of the axial nozzle	ℓ_a = 75 mm
Length of the tangential nozzle	ℓ_T = 84 mm
Tangential connecting pipe diameter	d_o = 38 mm
Angle of axial diffuser	θ = 7°
Angle of tangential diffuser	β = 4°8'

And in terms of ratios:

$$\frac{do}{D_e} = 2$$

$$\frac{D_t}{D_e} = 1.25$$

$$\frac{H}{D_e} = 1.3$$

$$\frac{D_o}{D_e} = 9.3$$

The pressure drop across the vortex diode was obtained by means of a strain gauge differential pressure transducer which was connected to the pipework one metre before and after the vortex

diode. A similar transducer was used to measure the pressure drop across the orifice plate. Water flooding of the differential pressure transducer in the case of the orifice plate was supplied by two cooling chambers. A multi input digital thermometer gave a direct reading of temperature from the copper/constantan thermocouples and two voltmeters were used for measurement of differential pressures. The pipework and vortex diode were well insulated to reduce the heat losses.

4.1.2 Procedure

During the test the upstream pressure, P_u, was kept constant by use of the throttle valve whilst the downstream pressure, P_d, was gradually increased by closing the throttle valve before the condenser. The characteristics for reverse and forward flow were obtained from P_u = 3 bar to 12 bar absolute at 1 bar intervals. The pressures upstream of the vortex diode and also at the orifice were read from the calibrated pressure gauges. The voltage readings from the pressure drops across the vortex diode and the orifice plate were converted to differential pressures by an available calibration chart.

It was originally feared that characteristics might have to be taken for different degrees of superheat but this turned out not to be the case and the characteristic for a given upstream pressure was unique regardless of the level of superheat, even very close to the saturation condition. Figure 4.6 shows that the diode

characteristic, in terms of a discharge factor (the parameter will be defined in Section 4.4.) at the choked condition, remains the same as the degree of superheat increases. The state point locus of the steam during its expansion through the diode could not be determined from the apparatus shown in Fig. 4.1 but will be shown later in Chapter 6. What can be determined from the present arrangement, however, are the end points of the expansion. Three such end points are shown in Fig. 4.7 for inlet pressure of 10, 7 and 4 bar absolute. It can be seen that the overall process is a throttling one, this observation is confirmed by consideration of the steady flow energy equation.

4.1.3 Results

Figure 4.8 shows the measured mass flow rates of steam through the diode for fixed inlet pressures ranging from 3 to 12 bar abs. The broken lines are simply an extrapolation of the measured values. Different maximum pressure ratios were achieved in different experiments due to the variable effects of atmospheric pressure, condenser cooling water supply, extractor pump seals, etc.

The choking of the diode is clearly seen in each characteristic where the mass flow becomes independent of downstream pressure. It is not absolutely clear at what pressure ratio the choking actually occurs, but it can be seem to be at a value of about 4-6; significantly different to the theoretical value of 1.86 for one-dimensional choking.

The corresponding data for the forward flow is shown in Fig. 4.9. Again the effect of choking is clearly seen, this time with the critical pressure ratio somewhere near its one-dimensional theoretical value. The maximum flow rate of steam used in the forward flow tests was about 1700 kg per hour and high velocities were produced in the pipework, particularly downstream of the diode where the steam specific value was much higher. As a result of the high velocities the second throttle valve in the rig presented a high resistance to the flow. This is the reason for the limited pressure ratio in the forward flow direction. Comparing the choked mass flow rates in Figs. 4.8 and 4.9. In Fig. 4.10 it can be seen that the ratio of the forward to reverse mass flow rates in the choked region is about 2.5 and already it is evident that the diode performance is substantially less than would be expected with incompressible flow.

4.1.4 Presentation of Data

Historically, vortex valve pressure-flow characteristics have been presented as a function of the Euler number, ξ, where

$$\xi = \frac{\Delta P}{\frac{1}{2}\rho v_e^2} \tag{4.1}$$

Euler number is the ratio of pressure forces to inertia force. ΔP represents the difference in pressure between two points in the flow, the $^1/2$ being inserted so that the denominator represents kinetic energy per unit volume or the dynamic pressure of the stream [77].

The Euler number can be thought of as a loss coefficient derived from the incompressible form of the energy (Bernoulli) equation. It is therefore most unlikely that this parameter is suitable for describing the characteristics of a flow control valve in highly compressible swirling flow. This was appreciated by George et al. [73]. Since, however, this is the first major study of the continuous static pressure characteristics of a vortex diode in compressible flow, it is likely that the performance parameter proposed in this work will be adopted by others working in this field. Bearing this in mind, it is proper to discuss the possible performance parameters in some detail, Euler number included.

(i) Validity of Euler Number

The data of Figs. 4.8 and 4.9 are shown in Figs. 4.11 and 4.12 in terms of Euler number using the usual approach of basing the density on the inlet pressure and the velocity as the inlet volume flow rate divided by the exit throat area. Figure 4.11, in particular, is most confusing since it suggests that the diode resistance rises, then falls, before rising again. This apparent fluctuation in the diode resistance is certainly not reflected in the basic data of Fig. 4.8. It must therefore be a false impression produced as a result of the incorrect application of equation (4.1). Indeed if equation (4.1) is considered more carefully, when the flow is choked both ρ and v will be constant and Euler number, therefore, becomes a simple linear function of ΔP. Figure 4.13 also shows the variation of the reverse flow Euler number, this time in terms of

downstream to upstream pressure ratio. The effect of choking can be seen at the pressure ratio of about 0.2 (P_u/P_d = 5) with a linear increase in the Euler number below this pressure ratio. Linear increase of reverse flow Euler number after choking was also reported by Zobel, as described earlier in Chapter 2 and shown in Fig. 2.6c. Vortex valve pressure-flow characteristics for incompressible fluid have been experimentally obtained by most workers by keeping the downstream pressure constant and changing the upstream pressures (usually exhausting to atmosphere). If experimental work had been carried out in this way, using steam as the working fluid, the characteristic would have been similar to those obtained with the incompressible flow and which have been presented by others. Figure 4.14 show a typical characteristic of the diode for steam which has similar shape as incompressible characteristic (data for Fig. 4.14 have been extracted from Fig. 4.11). Compressible flow characteristics of the diodes presented by Kumar [7] in terms of Euler number have also shown the effect of choking after a fall in Euler number. That a different characteristic can be obtained from different experimental techniques shows that the Euler number cannot produce a unique characteristic.

Evidently, therefore, Euler number is incapable of describing the pressure-flow characteristics of a vortex valve operating under compressible flow conditions - certainly not beyond the critical pressure ratio.

(ii) Isentropic Equation

A more suitable parameter was adopted by George et al. [73]. They compared the mass flow through a diode for a given pressure ratio to the ideal mass flow through an isentropic nozzle exposed to the same pressure ratio and having a throat area equal to the exit throat area of the diode. The resulting parameter is a discharge coefficient which immediately gives a measure of the effective resistance of the diode. George et al. presented their discharge coefficient as a function of an equivalent Mach number based on the pressure ratio. This is misleading and is also unnecessary since the pressure ratio itself is a more useful parameter. Furthermore, they only considered the case where their equivalent nozzle was choked, much of the data presented here is for pressures below those required for ideal choking. Consequently we may require an expression for the discharge coefficient when the ideal flow is supersonic and another for when the flow is subsonic. If M is the Mach number for the equivalent isentropic nozzle exposed to the same pressures as the diode, then

$$\frac{\dot{m}_{th}}{A_e} = \left[\frac{\gamma}{RT_u}\right]^{1/2} \frac{P_u M}{\left(1 + \frac{\gamma-1}{2} M^2\right) 2(\gamma-1)^{\gamma+1}} \qquad (4.2)$$

This is Shapiro's one-dimensional isentropic flow equation [78]. Condition of maximum flow per unit area can be found by setting M = 1 in equation (4.2). Thus,

$$\left(\frac{\dot{m}_{th}}{A_e}\right)_{max} = \left(\frac{\gamma}{R}\left(\frac{2}{\gamma+1}\right)^{\frac{\gamma+1}{\gamma-1}}\right)^{1/2} \frac{P_u}{\sqrt{T_u}} \qquad (4.3)$$

The discharge coefficient, Cd, is defined as the ratio of the actual flow to the isentropic flow rate.

$$Cd = \frac{\dot{m}_{act}}{\dot{m}_{th}} \tag{4.4}$$

Therefore for M < 1 (subsonic flow)

$$Cd = \frac{\dot{m}_{act} \left\{1 + \frac{\gamma-1}{2} M^2\right\}^{\frac{\gamma+1}{2(\gamma-1)}}}{\frac{A_e P_u}{\sqrt{T_u}} \left(\frac{\gamma}{R}\right)^{1/2} M} \tag{4.5}$$

and for M > 1 choked flow

$$Cd = \frac{\dot{m}_{act}}{\frac{A_e P_u}{\sqrt{T_u}} \left\{\frac{\gamma}{R} \left(\frac{2}{\gamma+1}\right)^{\frac{\gamma+1}{\gamma-1}}\right\}^{1/2}} \tag{4.6}$$

where

$$M = \left[\left(\left(\frac{P_u}{P_d}\right)^{\frac{\gamma-1}{\gamma}} - 1\right)\left(\frac{2}{\gamma-1}\right)\right]^{1/2} \tag{4.7}$$

The reverse flow data of Fig. 4.8 is shown in Fig. 4.15 in terms of Cd and it is seen that the data reduces almost to a single characteristic particularly for inlet pressures of 6 bar and above. The asymptotic value of 0.38 compares well with the value of 0.4 obtained by George et al. (who used a different design of vortex diode). When Syred and Roberts compared their data with that of George et al. they transformed ξ to produce a Cd for low pressure ratio data and they also obtained the minimum turning point shown in

Fig. 4.15 at a pressure ratio of about 1.

Although the graph in Fig. 4.15 does appear to represent a unique characteristic for the diode it is really the combination of two characteristics; one for the subcritical theoretical pressure ratio and another for the supercritical. The purpose of obtaining a single, dimensionless characteristic for the diode is so that a suitably scaled device can be designed for a given pressure and flow rate, whether the conditions be subsonic or supersonic. In this respect the use of Cd is not perfect since it is not represented by a single expression. Another parameter which could be adopted is a non-dimensional mass flow rate, i.e. multiplying the measured flow rate by suitable properties to obtain a dimensionless group. This non-dimensional mass flow rate, Cm, is given by:

$$Cm = \frac{\dot{m}\sqrt{R\,T_u}}{A_e\,P_u} \qquad (4.8)$$

Cm for reverse flow is shown in Fig. 4.16 where it is seen to be similar in shape to Fig. 4.15 but does not exhibit a minimum turning point at the lower pressure ratio.

Whilst this parameter does now give a single expression to the diode characteristic curve it is inferior to Cd in one respect. When the diode is choked, Cd approaches a value of 0.38 which has physical meaning in that it shows the diode is passing 38% of the flow that the equivalent ideal nozzle would pass. The asymptotic value of Cm, 0.25, on the other hand has no such meaning.

The parameters Cd and Cm both have their merits and weaknesses and there is little to choose between them. A useful parameter would be one that has the physical meaning of Cd and the single expression convenience of Cm. Such a parameter can be produced by adopting the expression given in equation (4.6), but using it over the whole pressure range, sub- and super-critical. Thus if we adopt this parameter, Cf, which is not truly a discharge coefficient since it does not strictly represent the incompressible regime, we can characterise the diode performance by,

$$Cf = \frac{\dot{m}}{\frac{A_e P_u}{\sqrt{T_u}} \left\{ \frac{\gamma}{R} \left(\frac{2}{\gamma+1} \right)^{\frac{\gamma+1}{\gamma-1}} \right\}^{1/2}} \qquad (4.9)$$

Since Cf is not a true discharge coefficient it is proposed that it be termed a "Discharge Factor". This discharge factor has also been adopted to investigate behaviour of the smaller diodes (D_e = 10 mm) at high pressure air, which will be given in the following section. Cf for the reverse flow data is shown in Fig. 4.17 where it can be seen that it acquires the same asymptotic value as Cd and displays the same subcritical form as Cm. The three parameters are compared in Fig. 4.18.

The forward flow data of Fig. 4.9 is presented in terms of the discharge factor, Cf, in Fig. 4.19. It can be seen that the data forms two similar asymptotes. These correspond to two different orifice plate sizes and clearly they should collapse together. Despite careful measurements and repeated tests, however, the

difference could not be accounted for and must be put down to experimental error. The asymptotic value of Cf for the bulk of the data in Fig. 4.19 is about 0.95 which shows that the diode presents very nearly the minimum possible resistance to the flow. Therefore in the forward flow direction the diode performance in compressible flow is comparable with that of incompressible flow. Finally, the forward and reverse flow characteristics of the diode, described by the discharge factor Cf, are shown together in Fig. 4.20.

4.2 **Air Characteristic of the Vortex Diode**

4.2.1 Experimental Apparatus and Instrumentation

Figure 4.21 shows a schematic of the characterisation rig used for the 10 mm throat vortex diodes. Although the figure shows four diodes, the basic characteristics were measured using just one diode. The configuration shown was used in the staging tests reported later in this section.

Air was delivered to the supply pipe at a maximum pressure of about 31 bar abs. and supplied to the vortex valves through a 50 mm pipe. A large Bellis and Morcom, 4-stage reciprocating compressure capable of providing air at the rate of 5 kg/s at 2.5 bar and 0.3 kg/s at 30 bar was used to supply the air. Air flow rate was measured upstream of the diodes in a 50 mm diameter pipe by an orifice plate with D and $^{D}/_{2}$ pressure tapping (BS 1042 [75]). A differential pressure transducer was used to measure differential pressure across the orifice plate. A digital voltmeter was used to

record the output voltage from the transducer. A dome loaded pressure controller was installed in the supply pipe for regulation of upstream pressure. Special hearing protection was necessary due to the very high level of noise, which was measured to be about 120 dB.

Four similar diodes were manufactured by numerically controlled machining from mild steel plate. The diodes were again of the Zobel design, Figs. 4.22 and 4.23.

The geometric values were as follows (see Fig. 2.9 for notation)

Inlet nozzle throat diameter	D_t = 12.7 mm
Axial throat diameter	D_e = 10 mm
Chamber height	H = 12.5 mm
Chamber outer diameter	D_o = 88.5
Length of the axial nozzle	ℓ_a = 39.5
Length of the tangential nozzle	ℓ_T = 42
Tangential connecting pipe diameter	d_o = 20
Angle of axial diffuser	θ = 7°
Angle of tangential diffuser	β = 4°8'

And in terms of ratios:

$$\frac{d_o}{D_e} = 2$$

$$\frac{D_t}{D_e} = 1.27$$

$$\frac{H}{D_e} = 1.25$$

$$\frac{D_o}{D_e} = 8.85$$

The same apparatus and instrumentation was used to characterise individual diodes and also the diodes in series. Figure 4.24 shows four diodes assembled in series.

4.2.2 Procedure

(i) Single diode

During the tests the upstream pressure, P_u, was gradually increased whilst the downstream, being the atmosphere, was kept constant. The characteristics for reverse flow were obtained for P_u = 2.7 bar to 31 bar absolute. The upstream pressures were measured using a calibrated pressure gauge. Reading of the voltage from the digital voltmeter was converted to pressure by an available calibration chart. Temperatures, at the exit of the last vortex valve were recorded by a digital thermometer through a Ni/Cr thermocouple.

(ii) Diodes in series

In order to be able to determine the reverse flow characteristics of more than one diode connected in series, and particularly to investigate the effect of increasing the number of diodes, the upstream pressure of the first diode (Fig. 4.21) in any combination (two, three or four diodes in series) was increased from

2.7 bar (40 psi) to 31 bar (450 psi) at 1.72 bar (25 psi) intervals. For each valve setting the upstream pressure of each diode in line and the temperature downstream of the last diode were recorded. Measurement of pressure differential across the orifice plate provided the data for calculation of the mass flow rate through diodes.

To provide a basis for comparison the diodes were replaced by orifice plates with 5 mm diameter and the above test was repeated.

4.2.3 Results

(i) Single diode

The results obtained for a single diode are plotted as discharge factor, Cf against pressure ratio $\frac{P_u}{P_d}$ in Figs. 4.25-4.28. The dimensions of the diodes differed very slightly and because of this, there is seen to be a small difference between their resistances, Fig. 4.29. The choking of the diode is seen in each characteristic at pressure ratio of about 4.

(ii) Diodes in series

By increasing the number of diodes in series from 1 to 4 the total resistance increased and hence the mass flow for a given overall pressure ratio decreased. This can be seen in Fig. 4.30. In Figs. 4.31-4.33 the characteristics for the individual diodes within the cascade are shown for 2, 3 and 4 diodes in series, respectively.

The discharge factor for each diode was calculated using the pressure measured at its inlet, although the whole characteristic in say, Fig. 4.33 is shown as a function of the overall pressure ratio $(\frac{P_{u1}}{P_d})$ across all the diodes. The discharge factor was calculated based on the upstream pressure of each individual diode. It can be seen that only the last diode in line, with a Cf value equal to 0.38, is choked, since it operates at the highest pressure ratio. Figure 4.35 shows comparison between diodes and orifices. The same equation (eq. (4.9)) was used to calculate values of Cf for the orifices.

4.3 **Discussion**

Diode characteristics measured with superheated steam and air have been shown to be similar. By using superheated steam, however, and condensing the flow at significantly sub-atmospheric pressures, the range of the inlet to outlet pressure ratio can be greatly extended. In the case of air the highest pressure ratio of about 30 was achieved by increasing the upstream pressure of the diode. Downstream was kept constant at atmospheric pressure. In reverse flow the diode is seen to choke at a pressure ratio of about 4. The theoretical pressure ratio for superheated steam in one-dimensional flow is 1.86 and for air is 1.89. When the flow is leaving the vortex chamber through the axial throat it has a large amount of swirl. The throat is the minimum area in the diode and it is here that the flow might be expected to choke. However, theoretical considerations together with the little experimental work available,

as discussed in Section 3.9, shows that choking in a swirling nozzle will not take place at the throat, since the axial Mach number is reported to be less than unity at the minimum cross-sectional area. In order to achieve a choking condition, a higher critical pressure ratio would be expected with swirling flow.

From Fig. 4.15 the discharge coefficient, Cd, is seen to fall to a minimum of 0.2 before rising to its asymptotic value of 0.38. In moving from a value of 0.2 to 0.38 the diode resistance can be considered as being halved. It is known, and was shown by King and Syred [79], that the high resistance in vortex valves is due mainly to the fluid dynamic blockage developed in the axial throat by the reversed flow zone associated with vortex breakdown in the exit and which was described in Section 3.6. As the pressure ratio in Fig. 4.15 increases from 1 to 4 so the axial component of velocity will be increasing until it reaches the local sonic velocity. At this point there will be no reversed flow in the exit throat since this is wholly incompatible with the concept of choking. In other words, the reversed flow zone has been swept downstream (the existence of vortex breakdown in supersonic flow will be discussed in Chapter 6). From this it can be seen that it is undesirable to operate a vortex diode at a pressure ratio greater than 4 and if possible it should be kept down to 2.

Comparing the choked mass flow rates in Figs. 4.8 and 4.9, the ratio of the forward and reverse mass flow rates is about 2.5 and already it is evident that the diode performance is substantially

less than would be expected with incompressible flow. This is shown more clearly in Fig. 4.10 where the ratio of forward to reverse flow for superheated steam falls rapidly from a value of about 6 in the subsonic region to the asymptote of 2.5 for the choked flow. It should be pointed out that the present investigation was instrumented to measure the relatively large pressure and flow rates found with compressible flow and therefore the accuracy of the data when the pressure ratio approaches one is suspect.

The forward flow characteristic of the diode, in Fig. 4.19, simply shows the effect of choking. It is perhaps surprising, considering the path through which the flow has to travel, that the measured flow is so close to the theoretical, one-dimensional critical mass flow.

Clearly a vortex diode operates at its best when exposed to pressure ratios just greater than one (i.e. incompressible flow) and certainly at pressure ratios somewhat less than four. In order to achieve this, diodes in series, such that they shared pressure drop between them, were tested. The diodes each had the same throat area, thus the pressure drop was shared almost equally, Fig. 4.34. A value of discharge factor, C_f,was calculated for the cascade by using the minimum area (i.e. diode throat) and the overall pressure ratio. This value was seen to fall from 0.38 to 0.14 by increasing the number of diodes to four, Fig. 4.35. As this shows, cascading of the diodes could be an ideal solution when throttling flow from a high initial pressure to a modest one.

It could also be argued, however, that simply cascading a number of equal diodes in series is bound to lead to a higher resistance but it also leads to a more tortuous path for the flow and hence the greater possibility of blockage. The argument for arranging diodes in series is that by doing so some of them will be operating with an incompressible pressure ratio and will hence recover some of their performance. If the diodes are of differing sizes the choking behaviour of the cascade will be different.

Consider two diodes in series: in compressible flow work it is usual for the inlet stagnation pressure and temperature to be kept constant while the downstream pressure (P_d) is gradually lowered.

If the second diode is the same size as the first, then it will choke first and as the downstream pressure is lowered further a shock moved down to the downstream of the second diode. However if flow can be choked at the second diode then flow upstream of this diode cannot be affected any more by lowering the downstream pressure. Although the seocnd diode has choked, the condition at the first diode remains unchanged and will not reach the critical condition. However, if the second diode is larger than the first, then by lowering the downstream pressure, p_d, the first diode may choke first. If on further lowering of the downstream pressure the flow can also be choked at the second diode then flow upstream of this diode cannot then be affected any more by lowering the downstream pressure. Therefore, if the Mach number reaches unity at at the second as well as the first, then from equation (4.8) the value of

$\left(\frac{\dot{m}\sqrt{RT_u}}{A_e P_u}\right)$ must have the same value at both diodes since $\dot{m}$, T_u and R will be very nearly constant. To obtain this with P_u at the first diode greater than P_u at the second, the second diode must therefore be larger than the first to avoid choked flow at the second diode. To achieve this condition the throat area of the second diode A_{e2} must be $= A_{e1} \times \frac{P_{u1}}{P_{u2}}$. However it has been shown that it is preferable to operate a diode in the unchoked condition and to this end it is advisable to arrange for the diodes in the cascade to be of the same size.

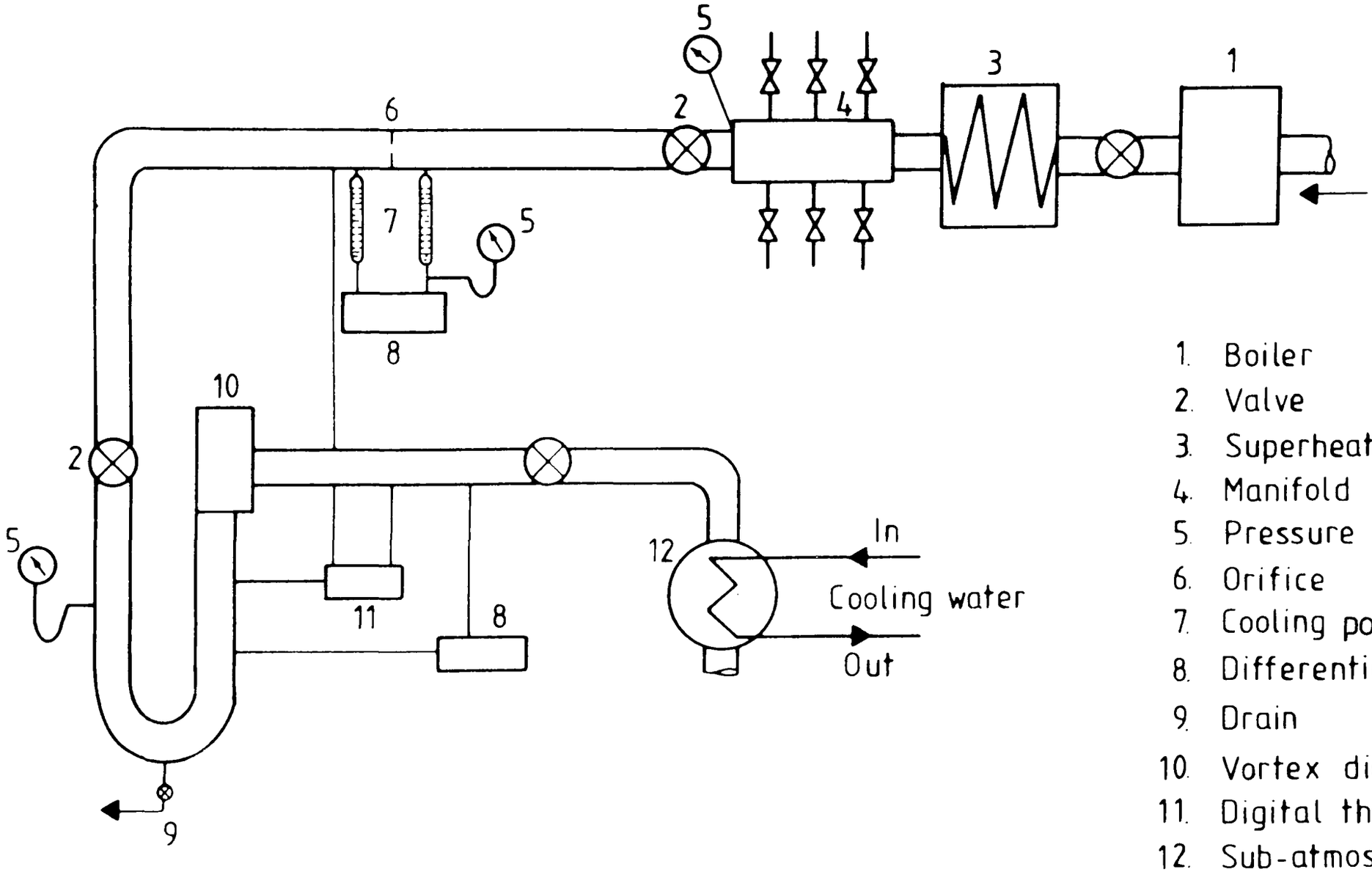

1. Boiler
2. Valve
3. Superheater
4. Manifold
5. Pressure gauge
6. Orifice
7. Cooling pots
8. Differential pressure transducer
9. Drain
10. Vortex diode
11. Digital thermometer
12. Sub-atmospheric condenser

Fig. 4.1 Vortex Diode Superheated Steam Characterisation Rig

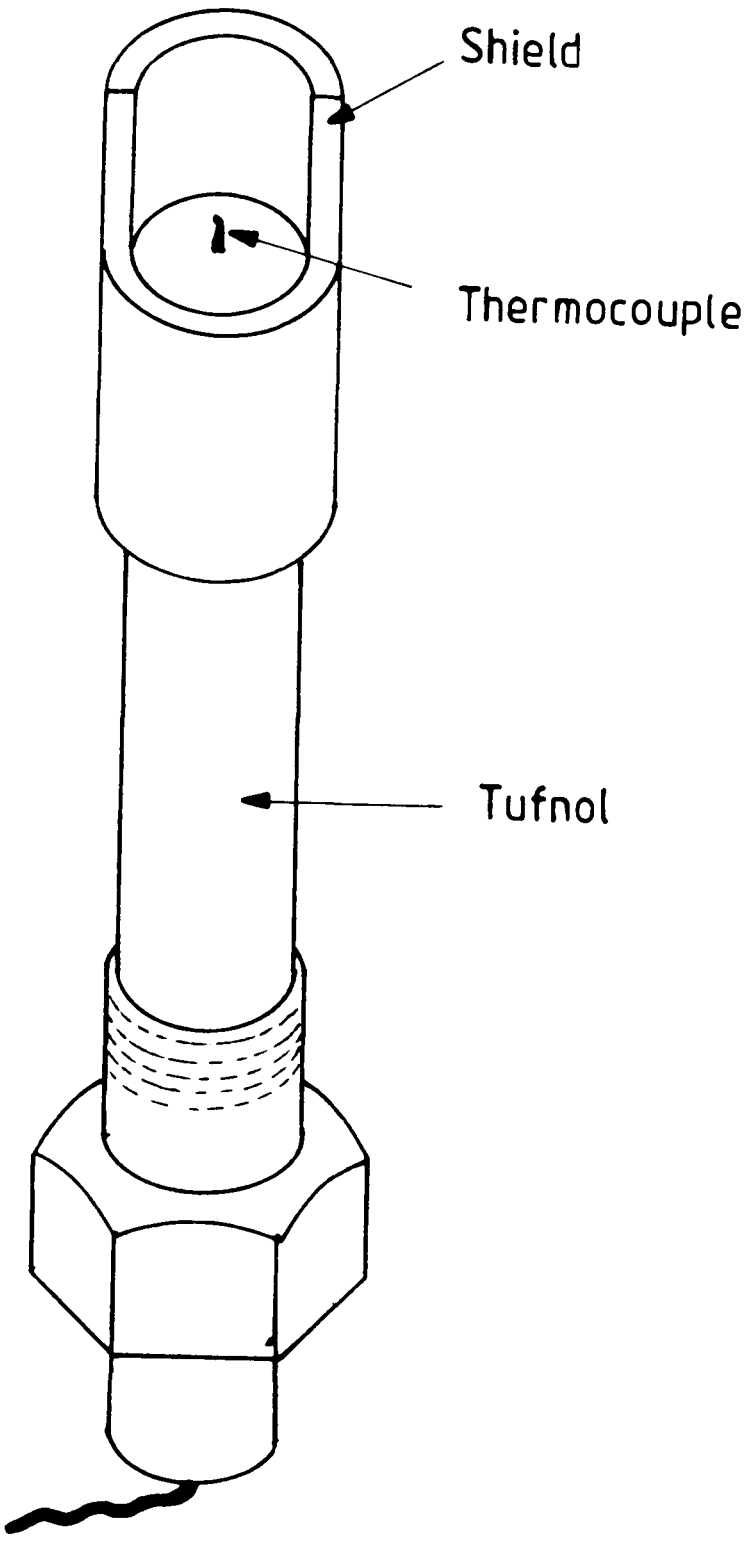

Fig. 4.2 Schematic Diagram of Half-Shielded Thermocouple Temperature Probe

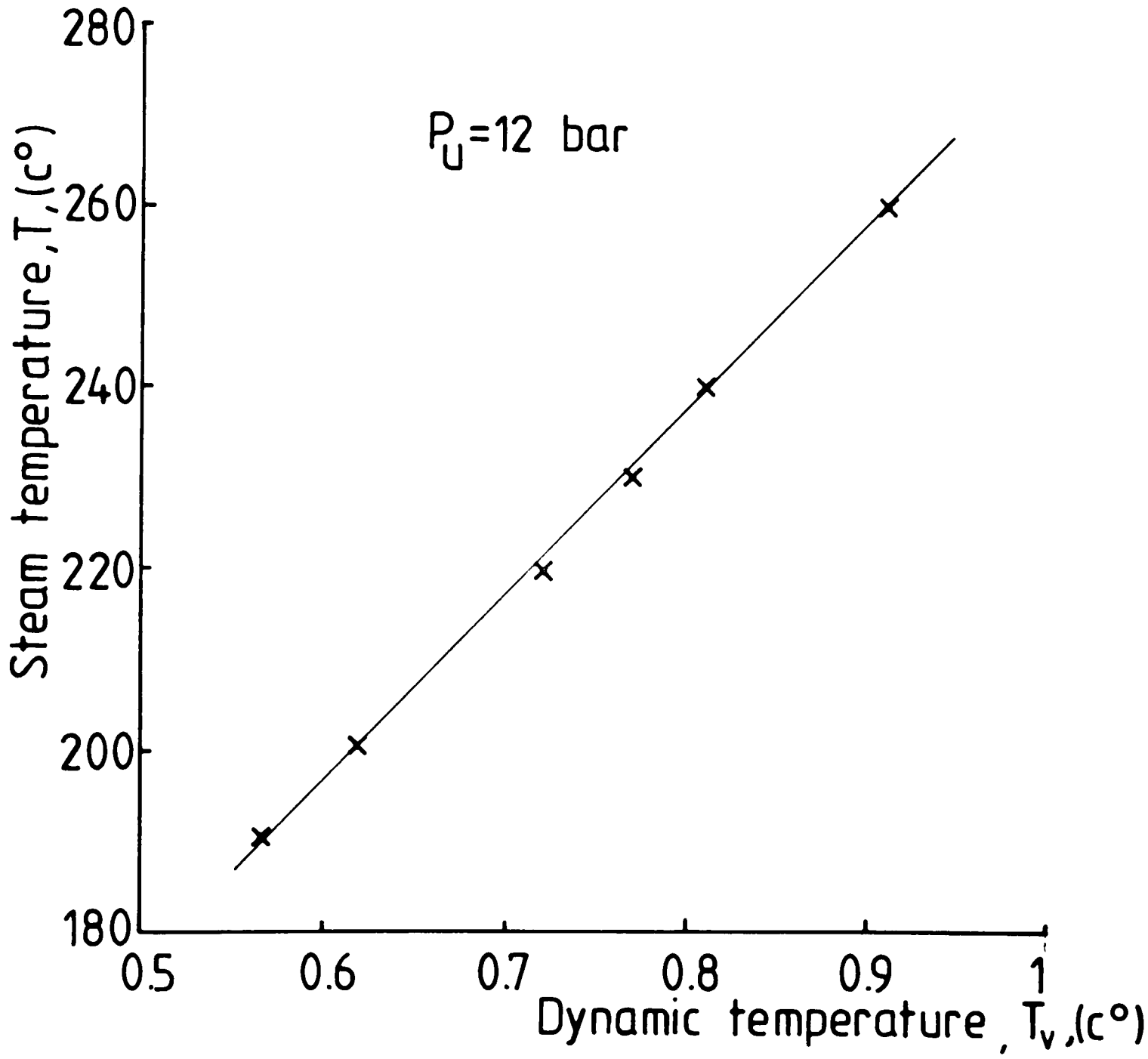

Fig. 4.3 Variation of Dynamic Temperature

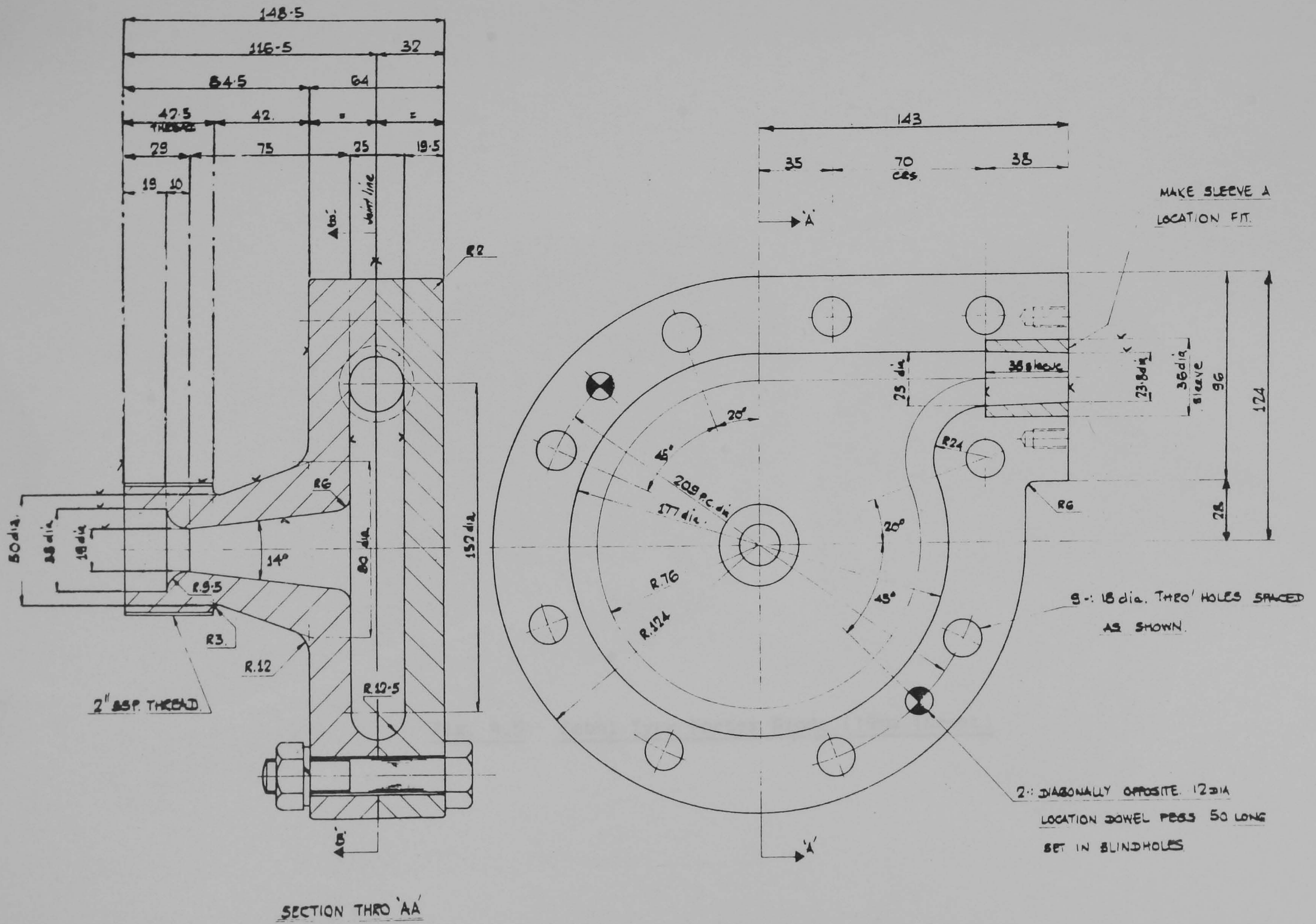

Fig. 4.4 Detail of Zobel Type Vortex Diode (19 mm Throat)

Fig. 4.5 Zobel Type Vortex Diode (19mm Throat)

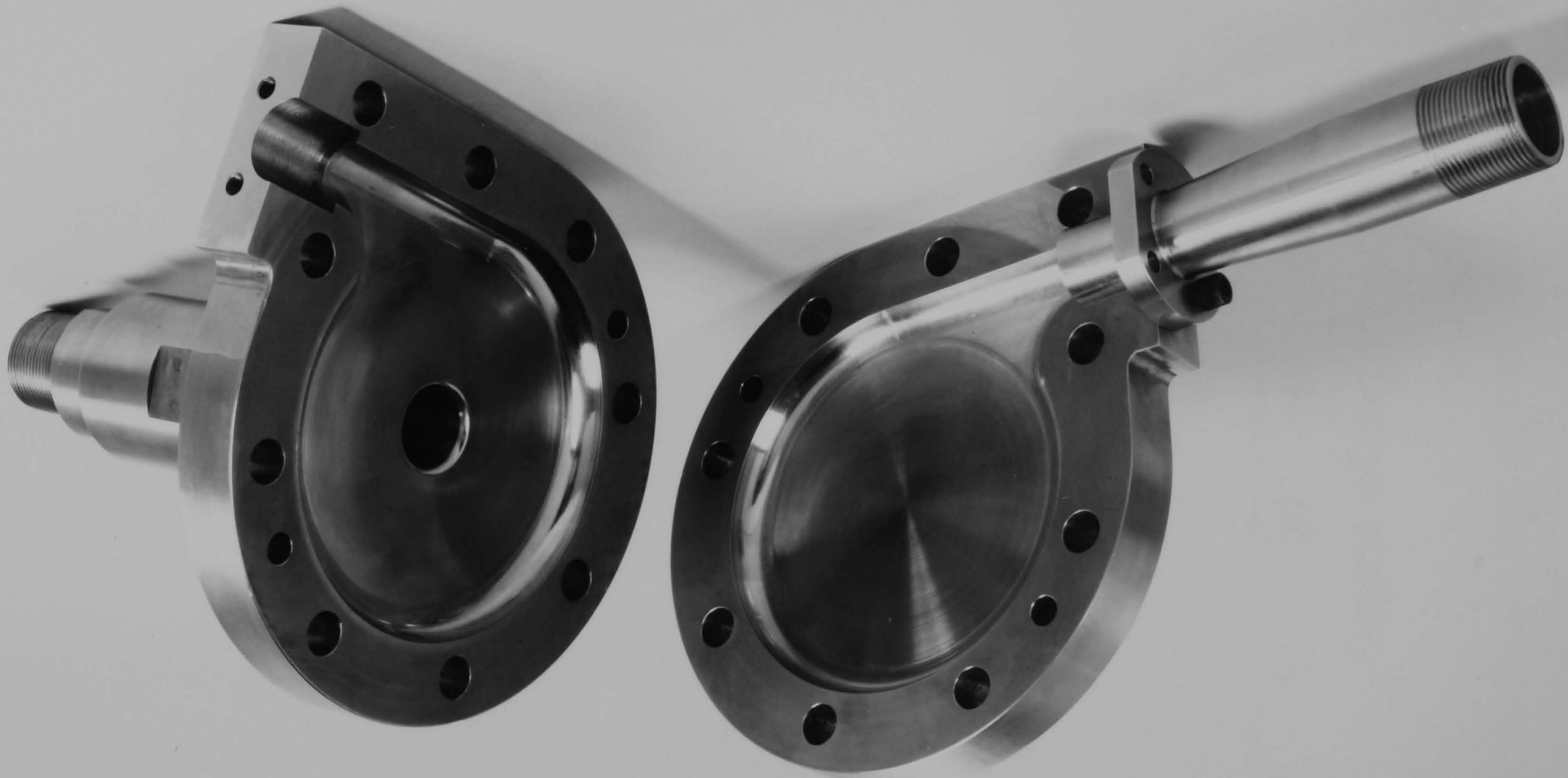

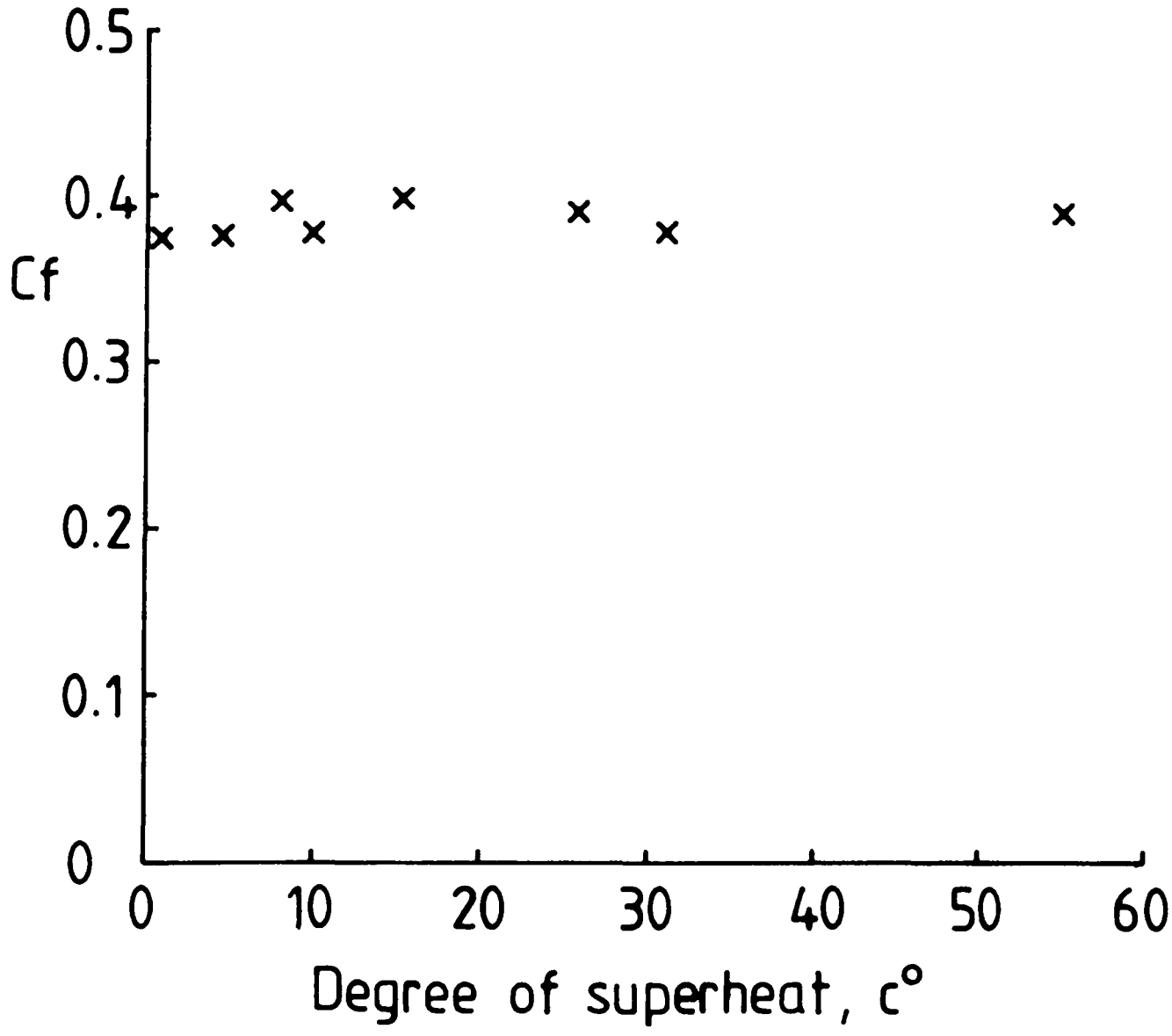

Fig. 4.6 Characteristic of Diode for Various Degree of Superheat

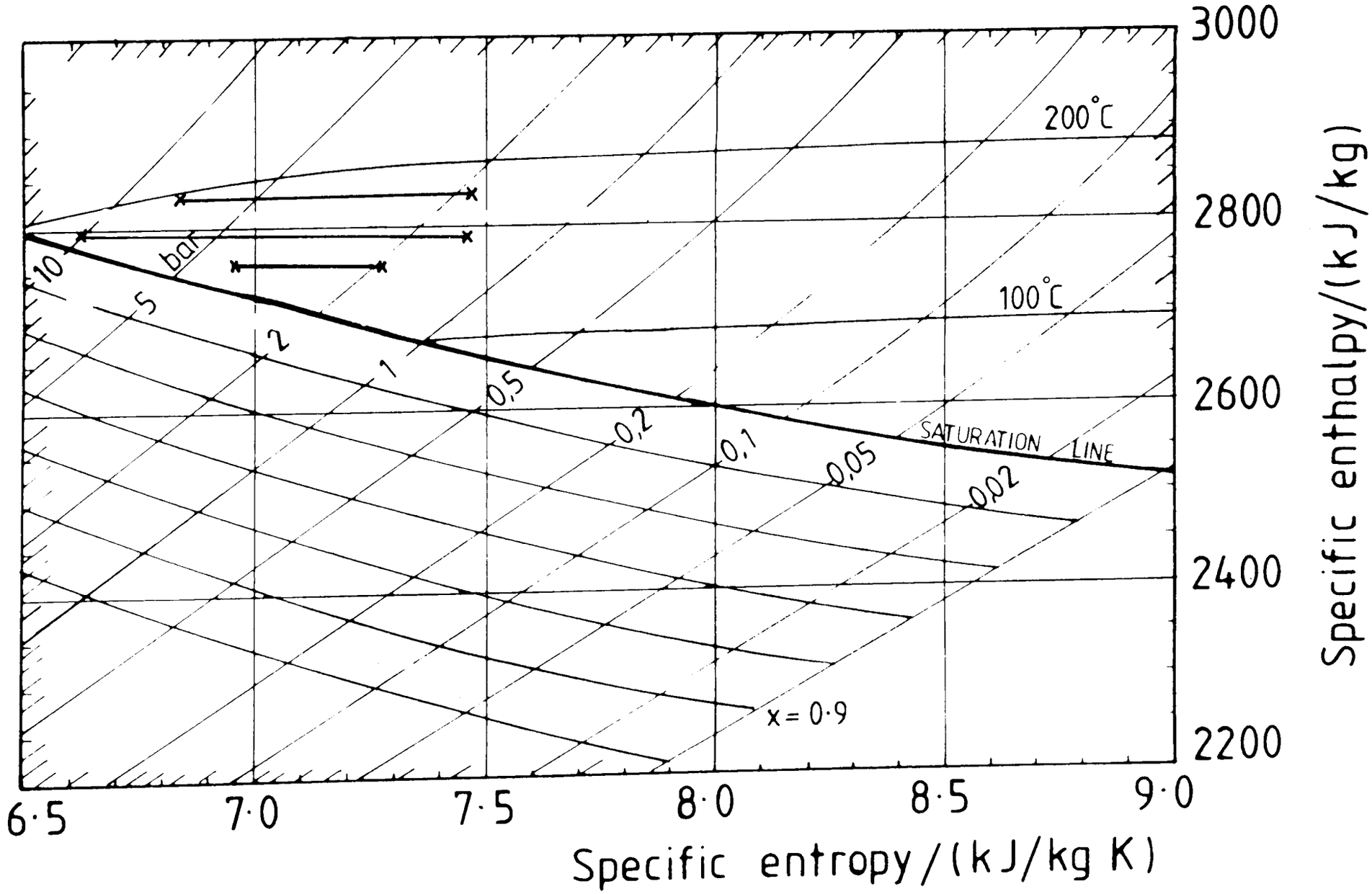

Fig. 4.7 Steam Conditions in Inlet and Outlet to Vortex Diode

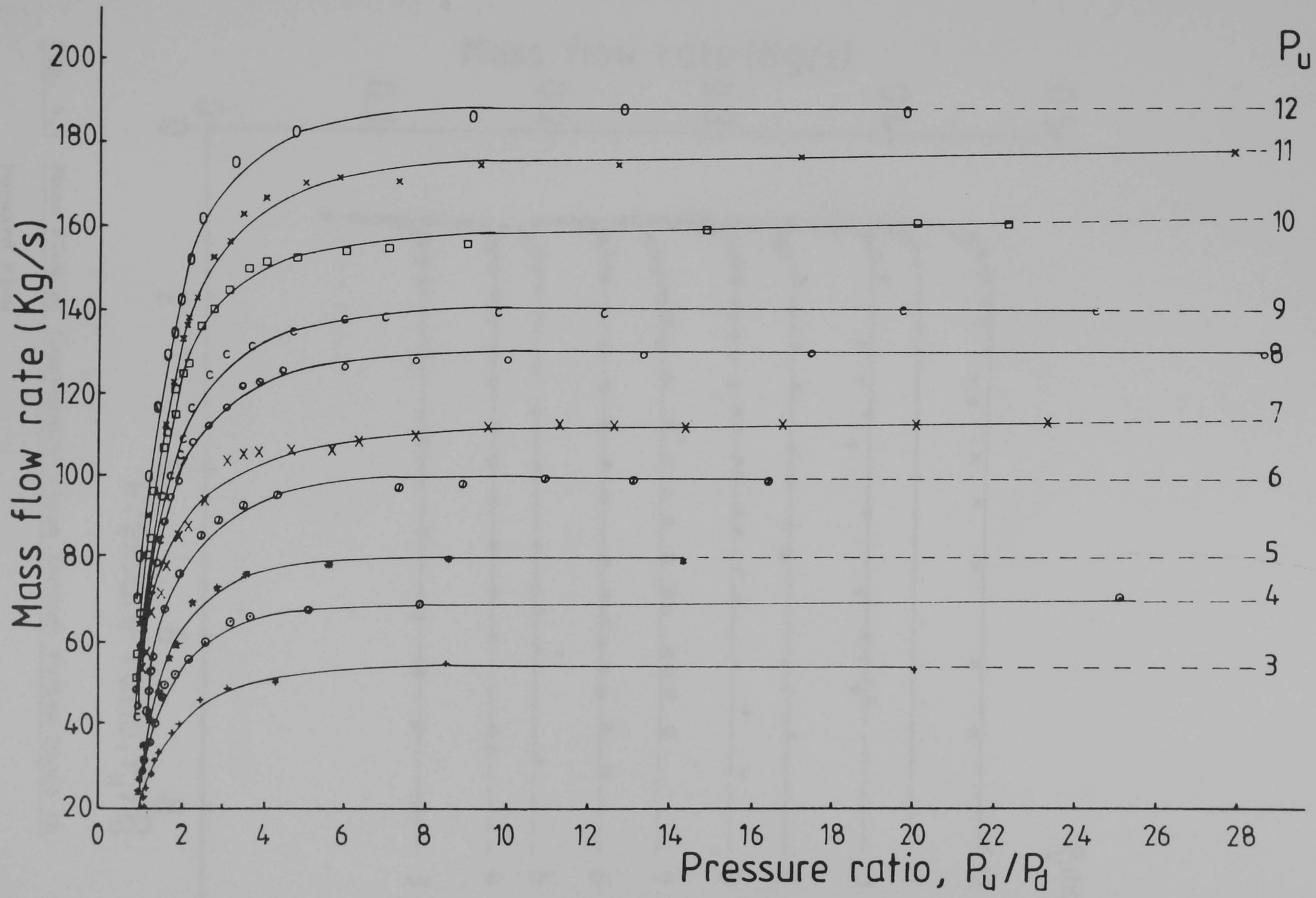

Fig. 4.8 Mass Flow of Superheated Steam Through Vortex Diode in Reverse Flow

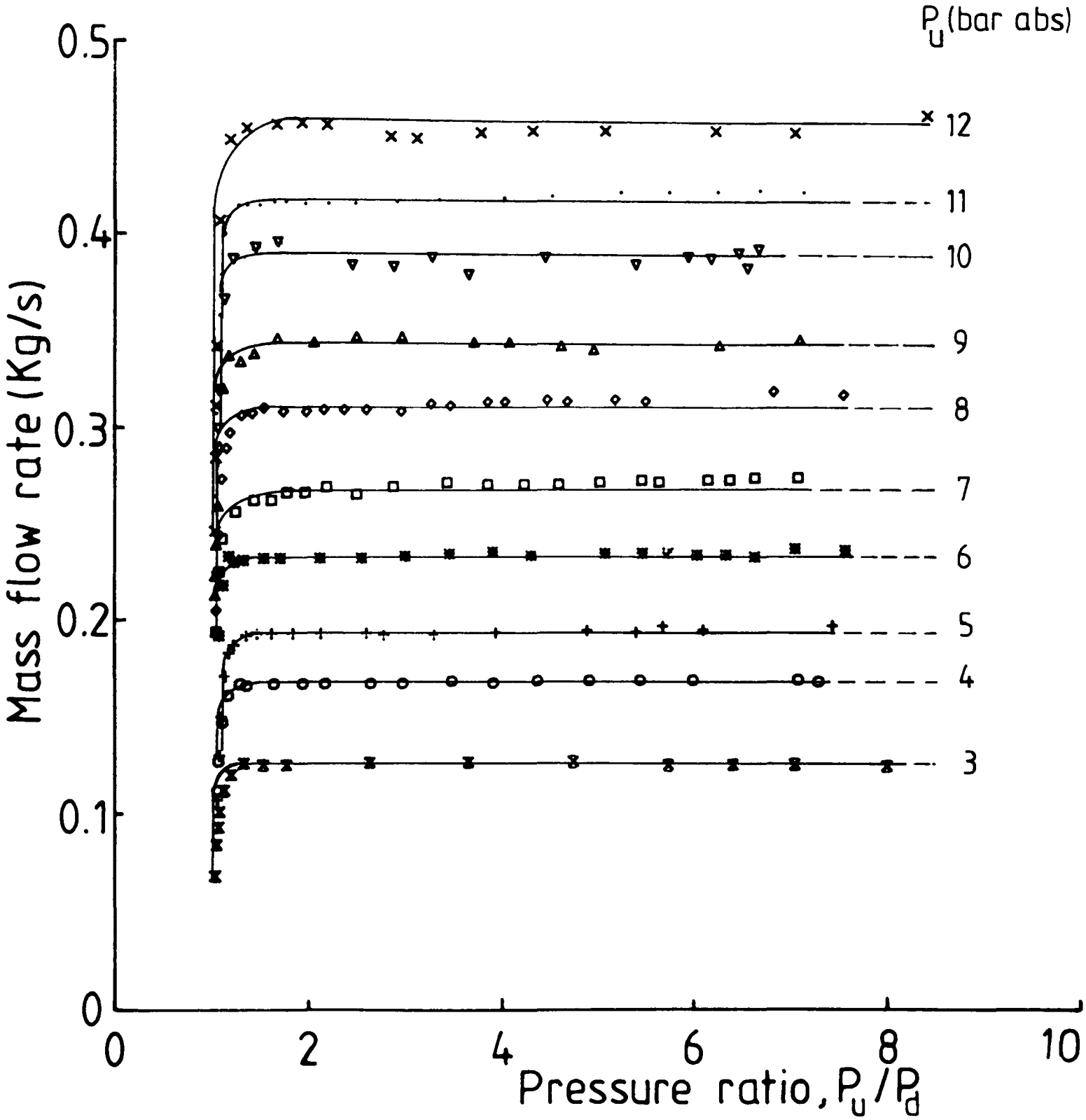

Fig. 4.9 Mass Flow of Superheated Steam Through Vortex Diode in Forward Flow

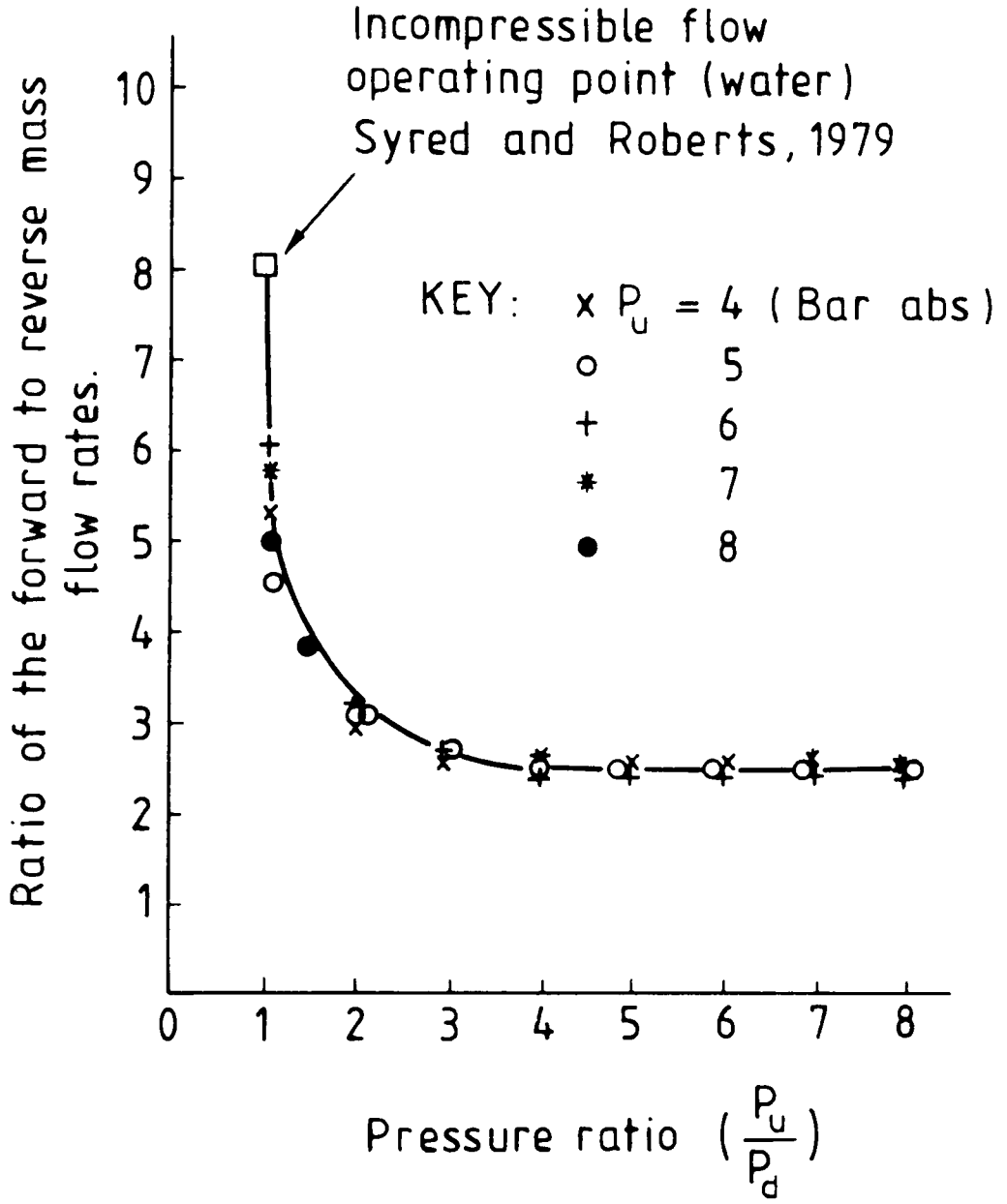

Fig. 4.10 Effect of Compressibility on Diode Performance

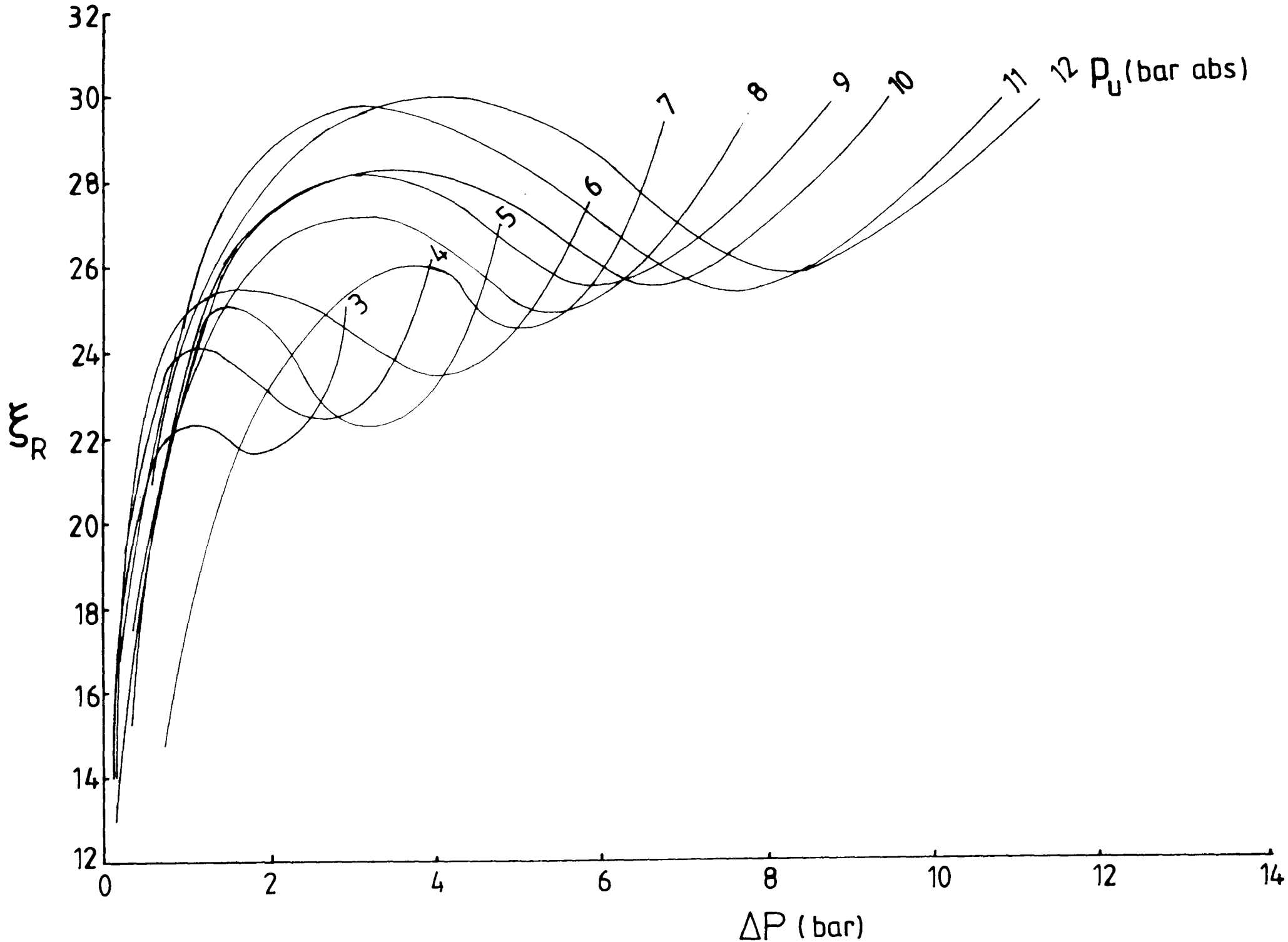

Fig. 4.11 Reverse Flow Euler Number

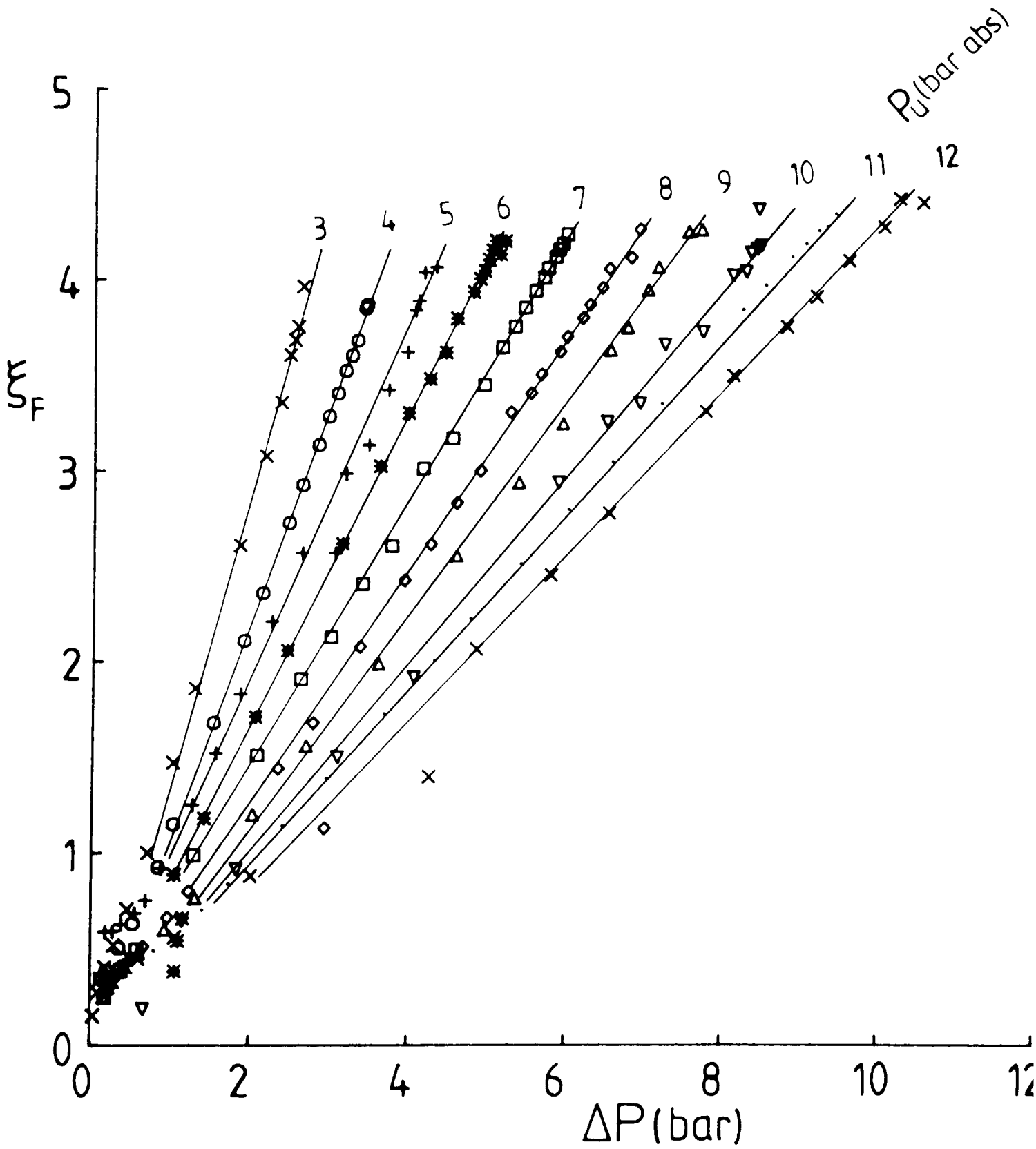

Fig. 4.12 Forward Flow Euler Number

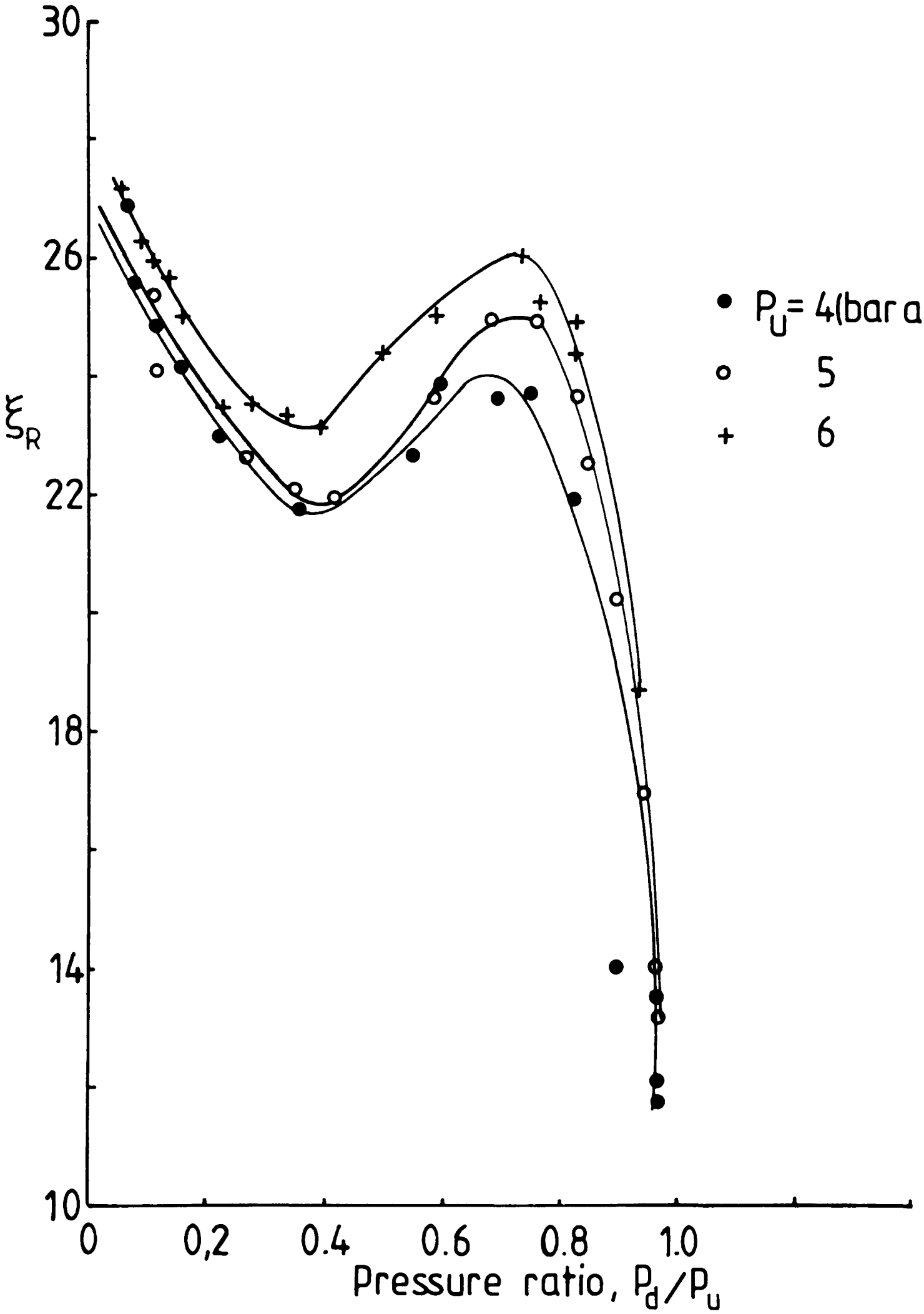

Fig. 4.13 Reverse Flow Euler Number

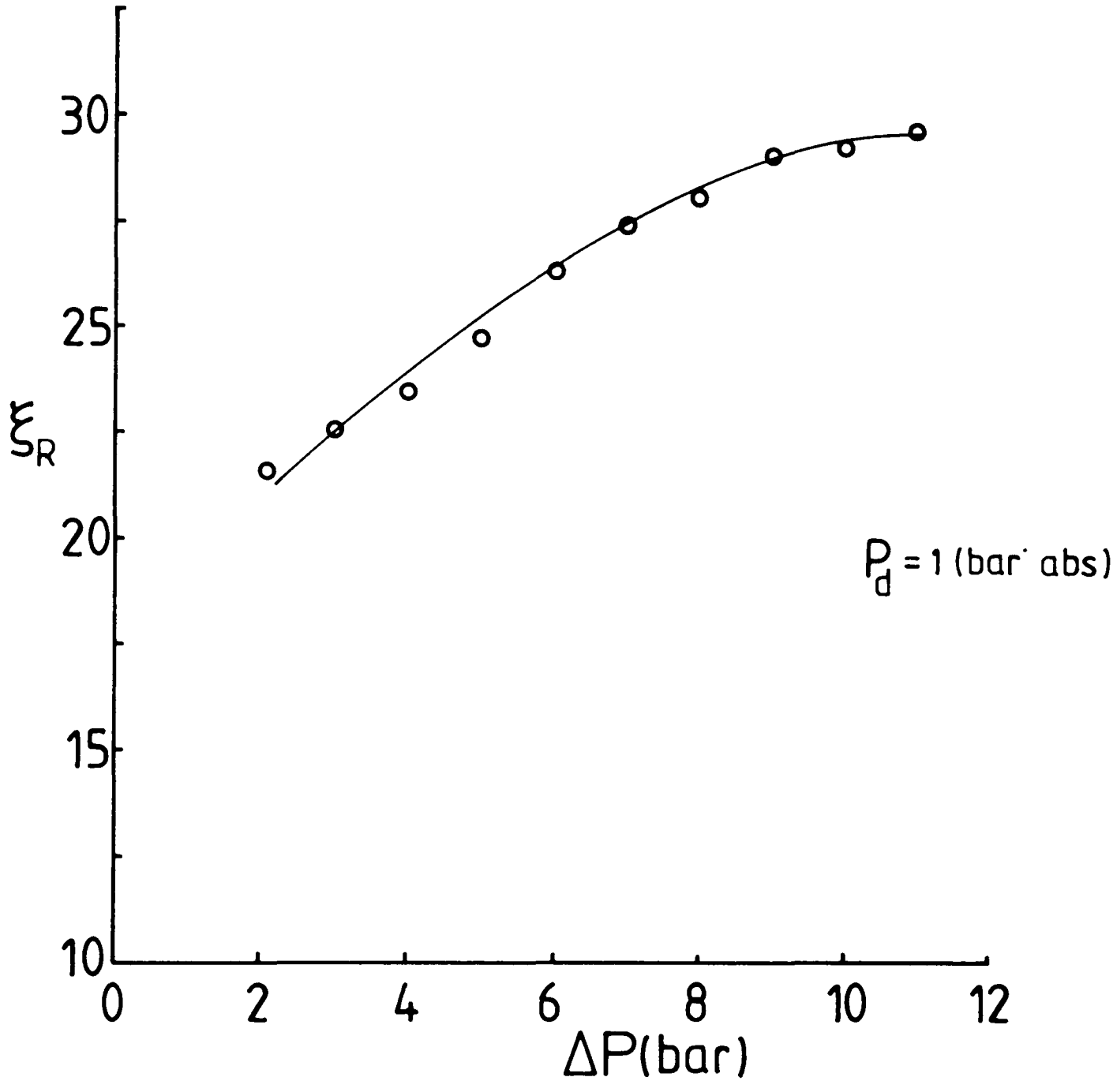

Fig. 4.14 Reverse Flow Euler Number

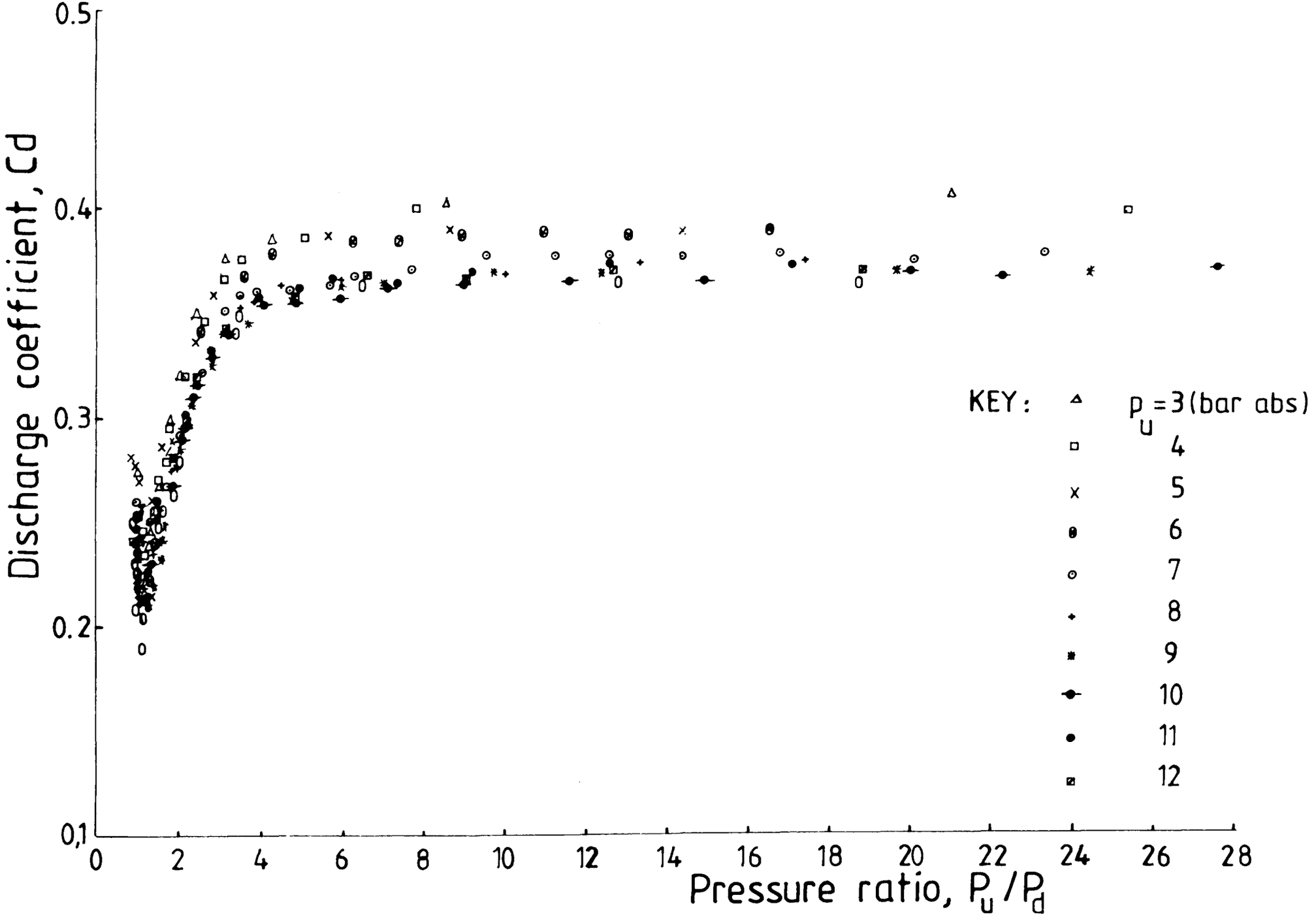

Fig. 4.15 Reverse Flow Discharge Coefficient

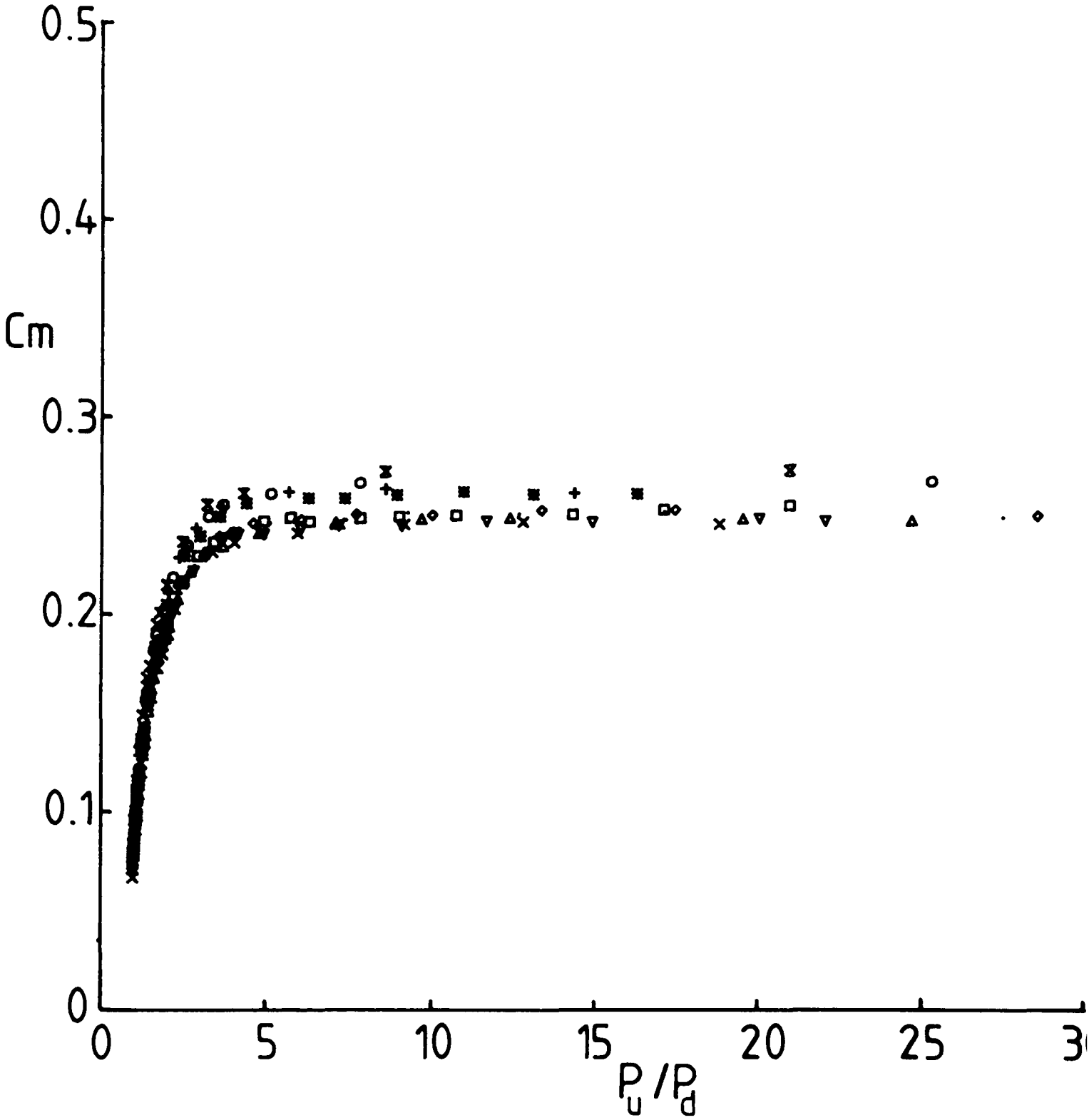

Fig. 4.16 Reverse Flow Non-Dimensional Mass Flow

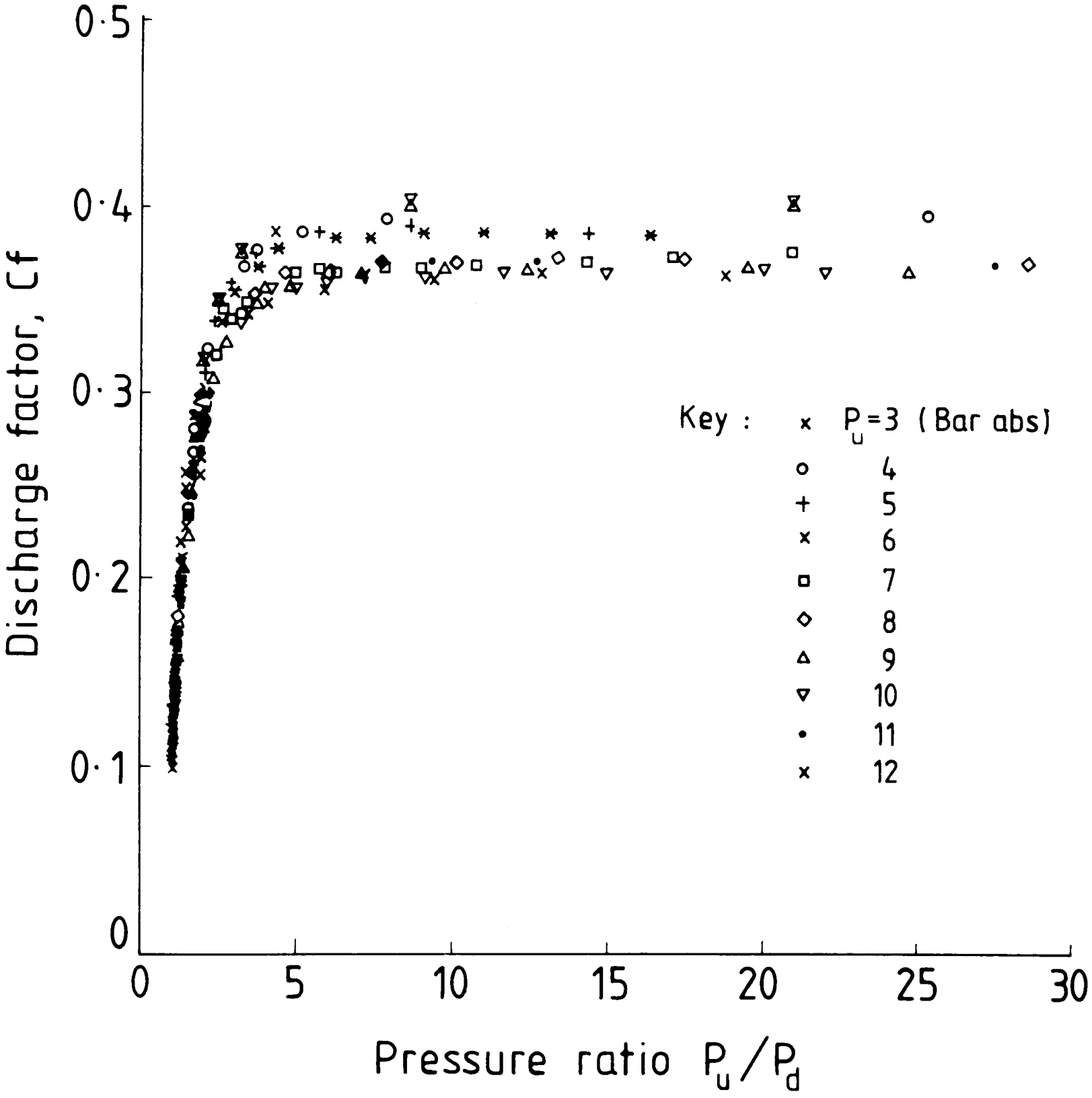

Fig. 4.17 Reverse Flow Discharge Factor

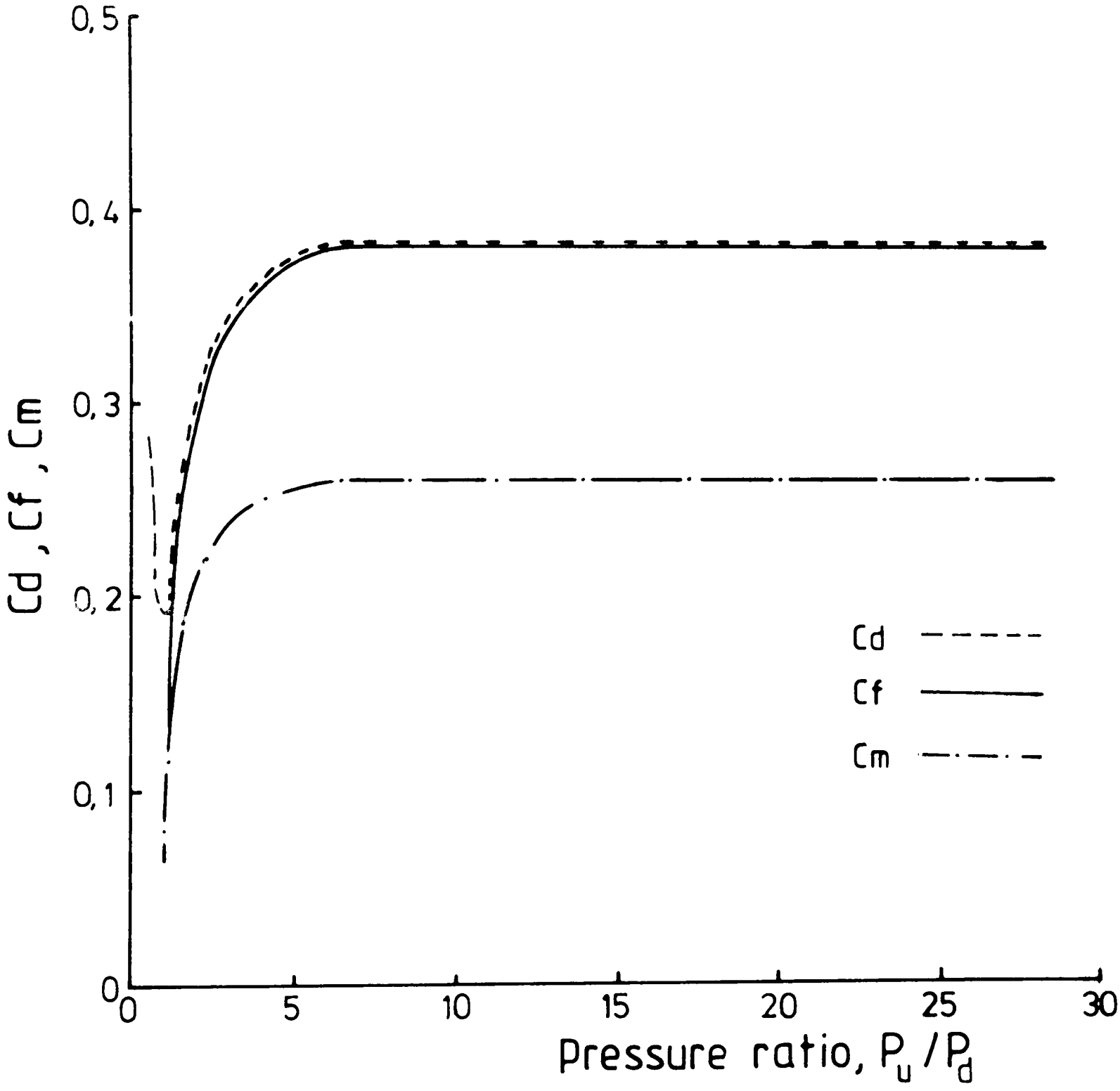

Fig. 4.18 Comparison of Cd, Cf, Cm

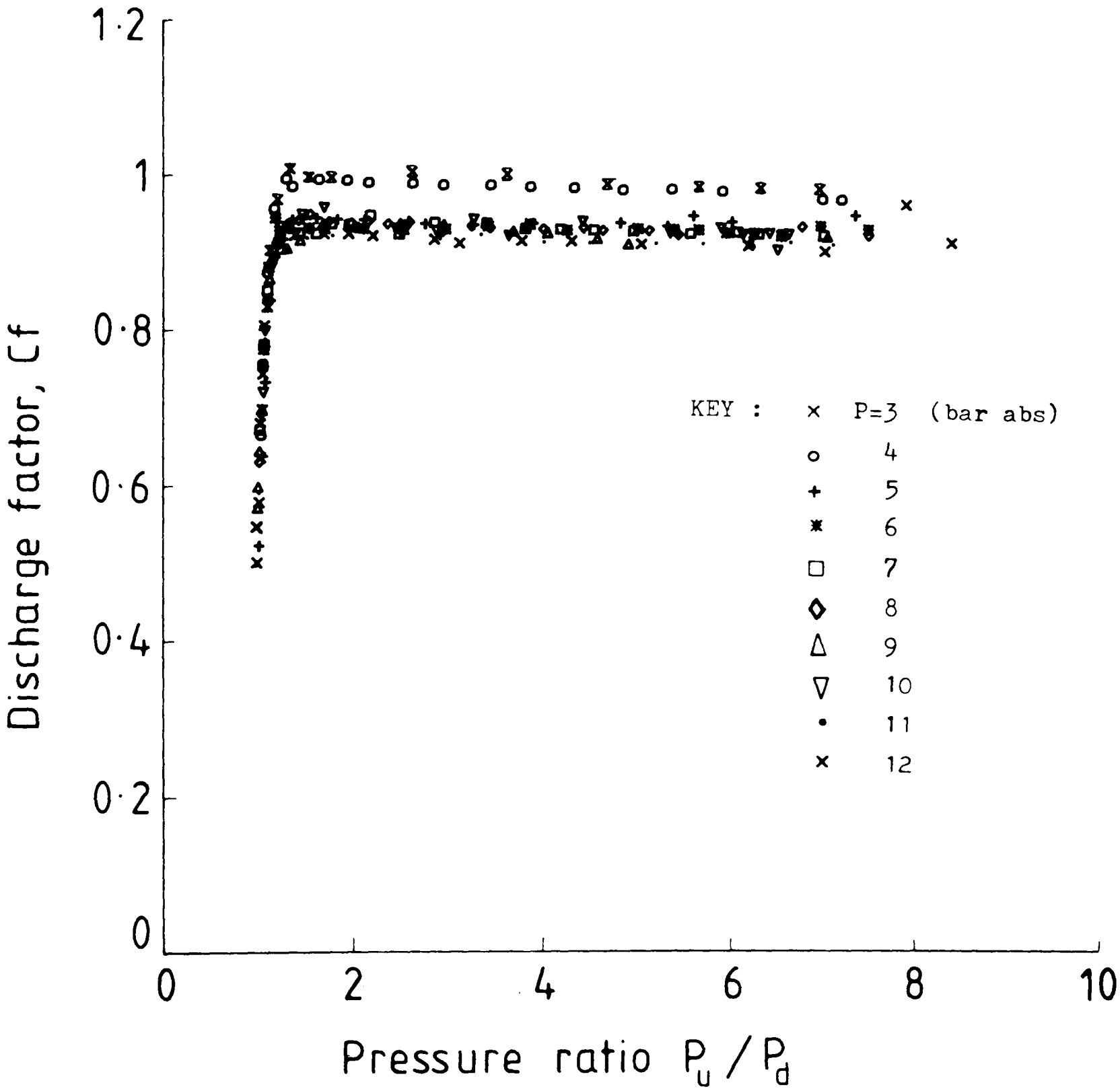

Fig. 4.19 Forward Flow Discharge Factor

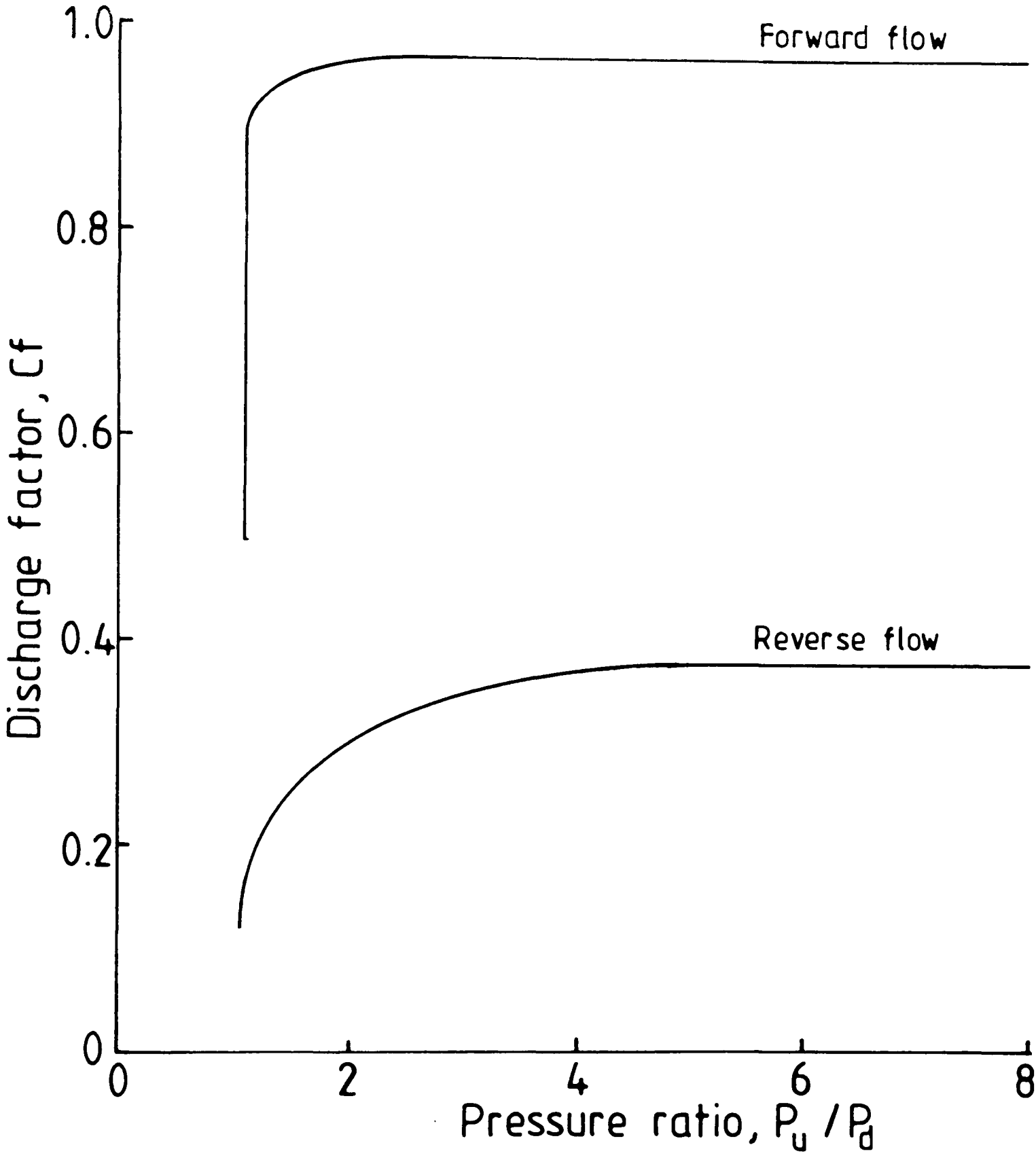

Fig. 4.20 Forward and Reverse Flow Characteristics

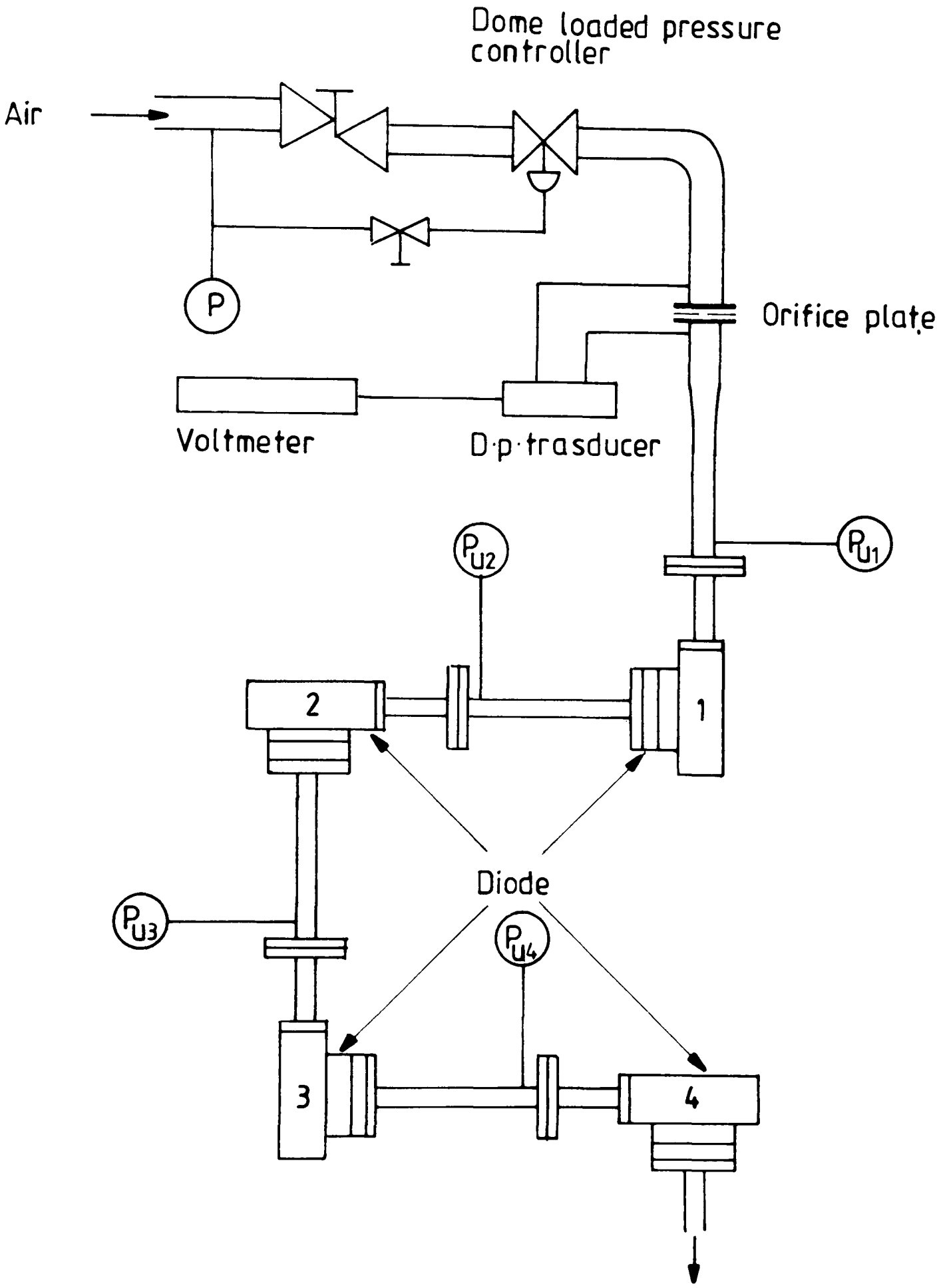

Fig. 4.21 Vortex Diode Air Characterisation Rig

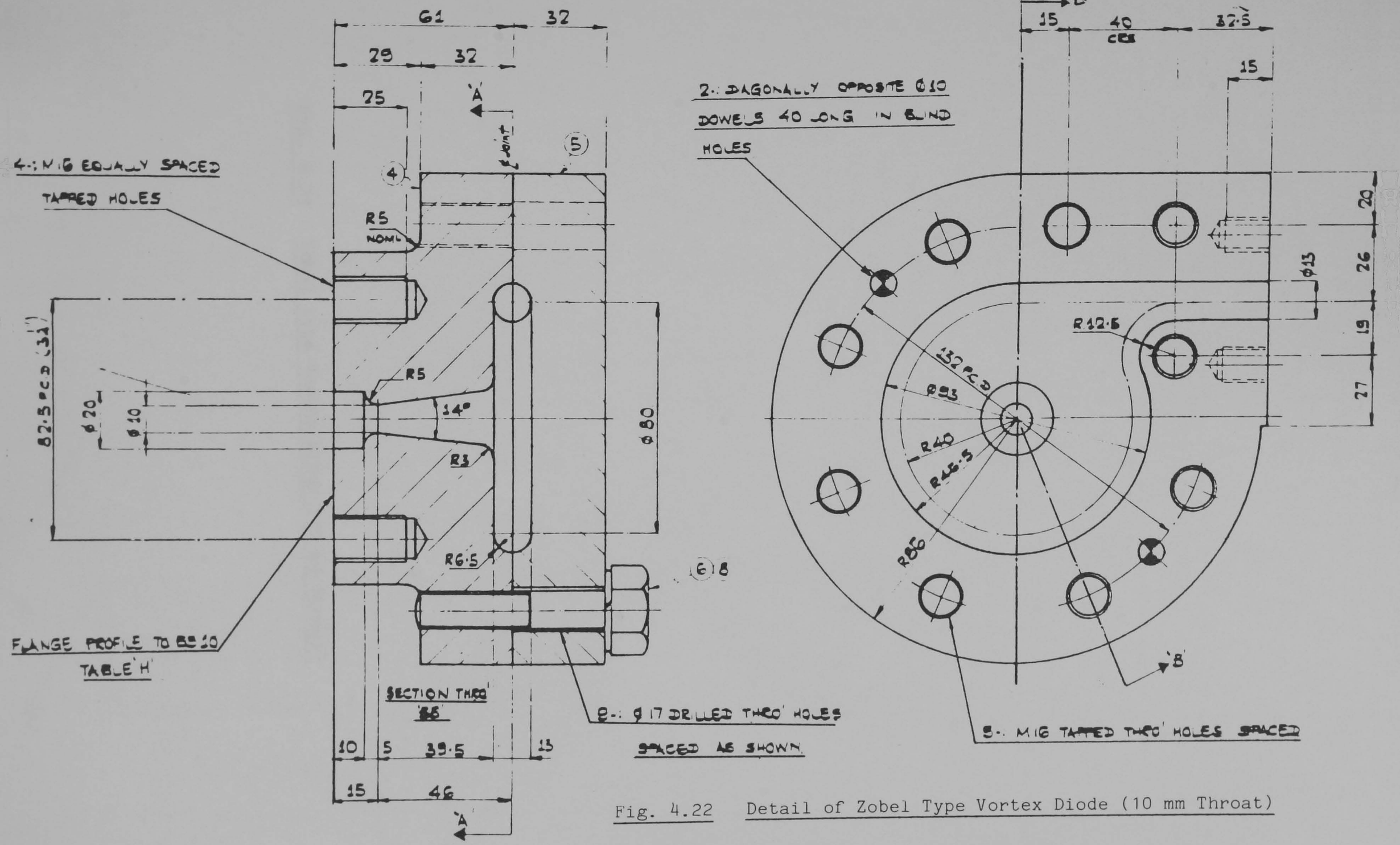

Fig. 4.22 Detail of Zobel Type Vortex Diode (10 mm Throat)

Fig. 4.23 Zobel type Vortex Diode (10 mm Throat)

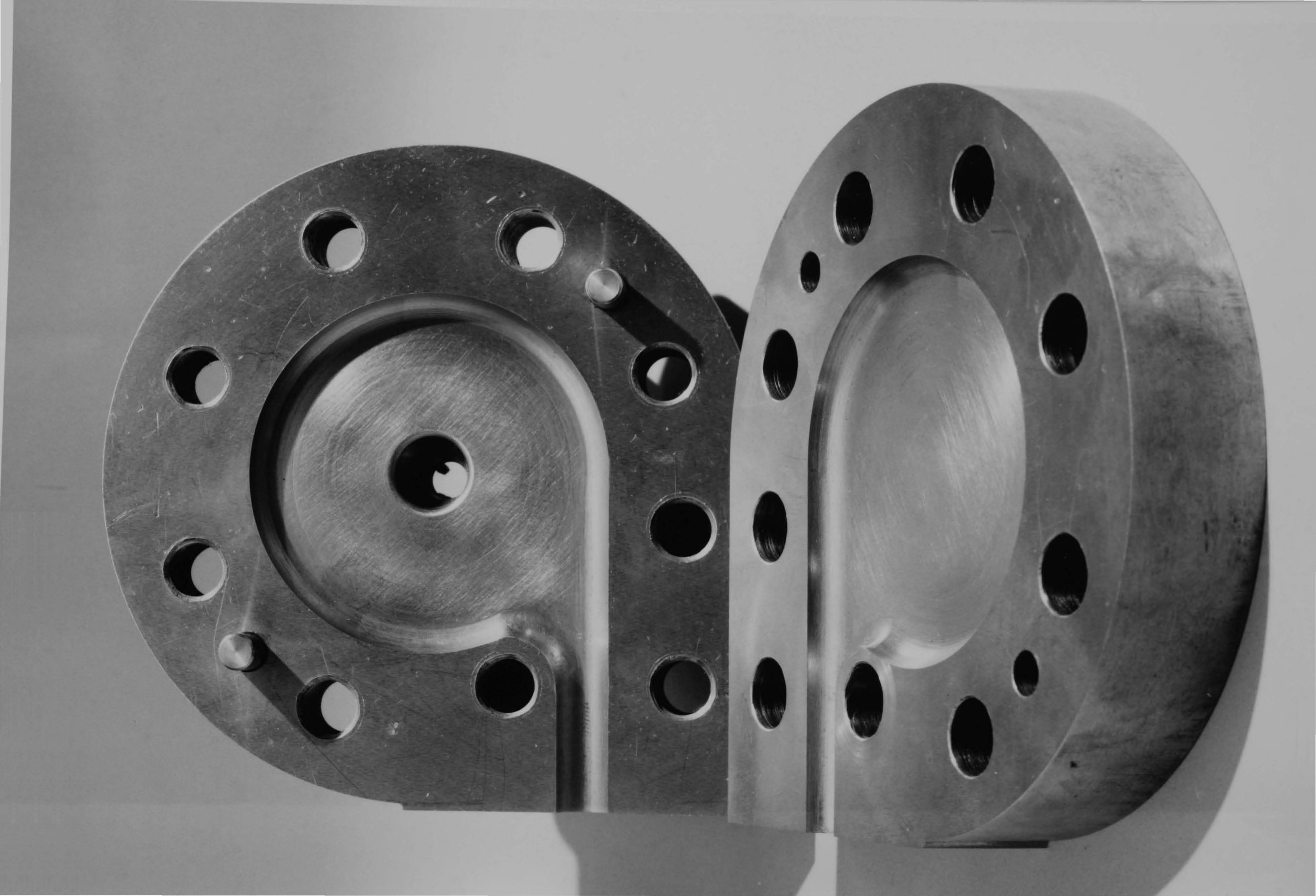

Fig. 4.24 Diodes in Series

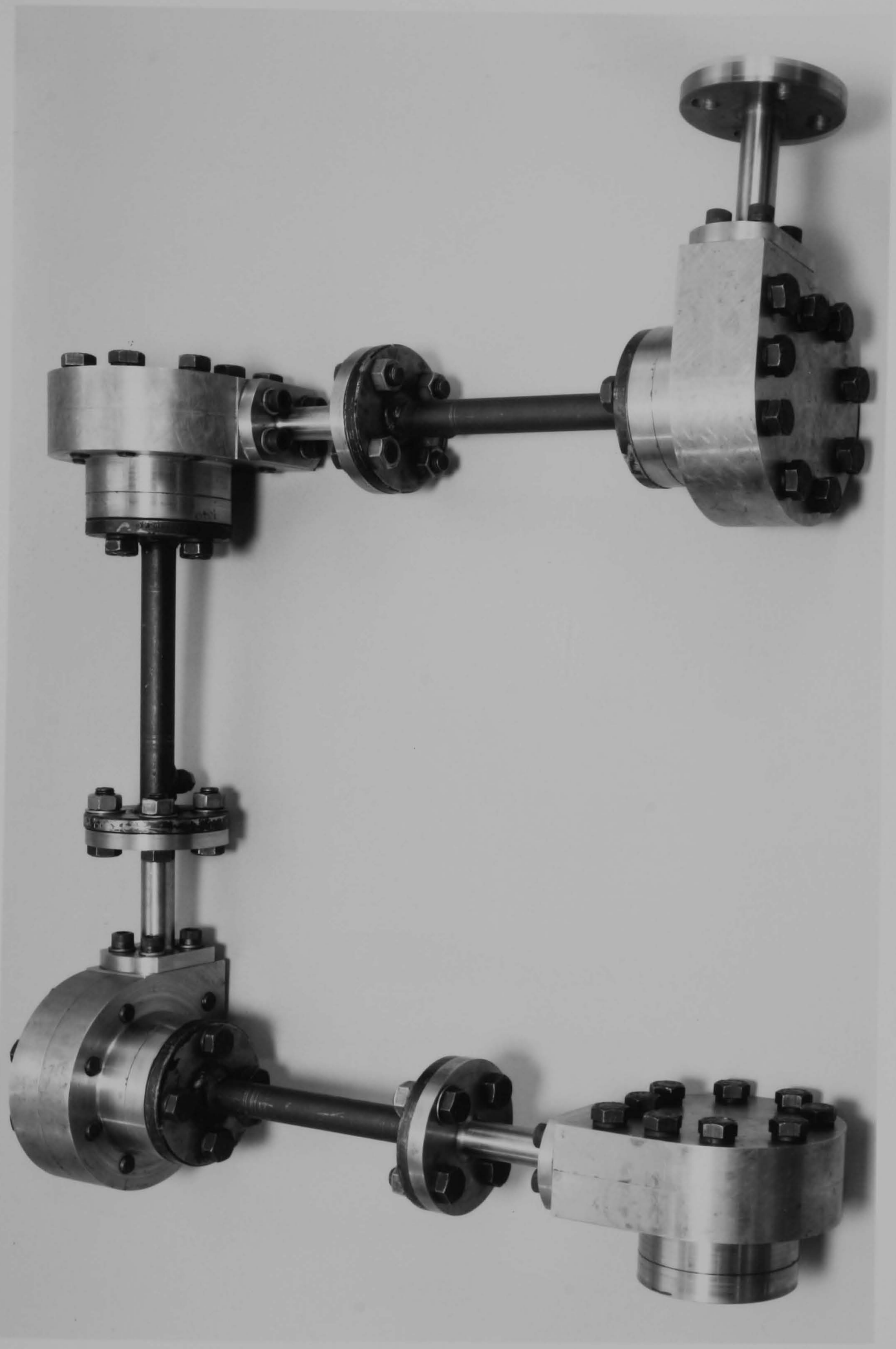

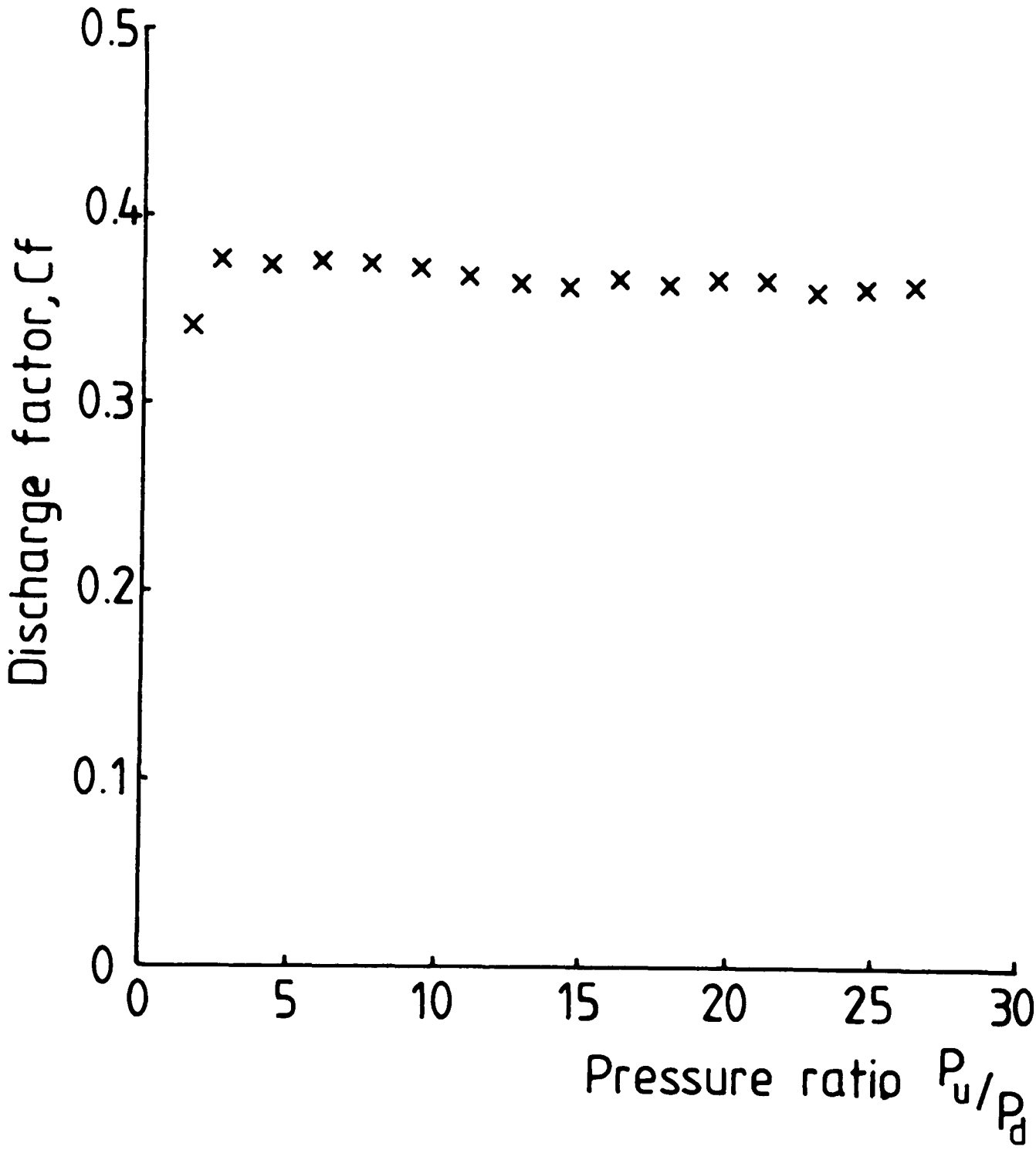

Fig. 4.25 Reverse Flow Discharge Factor (Diode No. 1)

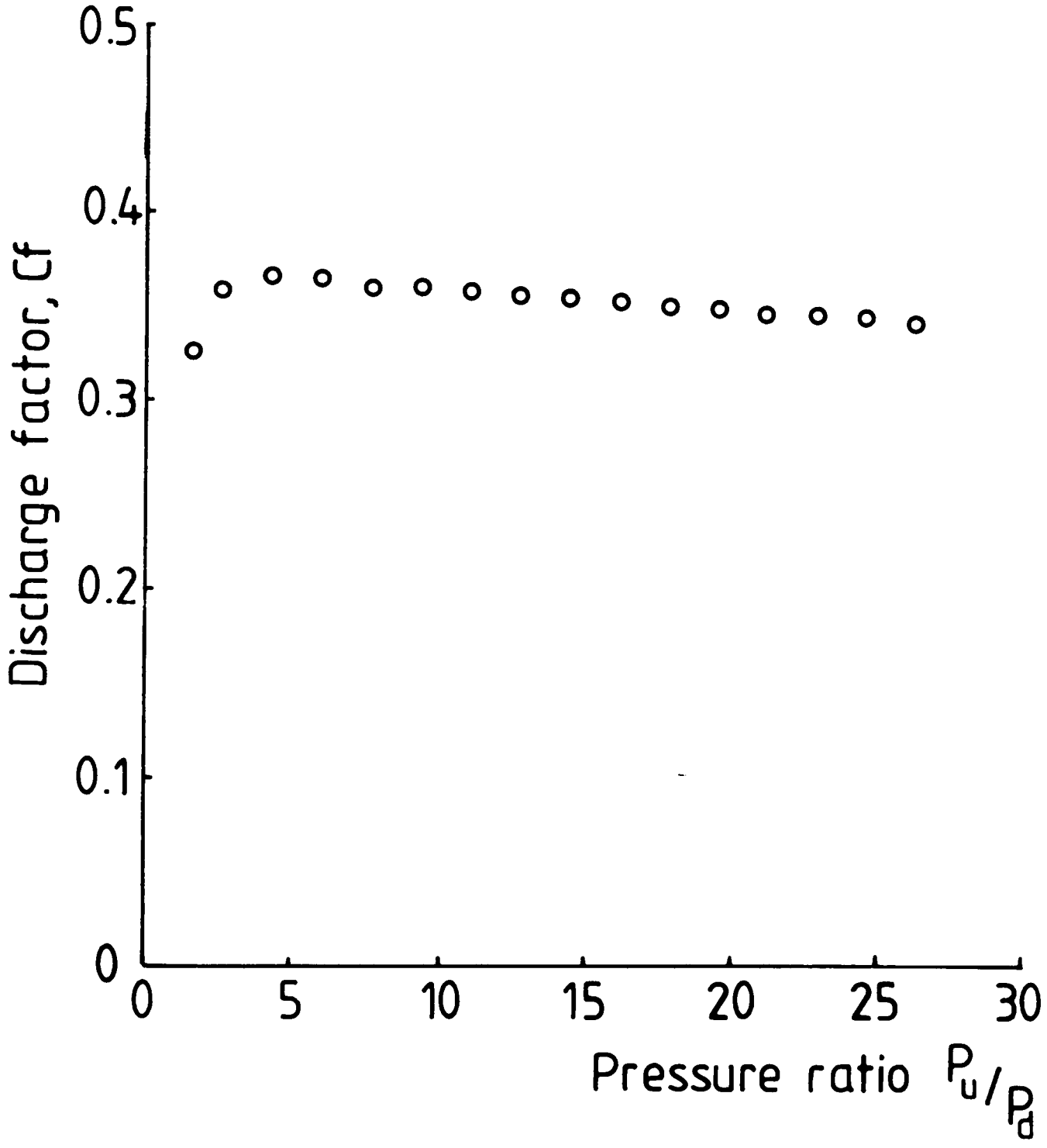

Fig. 4.26 Reverse Flow Discharge Factor (Diode No. 2)

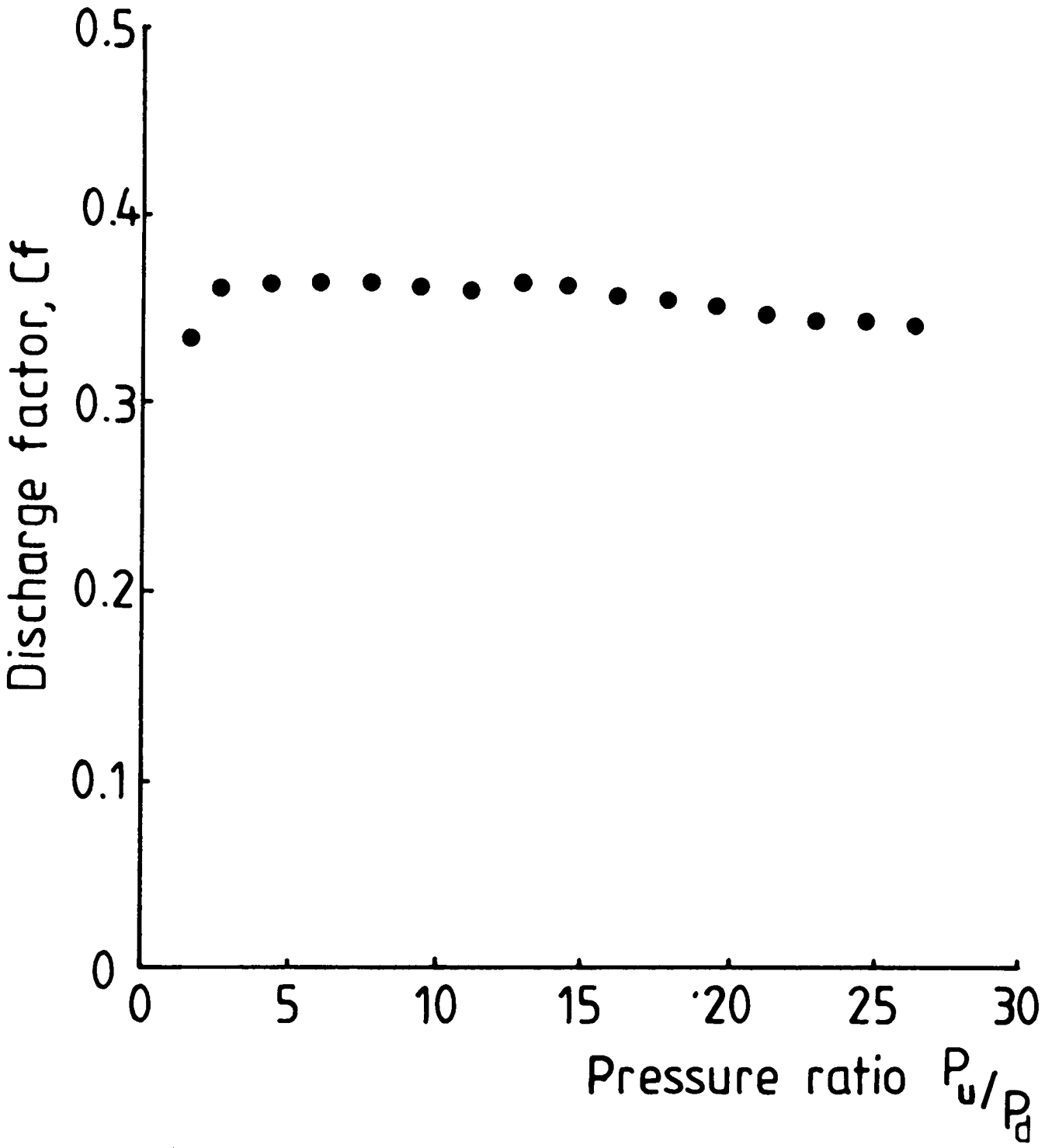

Fig. 4.27 Reverse Flow Discharge Factor (Diode No. 3)

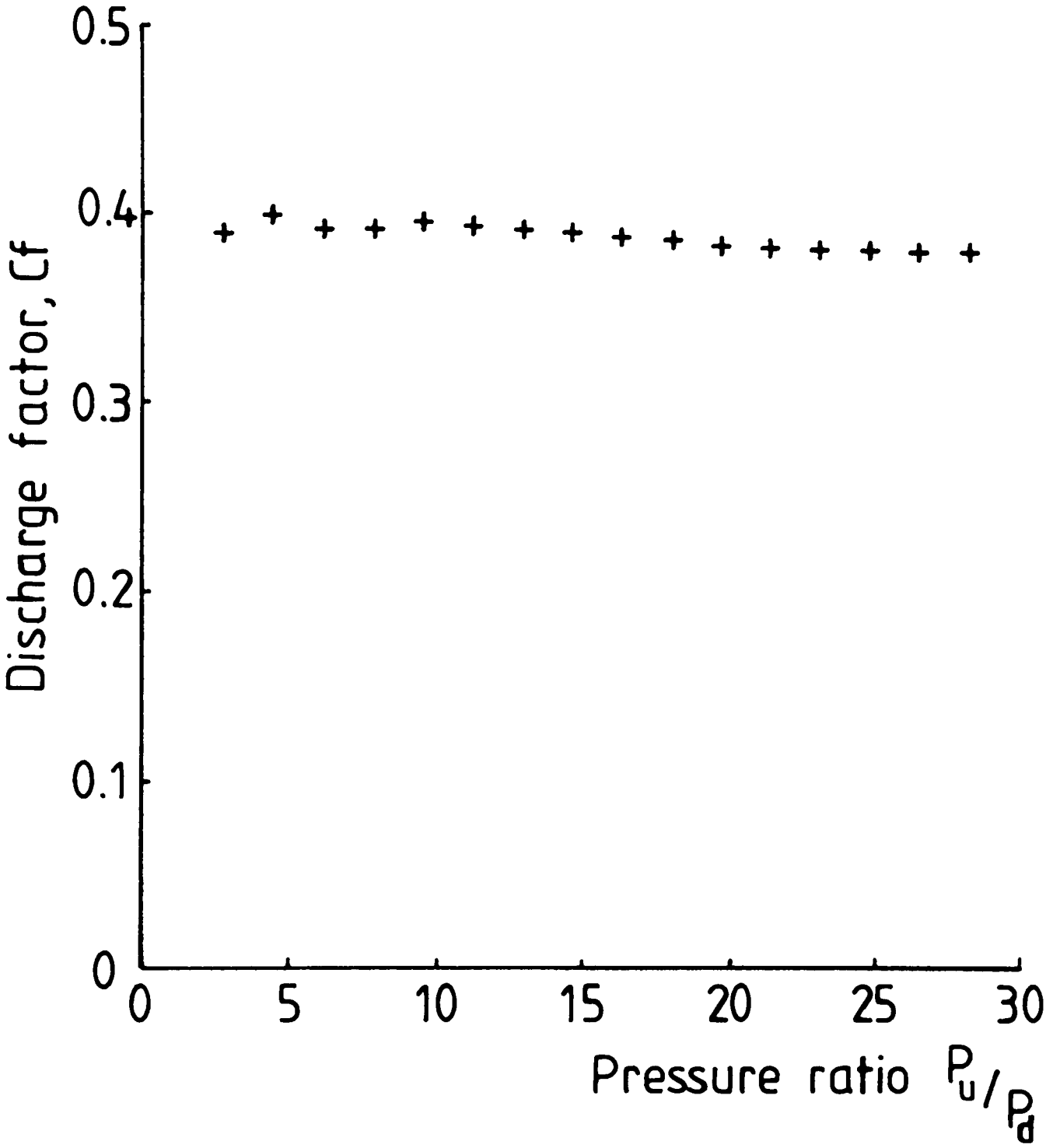

Fig. 4.28 Reverse Flow Discharge Factor (Diode No. 4)

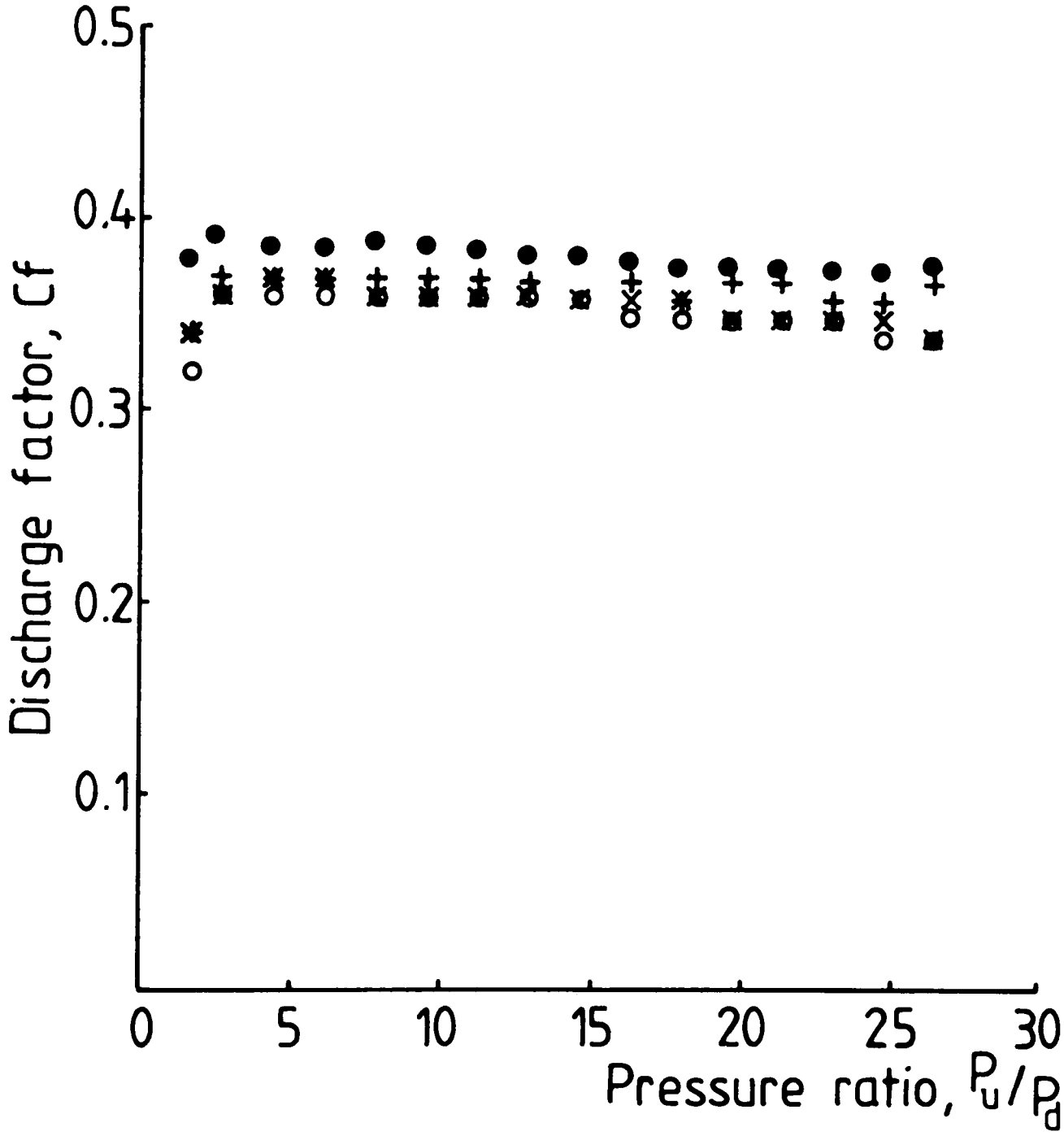

Fig. 4.29 Comparison of Reverse Flow Discharge Factor

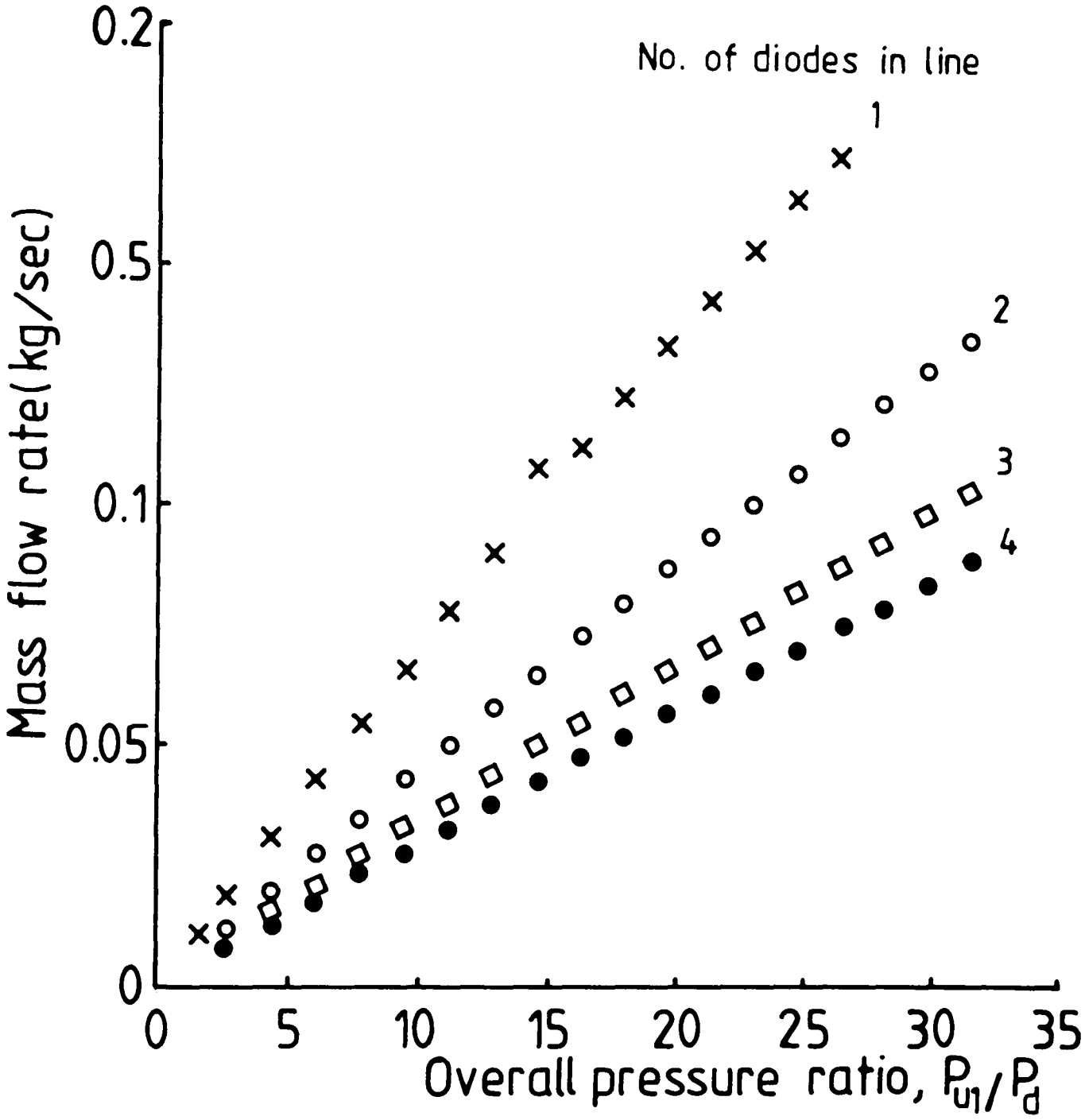

Fig. 4.30 Mass Flow Rate Through Diodes in Series

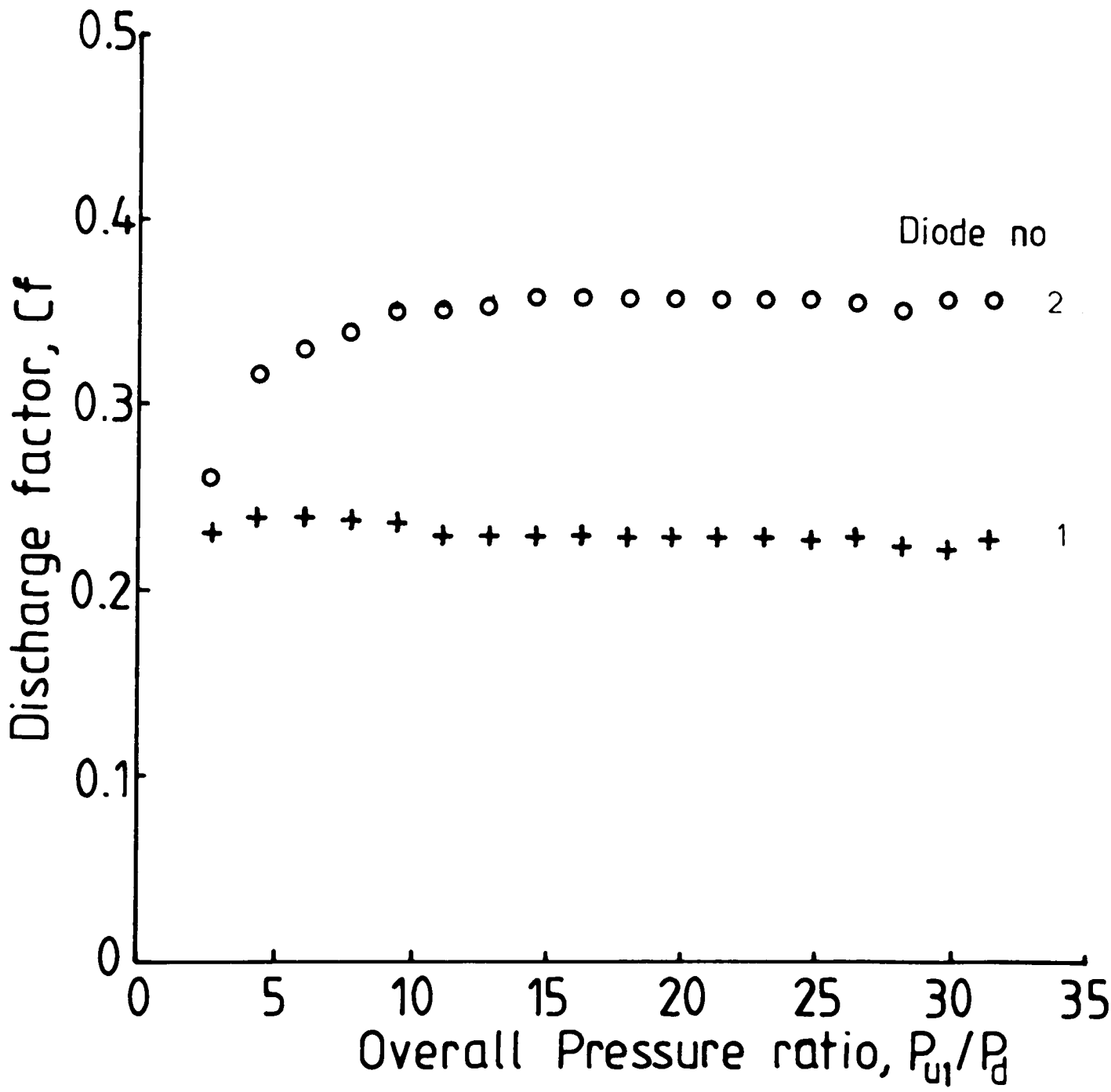

Fig. 4.31 Reverse Flow Discharge Factor Through 2 Diodes in Series

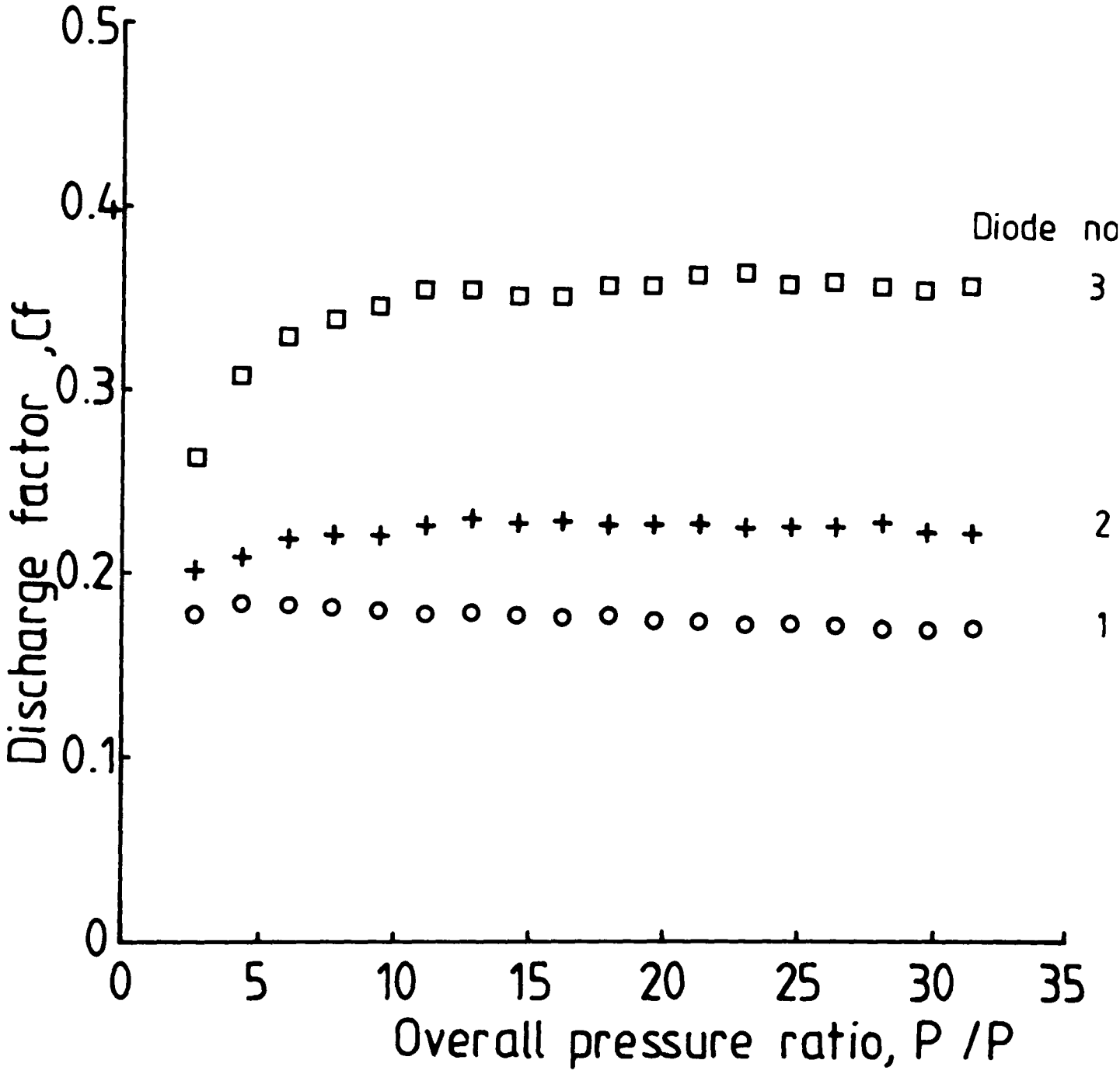

Fig. 4.32 Reverse Flow Discharge Factor Through 3 Diodes in Series

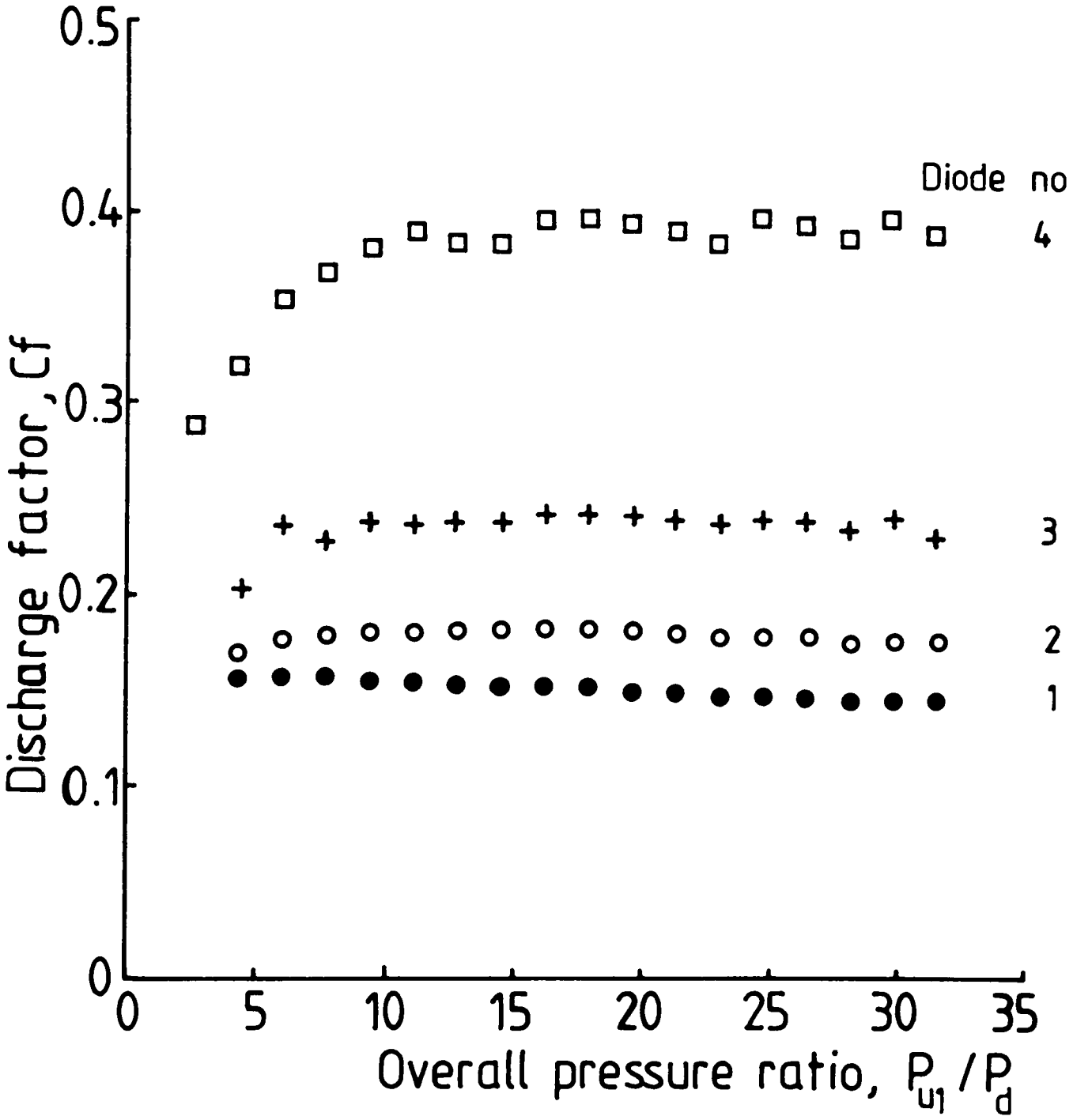

Fig. 4.33 Reverse Flow Discharge Factor Through 4 Diodes in Series

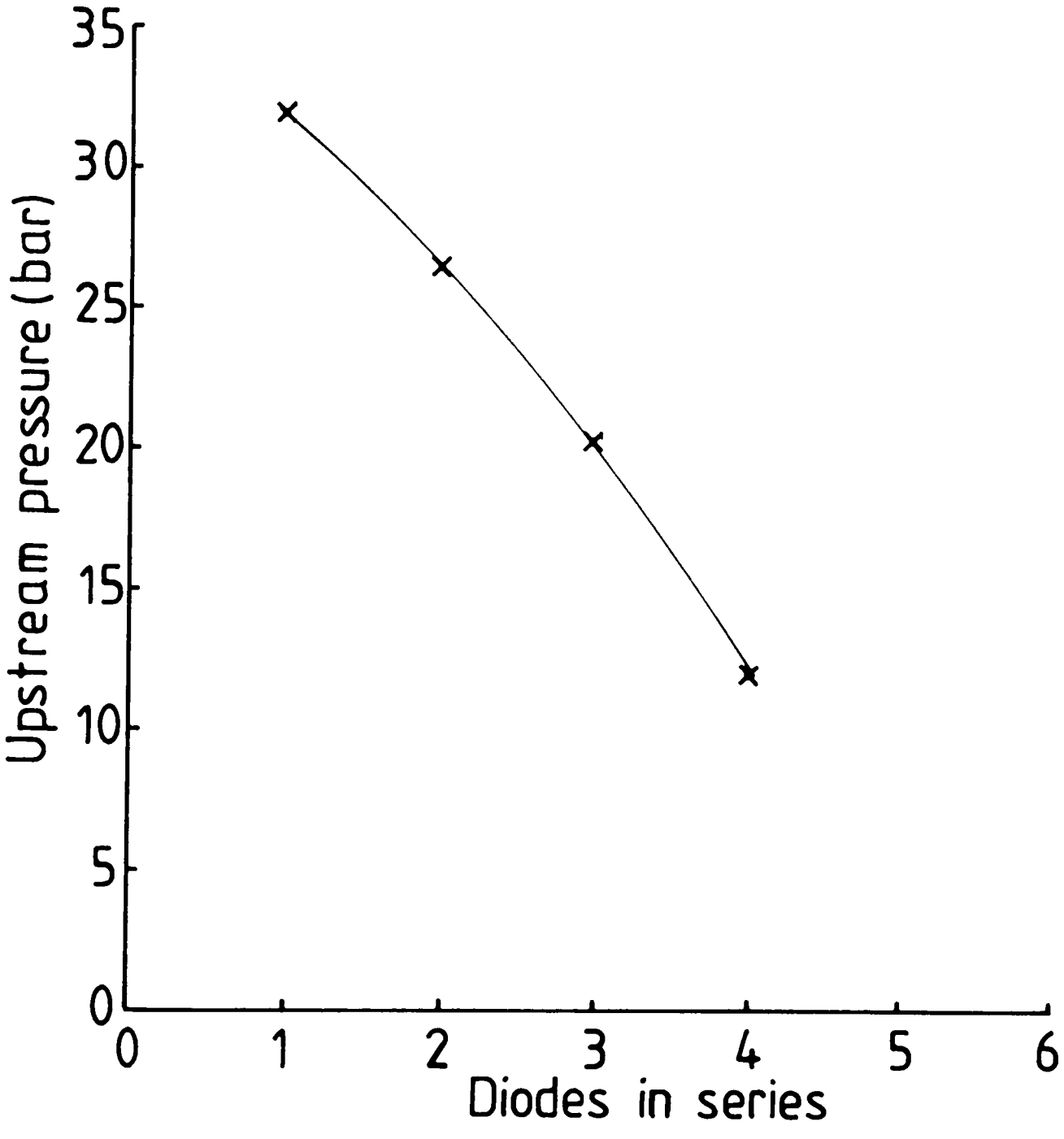

Fig. 4.34 Variation of Upstream Pressure for Diodes in Series

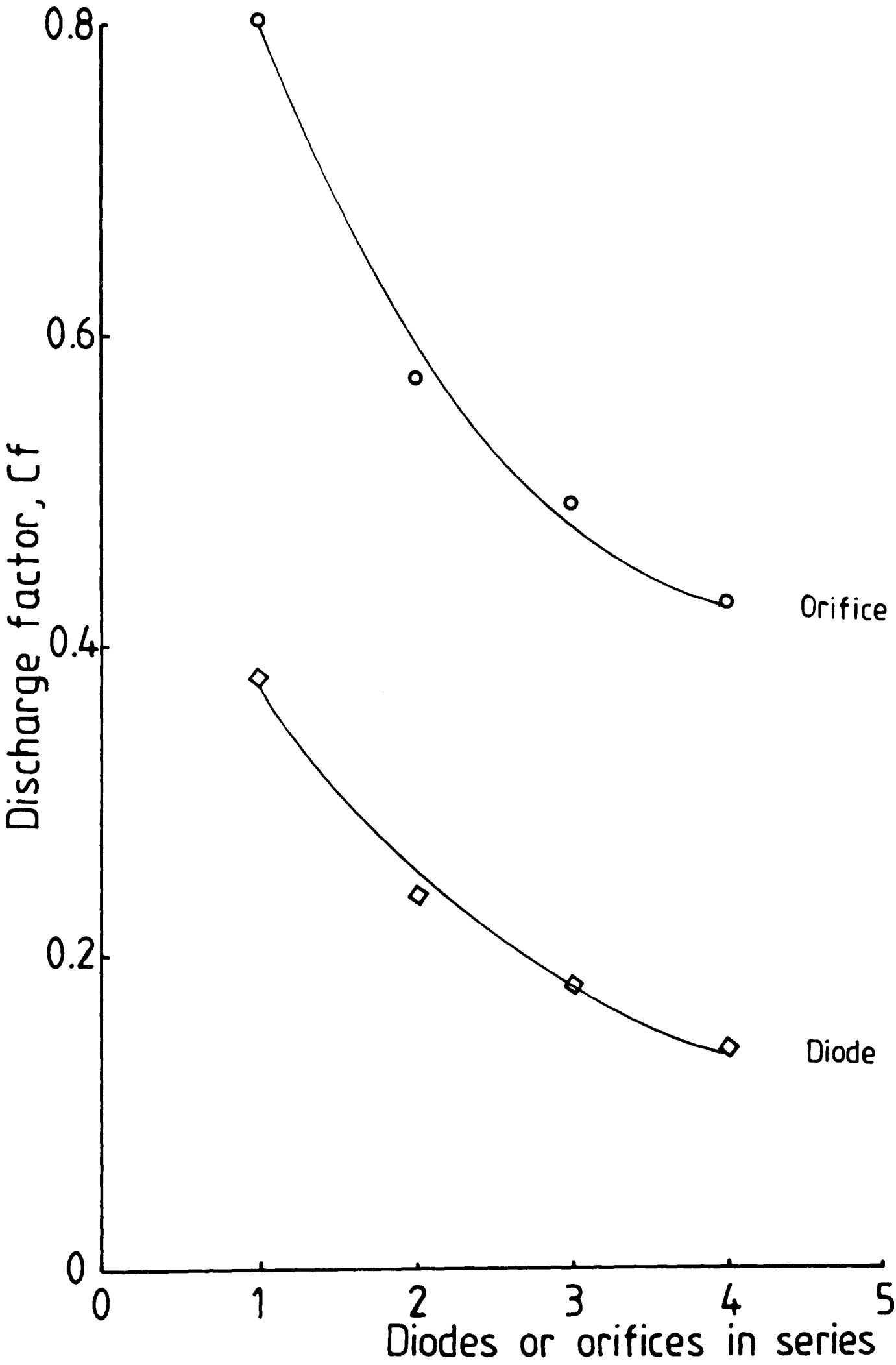

Fig. 4.35 Variation of Discharge Factor for Diodes (Reverse Flow) and Orifice in Series

CHAPTER 5

VORTEX DIODE CHARACTERISTICS IN COMPRESSIBLE WET STEAM

The attraction of power fluids lies in the supposed ability of the devices to handle difficult and dangerous fluids. With respect to single-phase corrosive and toxic fluids, their worth has been proven. The published literature also cites the ability of fluidic devices to handle multi-phase flows. Whilst there is some evidence to show that this is true for liquids containing suspended solids, there is no real evidence that this is true for gas-liquid flows.

A vortex diode is one of a number of non-moving part devices which have been used as flow control elements. Whilst their characteristics are now available for a variety of fluids over a wide range of operating conditions, however, there is no real data available for vortex valves operating with two-phase flow. Mori and Premoli [80] in their paper entitled "Vortex diodes in two-phase flow" showed that the diode performance was not significantly affected when tested with high temperature water at 258^{o}C. However the pressure at the diode inlet was 50 bar for which the corresponding saturation temperature is about 265^{o}C. The water was therefore sub-cooled at the inlet to the diode. It is known that, certainly in the high resistance direction, most of the pressure drop in the diode takes place at the exit throat. Furthermore, evaporation takes a finite time to occur and it is therefore unlikely that voidages would appear until the flow is leaving the axial port of the diode. In other words, the flow in Mori and Premoli's work was not, despite the

title of their paper, genuinely two-phase. Their diode was, in fact, experiencing severe cavitation. Burgess [81] used high temperature, sub-cooled water (1.14 bar with 100°C maximum) and reported that the high resistance of the diode is not significantly affected by flashing after the diode.

Wet steam flows such as those encountered in a steam main of a chemical or process plant can be considered as a high quality two-phase flow. Consequently the pressure losses in wet steam flows, whether they be frictional or singular, are usually assumed to be the same as would be measured for the gas phase alone. This is because in a well drained main the quality will normally be of the order of 95% and will rarely be less than 90%. For two-phase flows such as these the gas phase is practically unaffected by the liquid phase which exists both as drops entrained in the flow and as a film/rivulet on the pipe wall. The liquid is simply swept along by the gas and has little effect upon the loss-causing mechanisms. Thus the pressure drop measured across a length of pipe (frictional pressure drop) or across a valve (singular pressure drop) will be much the same in a dry steam flow as in a typical wet steam flow.

This Chapter describes forward and reverse flow characteristics of a Zobel type vortex diode in which the flow entering the diode was saturated wet steam of a known dryness fraction. The experimental work is an extension of the investigation described in Chapter 4, where the same diode was characterised using superheated steam. Much of the experimental equipment is common to both studies.

The only reliable method for producing wet steam of a known dryness fraction is to inject water of measured temperature and flow rate into superheated steam, whose temperature, pressure and flow rate are also known. By measuring the pressure of the resulting two-phase flow, the enthalpies before and after mixing can be equated and the dryness fraction calculated.

It has been observed that restricting the throughput of a wet steam flow under certain conditions of wetness, can lead to a build up of water which, after a time, will be picked up by the vapour and swept through the pipework. The effects of such an event on the behaviour of the diode have also been investigated.

5.1 **Experimental Apparatus and Procedure**

A schematic of the diode characterisation rig is shown in Fig. 5.1. The diode, is the same as that used and described in detail in Chapter 4. The mass flow rate of superheated steam to the rig was measured using an orifice plate according to B.S.1042 [75] before being de-superheated by using one, or two fine water sprays, depending on the amount of injected water required.

A Malvern laser diffraction particle sizer was used to characterise the water sprays. This instrument uses the principle of light diffraction from the drops to make a measurement. A schematic diagram of the system is shown in Fig. 5.2. A 5 mW visible laser transmitter produces a parallel, monochromatic beam of light which is arranged to illuminate the water droplets. On passing through the water spray, diffraction patterns are produced which are collected by

a Fourier transform lens, and focussed onto a multi-element photo-electric detector which produces an analogue signal proportional to the received light intensity. The detector is interfaced directly to a microcomputer allowing it to read the diffraction pattern and perform the necessary integration digitally. The computer uses the method of least squares analysis to fit the data to a particular size distribution. The result of the analysis is basically a size distribution by volume (weight), but it may be presented in a number of ways. A typical characteristic of a water spray is shown in Fig. 5.3.

To ensure thermodynamic equilibrium of the wet steam, it is necessary that the processes of heat and mass transfer between the superheated steam and water droplets be completed before the steam reaches the diode. The processes of drop and spray evaporation with relevant formaulae is decribed in detail in Appendix D.

A high pressure recriprocating pump, fitted with a surge vessel to damp out the pressure pulses, was used to supply water to the sprays. The water flow rate was measured using Rotameters. The pressure differentials across the diode and across the orifice plate were measured using differential pressure transducers. Stagnation temperatures were measured before and after the vortex diode as well as at the orifice plate using half-shielded thermocouples. Pressures at various positions in the rig were measured using calibrated pressure gauges. The outputs from the pressure transducers and the thermocouples were connected to a multi-pen chart recorder so that not only could the stable flow characteristics be recorded, but so

too could any flow instabilities which might occur. The pressures before and after the diode were controlled by two throttle valves. The flow was exhausted from the rig into a sub-atmospheric condenser.

During the course of the experiments it was not practicable to pre-select a particular dryness fraction since it was influenced by the steam flow rate, pressure and temperature, all of which changed when the water was injected. Therefore the controlled parameters during the experiment were the inlet and outlet pressures at the diode and the mass flow rate of the injected water.

The overall thermodynamic process from the inlet to the outlet of the diode is a throttling one. In Chapter 4 this was readily shown since both conditions were easily and uniquely measured with the steam being in the superheated condition. In the present work, when the steam inlet condition was not too wet (> 0.95), and there was a large enough pressure drop across the diode, the steam changed from being wet at the diode inlet to being dry downstream of the diode. The end points of such an expansion are shown in Fig. 5.4. The inlet condition was calculated from the enthalpies of the superheated steam and injected water flows; the outlet condition was measured directly. It can be seen that this confirms the process is a throttling one and serves to give confidence in the original calculation of the dryness fraction.

The pressure-flow characteristics were obtained by maintaining constant inlet pressures to the diode and systematically varying either the downstream pressure or the flow rate of the injected water independently. Inlet pressures from 5 to 8 bar absolute were used in the reverse flow direction and from 3 to 6 bar absolute in the forward flow direction. This range of inlet pressures is less than that used previously with superheated steam, but is sufficient to demonstrate the characteristics of the diode.

5.2 **Presentation of Data**

In Chapter 4, the diode was characterised by comparing the mass flow rate of the steam with the theoretical mass flow rate of an ideal gas through a choked isentropic nozzle with the same throat area as that of the vortex diode throat. It was thus observed that the vortex diode choked at an inlet to outlet pressure ratio of about 4 and in the choked condition passed 38% of the ideal nozzle flow rate. The flow rate through the diode was characterised by a discharge factor Cf which therefore, in the choked condition, was 0.38. The term 'discharge factor' was used since the parameter is only a true discharge coefficient in the choked region and the factor was used to describe the diode characteristics when the flow was both choked and unchoked. The use of this factor is discussed at some length in Chapter 4.

The above procedure allowed the data, in both forward and reverse flow directions, to be conveniently expressed by two independent characteristics. In this Chapter, the same approach has

been adopted for presenting the flow characteristics in wet steam. That is, the measured mass flow rate of the wet steam through the diode is expressed as a fraction of the mass flow rate of wet steam through a choked isentropic nozzle having the same throat area and inlet pressure as the diode.

Real wet steam differs considerably from the idealised two-phase systems dealt with in equilibrium thermodynamics. The following facts may play a more or less crucial role:

a. The state parameters are subjected to fast changes (e.g. during expansion).

b. The steam wetness at higher values of dryness fraction is mostly not bulk liquid (like films), but consists of finely dispersed drops and mist.

c. There is relative motion between the phases.

d. There is heat and mass transfer between the phases.

e. There is heat exchange with channel or container walls.

f. In the vapour phase, nucleation may occur.

g. Existing droplets grow or evaporate or link with each other or impact on walls and become absorbed in a bulk liquid film.

The behaviour of wet steam under given flow conditions is largely determined by the form in which the wetness is present (film or droplet, and the size or size distribution of the droplet), and by the total amount of condensed water (value of wetness fraction).

For practical purposes, it is important that a simple and yet reasonably representative model for the critical flow of wet steam be adopted; otherwise the purpose of the present study might lose its significance in the wider issue of critical two-phase flow.

A number of theoretical and semi-empirical formulations have been developed to describe two-phase flow in general, and critical two-phase flow in particular. In the present work we are dealing with a relatively high quality two-phase flow with the steam having dryness fractions greater than 0.88.

The simplest two-phase model is the frozen homogeneous model which assumes:

1. the average velocities of the phases are equal;
2. no heat or mass transfer occurs between the phases;
3. the vapour expands isentropically as a perfect gas, i.e. pv^{γ} is constant;
4. the kinetic energy is due solely to the vapour expansion;
5. the critical flow is defined by gas-dynamic principles.

In other words the flow is considered to be that of a perfect gas through an ideal nozzle and the water content is simply suspended in the flow as fine droplets with no slip and no evaporation.

The frozen homogeneous model used in the present work has been described by, amongst others, Henry and Fauske [82], (N.B. equation 43 in Ref. [82] is mis-typed) and by Deich et al [83].

Thus the critical mass flow rate, $\dot{m}_{cm}$, of wet steam is given by:

$$\dot{m}_{cm} = \frac{A_e}{V_m} \{2x_u P_u v_{gu} (\frac{\gamma}{\gamma-1})(1 - \varepsilon^{\frac{\gamma-1}{\gamma}})\}^{1/2} \qquad (5.1)$$

(the derivation of this formula is given in Appendix E)

where $\varepsilon = \left| \frac{2}{\gamma+1} \right|^{\frac{\gamma}{\gamma-1}}$ is the critical pressure ratio and v_m, the specific volume of the mixture at the throat of the nozzle is given by:

$$v_m = (1 - x_u)\, v_{fu} + x_u\, v_{gu}\, \varepsilon^{(-1/\gamma)} \qquad (5.2)$$

The critical flow equation for $\dot{m}_{cm}$ reduces to the one-dimensional critical gas flow equation when x = 1.

Cf, the discharge factor of the diode is therefore given by:

$$Cf = \frac{\dot{m}_m}{\dot{m}_{cm}} \qquad (5.3)$$

There is some controversy regarding what value should be taken for the isentropic index of expansion γ in wet steam flow. Mayhew and Rogers [84], for example, suggest a value of 1.35 for superheated steam and 1.135 for wet steam. Others argue [85] that γ has no physical meaning in two-phase flow and that to consider the homogeneous mixture as a single medium is misleading. In the present model it is assumed that the gas phase follows the laws of gas-dynamics, i.e. of the dry saturated steam. The value of γ which has been used is therefore 1.35.

Equation (5.1) is expressed graphically in Fig. 5.5. Although this model will not be accurate over the entire range of dryness fraction, it will be more representative at the higher dryness fractions where the water will be more dispersed and will suffer less thermal and mechanical disequilibrium. Furthermore, due to the fact that phase change is metastable and takes a finite time to occur there will be little or no phase change before the nozzle throat, thus satisfying some of the assumptions of the model.

5.3 **Results and Discussion**

5.3.1 Overall characteristics

in the previous study with superheated steam it was observed that the diode choked at the pressure ratio of about 4. In Fig. 5.6 the reverse flow discharge factor of the diode is shown for wet steam at a constant inlet pressure of 7 bar absolute and dryness fraction of 0.93 together with a corresponding curve for superheated steam from Chapter 4. From this limited wet steam data, it can be seen that the diode chokes at much the same pressure ratio as for superheated steam but with a higher discharge factor.

It was recognised that, in practice, steam supplies normally have pressures in excess of about 6 bar absolute and that a diode would normally be operated in the choked condition. Therefore, subsequent data was collected when the diode was operating well into the choked region.

In Fig. 5.7 the reverse flow discharge factor (in the choked region) is shown for dryness fractions ranging from 0.91 to 0.98 and for inlet pressures from 5 to 8 bar absolute. Also included is the corresponding data for superheated steam which has been assumed to be the same as that for dry saturated steam. This latter data fits in with the observed trend for wet steam. It can be seen that as the steam becomes wetter so the discharge factor rises from 0.38 for dry steam to 0.48 for steam at 0.93 dry. This reduction in the diode resistance is not due to extra mass being carried in the water content since this is allowed for in the model. In trying to explain this observed trend two other possibilities come to the fore. Firstly it is possible that the water content causes an increase in the apparent viscosity of the fluid and leads to an increase in viscous dissipation within the flow, this is known to occur in cyclone dust separators as the dust loading is increased [86]. Another possibility arose from observation of the flow in the vortex chamber. This was made through a glass wall which had been specially manufactured for this purpose. It will be seen later in this section that an annular condensation fog is observed in the exit region at the centre of the diode. It was argued in Chapter 4 that it is the flow in the exit throat of the vortex diode that governs its resistance properties. Condensation in this area (caused by the high velocities and hence low static temperatures) will enable more mass to pass through the throat. It is not clear why this effect might increase with an increased water content but it is known that drops

already existant in the flow can act as condensation sites. Neither of these explanations are wholly satisfactory but certainly their combination will lead to a deterioration in the diode resistance.

5.3.2 Oscillations

It was found that in the high resistance direction, as the water content was increased, so a point was reached where the resistance of the diode decreased suddenly and, at the same time, the flow of steam through the rig increased rapidly. This phenomenon did not occur at a particular value of dryness fraction and its onset could not be predicted with any accuracy. It occurred within an approximate range of dryness fraction between 0.93 and 0.91. This is shown in Fig. 5.7 as the transition region. A single oscillation is shown in Fig. 5.8 where, for approximately 15 seconds, the diode resistance falls and the steam flow rate rises in response. For dryness fractions below about 0.91 the oscillations become regular and it was impossible to take reliable measurements. Fig. 5.9 shows the regular nature of these oscillations which had a period of approximately 45 seconds.

To assist in the understanding of this behaviour the half of the diode body which formed the plane back wall was machined to accommodate a 125 mm diameter glass plate of 25 mm thickness. This enabled the flow in the vortex chamber to be seen. Fig. 5.10 shows dramatically the reason for the oscillations in Fig. 5.9. Fig. 5.10 shows four different stages during a single oscillation, with the flow being relatively dry in (a) to it being severely flooded in (d). On investigation, it became clear that for dryness fractions

less than about 0.93 the water content is not all carried with the steam but flows down to the 'U' bend in the rig, Fig. 5.1. Although the water is introduced as a fine spray, it is inevitable that much of it deposits on the pipe wall and is swept, either as a rivulet or as a film, through the pipework. This is the case with all wet steam flows. When the steam becomes too wet, reversal of the water flow can take place in upward vertical pipes, this is a well known feature in vertical two-phase flow [87]. The water accumulates in the 'U' bend until there is sufficient that some of it will be swept by the steam flow into the diode and the internal flow changes from (a) to (b). The tangential inlet is towards the lower left hand corner of the photographs. In (a) the water which has been deposited onto the glass wall can be seen tracing out the path of the flow in the boundary layer. The flow (a spiral vortex) is symmetrical around the axis of the chamber and the annular condensation fog discussed earlier can be seen clearly. This annular region coincides with the area of maximum velocity and hence minimum static temperature. In (b) the effect of the water on the flow structure is to reduce the size of the vortex and to move it over to the right hand side. The centre of the 'dry vortex' is shown in each photograph. Much of the resistance of the diode has now been lost and, as was shown in Fig. 5.9, the flow through the diode increases rapidly. The increased steam flow will now sweep the water from the 'U' bend and through the rig, Figs. (c) and (d). After the trapped water has been purged the steam becomes drier again and the vortex structure recovers. The cycle can then start again.

Therefore, the oscillations are as a result of the rig configuration and the effects of the excessive water on the diode internal flow structure. The purpose of a diode is to produce a high resistance and hence low velocity in the pipework. If the steam is too wet, water flow reversal can occur in any upward vertical run of pipe.

An experimental study of flooding in vertical tubes (38.1 mm internal diameter) with subcooled water injected from the wall into upward flowing steam by Fan & Schrook [88], has shown that for certain combinations of steam and water flow rates and liquid subcooling, the process can become transient and may involve a liquid plug bridging the pipe cross section, leading to sustained oscillations. These oscillations may cause forced mechanical vibration of components or system control problems. Therefore, it is of importance to predict the threshold of flow instabilities and to allow compensation for it in any engineering plant.

In the forward flow direction the diode presents a low resistance to the flow and hence the steam velocity was always high enough to sweep the water along with it. The forward flow discharge factor is shown in Fig. 5.11 where it can be seen that, as with superheated steam, the value approaches 1. This shows that the diode presents very nearly the minimum resistance to flow. There is a suggestion in the data that higher values of inlet pressure give higher values of Cf. This might be so, or it could be due to experimental error, since different size orifice plates were used for diode inlet pressures of 3 and 4 bar than for 5 and 6 bar.

Finally, in Fig. 5.12, the reverse and forward flow characteristics in the choked region are compared for different dryness fractions. The ratio of forward to reverse flow is seen to fall from about 2.5 to 2 as the steam dryness falls from 1 to 0.92.

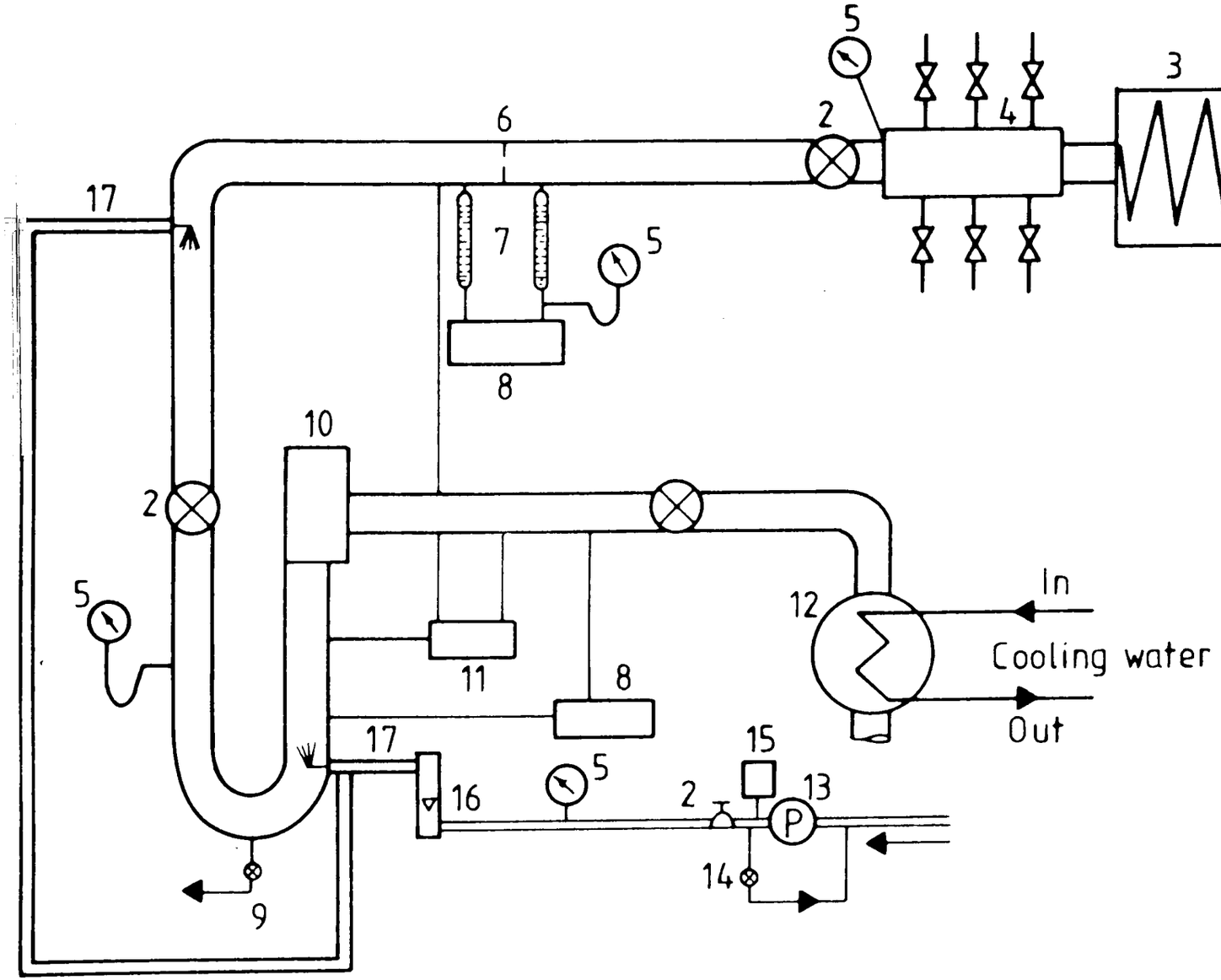

1. Boiler
2. Valve
3. Superheater
4. Manifold
5. Pressure gauge
6. Orifice
7. Cooling pots
8. Differential pressure transducer
9. Drain
10. Vortex diode
11. Digital thermometer
12. Sub-atmospheric condenser
13. Pump
14. Pressure relief valve
15. Surge vessel
16. Rotameter
17. Water spray

Fig. 5.1 Vortex Diode Wet Steam Characterisation Rig

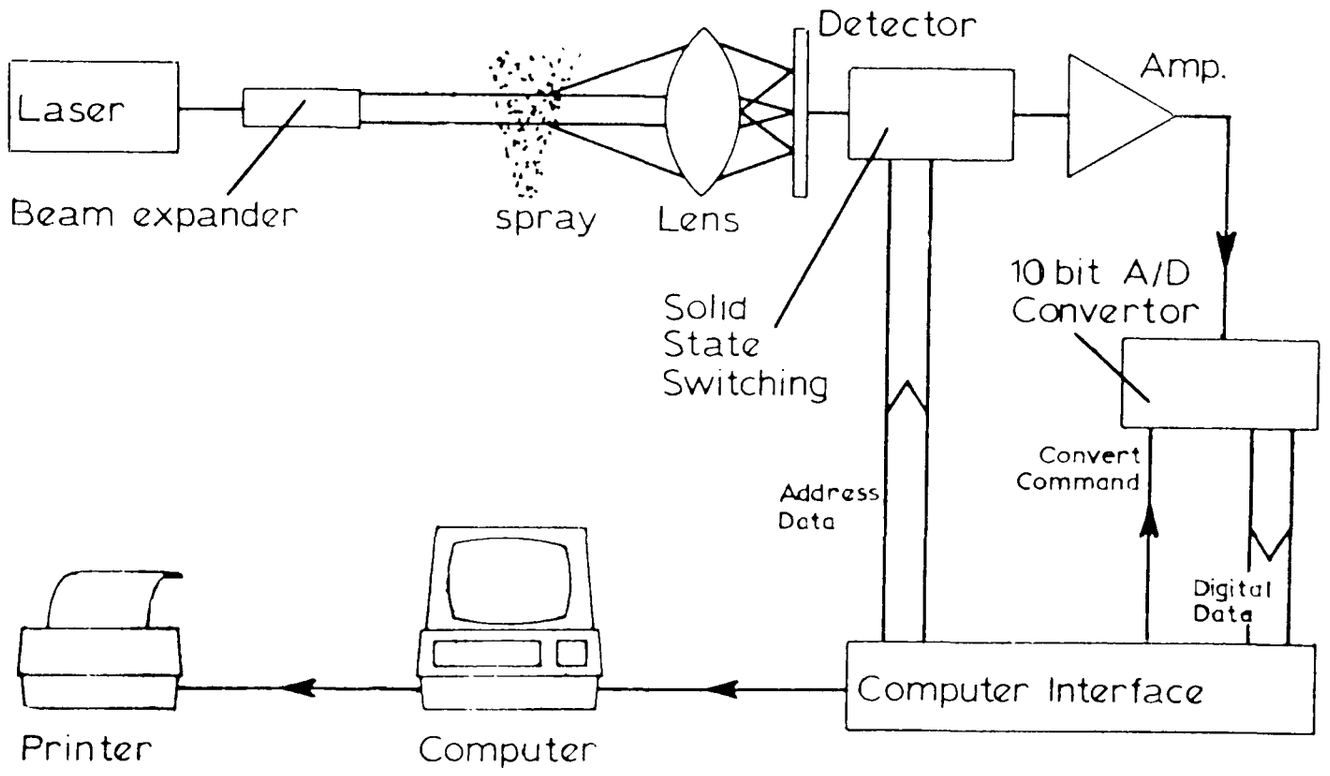

Fig. 5.2 Schematic Diagram of Malvern Laser Diffraction Particle Sizer

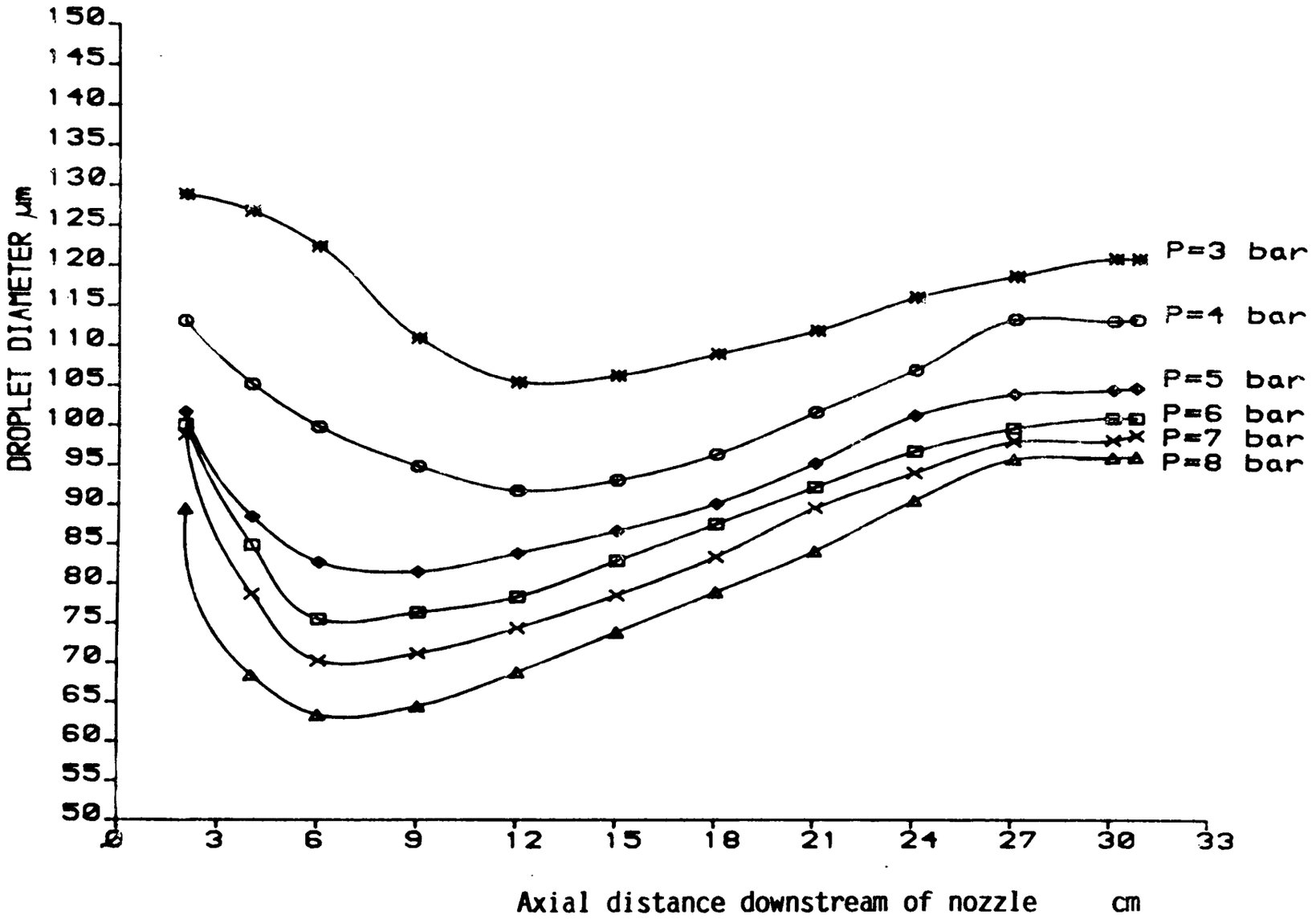

Fig. 5.3 Typical Spray Characteristics

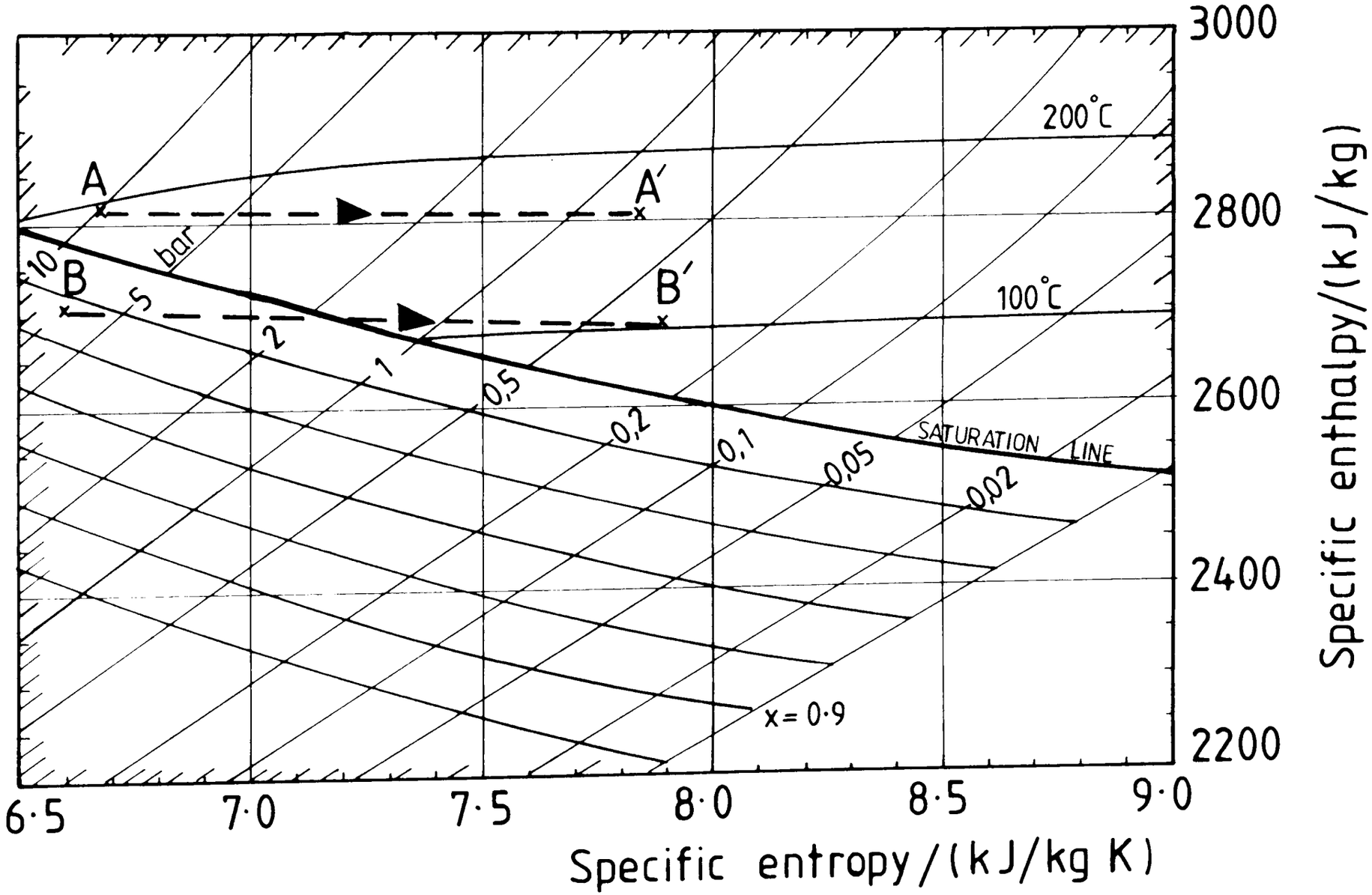

Fig. 5.4 Mixture Conditions in Inlet and Outlet to Vortex Diode

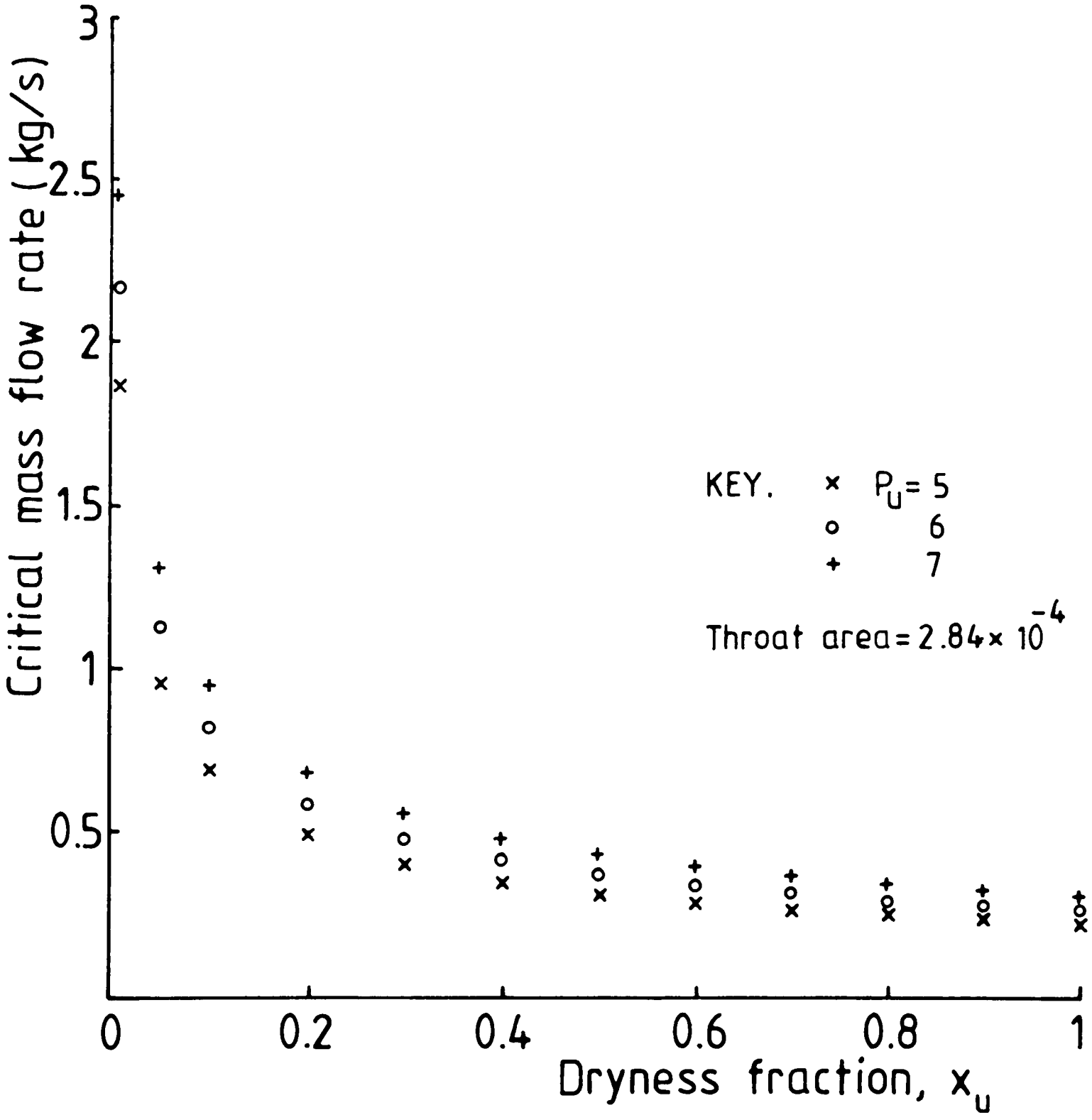

Fig. 5.5 Theoretical Two-Phase Critical Flow Through a Nozzle (Homogeneous Frozen Model)

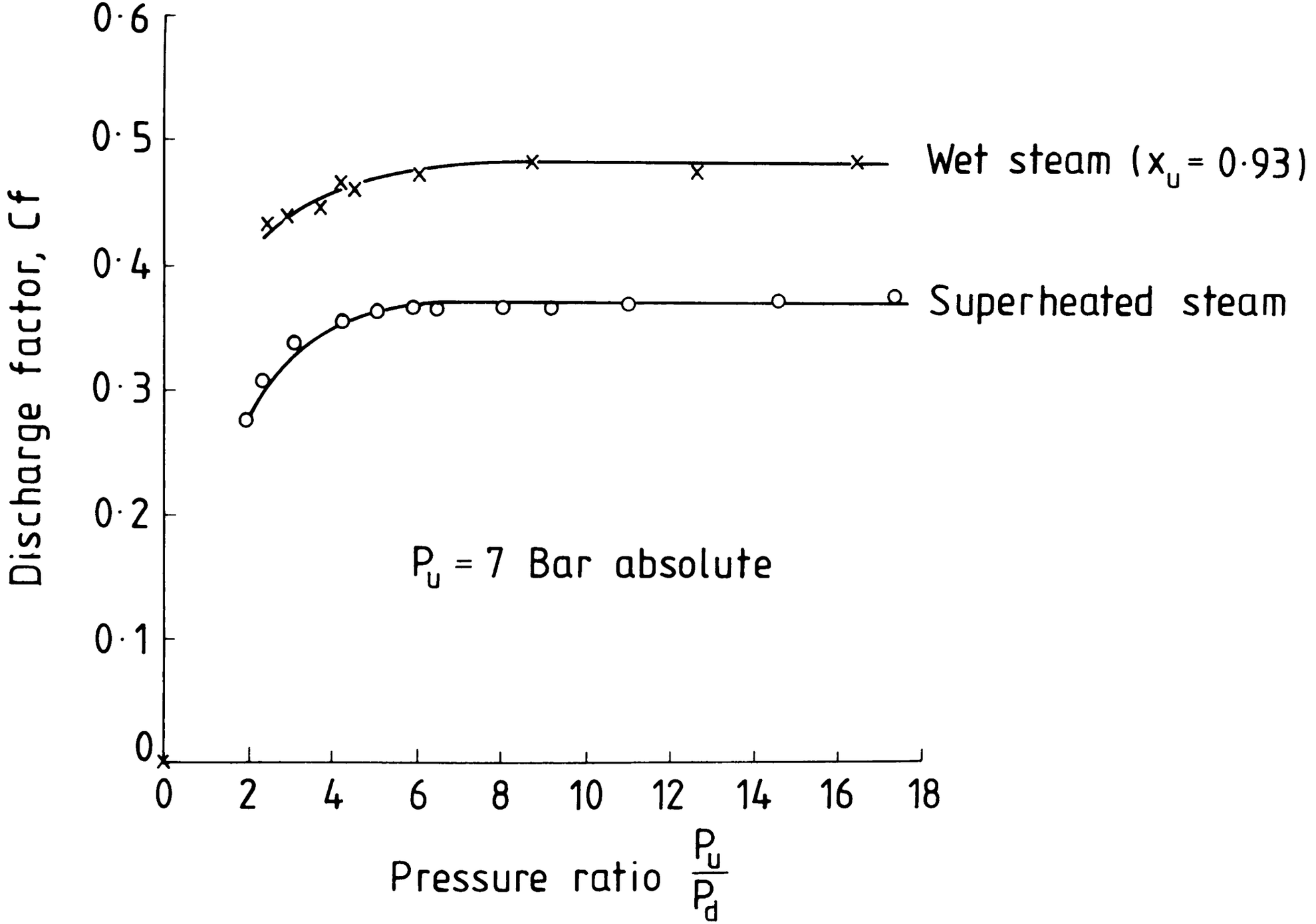

Fig. 5.6 Comparison of Reverse Flow Discharge Factor of Wet Steam and Superheated Steam

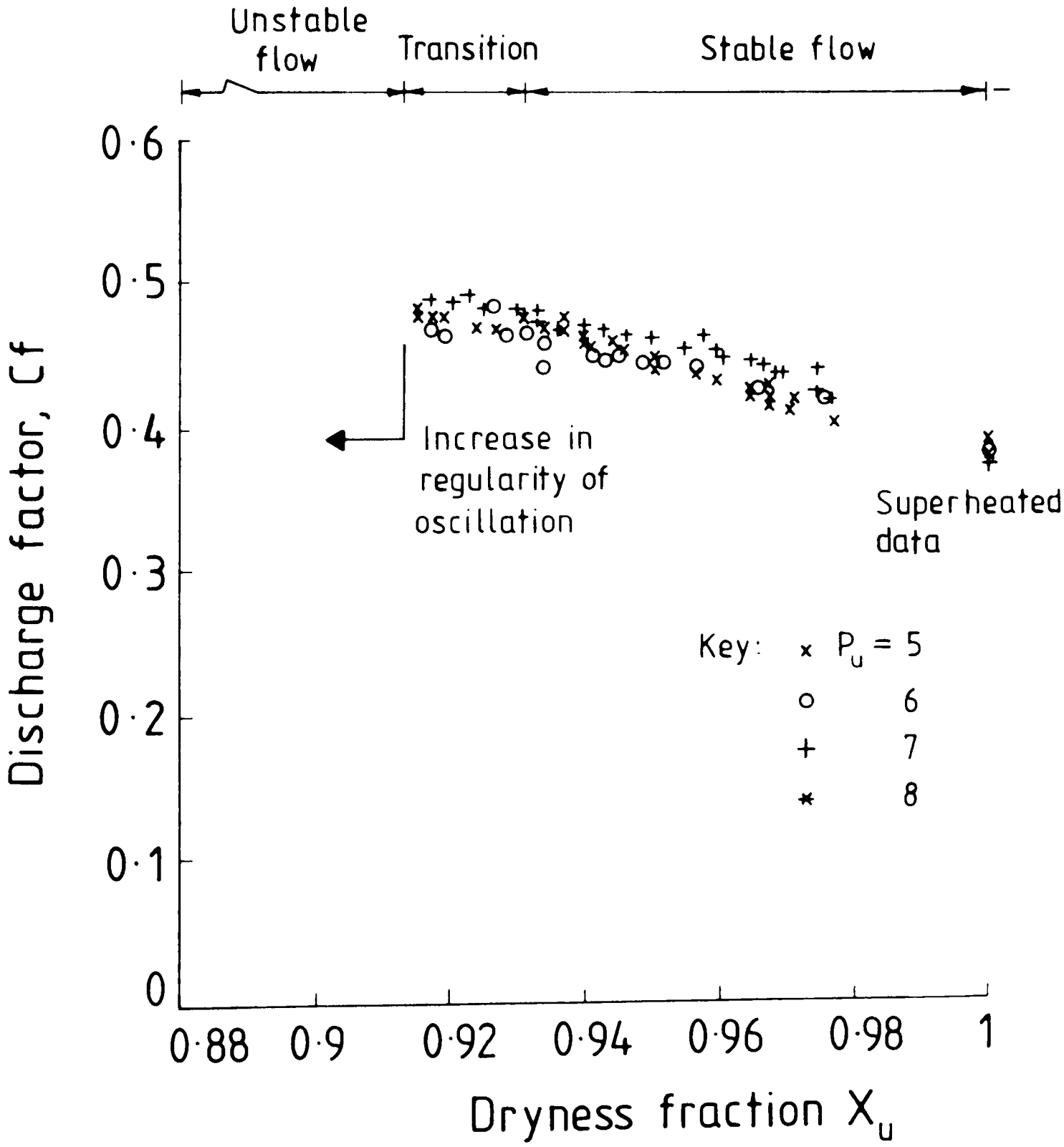

Fig. 5.7 Reverse Flow Discharge Factor for Wet Steam

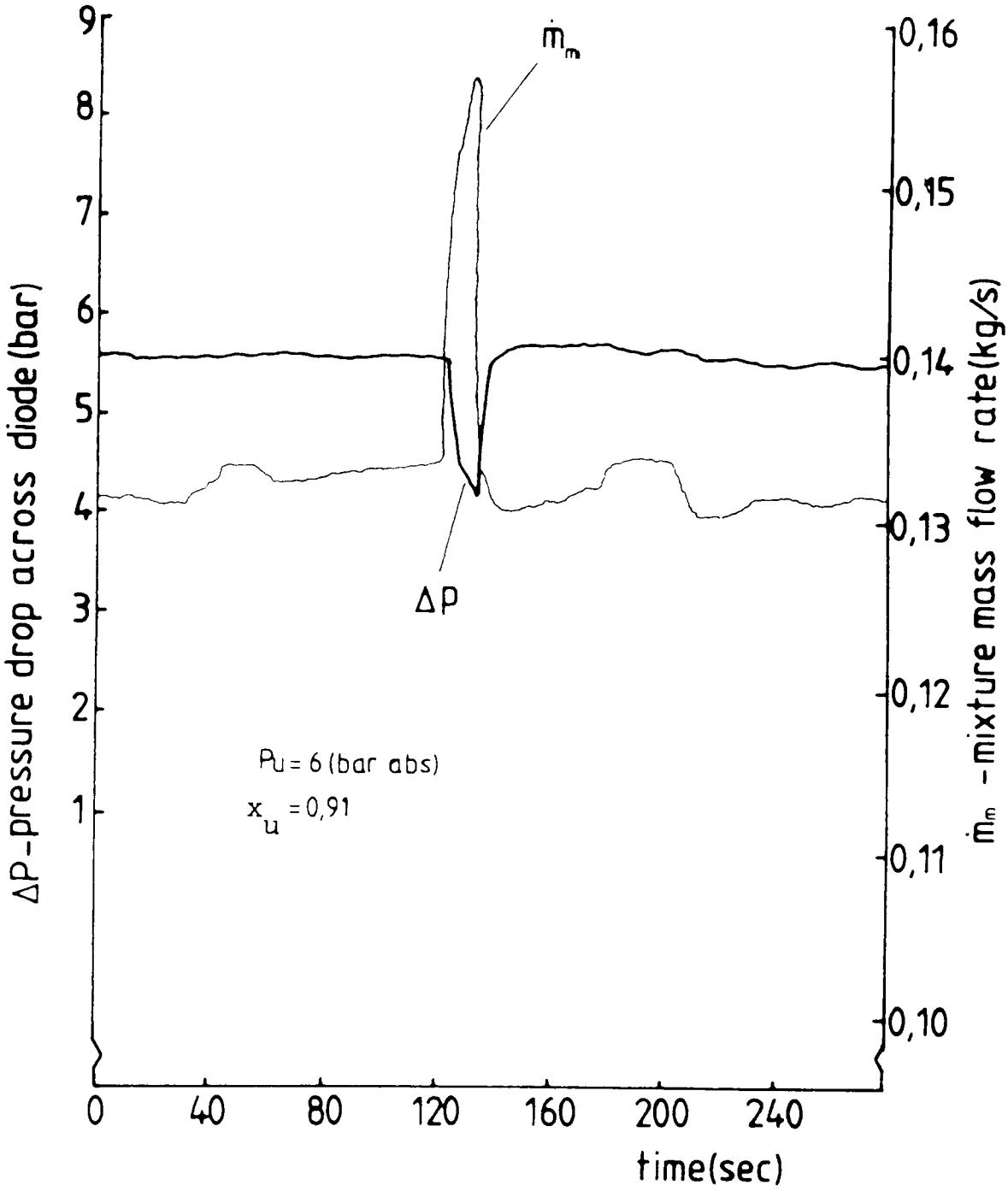

Fig. 5.8 Vortex Diode Single Oscillation in Wet Steam

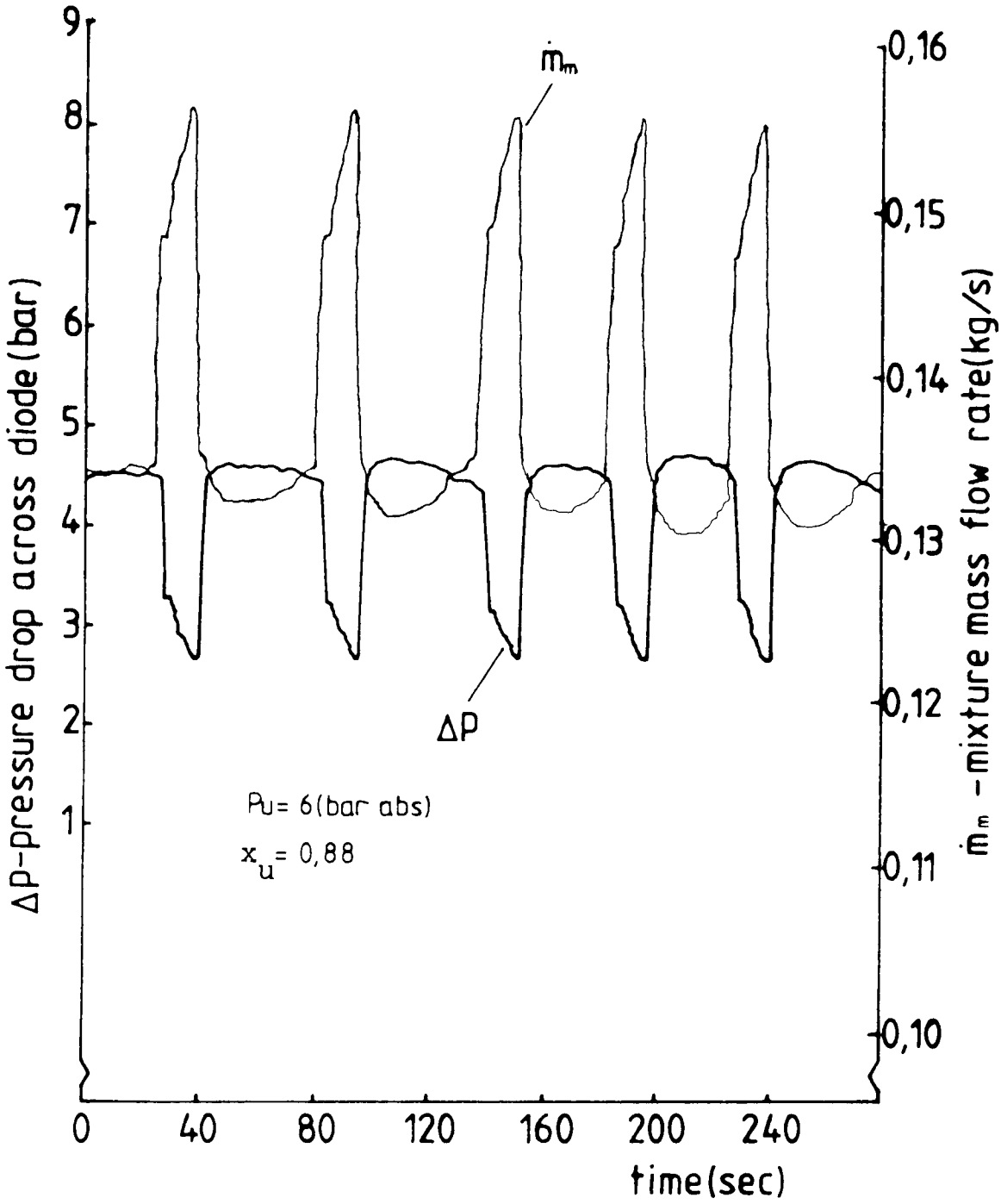

Fig. 5.9 **Vortex Diode Regular Oscillation in Wet Steam**

Fig. 5.10 Visualisation of Wet Steam Flow in Vortex Chamber During an Oscillation

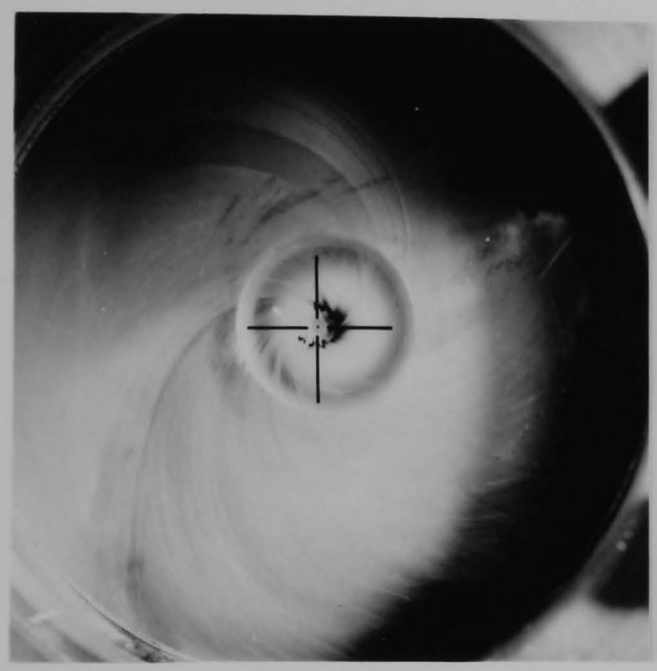

(a)

(b)

(c)

(d)

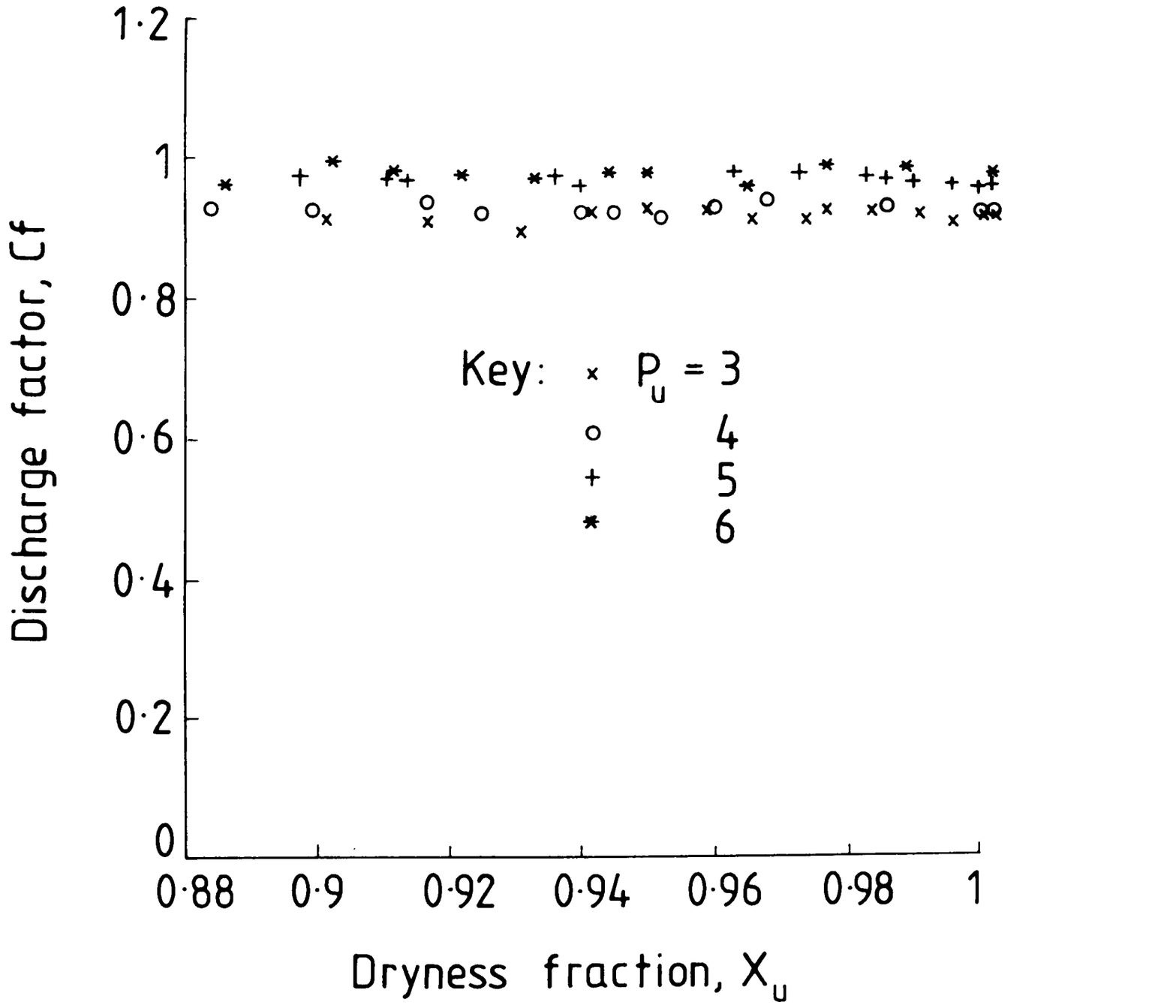

Fig. 5.11 Forward Flow Discharge Factor for Wet Steam (Choked Condition)

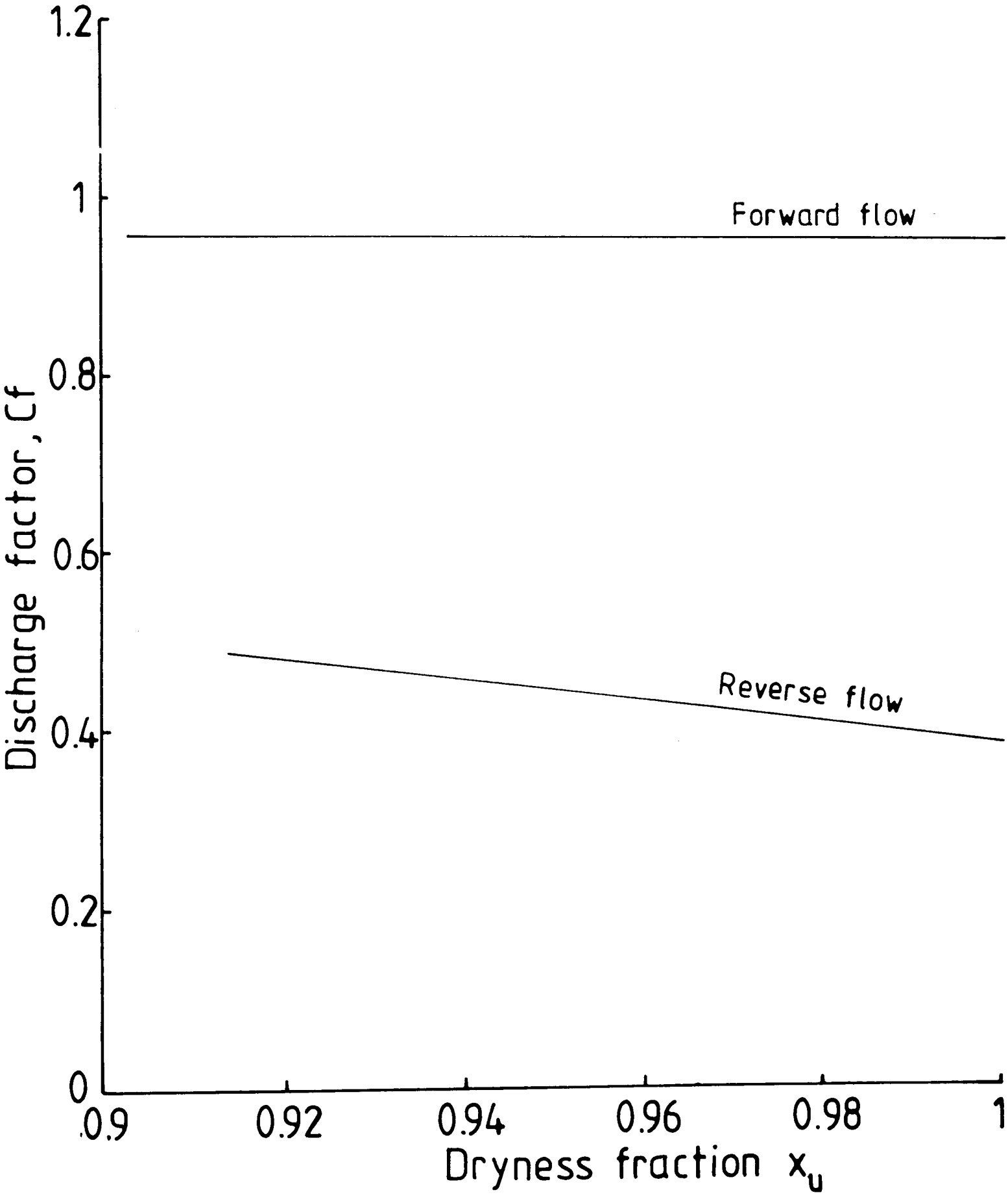

Fig 5.12 Forward and Reverse Flow Characteristics (Choked Condition)

CHAPTER 6

INTERNAL FLOW CHARACTERISTICS OF VORTEX DIODES

This chapter examines the internal flow in a simplified vortex chamber which was investigated experimentally using compressible superheated steam. The simplified geometry conforms to that of a vortex throttle (Section 2.1.4) and therefore the experimentation and subsequent flow analysis should strictly be applied only to that device. However, it is almost certain that the internal vortex of the vortex throttle and diode will be very similar, although the different exits of the two devices may influence the flows in that region. The vortex chamber was approximately twice the size of the previously used vortex diode (described in Figs. 4.4 and 4.5) to enable thermocouple and pressure tappings to be installed. The internal temperature and pressure distribution were measured for pressure ratios from 1.5 to 7.41, i.e. in the transonic region. From these experimental readings an analysis of the internal fluid mechanics was then used to determine flow velocity and the state point locus of the bulk flow.

The work was also extended to examine qualitatively the exhaust from the smaller Zobel type vortex diode (10 mm) which was characterised in Chapter 4 and shown in Figs. 4.21 and 4.22. Schlieren and Shadograph photography was used to visualise the air flow exhausting from the diode. The purpose being to examine and record the way in which the swirling flow exhausted from the axial

exit port. Also it was necessary to try and establish whether recirculation occurred in the diode exhaust flow. This phenomena, due to vortex breakdown is known to occur in other, comparable situations of swirling flow (see Chapter 3, Section 3.6).

6.1 Experimental Apparatus and Instrumentation

Figure 6.1 shows a schematic of the vortex chamber characterisation rig. Superheated steam was supplied to the vortex chamber via isolation and pressure reducing valves. Throttle valves were used to regulate the upstream and downstream pressures. The steam was condensed into a sub-atmospheric condenser which enabled relatively large upstream/downstream pressure ratios $\frac{P_u}{P_d}$ to be obtained. Upstream and downstream pressures were measured by calibrated pressure gauges. The corresponding half-shielded thermocouple temperature probes were similar to those described in Chapter 4, Section 4.1.

A third temperature probe was installed downstream of an orifice plate which was fitted to measure the mass flow rate of steam through the vortex chamber. The pressure drop across the orifice plate was measured by means of a strain gauge differential pressure transducer. Water flooding of the transducer pipework was maintained by condensate pots acting as cooling chambers near the line pressure tappings. The required orifice plate diameter was determined to be 30 mm and installed in accordance with B.S. 1042 [75].

Instrumentation was also fitted directly to the vortex chamber to measure local static pressures and internal wall temperatures. Ten static pressure tappings were drilled through the chamber wall, radially opposite the inlet port, as illustrated in Fig. 6.2. In addition to these a static pressure search tube was fitted through a gland in the centre of the chamber wall, Fig. 6.3. This could then slide along the axial centre line to measure static pressures through the exit duct and into the exhaust pipework. Individual radial or axial static pressures could then be determined using mercury U-tube manometers.

Ten internal surface temperature probes were fitted at 45° to the pressure tappings and at the same radii. These consisted of flush-mounted thermocouples in tufnol plugs bonded into flat-bottomed holes in the chamber internal wall, also shown in Fig. 6.2. The purpose of the tufnol was to thermally insulate the thermocouples from temperature gradients due to conduction in the steel wall. Flush mounting was necessary to prevent disturbance of the flow under investigation and to record local surface temperature only without disturbing the bulk flow. This method of pressure and temperature measurement was necessary for the calculation of velocity profile. Direct velocity measurements cannot be made, since the presence of a pitot tube will influence significantly the structure of the vortex flow. This was discussed previously in Section 3.5.

In order to log the thermocouple temperature readings for the

ten radial stations across the chamber they were connected to a multi-channel A/D converter. Each thermocouple provided an electrical e.m.f. analogue of the junction temperature at its radial position in the chamber wall. Analogue-digital conversion for each of the ten stations in turn produced a digital scan of the wall recovery temperatures.

Scanning and data-logging was controlled by a BBC micro-computer for which the program "DLOG8" was written as listed in Appendix F. Essentially consisting of two loops, the main program runs through the desired number of scans whilst an inner loop selects each channel in sequence. A/D conversion was controlled by a subroutine which was available from existing software. Accepting that conversion takes a finite time for each station, this sub-routine featured conversion completion with minimum delay.

The particular design of vortex chamber used for the quantitative investigation differs from the Zobel optimised diode although it operates in essentially the same manner. The detail of the vortex chamber is shown in Fig. 6.4.

The simplified design incorporates:

Tangential port diameter (cylindrical duct)	D_t = 50 mm
Axial exit diameter (cylindrical duct)	D_e = 38 mm
Chamber height	H = 50 mm
Chamber outer diameter	D_o = 350 mm
Tangential connecting pipe	d_o = 50 mm

And in terms of ratios:

$$\frac{D_t}{D_e} = \frac{H}{D_e} = 1.316$$

$$\frac{D_o}{D_e} = 9.2$$

$$\frac{d_o}{D_e} = 1.316$$

A flow straightener in the exit port was omitted but support "spiders" for the axial search tube were fitted in the pipework immediately downstream of the exit.

6.2 **Experimental Procedure**

6.2.1 Pressure-Flow Characteristics

Firstly the inlet and outlet steam conditions were obtained to observe the overall process across the vortex chamber. This treatment of the chamber as a "black box" was then continued to allow the high resistance pressure/flow characteristics to be determined for reverse flow conditions.

Within the limitation of pipework and fittings a range of constant upstream pressure, P_u, of 1 to 3 bar absolute were chosen (using 0.5 bar intervals). For each constant value of P_u, the downstream pressure, P_d was changed by throttling the flow into the condenser. Readings of upstream and downstream pressures and temperatures were recorded as were orifice plate downstream

temperature and d.p. transducer voltage. The voltage reading was linearly related to differential pressure which was determined by a simple calibration exercise (which had been carried out earlier). This enabled the mass flow rate through the orifice plate, and hence the vortex chamber, to be determined.

6.2.2 Internal Pressure Distribution

To determine the static pressure distribution through the vortex chamber section, radial and axial pressures were recorded for constant inlet pressure and temperature. It was therefore necessary to allow the system time to warm through and achieve steady-state conditions.

Static pressure readings were taken from one mercury manometer which was connected to each radial tapping in turn. A brief connection time was desirable for each tapping to minimise the collection of condensate in the manometer tubing.

With one exception, all the distributions were determined for a constant upstream pressure of 1 bar absolute. This was chosen so that all static pressures recorded would be sub-atmospheric and steam would not enter the instrumentation tubing and displace the mercury in the manometer. Initially the readings were found to be increasingly in error due to a steady build up of condensate in the manometer. This was attributed to molecular diffusion taking place between chamber steam and air in the tubing after their pressures had equalised. A glass reservoir chamber was therefore connected

into the tubing and partly filled with water to provide a surface upon which any diffusing vapour could condense.

Later sets of readings were also found to be inconsistent especially at the outer radial tappings. This was caused by slow "cycling" of the servo-actuated boiler control producing a variation in pressure of ± 50 mm Hg. This error was significant and was clearly unacceptable. Therefore, to maintain accuracy and repeatability of results the inlet steam pressure was carefully monitored and manually controlled throughout the experiment. This was achieved by permanently connecting the outer radial tapping to a separate U-tube mercury manometer with all adjoining tubing completely flooded with water. This head of water then had to be taken into account during the calculation of static pressure.

Atmospheric pressure (± 5 mm Hg) was maintained at the outer radial tapping by fine adjustment of the inlet steam throttle valve. Under these conditions the static pressure variation on the axis at the chamber wall was found to be generally less than 3 mm Hg.

In an attempt to record a pressure distribution for a pressure ratio greater than 5.56 the upstream pressure was increased to 2 bar absolute. At a pressure ratio of 7.41, one set of readings were taken. However a steam bubble became entrapped in the upstream monitoring manometer and so the fine control and consequent accuracy had to be abandoned for this test. Further difficulties with instrumentation resulted in no reliable pressure distributions being established for greater upstream pressures than 2 bar absolute.

6.2.3 Internal Temperature Distribution

Initial tests showed that the temperature at an individual station varied slightly at each scan. A running average of temperature at each station was therefore required with estimates of error. These calculations were built into the "DLOG8" program, introduced in Section 6.1 and listed in Appendix F.

If each reading is denoted by x_i then for n cycles, the mean of all readings in a set is:

$$x_m = \frac{1}{n} \sum_{i=1}^{n} x_i \qquad (6.1)$$

A simple statistical analysis to describe the data population is the sample standard deviation:

$$\sigma_{n-1} = \frac{\left[\sum_{i=1}^{n} (x_i - x_m)^2 \right]^{1/2}}{n - 1} \qquad (6.2)$$

Although primarily controlling the A/D converter, the program used dimensional arrays to store and update data from previous scans for the above calculations. Readings were taken under steady-state conditions at the same pressure ratios achieved in the pressure distribution tests. The upstream temperature was also adjusted to emulate inlet conditions and flow rates of Section 6.2.2. Each scan of readings took less than 6 seconds so just the last scan of 5 cycles was printed as a hard copy to log the incoming data.

6.3 Results and Discussion

6.3.1 Vortex Throttle Characteristics.

The reverse flow characteristics were obtained for constant upstream pressures, P_u. The overall process is a throttling one and is shown in Fig. 6.5. Variation of mass flow rate with upstream to downstream pressure ratio is shown in Fig. 6.6. The effect of choking can be seen at a pressure ratio of about 6. This critical pressure ratio differs slightly from the results of the previous work detailed in Chapter 4, but both differ considerably from the theoretical value of 1.86 for one-dimensional isentropic flow. Once again, as discussed previously, this can be attributed to the three-dimensional nature of the swirling flow in the exit port which will have both tangential and axial components of velocity. Investigations by Lewellen [68] indicated tangential Mach numbers as high as 1.4 may exist in the axial exit port of a transonic swirling flow. A greater pressure ratio will therefore be necessary to drive the vortex and to create velocities conducive with choked swirling flows.

Figure 6.7 shows the variation of discharge factor, Cf, (equation 4.9) with pressure ratio. The experimental points tend to fall onto one curve which implies that the discharge factor is a function of pressure ratio up to about 6 and then becomes independent beyond that point, i.e. the device is choked. The value of Cf approaches 0.28 in the choked region, i.e. the chamber exhausts only 28% of the ideal nozzle mass flow. This shows a

greater resistance to flow than for a Zobel type diode, as presented in Chapter 4, where Cf = 0.38 for similar pressure ratios. Although this represents a marked improvement in reverse flow performance it should be pointed out that the Zobel diode is an optimised design for both forward and reverse flow. The chamber under investigation lacks the conical diffusers at the axial and tangential ports and the rounding of the tangential port entry associated with the Zobel design. Clearly the different vortex chamber and exit port geometry is responsible for the improved reverse flow resistance and, presumably the different critical pressure ratio. The chamber diameter and height are twice those of the Zobel design; the effect of boundary layers on the vortex are therefore reduced.

6.3.2 Pressure Distribution

The static pressure distribution through the vortex chamber and exit pipe was obtained at steady state conditions for constant upstream to downstream pressure ratios. Non-dimensional static pressure readings are plotted against non-dimensional radial (chamber) and axial (exit pipe) positions on Fig. 6.8 for pressure ratios of 1.5 to 7.41. In Fig. 6.8 it can be seen that all of the pressure drop occurs in the vortex chamber, particularly within the inner third of the chamber radius. For the sub-critical cases it can be seen that much of the dynamic pressure is recovered in the exit duct as the flow expands in the 77 mm pipe into which it discharges. This leads to a strong adverse pressure gradient after the throat. In vortex valves operating with incompressible flow it

is known [59,79] that a strong reversed flow exists in the throat of the valve and that this blockage is largely responsible for the high resistance of the valve. It is believed that the adverse pressure gradient shown in Fig. 6.8 represents a similar reversed flow region. The pressure distribution for the supercritical case, on the other hand, shows only a weak pressure gradient. The concept of reversed flow is not compatible with choked and supersonic flows and a reversed flow zone would simply be swept downstream.

A noticeable feature of the vortex chamber operation was the creation of a high pitched whistling noise. This became loudest at a pressure ratio of about 2.8. Swirl in the chamber exhaust was observed qualitatively by the inability to stop the axial search tube rotating when inserted more than 85 cm through the chamber. Vibration of the search tube in the swirling flow caused the tube to fail by fatigue at its pressure tapping point on one occasion.

Upon stripdown the chamber wall showed evidence of boiler water carry-over. This was in the form of spirals converging to a single point which was displaced from the axis by 3 mm, opposite the inlet port. Considered two-dimensionally, although the mass flow is fed to the exit radially for a full 360°, the inlet flow is admitted and mixes with the existing vortex over about 90°. The resulting imbalance is sufficient to slightly distort the spiral vortex away from the inlet.

6.3.3 Temperature, Velocity Profile and Vortex Exponent

The static temperature within the vortex chamber can only be measured by an instrument which will not disturb the flow. Fluid nearest the internal surface is brought to rest by viscous effects and, if the flow were adiabatic, would reach stagnation temperature. However velocity changes very quickly near the surface and temperature gradients cause heat transfer within the boundary layer. Work is also done by shearing between adjacent fluid layers.

Assuming an adiabatic wall, fluid in contact with the surface is at a temperature between the total and static temperatures due to some degree of temperature recovery through the boundary layer. The recovery factor is established by Cheers, [89], as:

$$\alpha = \frac{T_r - T}{T_o - T} \quad \text{where } (0.75 < \alpha < 1) \tag{6.3}$$

T_r is the local internal wall temperature, or recorded temperature, measured by thermocouples.

Barrow and Ryley [90] developed an expression for the recovery factor in steam given by

$$\alpha = 1 - (1-Pr)4.45\ Re^{-\frac{1}{5}} \tag{6.4}$$

they suggested a useful working value of $\alpha = 0.9$. A simple expression was reported by Emmons and Brainend [47] in terms of Prandtl number only. For laminar flow over a flat plate with $0.5 < Pr < 2$ they proposed:

$$\alpha = Pr^{1/2} \tag{6.5}$$

and for flow over flat plates with higher Reynolds numbers they proposed

$$\alpha = Pr^{1/3} \tag{6.6}$$

In the present work the expression in equation (6.6) has been adopted. However to solve for static temperature it is still necessary to have another equation relating velocities and temperature. Bernoulli's equation was ineffective as a first step in an iterative procedure as it only holds for very small Mach numbers. Consequently a mathematical model of the vortex flow had to be chosen to provide another known variable.

The combination of the simplified momentum equation, ($\frac{dp}{dr} = \rho \frac{v_\theta^2}{r}$ equation 3.37), the equation of state ($P = \rho RT$) and tangential Mach number ($M_t = \frac{v_\theta}{\sqrt{\gamma RT}}$) yields:

$$M_t = \left(\frac{r}{\gamma P} \frac{dP}{dr}\right)^{1/2} \tag{6.7}$$

This equation was used as a basis for analysis of nitrogen flow by Kendall [91] and air by Holman and Moore [50], respectively. In the present work this tangential Mach number relation was used to estimate both static temperature and tangential velocity. Values of $\frac{dp}{dr}$ were determined by graphical construction of the available data from the pressure distribution measurements (Fig. 6.9). The procedure for calculating temperature and tangential velocity is

given in Appendix G.

The Navier-Stokes equation of motion as shown in Section 3.2 can be reduced to:

$$v_r \frac{dv_r}{dr} - \frac{v_\theta}{r} = - \frac{1}{\rho} \frac{dP}{dr} \qquad (6.8)$$

It should be noted that, in the simplification, constant density was assumed and strictly the above equation should only apply for incompressible flow. However when $v_r = 0$ it does reduce to the earlier inviscid relation. This is valid for such a compressible fluid because, with purely tangential flow, constant density would exist along a streamline.

From an initial state temperature estimate, the Prandtl number was determined to enable T to be recalculated. To solve equation (6.8), the radial velocity, v_r, was calculated from the continuity equation

$$\dot{m} = \rho v_r \, 2\pi r H \qquad (6.9)$$

where $\dot{m}$ is known from the chamber characterisation tests and ρ was determined from steam table by knowing pressure and temperature. Values of $\frac{dv_r}{dr}$ were obtained by graphical construction. The "NAVIER4" program was used to calculate values of $v_r \frac{dv_r}{dr} - \frac{v_\theta^2}{r}$ and $- \frac{1}{r} \frac{dP}{dr}$. (See Appendix H for "NAVIER4").

The validity of experimental data was checked by plotting experimentally derived values against calculated results on Fig. 6.10. A straight line correlation with unity slope is seen to exist. The variance about the line represents an error of ±0.1% in

the application of this equation to compressible vortex flow where the tangential velocity is by far the dominant component.

The static pressure distribution for the radial tappings only is shown on Fig. 6.9 as used to construct $\frac{dp}{dr}$ and used with the recovery temperature distribution to calculate static temperature and velocity profiles. These have been plotted in terms of radial and tangential Mach numbers on Figs. 6.11 and 6.12 respectively. As continuity predicts, the greatest increase in radial Mach number occurs within the inner radii of the chamber but should inevitably tend to a finite value at the chamber axis. The curves are not completed within the exit radius as the radial velocity here will vary across the chamber height as the flow takes on an axial component.

The tangential Mach number profile on Fig. 6.12 is also seen to increase as the vortex is being driven towards the exit radius. The maximum tangential Mach number is seen to peak at just over 0.8 at the inner instrumentation station. However the three-dimensional velocity components with the exit radius were not determined and for completeness the graph is drawn to represent transition to a forced vortex within that region.

In an attempt to gain further information from the calculated results, the tangential velocity has been plotted against radius on Fig. 6.13. If the flow was inviscid without chamber wall shear stresses restraining the vortex, the flow would be that of the free vortex.

$$v_\theta r^n = \text{constant}, \quad \text{where } n = 1 \tag{6.10}$$

since angular momentum must be conserved. The experimental data is therefore presented on a log plot to determine the degree it approximated the isentropic free vortex. The value of the vortex exponent, n, may be determined from the slope of the lines which were established by the method of least squares. The lines on Fig. 6.13 are very nearly parallel, indicating that the vortex exponent is relatively independent of pressure ratio or mass flow rate. The average slope of the straight lines on Fig. 6.13 was found to be 0.69. This gives a general vortex relation of:

$$v_\theta r^{0.69} = \text{constant} \tag{6.11}$$

for the vortex chamber, determined from experimental readings of recovery temperature and static pressure. Since the vortex exponent, $n \neq 1$ the flow is not an isentropic free vortex.

The ten thermocouple temperature readings, recorded using "DLOG8" showed very little variation across the chamber radius. The reading, or recovery temperature, T_r, generally peaked at stations 5 and 3 then fell to a minimum at the inner station 1 with a maximum recorded variation of 5°C. With the exception of the two inner stations, the calculated values of static temperature remained greater than 120°C given Pr greater than or equal to 1, and hence a recovery factor of 1. This then gives $T_o = T_r$ which implies that stagnation temperature, T_o, remains essentially constant across most of the vortex, where the radial flow is very small.

This confirms the assumption of constant stagnation temperature used by Holman and Moore [50] as a mathematical simplification to analyse velocity profiles from static pressures alone. They deduced a vortex exponent of 0.68 from a different analysis based on an energy balance, neglecting radial velocity. This correlates well with the exponent of 0.69 determined from the results of the present investigation. The similarity of these values is noteworthy when considering their vortex chamber design (5" diameter, 4" long and 0.75" exit diameter). Their analysis is however rather unclear and did not apply well to a 2" exit diameter chamber, [50].

For comparison purposes, an attempt has been made to apply their analysis to the experimental data of the present work in Fig. 6.14, where the vortex exponent should be represented by the slope of straight lines. The non-linearity at the outer chamber radii could be an effect of incoming steam mixing with the vortex flow. The average slope of the linear portions does however suggest a slope of 0.68, as for Holman and Moore's chamber, which supports the vortex exponent of 0.69 resulting from the analysis established uniquely in this project.

Holman and Moore also presented an expression for the polytropic exponent as:

$$n_1 = \frac{1}{1 - \frac{nR}{C_p}} \qquad (6.12)$$

Substituting experimental values into this gives a polytropic

exponent of 1.192 for the vortex chamber expansion. Comparing this with the isentropic index of γ = 1.335 again confirms a non-isentropic expansion process.

6.3.4 State Point Locus

The state point locus shown on the Enthalpy-Entropy diagram, Fig. 6.15, was plotted from the calculated values of static temperature and experimental pressure readings. For clarity, only two constant pressure ratios are shown, $\frac{P_u}{P_d}$ = 7.41 and 5 corresponding to upstream pressures of 2 and 1 bar absolute respectively. In both cases an almost isentropic expansion is seen to occur in the inner radii between stations 5 and 2 culminating with production of entropy to station 1 (Fig. 6.2). Having driven a strong vortex the chaotic, swirling flow then experiences an enthalpy recovery as it exhausts from the chamber throat. It is of note that in the case of $\frac{P_u}{P_d}$ = 5, for example, a minimum pressure of 0.067 bar absolute was recorded at the centre of the chamber wall. In order to reach that constant pressure line the state point locus would certainly need to cross the saturation line. In an equilibrium expansion, condensation would begin to form within the vapour when the saturated vapour line is reached. As the expansion continues below this line into the wet region, then condensation proceeds gradually and the dryness fraction of the steam would become progressively less. However in reality phase change is delayed and the vapour continues to expand as a supersaturated vapour until some point at which condensation occurs spontaneously.

The point at which this happens may be within the inner radii of the vortex chamber or within the exit pipe. Up to the point at which condensation takes place the steam is in a metastable state, although the introduction of the search tube can promote condensation.

In the event therefore we must recognise that although the pressure recorded at the centre of the chamber wall is well into the wet region this does not necessarily mean that the state point of the bulk of the flow has also reached that condition. Furthermore, since the expansion in the exit region is non-equilibrium it cannot be represented on the h-s diagram. Therefore Fig. 6.15 shows only the parts of the expansion which were satisfactorily measured.

6.4 **Exhaust Flow Visualisation**

In many engineering problems, flow cannot be viewed directly e.g. motion of air past models of aeroplane wings, exhausting jet flow, problems of convection, etc. In such cases the phenomena that are of interest frequently involve changes of the refractive index across the field to be investigated, which can then be visualised or photographed by using optical methods that depend on the effects of refractive index changes on the transmission of light. Of the techniques available, Schlieren and Shadowgraph photography are probably the most popular. Extensive use is made of flow visualisation in aerodynamic research for studying high speed air flow, where the changes of refractive index that accompany the

density changes across the flow field can be readily observed.

In this part of the work, flow visualisation was adopted for observing the swirling air flow exhausting into the atmosphere from a Zobel type vortex diode with 10 mm throat diameter.

6.4.1 Experimental Apparatus and Procedure

Figure 6.16 shows a schematic of the flow visualisation experimental rig. Air was supplied at pressures up to 33.5 bar (470 psig) by a large Bellis and Morcom 4-stage reciprocating compressor and delivered through a 50 mm supply pipe. A dome loaded pressure controller was installed in the diode supply pipe for regulating the upstream pressure. To enable the exhaust flow to be observed the diode body was machined to the extent that the exit port consisted only of a converging nozzle, as shown in Fig. 6.17. This diode is similar to one which was used for the air characterisation (Chapter 4, Section 4.2.1) and shown in Figs. 4.22 and 4.23.

The Schlieren apparatus used was conventional and consisted of an argon arc spark light source, condensing lenses, two knife edges, two 10 cm diameter concave mirrors of 122 cm focal length, and a camera. Problems were encountered during the experimental work in the correct positioning of the various components with respect to each other; this was overcome with experience. In setting up the Schlieren equipment the argon jet light source was placed in approximately the correct position (focus of first mirror). The first adjustment was to locate the horizontal knife edge at the

focus of the first lens. The light passed through the second lens and was converged to its focal point before being diverged onto the first mirror. The first mirror was rotated until the light beam passed through the exit port of the diode. The next adjustment was to set the parallel light beam formed by the first mirror so that it passed through the exit port in the direction perpendicular to the exhaust flow. The second mirror was moved laterally and vertically until it was filled by the parallel beam emerging from the working section and was rotated until the light reflected from it passed through the second knife edge and formed an image of the flow on the viewing screen. The knife edge was set in the focal plane of the second mirror, and its position was adjusted. The edge was then set on that the required fraction (usually half) of the image of the source was cut off. The amount of cut-off was estimated approximately by holding a white card immediately behind the knife edge so that the amount of light intercepted could be adjusted and the intensity of the remaining light observed. In order to maintain the light rays parallel and to avoid aberration difficulties, the angle θ_1 was set approximately equal to θ_2 and both angles kept as small as possible (see Fig. 6.16).

It was found that the appearance of the images of the flow (shock waves, boundary, etc.) in the neighbourhood of large density gradients were more sensitive to the focussing of the apparatus than was the sharpness of the geometrical image of the flow. The focussing was found to be more accurate when carried out with the high speed air flow present and exhausting to the atmosphere.

Schlieren images of the exhaust air flow were observed by projecting parallel light rays from the collimated light source across the flow field between mirrors. The rays leaving the second mirror, converged to its focal point where a knife edge was placed and then diverged onto a camera fitted with a zoom lens. The knife edge acts as an optical filter and only allowed approximately half of the light to be transmitted to the camera. This filter established better contrast between that light which was undisturbed and that light which had been disturbed on passing through the flow containing a density gradient. Because of the refractive index changes in the flow, light passing through the flow will diverge and regions of the flow will appear relatively dark or bright compared with the average background intensity. By removing the knife edge, shadowgraph images of the flow were observed. Shadowgraphs are sensitive only to second derivative changes in the density of the flow field and it is useful for examining rapid changes in the flow field, such as appearance of shock waves.

The Schlieren technique is sensitive to first derivative changes in the density of the flow field and reveals more detail of the flow compared with shadowgraphs.

Alternative shadowgraph and Schlieren images were photographed by removal or repositioning of the knife edge. Instantaneous flow behaviour was observed using a capacitor-discharged spark in an argon atmosphere as a light source. Such brief exposures were made in a darkened laboratory whilst holding open the camera shutter.

Exposures were made for inlet pressure increasing in increments of 0.7 bar (10 psig) up to 32.4 bar (470 psig).

6.4.2 Results

Schlieren photographs, taken with a horizontal knife edge, of the flow of air exhausting from a vortex diode are shown in Fig. 6.18 for increasing inlet pressures. In Fig. 6.19 the flow field can be seen when photographed using a vertical knife edge. Figure 6.20 shows a typical shadowgraph of the flow. These photographs are only a selection of the many that were taken during the investigation.

The swirling exhaust flow of air with upstream pressure greater than 10 bar (145 psig) were visible to the naked eye using only local room lighting. This indicated that significant air density gradients existed in the region within about 3 exit diameters of the outlet.

In the first set of photographs, (Fig. 6.18) the knife edge was perpendicular to the exhausting flow so that the components of the density gradients parallel to the flow direction are visualised. The shock waves appear as regions of increased illumination. In the second set of photographs, Fig. 6.19, the knife edge was vertical and hence parallel to the flow; in this case component of density gradients perpendicular to the flow direction are visualised.

A sketch of the flow pattern of the photograph shown in Fig. 6.18g is shown in Fig. 6.21. The photograph indicates the possible existence of recirculation zone at the exit of the diode, and shows clear evidence of the shock wave, which occur at about one diameter downstream of the diode exit.

6.4.3 Discussion

As stated earlier, the high resistance of vortex chambers operating with incompressible fluids is largely attributed to the blocking effect of strong reversed flows, or backflows in the outlet throat. The initiation stages of an external backflow occur as rapid decelerations in a limited region, being known as "vortex breakdown". This can be defined as the stagnation of the axial flow followed by the occurrence of a region of reversed axial flow near the vortex centreline.

This concept is not compatible with choked and supersonic flows and was investigated by Lewellen et al. [68] who proposed that in the subsonic case, a backflow can exist from downstream of the exit, along the axis to the chamber wall. Then, by increasing the flow rate to transonic flow, the minimum cross section becomes choked and the backflow forms into two distinct cells as on Fig. 6.22. Sarpkaya [57] observed this external cell as an ovoid region of circulating incompressible fluid. A similar flow structure in air is described by Gore and Ranz [92] as an almost spherical external recirculation zone with a clearly defined upstream

stagnation point. This "bubble" type of vortex breakdown is described by Leibovich [56] as looking like a body of revolution placed in the flow.

Another form is the "spiral" type appearing as a spiral shape rotating about the axis in the same sense as the fluid. A classic example of this phenomena is its appearance in the leading edge vortex flows formed above a delta wing. In either form a stagnation point appears on the vortex axis followed by a limited region of reversed axial flow near the centreline. An expanding swirling flow such as that in the axial exit port of the vortex diode is known to cause vortex breakdown as a result of substantial swirl velocities increasing the pressure along the axis.

Hall [66] discussed in some detail the physical effects of compressibility on vortex cores. In particular he considered the relative changes in the axial velocities at the centreline and at the core boundary. When a fluid with strong swirl is flowing along a duct there is a tendency for it to be centrifuged towards the wall. By continuity, the axial component of velocity is therefore greater near the wall than on the centreline. Coupled with the effects of wall shear stress, this produces an axial velocity profile symmetrical around the axis of the duct with a peak towards the wall and a lower velocity region at the centreline. This is true whether the flow is compressible or incompressible.

When a subsonic flow such as that described above reaches an expansion, the axial velocity reduces. The centreline velocity,

being lower than at the core boundary will stagnate and then reverse - vortex breakdown will have occurred and a reverse flow zone formed. LDA measurements of swirling flow by Uchida et al. [93] showed the axial velocity at the centre of the core decreasing rapidly to zero just at the tip of the bubble breakdown, Fig. 6.23. However, for a supersonic flow, although the centreline axial velocity will again be less than that at the core boundary; both will be increasing - stagnation and flow reversal will not occur.

If this concept is now related to the swirling flow exhausting from the vortex chamber, then at some region in the exit duct the flow will choke when the axial Mach number reaches unity. (Clearly from the present discussion this will not occur at a plane section.) After this region the flow will accelerate and the axial velocity profile described above will be produced. The crude nozzle design ensures that the jet is underexpanded as it leaves the throat and the flow will encounter a complex shock wave and become subsonic. The conditions necessary for vortex breakdown have already been established in the supersonic region and thus flow reversal will occur very soon after the shock wave. In relation to the vortex diode, therefore, a reverse flow zone will exist but it will be downstream of the exit port and will have no influence on the diode resistance - hence the reduction in performance of the diode in going from conditions of incompressible to compressible flow.

The Schlieren photographs, Figs. 6.19 a-h show the effect of increasing inlet pressure (and hence, pressure ratio) on the vortex

chamber exhaust flow. These photographs indicate changes in the fluid density and cannot give an indication of flow direction. At P_u = 50 psig the bulk flow is seen to be confined to an annular region where the high axial velocities will be formed. Vortex breakdown is not apparent here although an axial reversed flow may exist into the nozzle exit. Fig. 6.19c shows a choked nozzle at P_u = 100 psig (P_u/P_d = 7.8). In this case there is a step change from supersonic to subsonic flow depicted as a curved shaped shock wave just downstream of the exit port. The densely turbulent flow existing for a further three or so exit diameters downstream may represent a region of reversed flow following further rapid deceleration after the shock wave. This can be more readily visualised from Fig. 6.19g with P_u = 350 psig. The curved shock here appears further away from the exit port as the upstream face of an ovoid, recirculating region. To reach stagnation conditions the flow first becomes subsonic through the shock before decelerating into a vortex breakdown. The reverse flow zone is followed by a less dense wake region before the onset of spiral vortex breakdown at the top of the photograph. (See also Fig. 6.21).

The exit port in the photograph forms an under-expanding nozzle, having no diverging portion at all. The shape of the shock wave in the expanding swirling jet forms an ideal geometry after which a "bubble" type vortex breakdown may form. Fig. 6.19g also clearly illustrates the radiation of sound waves from the source at the nozzle exit. This phenomenon was investigated in depth by Davies and Oldfield [94].

The shadowgraph on Fig. 6.20 shows an extremely turbulent exhaust flow. It can be seen that a shock wave (dark band) appears to be located at about one diameter from the exit followed by a curved region which may represent the recirculating zone.

On all photographs a region of high density can be recognised and it moves downstream as the upstream pressure of the diode increases. All this evidence, perhaps, confirms the existence of the vortex breakdown but it is still possible that these photographs represent a complicated three-dimensional Mach intersection.

In order to enhance the effect of local change of density, localised heating of the exhaust jet was carried out by suspending a resistance heated wire across the exit plane. This was supplied at 30V, 15 amp. A.C. from a mains transformer. A series of photographs taken at varying wire heights and inlet pressure showed no significant change on flow pattern. It was hoped that if reverse flow was present it would be seen.

The diode rear wall was then drilled axially for the purpose of gas injection. By injecting a gas with a high density it was thought that it might be held in a reverse flow zone and be indicated on the photograph. This position for the hole was chosen as the quantitative pressure distribution shows the pressure here to remain less than the exit pressure and should consequently draw gas in when exhausting to atmosphere. This was found only to apply for inlet pressures less than 5.86 bar (85 psig) $(\frac{P_u}{P_d} = 6.8)$ above

which, the exit pressure was exceeded at the back wall. A series of photographs using argon injection produced results identical to initial observations without any noticeable pictorial enhancement.

It has been strongly inferred in this and in earlier chapters of this thesis that the change in the high resistance properties of the vortex diode between incompressible and choked flow can be attributed to the displacement of the reverse flow zone from the exit region as the flow reaches the critical condition. There are, however, other areas of flow within the valve which contribute to its resistance and these should also be considered.

If the vortex diode is considered as being made up of a tangential nozzle, a swirl chamber and an exit region then the likely changes in resistance of each of these, as the pressure ratio across the diode is increased, can be assessed.

Considering first the tangential inlet, then the losses here are very similar to that of a nozzle or contraction. Although the diode may be exposed to a pressure ratio which causes the exit flow to become highly compressible; the inlet region remains very much in the incompressible region. For example, for an inlet pressure of 12 bar as the inlet to outlet pressure ratio is increased from 1.2 to 19 the inlet Reynolds number based on the inlet diameter changes only from 2.7×10^5 to 6×10^5. The localised flow remains therefore very much in the same regime and the nozzle resistance is unlikely to change significantly.

In the flow through the vortex chamber, it was seen earlier in this Chapter that the vortex exponent has a value of 0.69 and is reasonably constant for pressure ratios from 1.5 to 7.41. This compares with a value of 0.58 obtained by Syred [95] in air at low pressures. The vortex field and hence the radial pressure gradient does not appear to be significantly affected by the increase in pressure ratio. The resistance of the vortex chamber can also be influenced by the presence of reversed radial flow caused by the strong centrifugal field and the ability of the fluid to by-pass the centre of the vortex chamber via the end-wall boundary layers. This behaviour was discussed earlier in Section 3.5. A visual manifestation of this phenomenon is the appearance of a spinning body of stagnant fluid. This feature was examined by Wormley [96] who used water in a 7 in. diameter, 1.75 in. height vortex chamber. He observed that this "doughnut" region filled the chamber to a radius of 0.68 r_o at $\lambda = \frac{v_\theta}{v_r} = 407$ and to a radius of 0.38 r_o for $\lambda = 58$. As λ was decreased the radial flow was seen to penetrate further into the chamber mid-plane and the size of the "doughnut" decreased, at $\lambda = 24$ the "doughnut" disappeared. In the present work the Zobel diode had a value of $\lambda = 27$. It is therefore unlikely that radial reverse flow occurs within the chamber, particularly in view of the fact that the chamber height in the vortex diode is much less than that of Wormley's vortex chamber.

Considering the above comments together with the measured pressure profiles and the deduced velocity profiles it appears that there are not significant changes in the fluid behaviour which would

cause a large change in resistance.

If the exit region is considered as a nozzle with swirling flow then the work of Norton et al. [69] and also Lewellen et al. [68] can be brought directly to bear. Fig. 3.15, after Norton et al., shows the effect of increasing the swirl level in a choked nozzle. Their mass flow parameter $\dot{m}a_o/p_oA_e$ is proportional to the discharge factor, Cf, used in the present work. It can be seen that as the swirl level increases so the mass flow falls significantly. To relate this to the vortex diode, if the area ratio A/A_e is taken to be the area of the vortex chamber to the exit then a value of about 87 is obtained, the swirl level for the diode ($r_R\omega/a_o$) is about 0.15. The mass flow parameter on Fig. 3.15 for these conditions is about 0.45. This corresponds to a discharge factor, C_f, of about 0.55.

Therefore, returning now to the vortex diode, which as a discharge factor of about 0.4, the exit nozzle alone has a discharge factor of about 0.55 and the contribution to the valve resistance from the inlet and vortex chamber accounts for the rest. Even in the choked condition, when the valve has a relatively low resistance, most of that is still provided by the exit. As the pressure ratio is reduced the resistance of the inlet and the vortex chamber changes little. In the exit region, however, the vortex breakdown will be able to re-establish itself in the exit port and, as described by Syred and Beer [65], will occupy up to 80% of the flow area, thus significantly affecting the overall resistance and

providing the high resistance performance of the diode which is seen for incompressible flow.

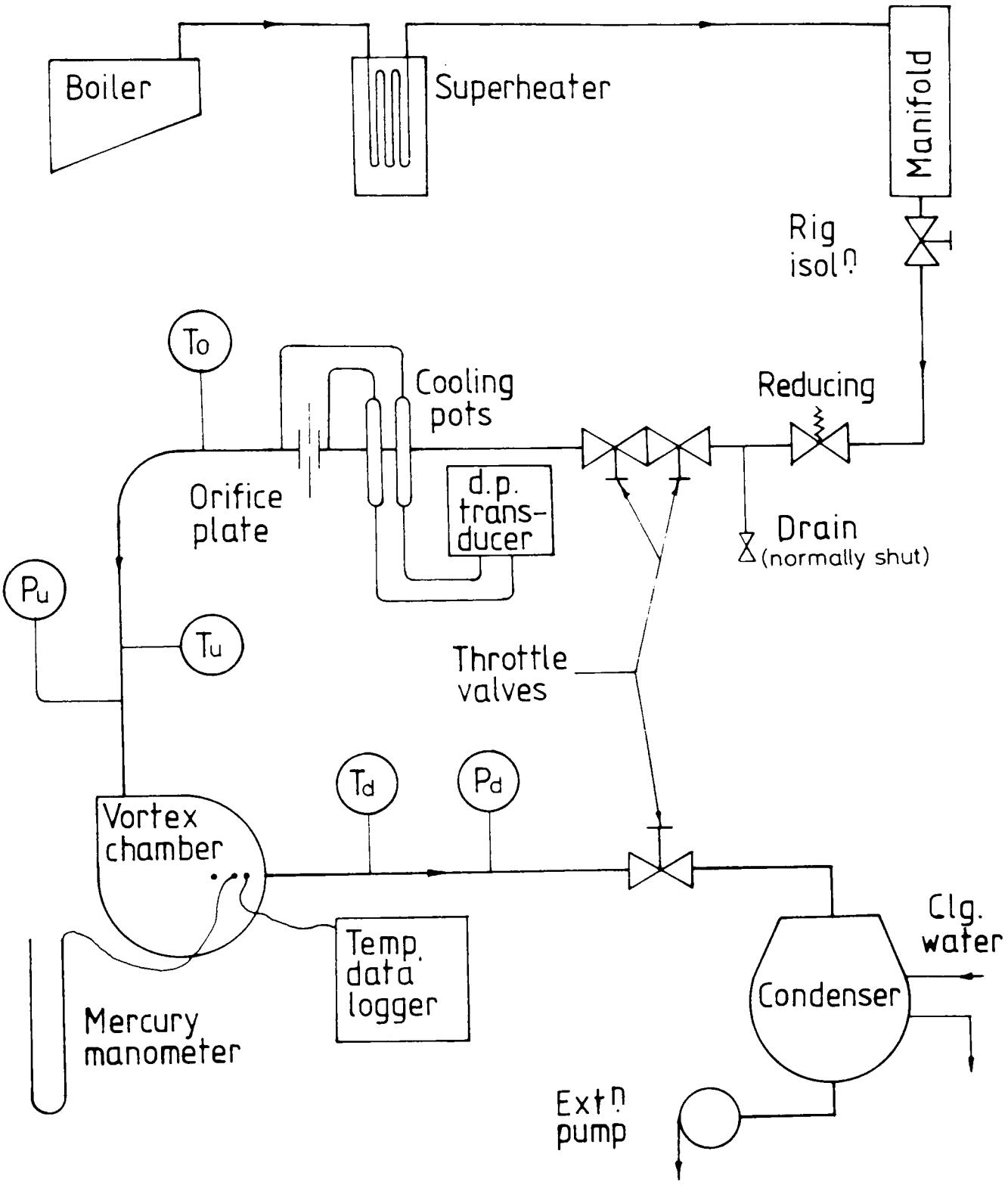

Fig. 6.1 Internal Flow Characterisation Rig

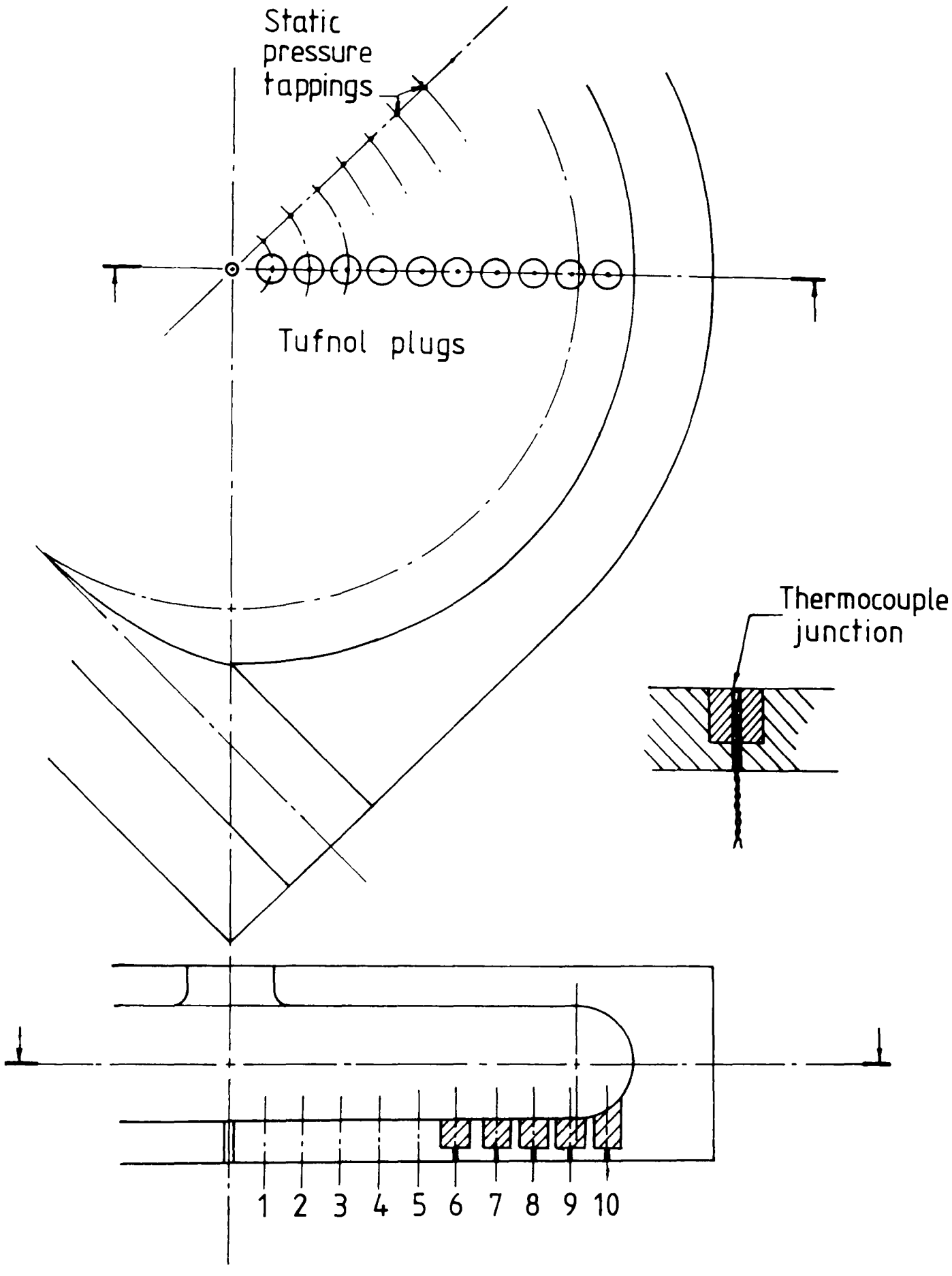

Fig. 6.2 Vortex Chamber Radial Instrumentation

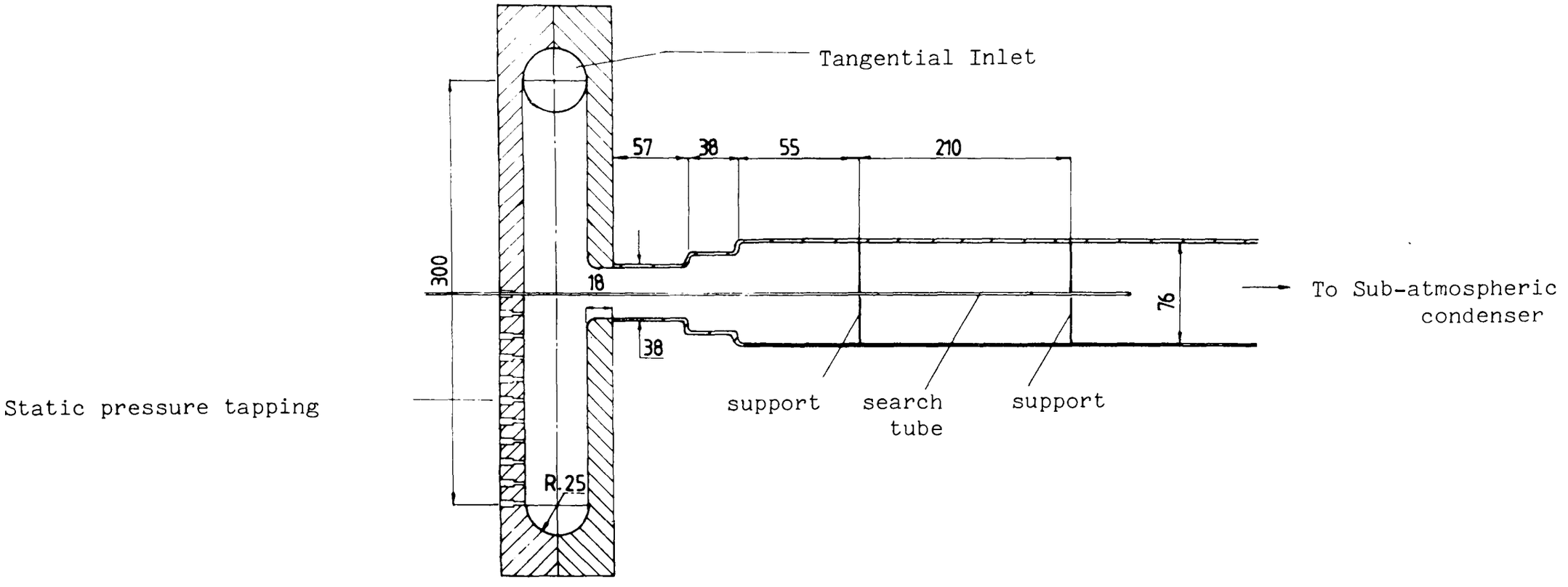

Fig.6.3 Vortex Chamber used for measurement of pressure distribution

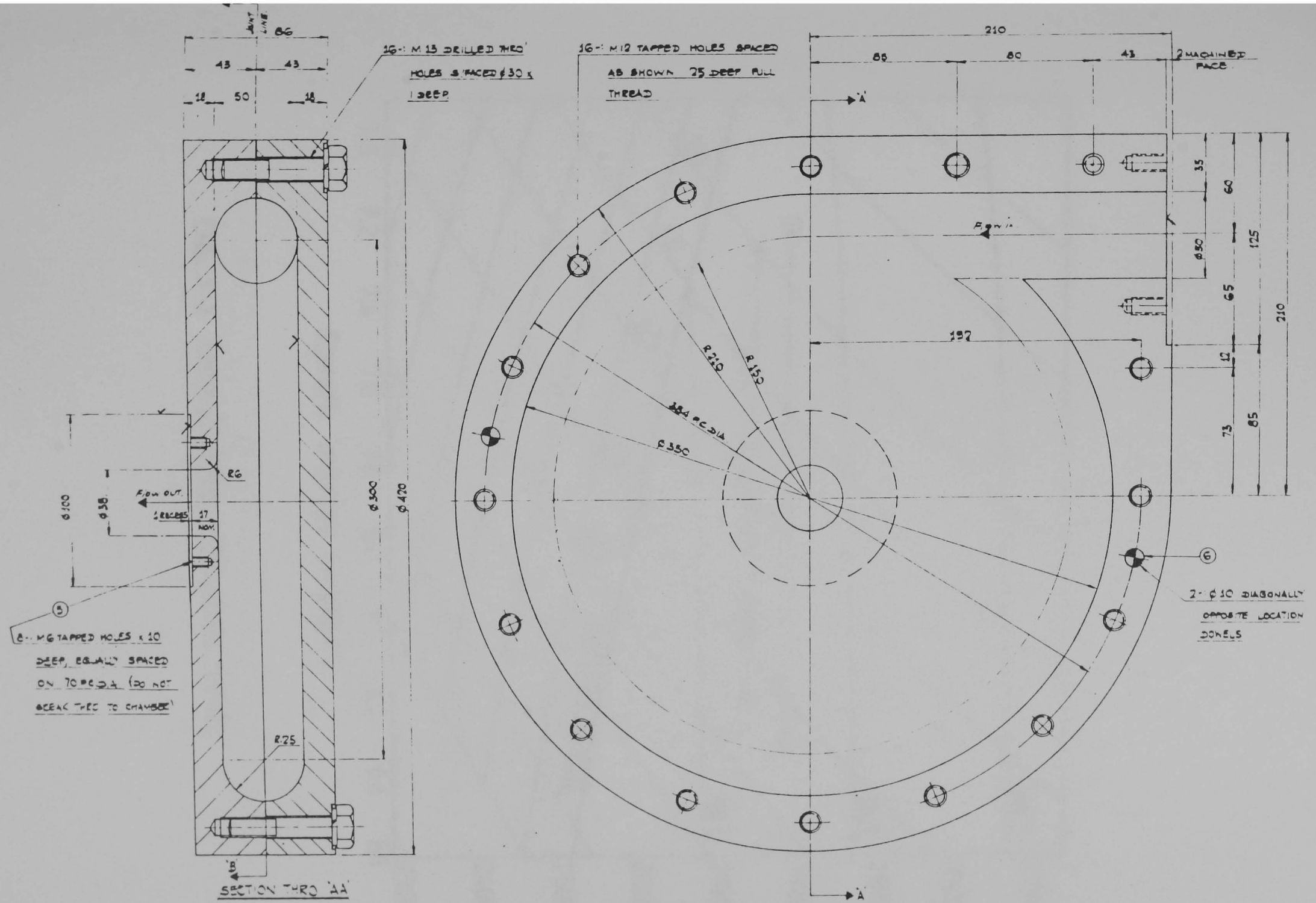

Fig. 6.4 Detail of Vortex Throttle

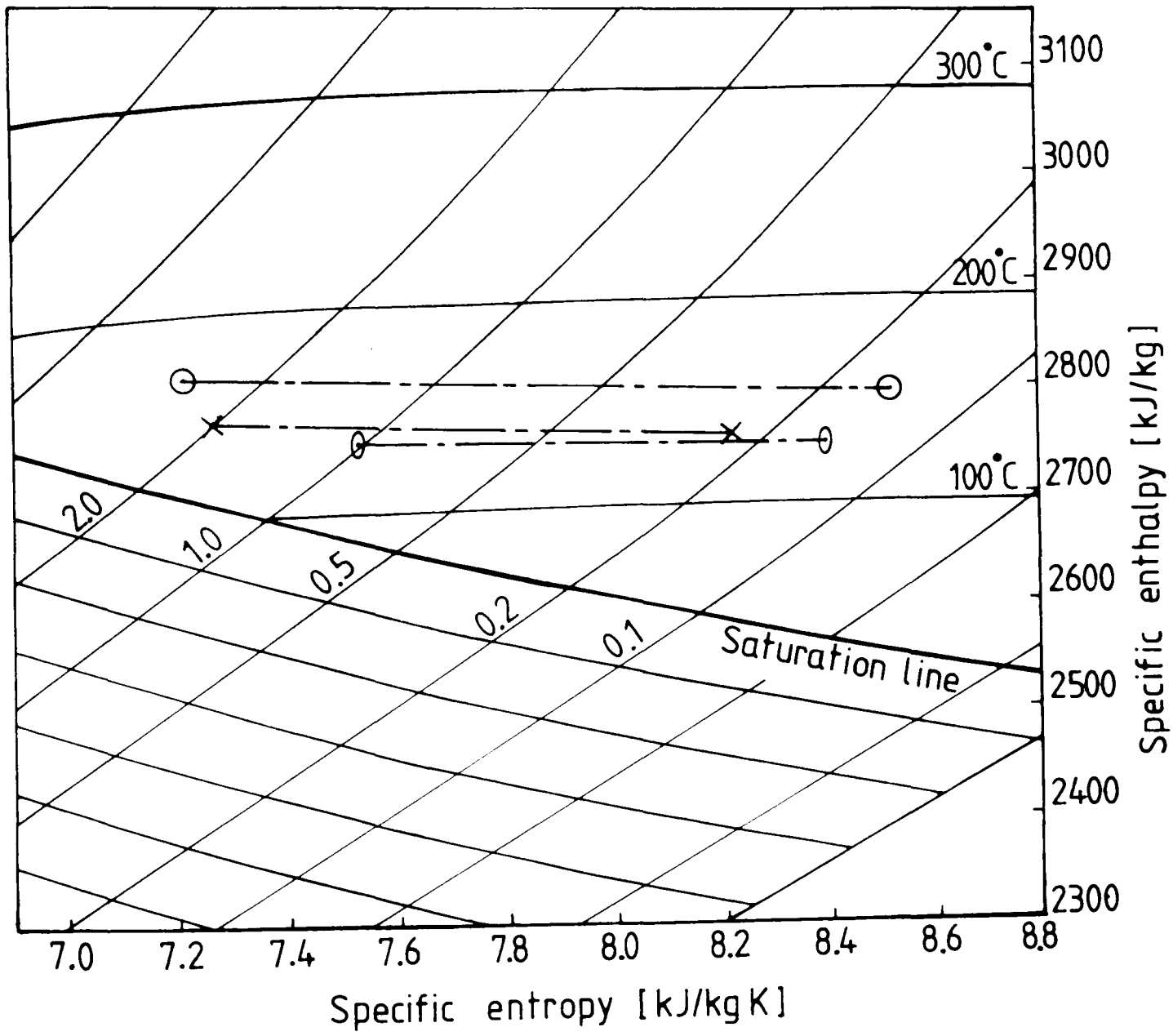

Fig. 6.5 Vortex Chamber - End State Points

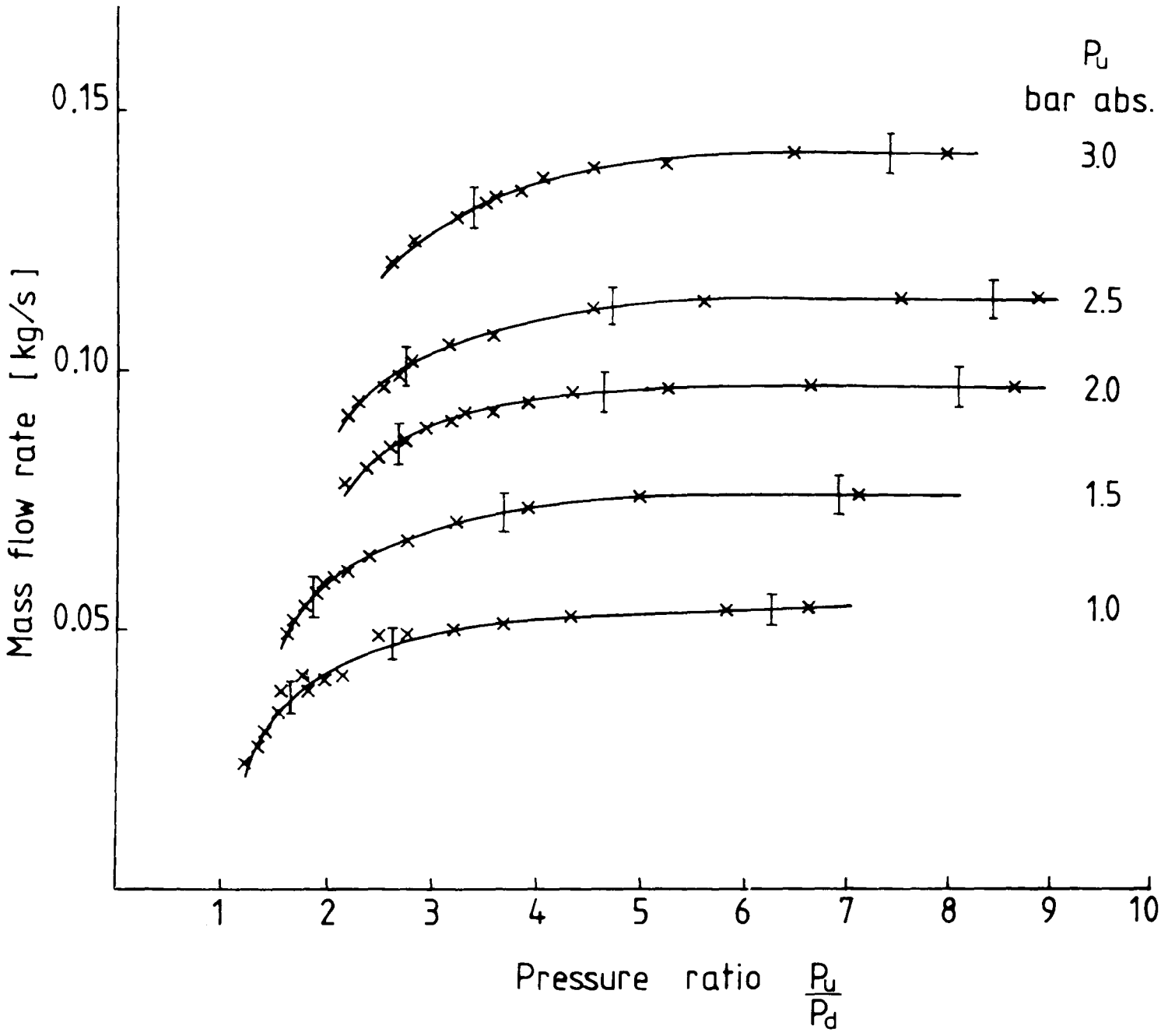

Fig. 6.6 Mass Flow Through Vortex Chamber in Reverse Flow

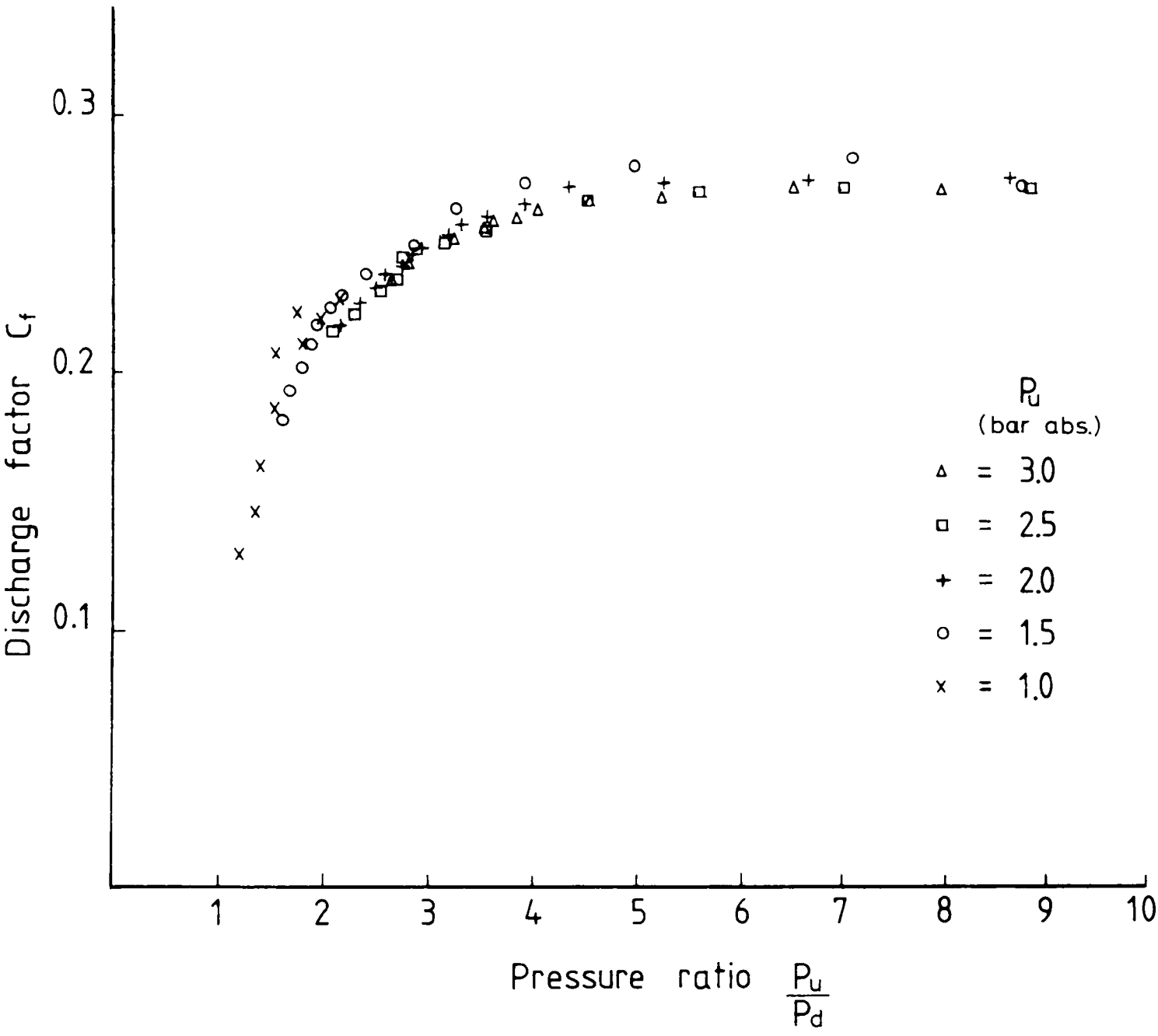

Fig. 6.7 Reverse Flow Discharge Factor

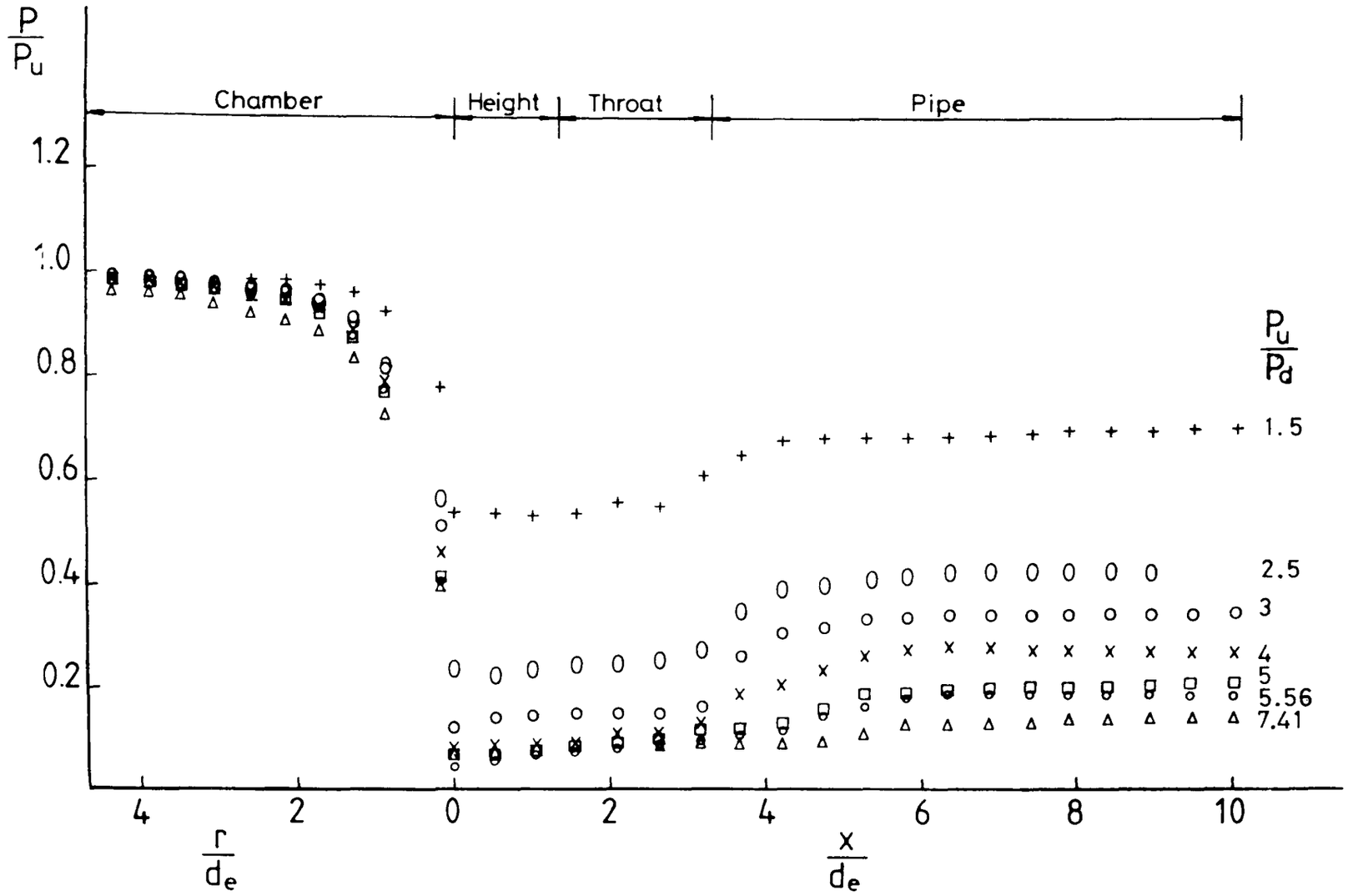

Fig. 6.8 Static Pressure Distribution

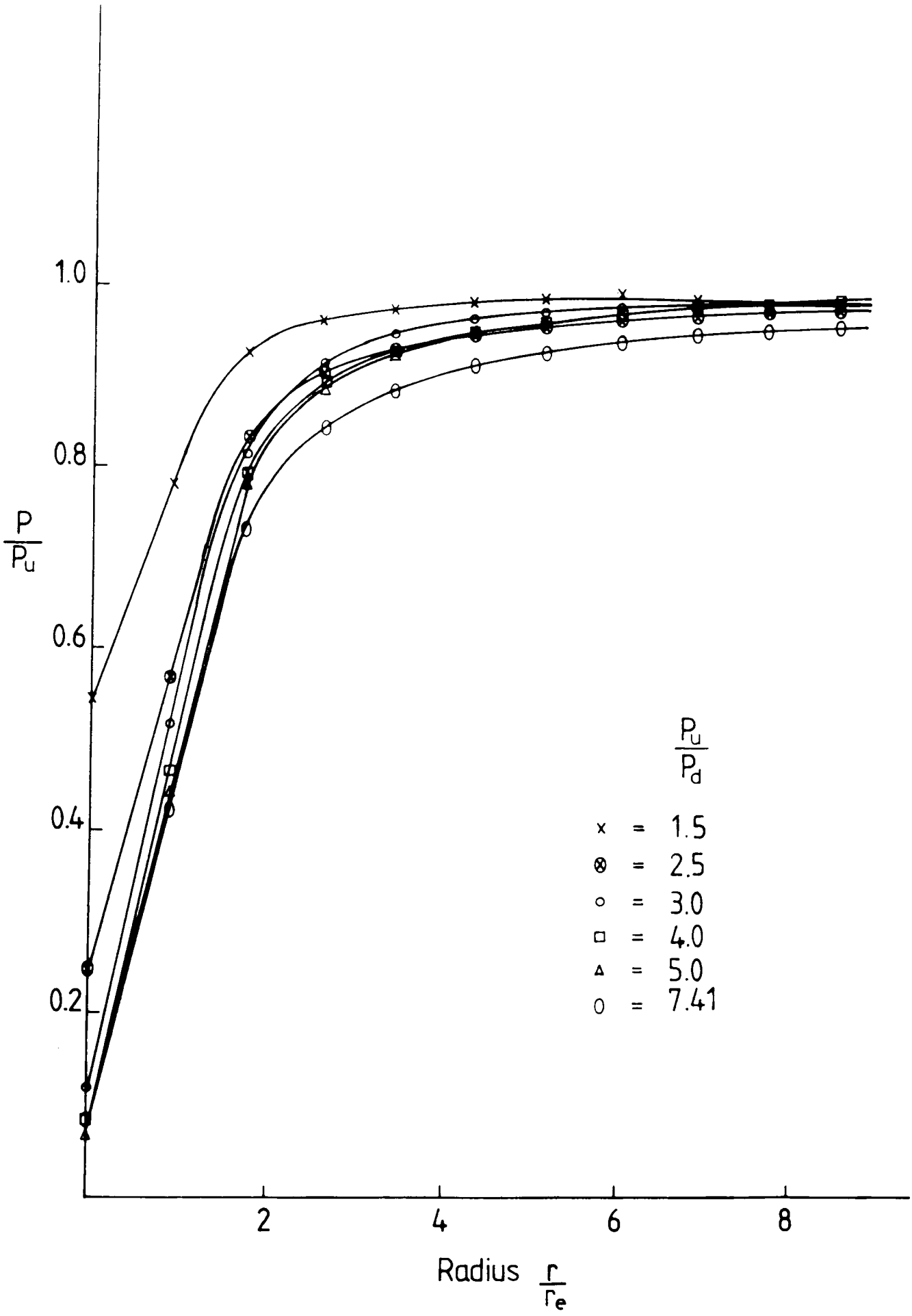

Fig. 6.9 Radial Pressure Distribution

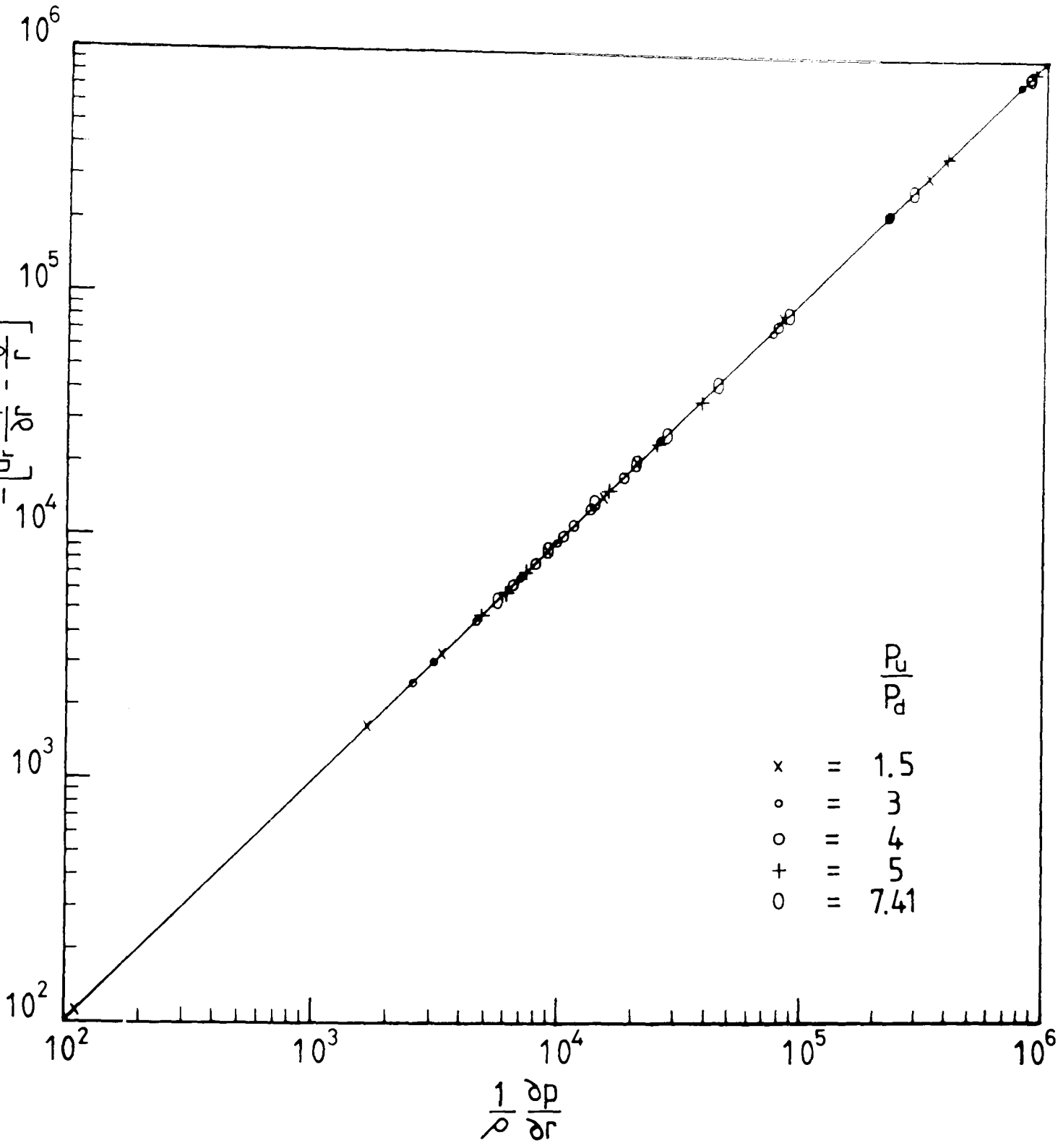

Fig. 6.10 Validity of Tangential Velocity Equation

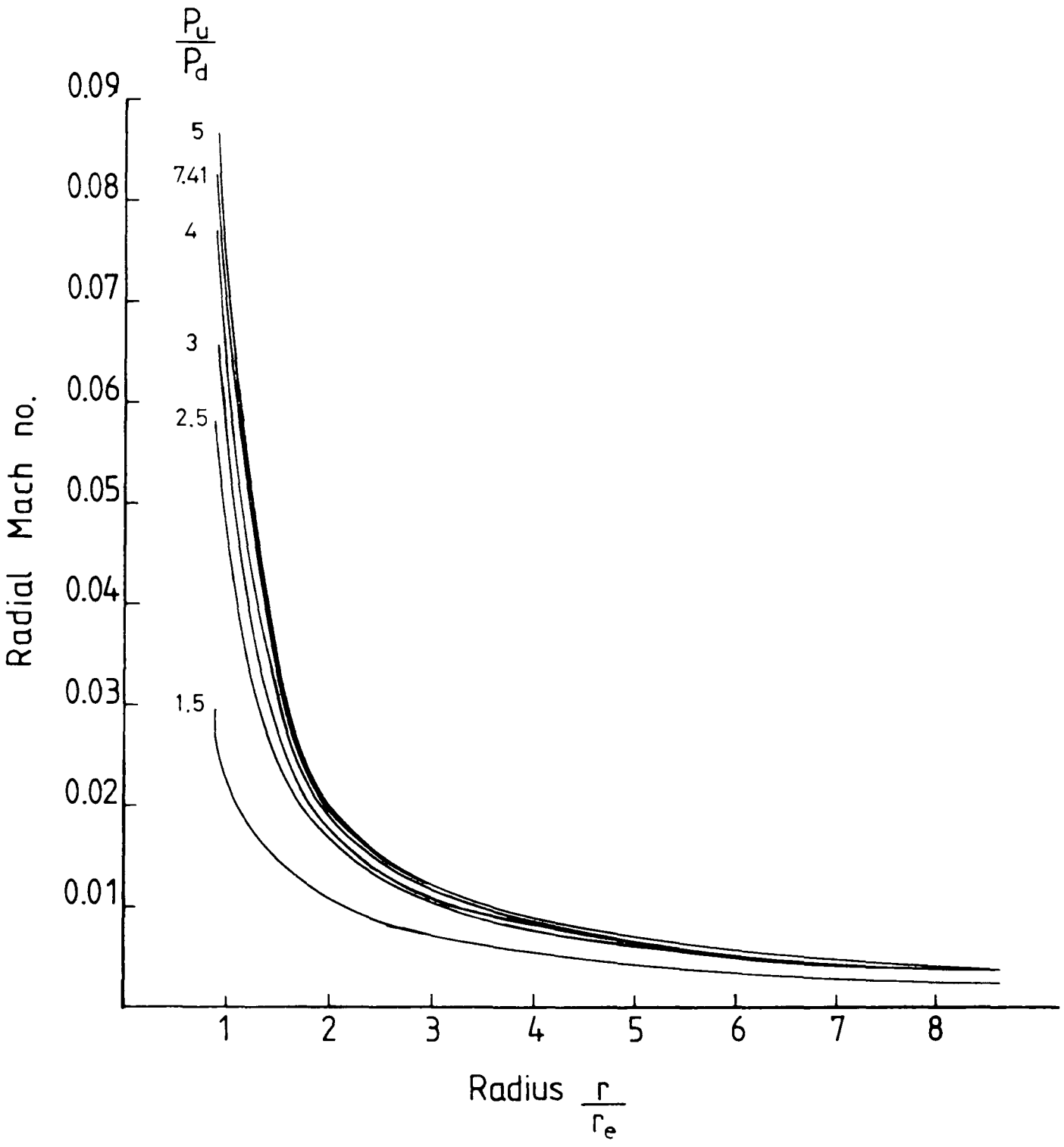

Fig. 6.11 Radial Mach No. Profile

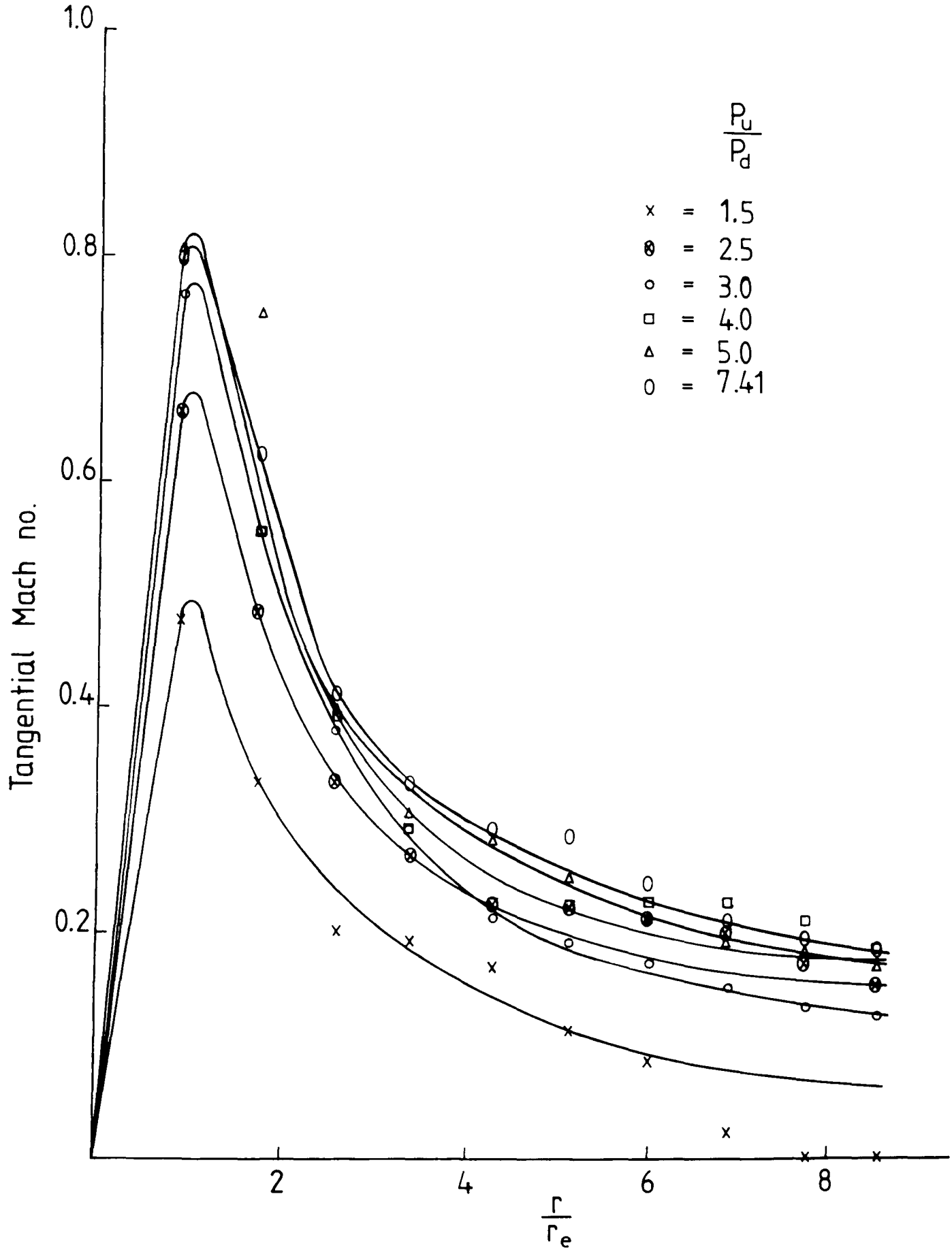

Fig. 6.12 Tangential Mach Number Profile

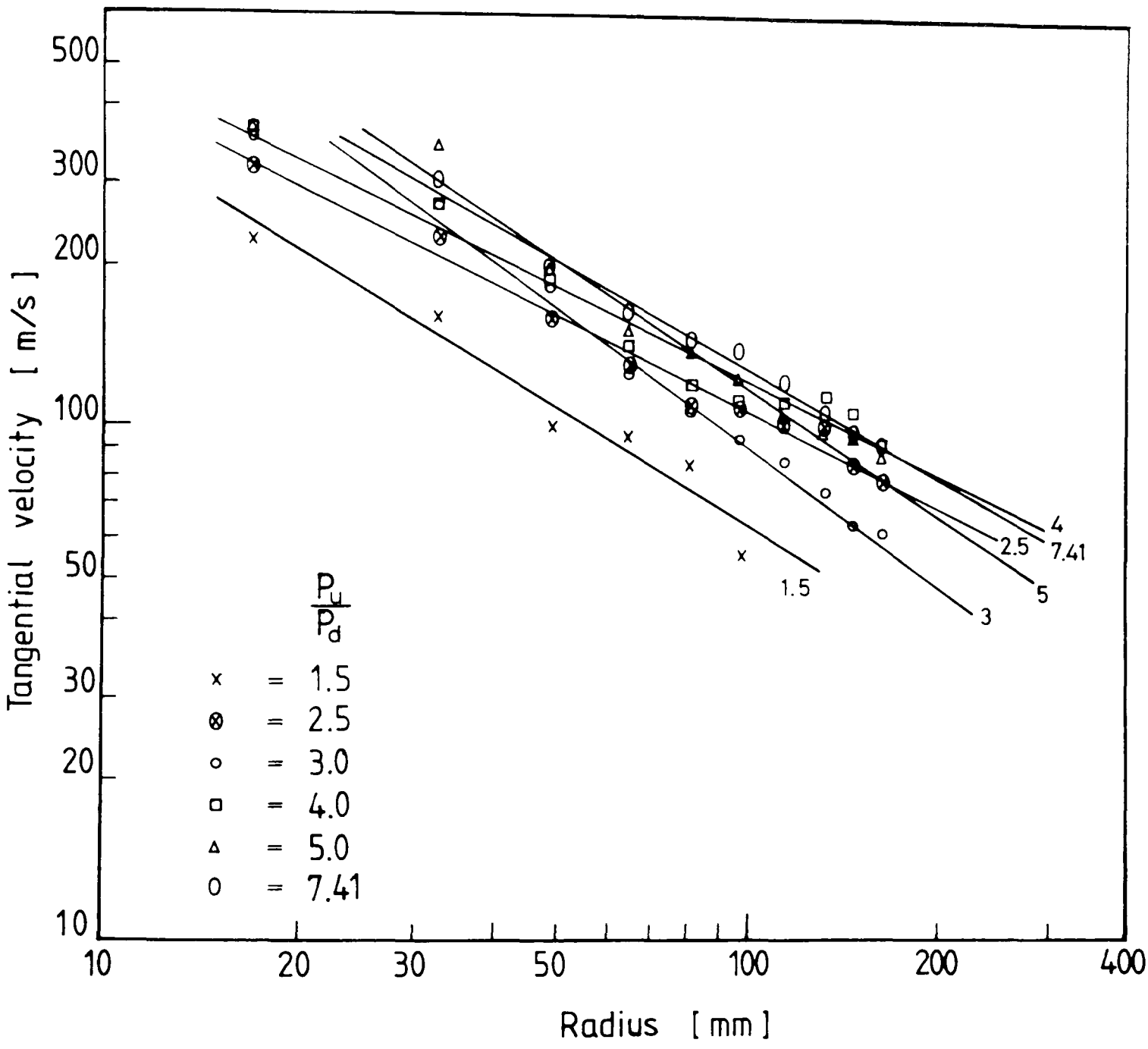

Fig. 6.13 Determination of Vortex Exponent

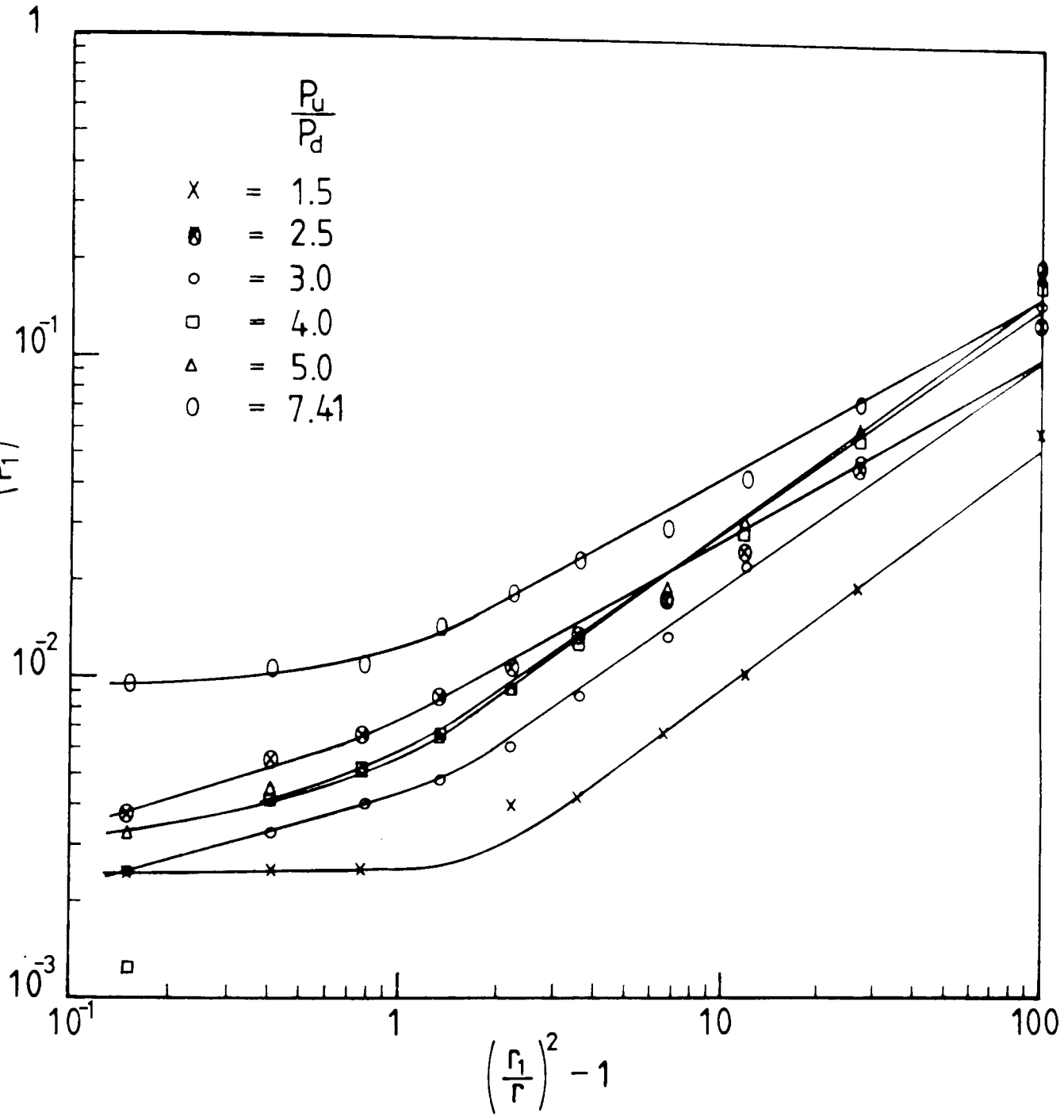

Fig. 6.14 Vortex Exponent by Energy Equation

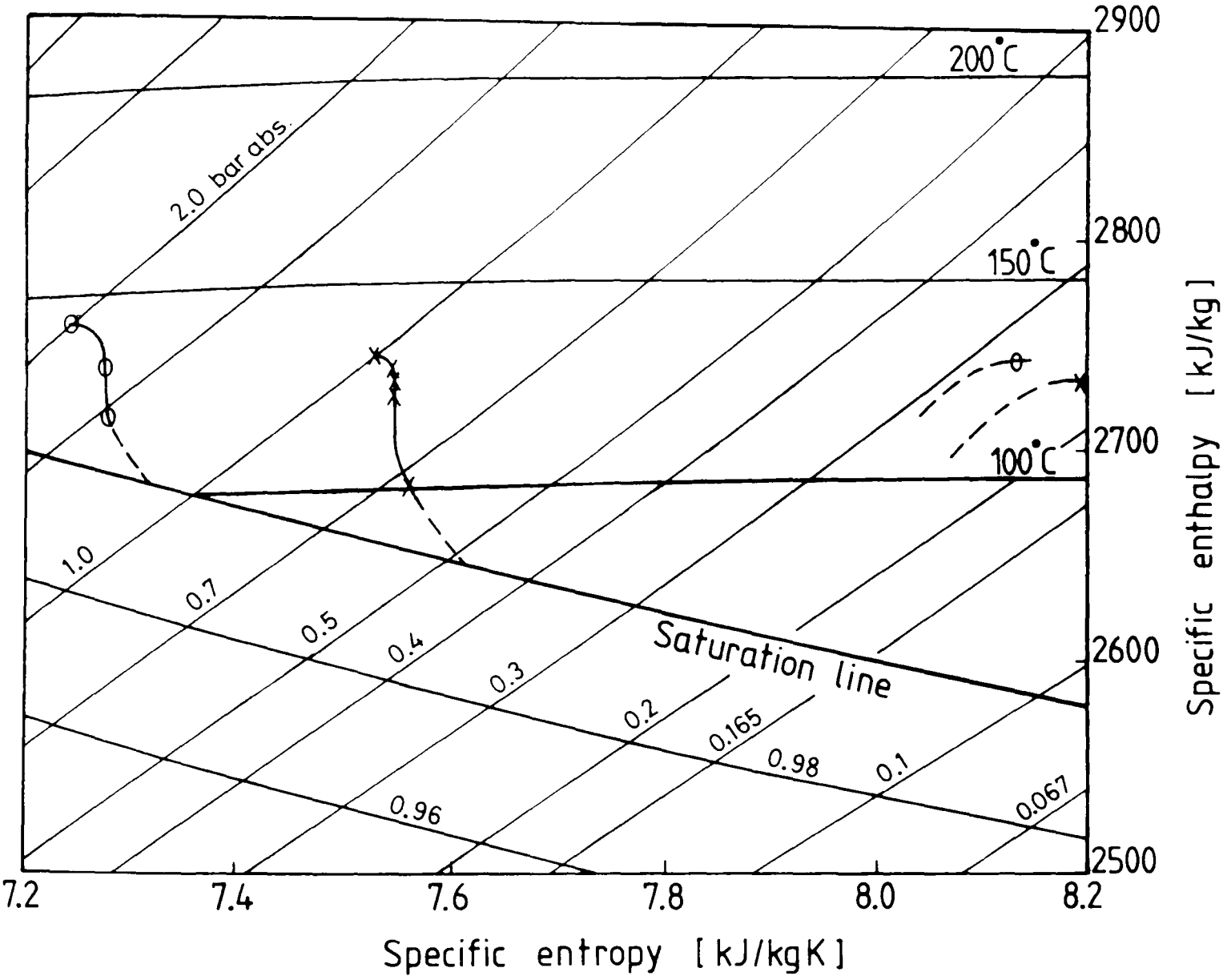

Fig. 6.15 Vortex Chamber - State Point Locus

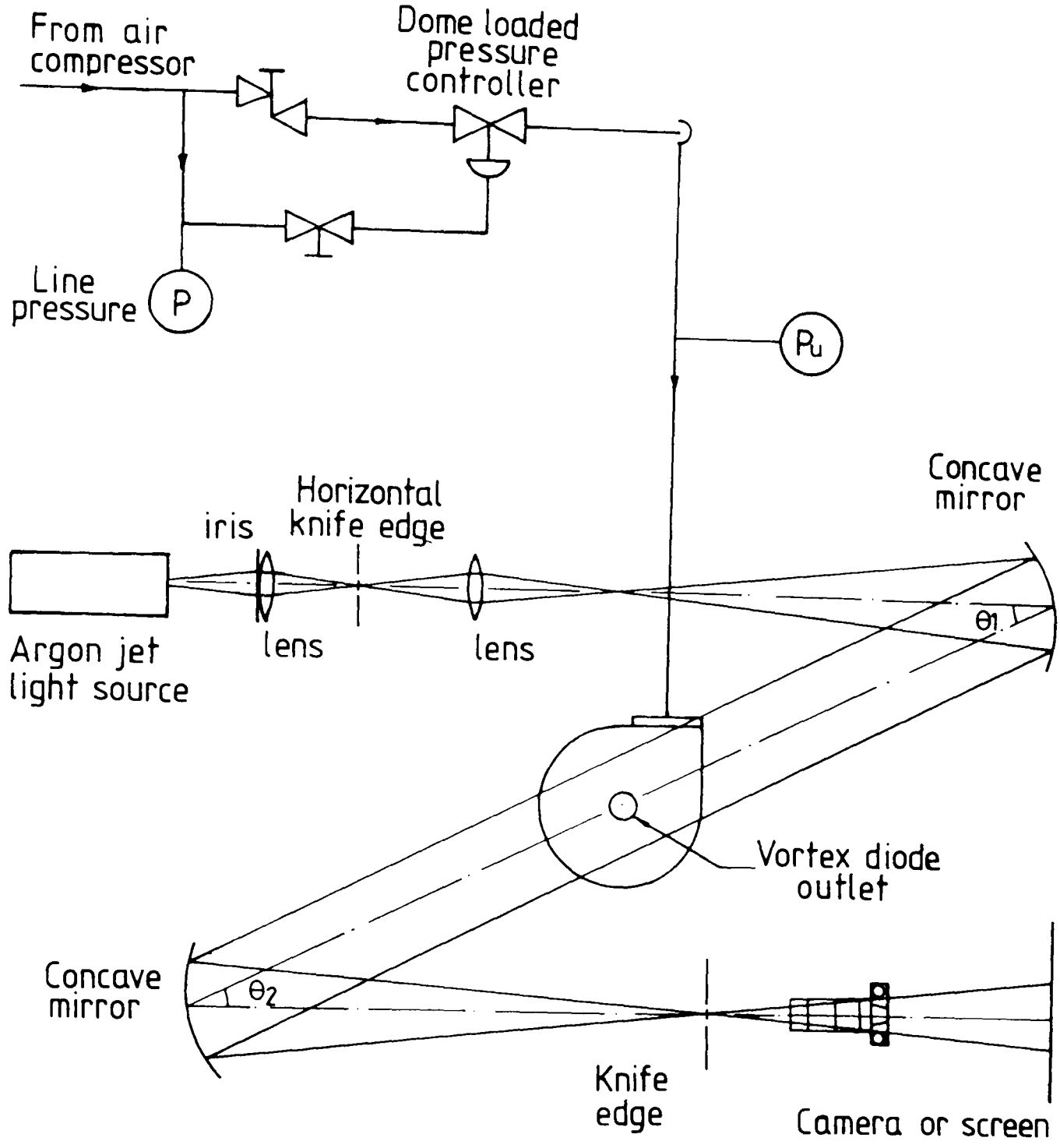

Fig. 6.16 Arrangement of Flow Visualisation Rig

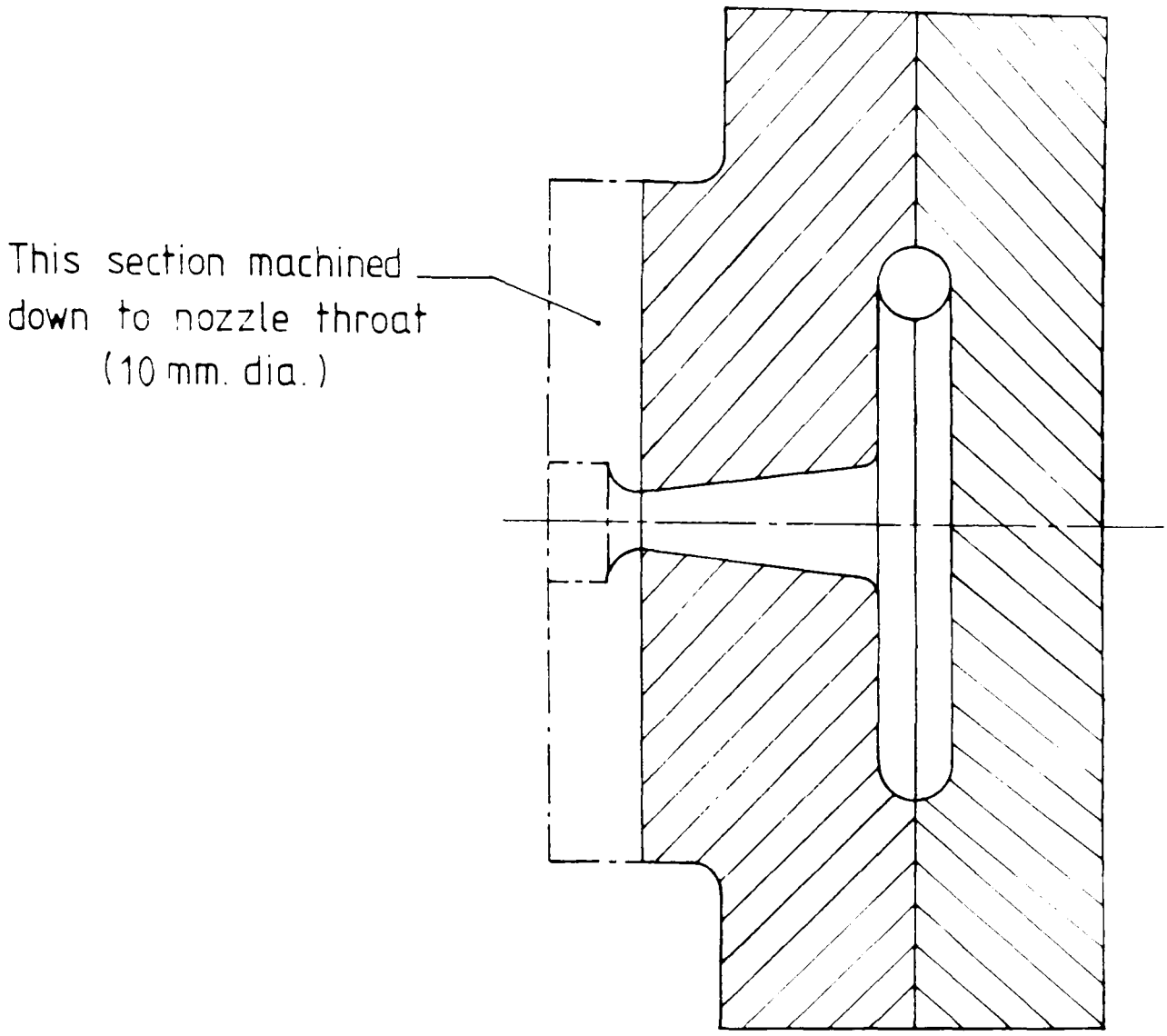

Fig. 6.17 Modifications to Zobel Type Diode

Fig. 6.18 Schliern Photographs with Horizontal Knife Edge, at Upstream Pressure of (a) 20 psig, (b) 50 psig, (c) 100 psig, (d) 150 psig, (e) 200 psig, (f) 250 psig, (g) 350 psig and (h) 400 psig.

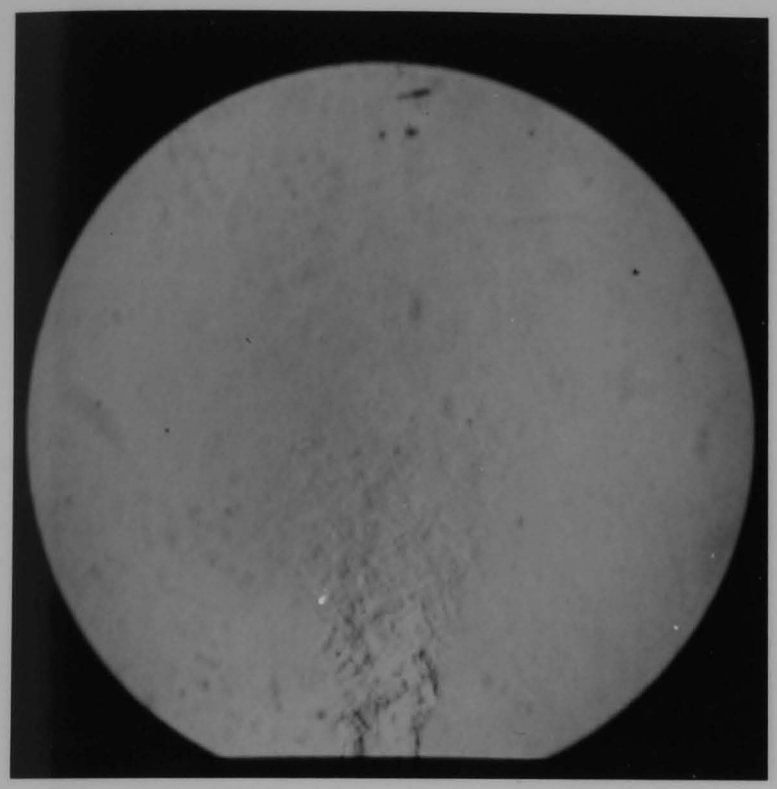

(a)

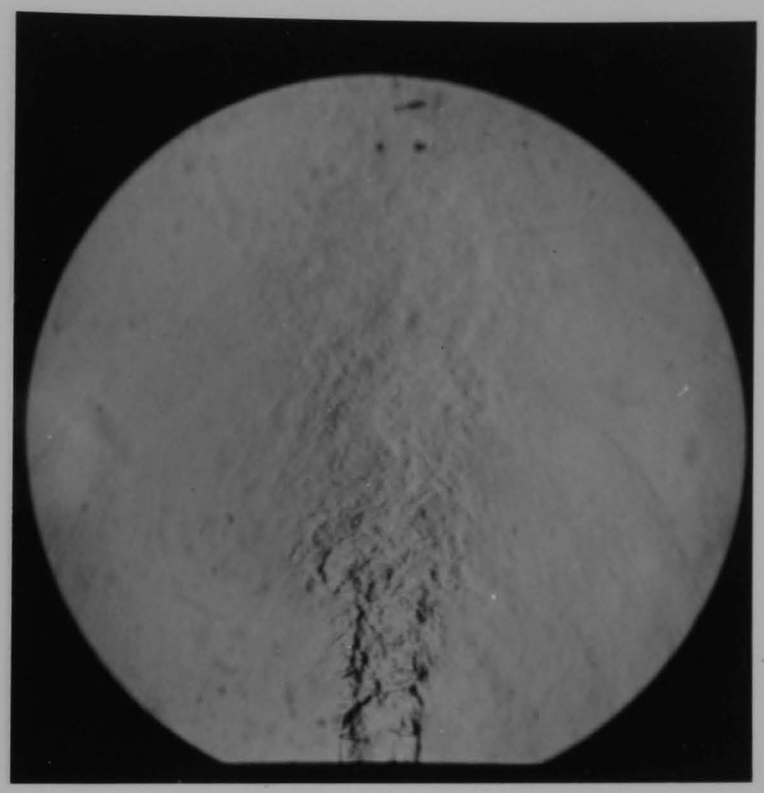

(b)

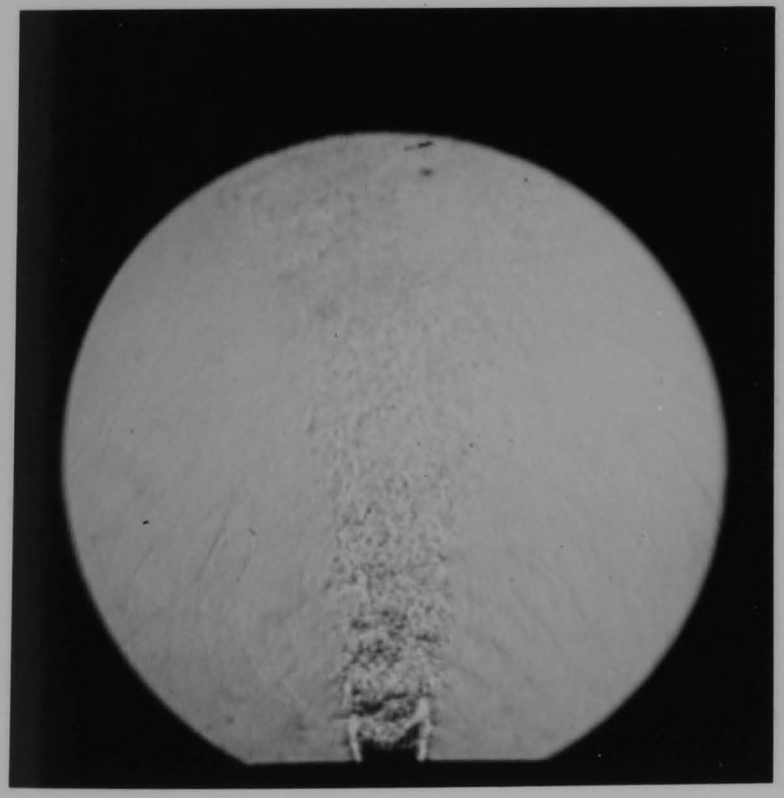

(c)

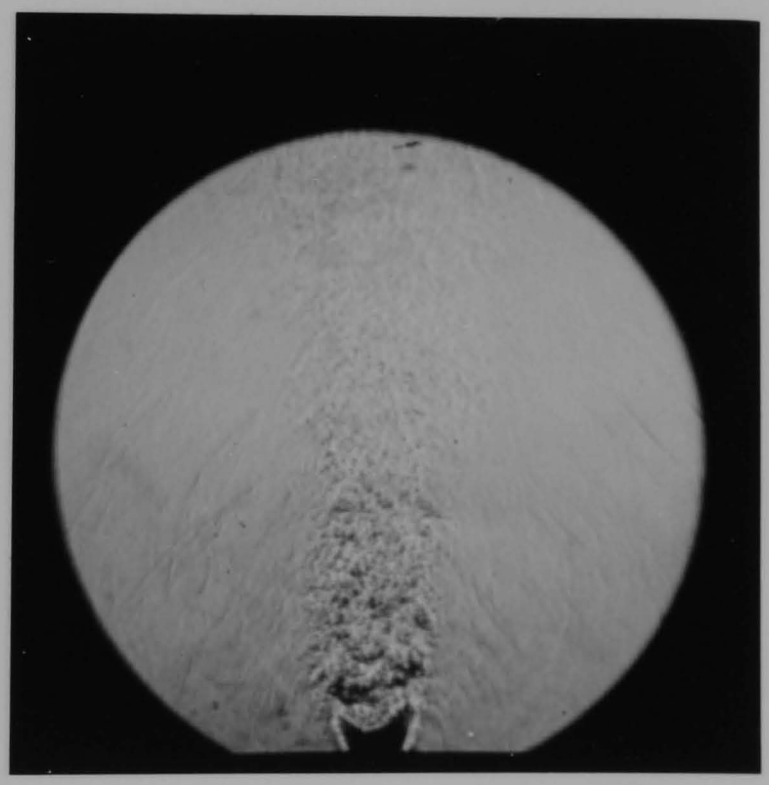

(d)

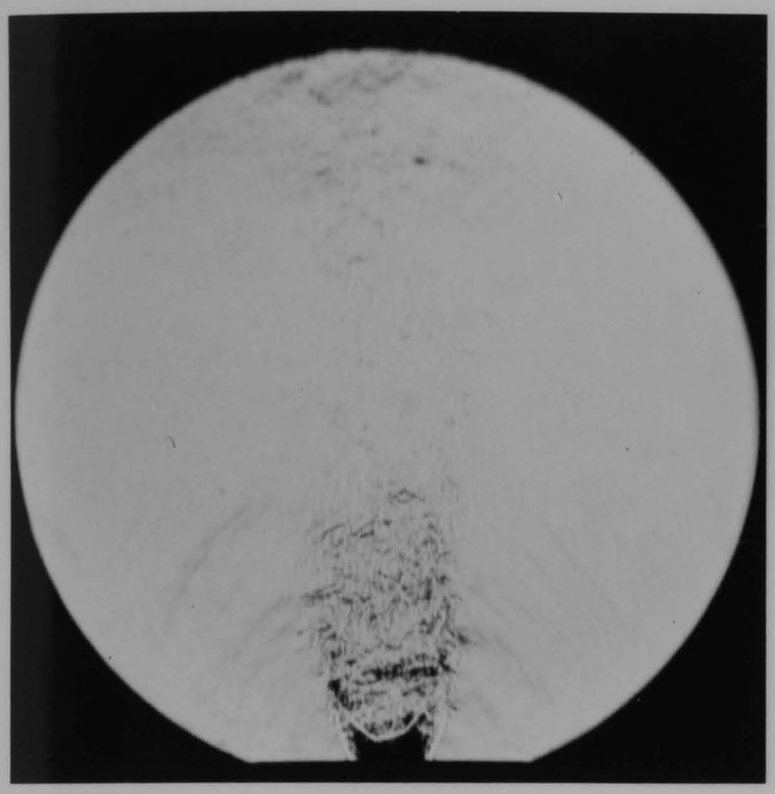

(e)

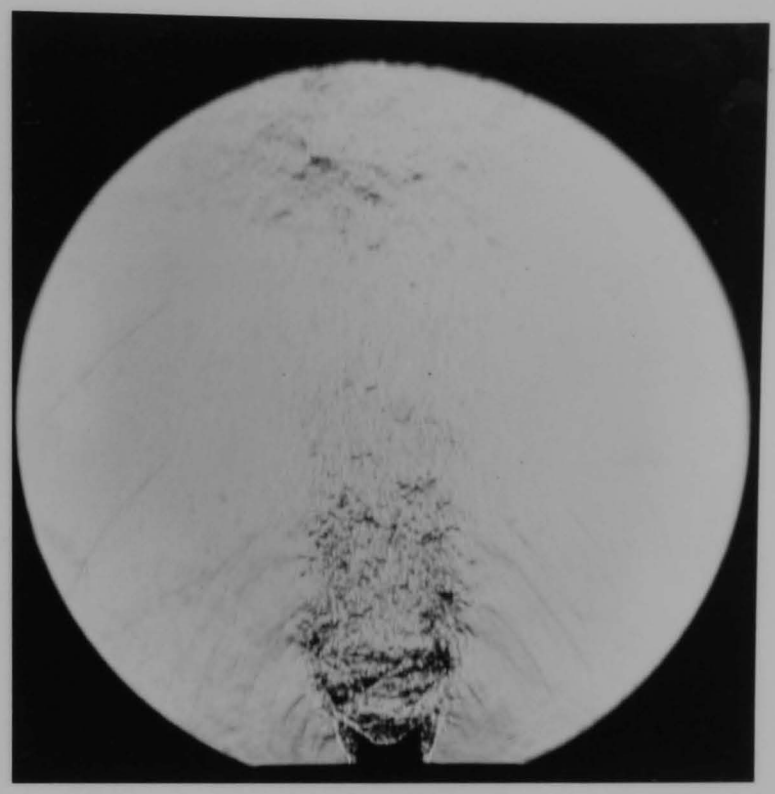

(f)

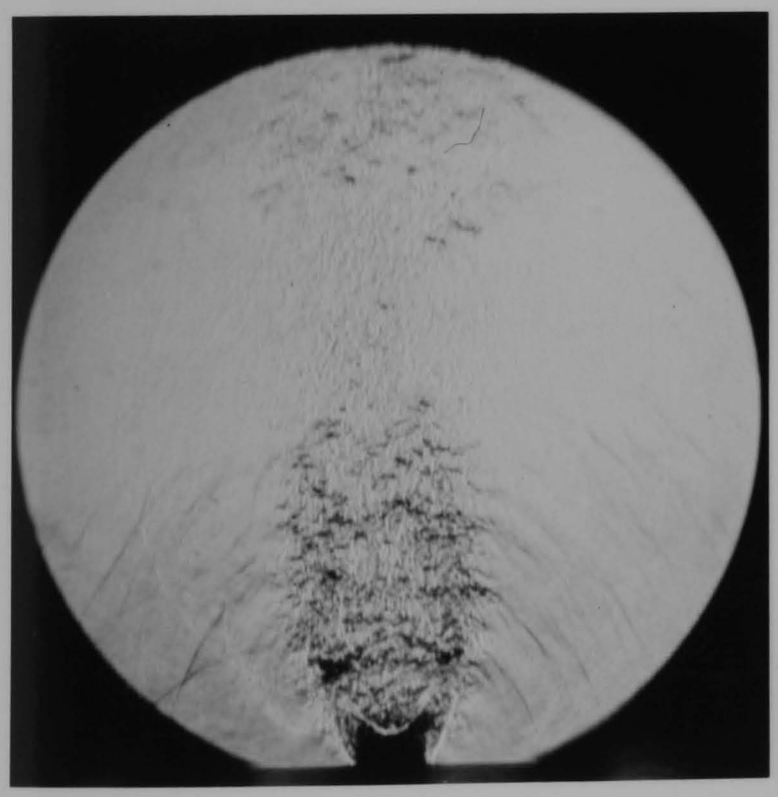

(g)

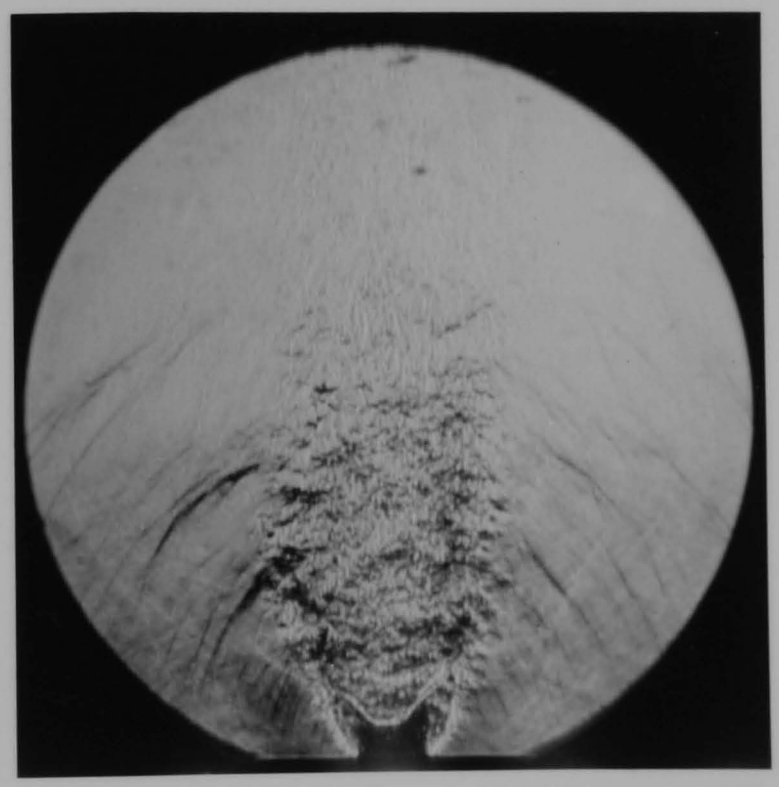

(h)

Fig. 6.19 Schlieren Photographs with Vertical Knife Edge, at Upstream Pressure of (a) 360 psig, (b) 380 psig, (c) 440 psig and (d) 460 psig.

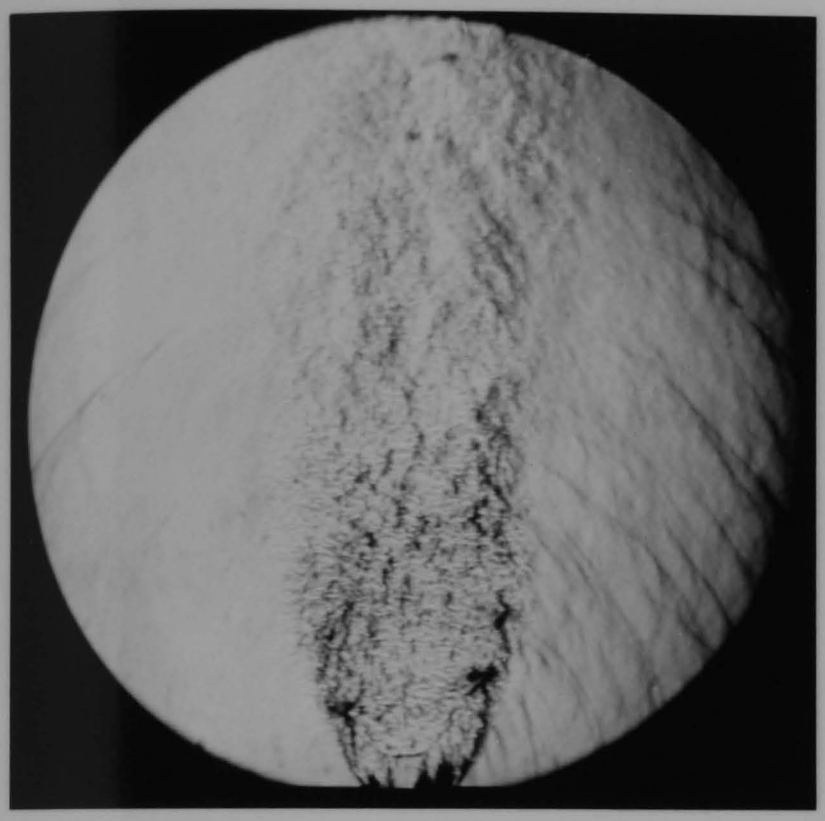

(a)

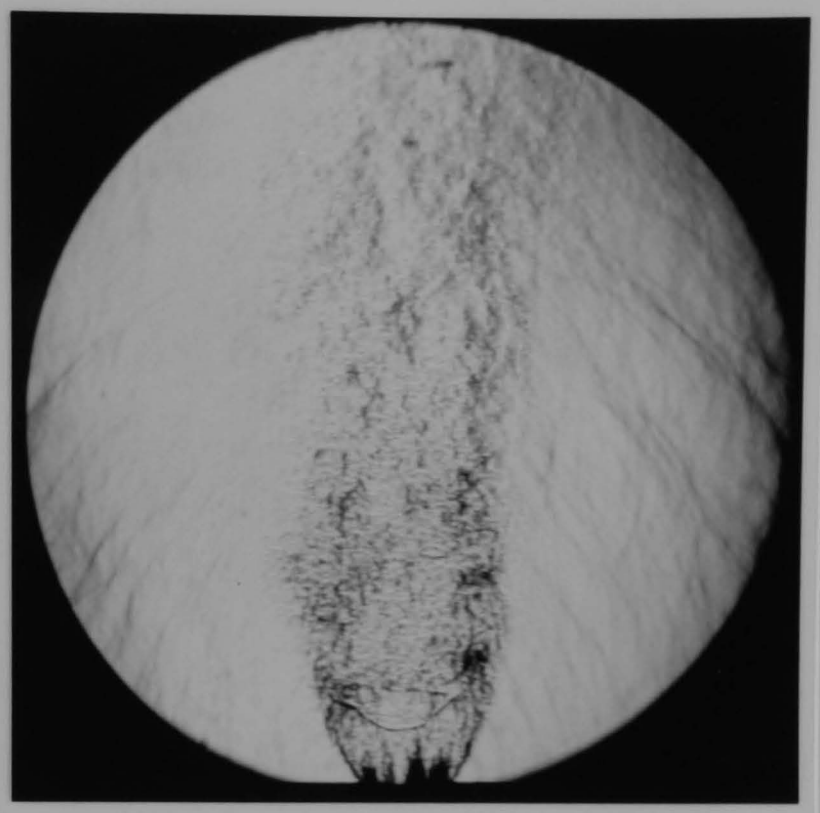

(b)

(c)

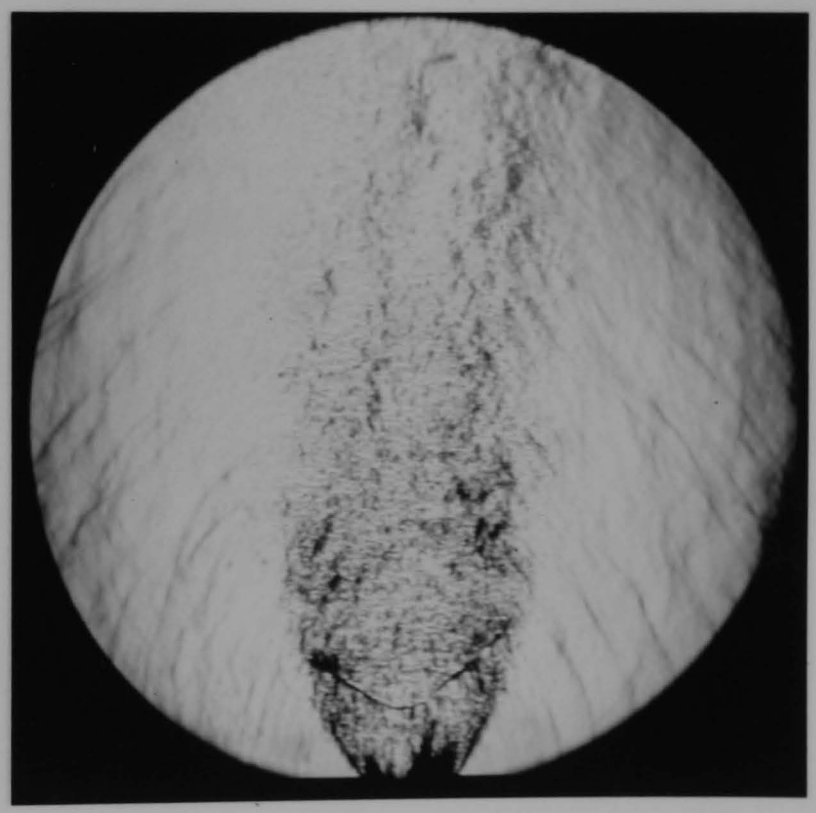

(d)

Fig. 6.20 Shadowgraph of Swirling Flow Exhausting into Atmosphere with Upstream Pressure of 180 psig.

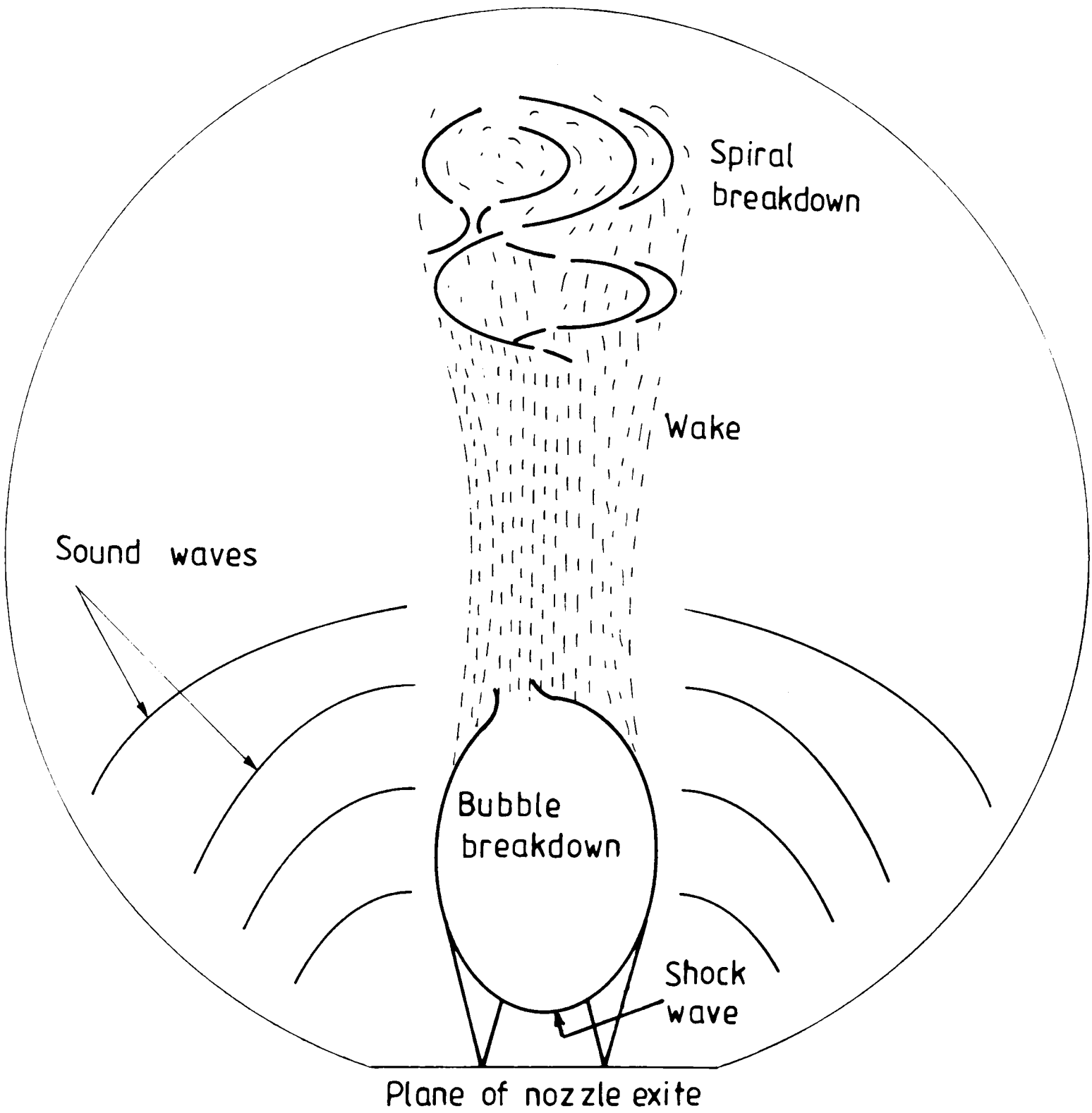

Fig. 6.21 Flow Pattern of the Vortex Breakdown

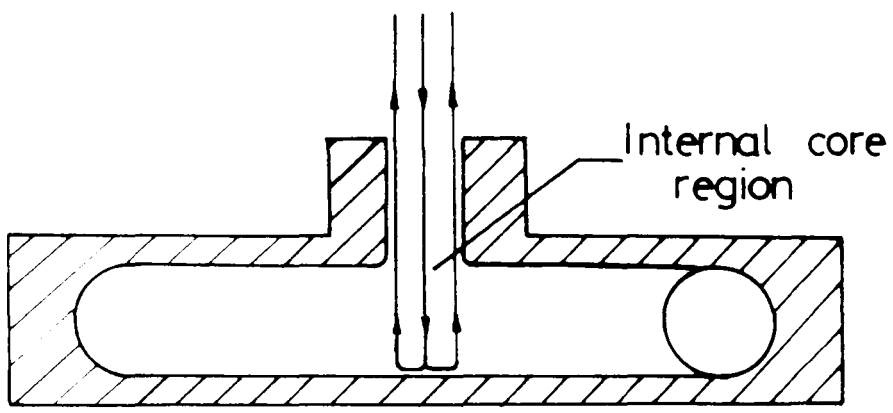

Subsonic cell structure

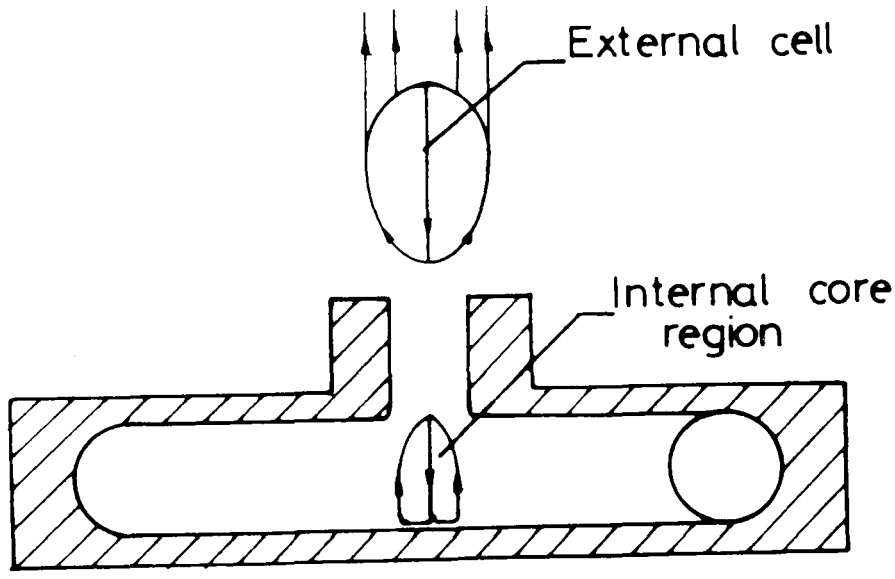

Supersonic cell structure

Fig. 6.22 Position of Recirculation Zones

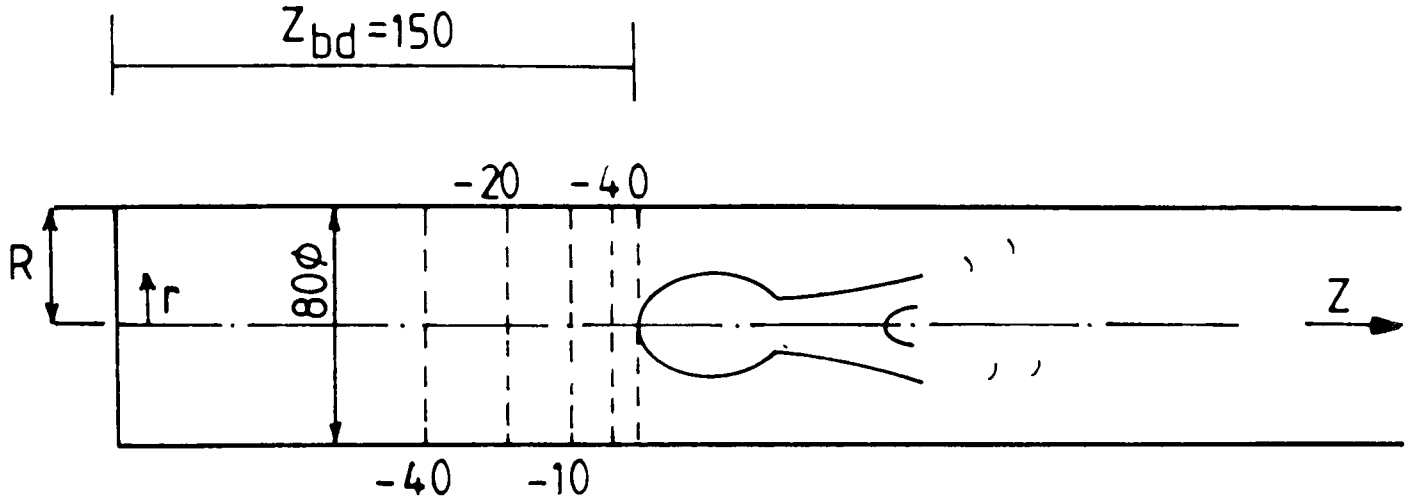

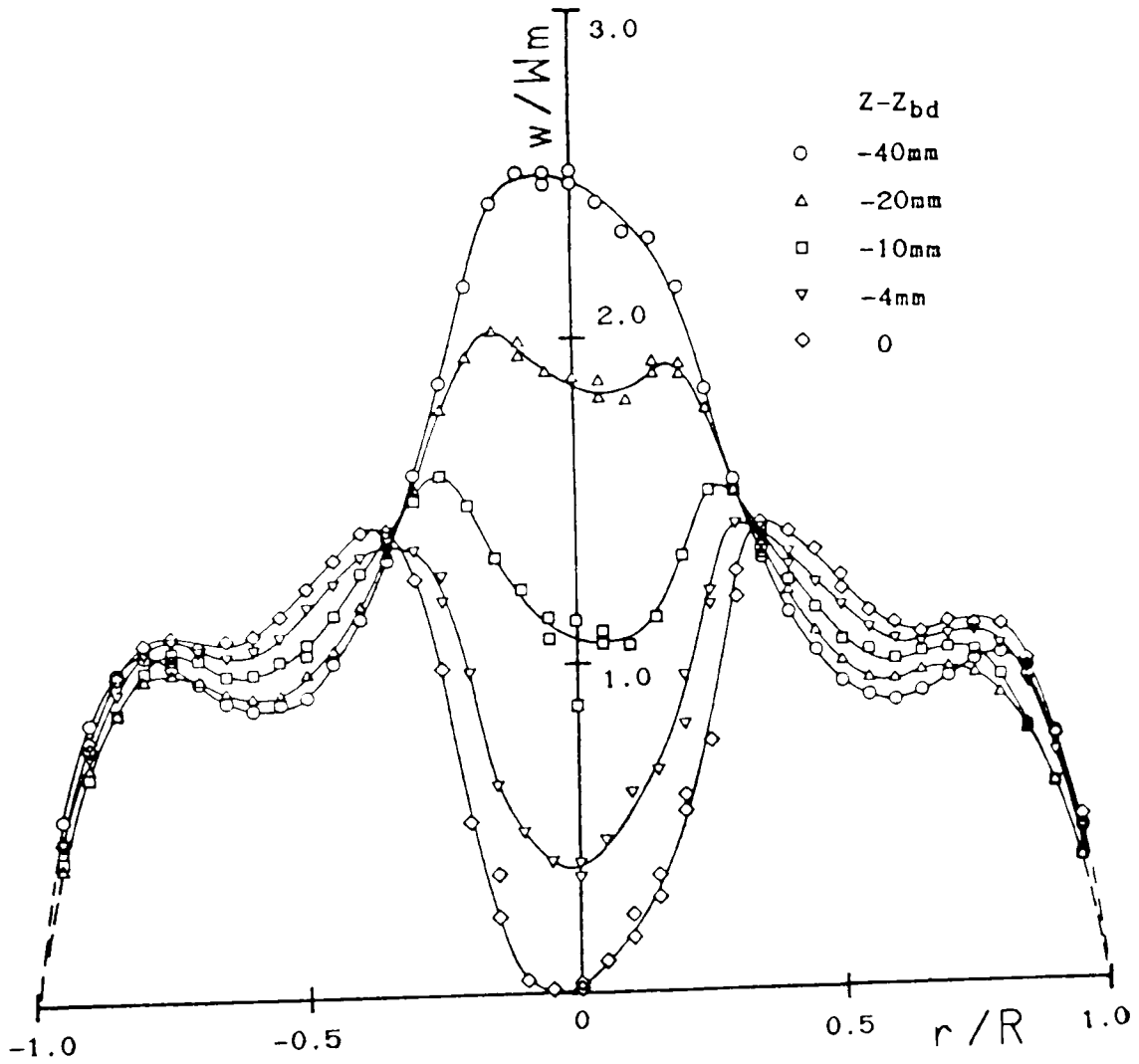

Fig. 6.23 Component of Axial Velocity Upstream of Vortex Breakdown

CHAPTER 7

CONCLUSIONS AND FUTURE WORK

The investigation reported in this thesis has concentrated on the characterisation of a Zobel type vortex diode in steam flow. Superheated steam and air were used to obtain compressible flow characteristics (Chapter 4) whilst an equilibrium steam-water mixture was used to investigate the behaviour of the vortex diode in a wet steam two-phase flow, typical of that found in a steam main (Chapter 5). Internal flow characteristics such as pressure and velocity distribution were carried out in order to gain a better understanding of the fluid dynamics that occur inside the diode, and at the exit, (Chapter 6).

The conclusions to the various aspects of this research which has been undertaken, can be summarised from each of the relevant Chapters.

7.1.1 Chapter 2

An extensive literature survey of the available vortex devices has shown that there are many engineering applications for fluidic devices. Mechanical reliability, simple construction, lack of moving parts and the ability of components to handle difficult fluids are the main advantages of using these devices. These advantages have been attractive, especially to the nuclear industry but this is certainly not the limit to the applications. Further applications will be, and are being, found in the wider fields of chemical and

process engineering.

Simplicity of devices does not necessarily mean that the fluid dynamics of them are also simple. Different devices can have significantly different characteristics, which also depend on the working fluid and the conditions of operation. This points to the need for additional knowledge of the internal fluid flow, to help understand the behaviour of each individual component.

7.1.2 Chapter 3

A review of available literature was used to reveal information about highly complex three-dimensional vortex flows. Many vortex flow theories have been established, the majority of which are aimed at the case of incompressible flows. It seems that further work needs to be done with compressible flows, apart from the need for solutions to existing problems.

Highly three-dimensional complex phenomena such as vortex breakdown should be considered at higher Reynolds and Mach numbers. This is particularly true in the case of compressible and supersonic flows where compressibility has an important effect on the nature of the vortex breakdown and needs further substantial experimental work.

Most of available experimental work has been conducted by conventional methods, for example, the measurement of velocity by the use of probes which disturb the flow. The measurement of the internal vortex flow field by probe insertion has proved impossible

in the present study. Although it was not attempted, it will also be very difficult to measure the exhaust flow field by probe insertion. There is therefore a strong case for investigating the areas using a non-intrusive technique, such as laser anemometry.

7.1.3 Chapter 4

The compressible flow characteristics have been measured for a Zobel type vortex diode with 19 mm throat diameter in which super-heated steam was used as the working fluid in both the forward and reverse flow directions (low and high resistance). A discharge factor Cf has been used to describe the diode resistance. In the reverse flow direction, Cf has a minimum vale of 0.2 at pressure ratio of about 1 and choking was seen to occur at a pressure ratio of about 4, beyond which Cf had a constant value of 0.38. In the forward direction, the flow was seen to choke at a pressure ratio of about 2, and Cf had a constant value in the choked region of about 0.95. The ratio of forward to reverse flow is therefore about 2.5, a very low value compared to vortex diodes operating with incompressible flow.

It has been shown that the high resistance performance of the diode is significantly reduced as the flow changes from subsonic to supersonic and choked flow. The reason for this is believed to be largely due to the absence of reversed flow in the exit throat of the diode.

7.1.4 Chapter 5

It was shown in this Chapter that the characteristics of a vortex diode operating in wet steam are, broadly, similar to those obtained with superheated steam; although there is a reduction in the high resistance performance as the steam quality is reduced. For the present rig configuration a practical lower limit of 0.93 was found below which the diode will not operate in the reverse flow direction without experiencing the oscillations which have been described. This limit is not universal, however, and relates solely to the present experimental rig. If, for example, the pipework consisted only of horizontal or downward vertical runs the build-up of water would not occur. Also, the pipework used in the present rig has an internal diameter of 77 mm and was oversized in relation to the diode. A smaller bore pipe will have higher steam velocities and could therefore accommodate higher wetness fractions before experiencing flow reversal.

In general, however, pipework will have upward vertical runs, valve and other fittings, all of which can lead to a build-up of water. It would be prudent to install a water separator in the pipework before a diode if it is to operate in wet steam. Baffle type separators, for example, have a separator efficiency better than 70% and would stop the diode being flooded. Steam traps, located at suitable positions in the pipework would also prevent a build-up of water. Precautions such as these will enable the diode to operate in wet steam with a performance comparable with that which might be expected in a dry compressible flow.

However, as was discussed at some length in Chapter 4, the high resistance properties of a vortex diode are significantly reduced in compressible flow compared with that obtained in incompressible flow.

7.1.5 Chapter 6

The effect of compressibility on the operating characteristics of a fluidic vortex valve is to impair its high resistance capability. This feature has been explained in the present work by investigating the flow through a thin vortex chamber using both steam and air. The internal flow of the vortex chamber produces a vortex described by:

$$V_\theta r^{0.69} = \text{constant}$$

The vortex exponent compares well with work by Holman and Moore [50] who used a vortex chamber with a much greater chamber height. The general form of the vortex appears therefore to be relatively independent of the chamber height, which is somewhat surprising since, intuitively, the wall shear would be expected to impose a greater influence on the flow in the thinner chamber. The polytropic index of the expansion for steam flow in the vortex was found to be 1.192 compared with the isentropic value of 1.335.

The vortex chamber was found to choke at an inlet to outlet pressure ratio of about 6 and passed about 28% of the mass flow of the equivalent ideal one-dimensional nozzle. The corresponding

values measured for a Zobel type vortex diode in Chapter 4 were 4 and 38%. Clearly these values are influenced by the geometry of the vortex device.

The reduction in vortex chamber resistance as the flow becomes compressible has been considered through a discussion of vortex breakdown in expanding swirling flows such as those found in the exit port of the vortex chamber. The discussion has been supported by Schlieren photography of the flow field in the exit region. It has been concluded that the aerodynamic blockage, which is largely responsible for the high resistance, is swept out of the axial port as the flow becomes compressible. This view is further supported by measurements of the static pressure along the centreline of the exit. An assessment of the affects of compressibility on the resistance of the tangential inlet, vortex chamber and outlet nozzle confirms that only the latter is significantly affected as the pressure ratio across the device is increased. This supports the view that it is the flow within the exit region that is responsible for the loss of high resistance under conditions of compressible flow.

7.2 **Future Work**

This report has decribed the findings of a new area of research into the behaviour of vortex diodes in steam and into the effects of compressibility and also wetness on diode performance. Since this is the first serious venture into these areas, it is not surprising that a number of new questions have been raised. These should form the

basis of future work.

(i) Two-Phase Flow - The behaviour of diodes operating with wet steam having wetness fractions typical of those found in plant, resulted in a decrease in total resistance of the diode, and wetness fraction higher than 0.93 caused a serious instability and a collapse of the vortex. A vortex diode not capable of forming a vortex would not be effective and the oscillation could cause mechanical damage to the system.

A survey of available papers has shown that there is no real data available for vortex valves operating in the area of two-phase flows, therefore, it is prudent to consider a programme of work to investigate the behaviour of vortex valves in two-phase flows ranging from single-phase liquid to single-phase gas. Initially, it would be easier, and cheaper, to consider the behaviour of vortex valves in air/water flows in both directions, with the aim of understanding how to correlate the data. This future work would shed some light on an area which is very important to the future of power fluidics. This work could be extended to gather more information about other types of two-phase flows, such as steam and water mixtures for different geometrical configuration of experimental rigs.

(ii) Internal Flow - The existence of recirculation zones has been discussed in some detail in Chapter 6, and supported by Schlieren photography of the flow exhausting into the atmosphere where the structure of the flow changes suddenly at the exit of the vortex diode. It seems that when the flow is choked, the

position of the recirculating zone does not change with variation of upstream pressure. A perspex tube could be used to confine the exhausting flow and to examine the position of the recirculation zone. Non-contact optical instruments, such as LDA, could also be used to locate the position of vortex breakdown by measurement of velocities. This could give more accurate information about the structure of the vortex flow at the exit pipe in supersonic conditions.

(iii) Diodes in series - It has been shown in Chapter 4 that the compressible flow performance of the diode can be restored by connecting a number of diodes with the same geometry in series. This work could be extended in the future to investigate the possibility of using different size diodes in series. This proposal should be tested and the information used to reveal better combinations and thus improving the resistance to the flow.

(iv) Vortex throttle - If a diode is to be installed into a system simply as a restrictor, as described by Priestman and Tippetts [13], then the design will change. It has been shown in Chapter 6 that the discharge factor of a vortex throttle is about 25% lower than that of comparable Zobel type vortex diodes. The throttle forward flow characteristics should be established under compressible and choked conditions. If the forward flow resistance of the two devices were found to be similar, then the throttle should be used to replace the diode for supercritical pressure ratios.

REFERENCES

1. Lugt, J.H. — "Vortex flow in nature and technology", John Wiley & Sons, 1983.

2. Kemp, M. — "Leonardo Davinci, the marvellous works of nature and man", j.M. Dent & Sons Ltd., 1981.

3. Zobel, R. — "Experiment on hydraulic reversing elbow", U.K.A.E.A. Risley Translation, No. 439.

4. Syred, N. Roberts, P.J. — "Use of vortex diodes applied to post accident heat removal systems", A.S.M.E. Paper 79-HT-9.

5. — "Applying fluidics to reactor safety and reprocessing", Nuclear Engineering International, Dec. 1984.

6. Thoma, D. — "Transactions of the first world power conference", London, 1924, Paper 100.

7. Kumar, H.S. — "A study of the effect of geometry on vortex diode performance", Power Fluidics Section, U.K.A.E.A. Internal Report, August 1984.

8. Jacobs, B.E.A. — "The steady state and transient performance of some large scale vortex diodes", 5th Cranfield Fluidics Conference, 13-16 June, 1972, Uppsala, Sweden.

9. Baker, P.J. — "A comparison of fluid diodes", 2nd Cranfield Fluidics Conference, 3-5 Jan., 1967, Cambridge, Paper D6.

10. Markland, E. — "Selection of optimum Siso diodes", Report to U.K.A.E.A., April, 1986.

11. Tippetts, J.R. Syred, N. — "Flow control circuit for toxic fluids", Fluidics Technology, Agadograph, No. 215, 1976.

12. Roberts, P.J. Syred, N. — "Fluidic two-diode pump systems for hot and cold liquids", Fluidic Quarterly, Vol. 10, No. 3, July, 1978.

13. Priestman, G.H. Tippetts, J.R. — "Cavitation in vortex diodes and its significance in diode pumps", Journal Mechanical Engineering Science, I.Mech.E. Vol. 24, No. 4, 1982.

14. Brombach, H. "Vortex flow controllers in sanitary engineering", Journal of Dynamic Systems, Measurement and Control, Vol. 196, pp. 129-133, June, 1984.

15. Hamid, S.
Reid, K.N. "Steady-state characteristics of hydraulic vortex resistors", I.F.A.C. Pneumatic and Hydraulic Components, Warsaw, Poland, 1980.

16. Dilly, N.
Roberts, P.J.
Syred, N. "Characterisation of recent developments in the design of thin chamber vortex diodes", Report to U.K.A.E.A., Oct. 1977.

17. Syred, N.
Roberts, P.J.
Sidhu, B.S. "Vortex diode", British Patent, Serial No. 1571287, 9 June, 1977.

18. Lamaici, A. "Characterisation of high performance vortex diodes", Report No. 328, 1977, U.C.C. Mechanical Engineering and Energy Studies Department.

19. Fujio, N.
Nishiwaki, K.
Kato, K.
Ijima, T. "Prevention of backflow in a crankcase - Scavenged two-stroke engine by fluid diodes" Bull. J.S.M.E, Vol. 14, No. 71, 1971.

20. Sher, E. "Improving the performance of a crankcase scavenged two-stroke engine with a fluid diode", Proceedings of the Inst. of Mechanical Eng., Vol. 196, No. 1, 1982.

21. Mayer, E.A.
Maker, P. "Control characteristics of vortex valves", Proceedings of the Fluid Amplification Symposium, Washington D.C., 1964.

22. Greber, I.
Koerper, P.E.
Taft, C.K. "Fluid vortex amplifier optimisation", Proceedings of the Fluid Amplification Symposium, Washington D.C., 1965.

23. Chow, S.K. "An experimental study on the characteristics of vortex valves", Int. Federation of Automotive Control Symposium on Fluidics, London, 1968.

24. Tippetts, J.R. "Vortex amplifier controlled ventilation system for nuclear fuel reprocessing plants", Fluidic Quarterly, Vol. 10, No. 3, July 1978.

25. Brombach, H. "Vortex valve for run off control in retention basins", Proc. Symp. Power Fluidics for Process Control, Inst. Meas. and Control, Surrey, 1973.

26. Tylor, A.F. — "Vortex devices in aircraft fluid systems", 4th Cranfield Fluidics Conf., 17-20 March, 1970, Coventry Paper B2.

27. Hilsch, R. — "The use of the expan of gases in a centrifugal field as cooling process", Rev. Sci. Inst., Vol. 18, 1947, pp. 108-113.

28. Aronson, R.B. — "The vortex tube : Cooling with compressed air", Machine Design 48, 9 December, 1976, pp. 140-143.

29. Takahama, H. Yokosawa, H. — "Energy separation in vortex tubes with a divergent chamber", Journal of Heat Transfer, Vol. 103, May 1981, pp. 196-203.

30. Westley, R. — A bibliography and survey of the vortex tube", College of Aeronautics, Cranfield, Note 9, March 1954.

31. Takahama, H. Kawamura, H. Kato, S. Yokosawa, H. — "Performance characteristics of energy separation in a steam operated vortex tube", Int. Journal of Engineering Science, Vol. 17, 1979, pp. 735-744.

32. Sarpkaya, T. — "Forced and periodic vortex breakdown", Journal of Basic Engineering, Trans. ASME, Series D, Vol. 89, No. 3, Sept. 1967, pp. 609-616.

33. Paynter, H.M. — "Fluidic transients in engineering systems", Section 20 in Handbook of Fluid Dynamics, 1st Ed., edited by Streeter, V.2, McGraw-Hill, N.Y., 1961, pp. 20-21.

34. Sarpkaya, T. Pavlin, C. Phasook, S. — "A theoretical and experimental investigation of a confined vortex oscillator", Trans. of ASME, pp. 750-754, Dec. 1969.

35. Parker, S.P. — "Mcgraw-Hill Encyclopaedia of Energy", 2nd Edition, 1981.

36. Roberts, A.G. Raven, P. Phillips, R.N. Barker, SD.N. Pillal, K.K. Wood, P. — "PFBC - A 1000 hour programme", Proc. of Conference Organised by Inst. Energy. Fluidised Combustion, London, Nov. 1980.

37. Ernest, M. Hoke, R.C. Siminski, V.J. — "Evaluation of a Cyclone dust collector for high temperature, high pressure, particulate control", Ind. Eng. Chem. Process, Vol. 21, pp. 158-161, 1982.

38. Stairmand, C.J. — "The design and performance of Cyclone separators", Trans. Inst. Chem. Engrs., Vol. 29, Part 3, pp. 356-373, 1951.

39. Chapman, R.A. — "Development of a solid waste fired gas turbine system", 1st Int. Conf. and Tech. Exhibition on Conversion of Refuse to Energy, Montreux, Switzerland, Nov. 1975.

40. Vonnegut, B. — "A vortex whistle", The Journal of the Acoustical Soc. of America, Vol. 25, No. 1, Jan. 1954.

41. Michelson, I. — Theory of vortex whistle", The Journal of the Acoustical Soc. of America, Vol. 27, No. 5, Sept. 1955.

42. Kirshner, J.M. — "Fluid amplifiers", Mc-Graw Hill Book Co., p. 42, 1966.

43. Welty, J.R. Wicks, C.E. Wilson, R.E. — "Fundamentals of momentum, heat and mass transfer", John Wiley & Son, p. 144, 1969.

44. Mack, L.M. — "The compressible viscous heat conducting vortex", Journal of Fluid Mechanics, 1960, 8, pp. 284-292.

45. Alexander, R. M. — "Fundamentals of Cyclone design and operation", Proc. Aus. IMM (Inc), N.S. Nos. 152-153, p. 204, 1949.

46. Roschke, E.J. Pivirotto, T.J. — "End wall pressure distribution in a confined vortex", AIAA Journal, Vol. 5, pp. 817-819, April 1967.

47. Emmons, H.W. Brainerd, J.G. — "Temperature effects in a laminar compressible boundary layer along a flat plate", Journal App. Mech. 8, 105, 1941.

48. Savino, J.M. Keshock, E.G. — "Experimental profiles of velocity components and radial pressure distribution in a vortex contained in a short cylindrical chamber", NASA TN D-3072, Oct. 1965.

49. Owen, I. Motamed-Amini, A. — "Compressible flow characteristics of a vortex diode operating with superheated steam", presented at the Winter Annual Meeting of ASME, Anaheim, California, Dec. 1986.

50. Holman, J.P. Moore, G.D. — "An experimental study of vortex chamber flow", Journal of Basic Engineering, Trans. ASME, pp. 632-636, Dec. 1961.

51. Taylor, G.I. — "The boundary layer in the converging nozzle of a swirl atomiser", Quart. Journal of Mech. Appl. Math., Vol. 3, p. 129, 1950.

52. Rosenzweig, M.L. Lewellen, W.S. Ross, D.H. — "Confined vortex flows with boundary-layer interaction", AIAA Journal, Vol. 2, pp. 2127-2134, Dec. 1964.

53. Wormley, D.N. — "An analytical model for the incompressible flow in short vortex chamber", Trans. ASME Journal of Basic Eng., Vol. 91, 1964.

54. Kotas, T.J. — "Turbulent boundary layer flow on the end wall of a cylindrical vortex chamber", Proc. Inst. Mech. Engrs., pp. 305-315, Vol. 189, 1975.

55. Peckham, D.H. Atkinson, S. — British Aero. Res. Council, No. 508, 1957.

56. Leibovich, S. — "Vortex stability and breakdown", Survey and Extension, AIAA Journal, Vol. 22, No. 9, p. 1197, 1984.

57. Sarpkaya, T. — "On stationary and travelling vortex breakdowns", Journal of Fluid Mechanics, Vol. 45, Par. 3, pp. 545-559, 1971.

58. Jones, J.P. — "The breakdown of vortices in separated flow", Univ. of Southampton, U.S.A.A. Rep. No. 140, 160.

59. Brook, Benjamin, T. — "Theory of the vortex breakdown phenomenon", J. of Fluid Mechanics, pp. 593-629, Vol. 14, 1962.

60. Sarpkaya, T. — "Vortex breakdown in swirling conical flow", AIAA Journal, Vol. 9, No. 9, pp. 1792-1799, 1971.

61. Escudier, M.P. Zehnder, N. — "Vortex flow regimes", Journal of Fluid Mech., Vol. 115, pp. 105-121, 1982.

62. Garg, A.K. Leibovich, S. — "Spectral characteristics of vortex breakdown flow fields", Phys. Fluids, Vol. 22, p. 2053, 1979.

63. Boucher, R.F. Asquith, R.W. Royle, J.K. — "Vortex flow controllers design, stability and applications", Proc. 1st Symposium on Power Fluidics for Process Control, organised by the Inst. Measurement and Control, Univ. of Surrey, April 1973.

64. Syred, N.
Gupta, A.K.
Beer, J.M.
"Temperature and density gradient change arising with the precessing vortex core and vortex breakdown in swirl burners", Proc. 15th Syposium (Int.) Combustion, pp. 587-597, 1974.

65. Syred, N.
Beer, J.M.
"Vortex core precession in high swirl flow", 2nd Int. J.S.M.E. Symposium, Fluid Machinery and Fluidics, Tokyo, Sept. 1972.

66. Hall, M.G.
"The structure of concentrated vortex cores", Aeronautical Science, Vol. 7, pp. 53-110, 1966.

67. Gaudet, L.
Winter, K.G.
"Preliminary measurement of the flow field on the leeside of a delta wing of unit aspect ratio at a Mach number of 2.6 and an incidence of 15°", R.A.E. TN. No. Aero 2787.

68. Lewellen, W.S.
Burns, W.J.
Strickland, H.J.
"Transonic swirling flow", AIAA Journal, Vol. 7, pp. 1290-1297, July 1969.

69. Norton, D.J.
Farquhar, B.W.
Hoffman, J.D.
"An analytical and experimental investigation of swirling flow in nozzles", AIAA Journal, Vol. 7, No. 10, pp. 1992-2000, Oct. 1969.

70. Hsu, C.T.
DeJoode, A.D.
"Inviscid swirling flows through a choked nozzle", AIAA Journal, Vol. 11, pp. 1564-1566, Nov. 1973.

71. Binnie, A.M.
"The passage of a perfect fluid through a critical cross section or 'throat'", Proc. of the Royal Society, London, Ser. A, Vol. 197, pp. 543-551, 1949.

72. Carpenter, P.W.
"A general one-dimensional theory of compressible inviscid swirling flows in nozzles", Aero. Quarterly, Vol. 27, pp. 201-216, Aug. 1976.

73. George, P.J.
Ward, J.R.
Mitchell, F.M.
"Vortex diode characteristics at high pressure ratios", Proc. Conf. Process Control by Power Fluidics, Inst. Meas. Control, London, Paper 10, 1975.

74. Kline, S.J.
McClintock, F.A.
"Describing uncertainties in single-sample experiments", Mechanical Engineering, pp. 3-8, 1953.

75. British Standard
"British Standards methods of fluid flow in closed conduits", Part 1, B.S.1042, Section 1.1, 1981.

76. Benedict, R.P. — "Fundamentals of temperature and flow measurements", John Wiley & Sons, Inc., 1969.

77. Massey, B.S. — Mechanics of Fluids", 2nd Edition, Van Nostrand Reinhold Co., p. 217, 1970.

78. Shapiro, A.H. — "The dynamic and thermodynamics of compressible fluid flow", Vol. 1, p. 84, 1953.

79. King, C.F. Syred, N. — "An investigation of vortex phenomena associated with the development of axial flow reversal in a high Reynolds number confined flow", ASME Winter Annual Meeting, Chicago, 1980.

80. Mori, G. Premoli, A. — "Vortex diodes in two-phase flow", European Two-phase Flow Group Meeting, Brussels, 4-7 June, 1973, Paper A5.

81. Burgess, M.H. — "Two-phase choked flow in vortex diodes", AEEW-M1409, Winfrith, July 1976.

82. Henry, R.E. Fauske, H.K. — "The two-phase critical flow of one component mixtures in nozzles, orifices and short tubes", Trans. ASME, J. Heat Transfer, pp. 179-187, May 1971.

83. Deich, M.E. Danilin, B.S. Tsiklauri, G.V. Shanin, V.K. — "Investigation of the flow of wet steam in axisymmetric Laval nozzles over a wide range of moisture content", Moscow Power Engineering Inst. Translated from Teplofizikia Vysokikh Temperature, Vol. 7, No. 2, pp. 327-333, March-April 1969.

84. Mayhew, A.R. Rogers, G.F.C. — "Thermodynamic and transport properties of fluids", 2nd Edition, Blackwell, 1973.

85. Ryley, D.J. — "Communication on the invalid use of an isentropic expansion index for wet steam", Journal of Mech. Eng. Science, Vol. 12, No. 3, 1970.

86. Sproll, W.T. — "Effect of dust concentration upon the gas flow capacity of a Cyclonic collector", Journal of the Air Pollution Control Association, Vol. 16, No. 8, Aug. 1966.

87. O'Brien, S.A. Such, D.R. Mills, A.F. — "The effect of fluid flow rate on flooding in vertical annular counter-current two-phase flow", Int. J. Multiphase Flow, Vol. 12, No. 4, pp. 699-704, 1986.

88. Fan, C.K.
Schrock, V.E.
"Steam-water interactions in a vertical tube", Nuclear Engineering and Design, Vol. 95, pp. 129-141, 1986.

89. Cheers, F.
"Elements of compressible flow", John Wiley & Sons Ltd., 1963.

90. Barrow, H.
Ryley, J.R.
"Temperature recovery factors in steam", The Engineer, pp. 903-906, May 1960.

91 Kendall, J.M.
"Experimental study of a compressible viscous vortex", J.P.L. Technical Report No. 32-930, June 1962.

92. Gore, R.W.
Ranz, W.E.
"Backflow in rotating fluids moving axially through expanding cross sections", AIChE J., Vol. 19, pp. 83-88, Jan. 1964.

93. Uchida, S.
Nakamura, Y.
"Experiments on the axysymmetric vortex breakdown in a swirling air flow", Trans. Japan Soc. Aero. Space Sci., Vol. 27, No. 78, pp. 206-216, Feb. 1985.

94. Davies, M.G.
Oldfield, D.E.S.
"Tones from a choked axyisymmetric jet, I.Cell Structure, eddy velocity and source locations", Acustica, Vol. 12, No. 4, 1962.

95. Syred, N.
"An investigation of high performance vortex valves and amplifiers", Ph.D. Thesis, Dept. of Mech. Eng., University of Sheffield, 1969.

96. Wormley, D.N.
"An analytical model for the incompressible flow in short vortex chambers", Trans. ASME, pp. 264-276, June 1969.

97. Schlichting, H.
"Boundary layer theory", McGraw-Hill Inc., p. 255, 1968.

98. Ryley, D.J.
Lee, K.
"The evaporation of water droplets in superheated steam", presented to the ASME/ AIChE Heat Transfer Conf., Philadelphia, August, ASME Paper No. 68-HT-11, 1968.

APPENDIX A

Some Mathematical Definitions

The vector differential operator DEL, written ∇, is defined by:

$$\nabla = \frac{\partial}{\partial x} i + \frac{\partial}{\partial y} j + \frac{\partial}{\partial z} k$$

This vector operator possesses properties analogous to those of ordinary vectors.

The Gradient ∇P

Let P(x,y,z) be defined and differentiable at each point (x,y,z) in a certain region of space. Then the gradient of P written as ∇P or grad P is defined by:

$$\nabla P = \left(\frac{\partial}{\partial x} i + \frac{\partial}{\partial y} y + \frac{\partial}{\partial z} k\right) P$$

$$= \left(\frac{\partial P}{\partial x} i + \frac{\partial P}{\partial y} j + \frac{\partial P}{\partial z} k\right)$$

∇P in cylindrical co-ordinates is:

$$\nabla P = e_r \frac{\partial P}{\partial r} + e_\theta \frac{1}{r} \frac{\partial P}{\partial \theta} + e_z \frac{\partial P}{\partial z}$$

The Divergence $\nabla.V$

V defines a differentiable vector field then the divergence of V, written $\nabla.V$ or div.V, is defined by:

$$\nabla.V = \left(\frac{\partial}{\partial x} i + \frac{\partial}{\partial y} j + \frac{\partial}{\partial z} k\right).\left(v_1 i + v_2 j + v_3 k\right)$$

$$= \frac{\partial v_1}{\partial x} + \frac{\partial v_2}{\partial y} + \frac{\partial v_3}{\partial z}$$

In cylindrical co-ordinates:

$$\nabla.V = \frac{1}{r}\frac{\partial (rv_r)}{\partial r} + \frac{1}{r}\frac{\partial v_\theta}{\partial \theta} + \frac{\partial v_z}{\partial z}$$

$$= \frac{\partial v_r}{\partial r} + \frac{v_r}{r} + \frac{1}{r}\frac{\partial v_\theta}{\partial \theta} + \frac{\partial v_z}{\partial z}$$

$\nabla.V \neq V.\nabla$

The Curl ∇xV

If V(x,y,z) is a differentiable vector field, then the curl or rotation of V, written ∇xV, curl V, is defined by:

$$\nabla xV = \left(\frac{\partial}{\partial x}\, i + \frac{\partial}{\partial y}\, j + \frac{\partial}{\partial z}\, k\right).(v_1 i + v_2 j + v_3 k)$$

$$= \begin{vmatrix} i & j & k \\ \frac{\partial}{\partial x} & \frac{\partial}{\partial y} & \frac{\partial}{\partial z} \\ v_1 & v_2 & v_3 \end{vmatrix}$$

$$= \left(\frac{\partial v_3}{\partial y} + \frac{\partial v_2}{\partial z}\right) i + \left(\frac{\partial v_1}{\partial z} - \frac{\partial v_3}{\partial x}\right) j + \left(\frac{\partial v_2}{\partial x} - \frac{\partial v_1}{\partial y}\right) k$$

and in cylindrical co-ordinates:

$$\nabla xV = e_r \left[\frac{1}{r}\left(\frac{\partial v_a}{\partial \theta} - \frac{\partial_r v_\theta}{\partial z}\right)\right] + e_\theta \left(\frac{\partial v_r}{\partial z} - \frac{\partial v_z}{\partial r}\right) + e_z \left[\frac{1}{2}\left(\frac{\partial_r v_\theta}{\partial r} - \frac{\partial v_r}{\partial \theta}\right)\right]$$

Laplacian Operator ∇^2

Laplacial operator is defined by:

$$\nabla^2 = \frac{\partial^2}{\partial x^2} + \frac{\partial^2}{\partial y^2} + \frac{\partial^2}{\partial z^2}$$

In cylindrical co-ordinates Laplacian of scalar u is:

$$\nabla^2 u = \frac{1}{r}\frac{\partial}{\partial r}\left(r\frac{\partial u}{\partial r}\right) + \frac{1}{r^2}\frac{\partial^2 u}{\partial \theta^2} + \frac{\partial^2 u}{\partial z^2}$$

$$= \frac{\partial^2 u}{\partial r^2} + \frac{1}{r}\frac{\partial u}{\partial r} + \frac{1}{r^2}\frac{\partial^2 u}{\partial \theta^2} + \frac{\partial^2 u}{\partial z^2}$$

and of a vector V is:

$$\nabla^2 V = e_r \nabla^2 v_r + e_\theta \nabla^2 v_\theta + e_z \nabla^2 u_z$$

Total Derivative $\frac{d}{dt}$

In cylindrical co-ordinates:

$$\frac{d}{dt} = \frac{\partial}{\partial t} + v_r \frac{\partial}{\partial r} + \frac{v_\theta}{r}\frac{\partial}{\partial \theta} + v_z \frac{\partial}{\partial z}$$

APPENDIX B

The Recovery Factor

The temperature changes brought about by the dynamic pressure variation in a compressible flow are important for its balance. In particular, it appears useful to compare the temperature differences which result from the heat due to friction, with those caused by compression. Integration of the energy equation for the case of zero heat conduction in frictionless flow [97], gives:

$$C_p\ (T - T_\infty) = \int_{P_\infty}^{P} \frac{dP}{\rho} \tag{B1}$$

and from Bernoulli's equation for compressible flow:

$$\frac{v^2}{z} + \int \frac{dP}{\rho} = \text{const} \tag{B2}$$

so that temperature increase

$$T - T_\infty = \frac{1}{2C_p}\ (v_\infty{}^2 - v^2) \tag{B3}$$

for stagnation condition v = 0, i.e.

$$T_o - T_\infty = \frac{v_\infty{}^2}{2C_p} \tag{B4}$$

where ∞ refers to free stream condition.

This difference between stagnation and the free-stream temperature is

called adiabatic temperature increase. This change is due to frictional heat. In the case of an adiabatic wall (flat-plate thermometer) the above relation can be written in terms of local Mach number as:

$$T_o = T_\infty \left(1 + \frac{\gamma - 1}{2} M_\infty^2\right) \tag{B5}$$

Since $M_\infty = \frac{v_\infty}{a}$ and $a^2 = (\gamma - 1)\, C_p\, T_\infty$, this relation is valid for Pr number of unity. In the case of compressible fluid where Prandtl numbers are not unity, (e.g. Pr of air is less than one and for steam is between 1 and 2), the deviations in wall temperature caused by compressibility effects are very slight, as shown by Emmons et al [47] for laminar compressible flow, thus the equation is:

$$T_o = T_\infty + Pr^{1/2} \frac{v_\infty^2}{2C_p} \tag{B6}$$

In the case of turbulent flow, Emmons et al found that:

$$T_o = T_\infty + Pr^{1/3} \frac{v_\infty^2}{2C_p} \tag{B7}$$

In summary, when the Prandtl number of a gas differes from one, total temperature reduces to a concept. Under these conditions, even the adiabatic probe which completely stagnates a real gas locally, will not indicate the total temperature, thus:

$$T_o = T_\infty + \alpha \frac{v_\infty^2}{2C_p} \tag{B8}$$

where α is known as the recovery factor which, if based on local values of

directed velocity and static temperature, is approximately dependent on Mach and Reynolds numbers, and is well represented by $\alpha = Pr^{1/2}$ for laminar flow and by $\alpha = Pr^{1/3}$ for turbulent flow, [47].

Barrow and Ryley [90] gave the recovery factor for steam as:

$$\alpha = 1 - (1 - Pr)\ 4.45\ Re^{-1/5} \qquad \text{(B9)}$$

APPENDIX C

Estimation of Errors

The range of experimental error in the basic data has been calculated in accordance with Ref. [74] and reflects the reliability of the instrumentation and the accuracy with which it could be read.

If variables such as $\dot{m}$, T_u and D_e and P_u in equation (4.9) measured with uncertainties, $\delta\dot{m}$, δT_u, δD_e and δP_u, and the measured values used to compute the value of discharge factor, Cf ($\dot{m}$, T_u, D_e, P_u) the uncertainty in value of Cf can be calculated as follows.

Equation (4.9) could be simplified by neglecting constant values:

$$Cf = \frac{\dot{m}\sqrt{T_u}}{P_u D_e^2} \qquad (1)$$

The error in value of Cf is:

$$\delta Cf = \left[\left(\frac{\partial Cf}{\partial \dot{m}}\delta\dot{m}\right)^2 + \left(\frac{\partial Cf}{\partial T_u}\delta T_u\right)^2 + \left(\frac{\partial Cf}{\partial}\delta P_u\right)^2 + \left(\frac{\partial Cf}{\partial D_e}\delta D_e\right)^2\right]^{1/2} \qquad (2)$$

Differentiating equation (1) in respect to $\dot{m}$, T_u, P_u and D_e and substituting into equation (2) and divididing it by equation (1) yields:

$$\frac{\delta Cf}{Cf} = \left[\left(\frac{\delta\dot{m}}{\dot{m}}\right)^2 + \left(\frac{1}{2}\frac{\delta T_u}{T}\right)^2 + \left(\frac{\delta P_u}{P_u}\right)^2 + \left(2\frac{\delta d_e}{d_e}\right)^2\right]^{1/2} \qquad (3)$$

This equation could be used to calculate errors in Cf as illustrated in the following example:

Example

Let us consider a case with P_u = 4 bar, i.e. error from measuring instrument can be listed as follows:

$P_u = 4 \pm 0.1$ bar

$D_e = 19 \pm 0.1$ mm

$T_u = 152 \pm 1^{o}C$

value of $\delta\dot{m}$ was calculated using similar procedure as above, and found to be about 5%, i.e.

$$\frac{\delta Cf}{Cf} = \left[\left(\frac{5}{100}\right)^2 + \left(\frac{1}{2}\,\frac{1}{152}\right)^2 + \left(\frac{0.1}{4}\right)^2 + \left(2\,\frac{0.1}{19}\right)^2\right]^{1/2}$$

$$= 0.057 \simeq 0.06$$

Therefore,

δCf = 6%.

The distribution of static pressure in Chapter 6 was determined to ± 1% error by fine control of inlet steam pressure. Thermocouple temperature reading error was monitored by scanning each section five times, logging the running average temperature and the sample standard deviation. This remained consistently less than $0.2^{o}C$ which, for a reading range of only $5^{o}C$, represents ± 4%.

APPENDIX D

EVAPORATION OF DROPLET IN SUPERHEATED STEAM

At the point of injection, considerable differences in velocity and temperature of the phases exist in general. Spray droplets may be distorted or even shattered into smaller droplets as a result of interaction with the superheated steam. The distribution of droplets are not usually uniform. Condensation may take place, making the droplets grow in size and even cause them to fall under gravity to form a thin film on the pipe wall. It is also possible that evaporation of the drops could take place. Whatever the processes, there becomes only a moderate or even negligible difference between velocity and temperature of drops and the steam after a short period of time. The calculations of heat, mass and momentum exchange between spray droplets and its gaseous surroundings are not simple. However, it is necessary and important to understand the transport processes between the steam and droplets. For simplicity, steam carrying a large number of dispersed droplets may be considered as being subdivided into cells, each cell containing one droplet. The size of droplet can be taken as the mean value of the spray distribution. Derivation of formulae by Ryley and Lee [98] for the evaporation of a single droplets has been chosen and a sample calculation is given below.

The temperature of the injected water is lower than the steam temperature, the total heat transferred, Q, from the steam to the droplet at saturation condition is:

$$Q = Q_{ev} + Q_{v} \tag{D1}$$

where:

Q_{ev} is the heat transfer to vaporise the liquid, and Q_v is the heat transfer to be carried back with the diffusing vapour in the form of superheat. However, the amount of Q_v is very small and can be neglected. Therefore,

$$Q = Q_{ev} \tag{D2}$$

$$\frac{dQ_{ev}}{dt} = h' A_p \Delta T \tag{D3}$$

where Ap is the surface area of the drop (πd_p^2). The average heat transfer coefficient, $h' = \frac{K'Nu}{d_p}$

$$\frac{dQ_{ev}}{dt} = \pi d_p K' \Delta T Nu \tag{D4}$$

The evaporation rate from the droplet is determined as:

$$\frac{dm_p}{dt} = \frac{1}{h_{fg}} \frac{dQ_{ev}}{dt} \tag{D5}$$

Combining equation (D4) and (D5) yields:

$$Nu = \frac{dm_p}{dt} \left(\frac{h_{fg}}{\pi d_p K' \Delta T}\right) \tag{D6}$$

For a flat plate, the Nusselt number is approximately proportional to $Re^{0.5} Pr^{0.33}$. and at Re = 0, Nu = 2. Therefore,

$$Nu = 2 + C_1 Re^{0.5} Pr^{0.33} \tag{D7}$$

From (D6) and (D7),

$$\frac{dm_p}{dt} = \frac{\pi d_p \, K'\Delta T}{h_{fg}} \left(2 + C_1 \, Re^{0.5} \, Pr^{0.33}\right) \tag{D8}$$

and since $m_p = \frac{\pi d_p^{\,3} \, \rho_w}{6}$

$$\frac{d_p}{2 + C_1 \left(\frac{V_s}{V_g}\right)^{0.55} Pr^{0.33} \, d_p^{\,0.5}} \, dd_p = \frac{2K' \, \Delta T \, d_t}{\rho_w \, h_{fg}} \tag{D9}$$

When the property values are constant equation (D9) becomes:

$$\int_{d_{p1}}^{d_{p2}} \frac{d_p}{2 + C_3 \, d_p^{\,0.5}} \, dd_p = \int_0^{t_{ev}} C_2 \, dt \tag{D10}$$

where $C_2 = \frac{2 \, K'\Delta T}{\rho_w \, h_{fg}}$ (constant) (D11)

and $C_3 = C_1 \left(\frac{V_s}{V_g}\right)^{0.5} Pr^{0.33}$ (constant) (D12)

The integration of equation (D10) yields:

$$t_{ev} = \frac{1}{C_2} \left[\frac{2(d_{p2}^{\,1.5} - d_{p1}^{\,1.5})}{C_3^{\,2}} - \frac{2(d_{p2} - d_{p1})}{C_3^{\,2}} + \right.$$

$$\left. \frac{8(d_{p2}^{\,0.5} - d_{p1}^{\,0.5})}{C_3^{\,3}} - \frac{16}{C_3^{\,4}} \ln \left(\frac{2 + C_3 \, d_{p2}^{\,0.5}}{2 + C_3 \, d_{p1}^{\,0.5}}\right)\right] \tag{D13}$$

A value of $C_1 = 0.738$ was determined experimentally by Ryley and Lee.

Returning now to the injected water in the present work, the mass of water spray can be related to the number of drops of diameter d_{p1} as follows:

$$\dot{m}_w = \frac{\pi}{6} d_{p1}^3 \rho_w N \tag{D14}$$

The mass of injected water evaporated is given by:

$$\Delta\dot{m} = \dot{m}_w - \dot{m}_f$$

and this can be related to the size change in each drop by:

$$\Delta\dot{m} = \frac{\pi}{6} (d_{p1}^3 - d_{p2}^3) \rho_w N \tag{D15}$$

From equation (D15), the new diameter d_{p2} of the drop after it has evaporated and reached thermodynamic equilibrium may be obtained, and the time for this evaporation to occur, t_{ev}, is given by equation (D13).

Consider now the period for heating the initially subcooled drop to its saturation condition. For convection heat transfer to a fully immersed sphere in the absence of phase change,

$$Nu = \frac{h' d_p}{K'} \tag{D16}$$

the enthalpy given to the sphere in time t_h (for the heating up of a drop), may be equated to the heat transfer through the surface, i.e.

$$Q_h = t_h h' A_p \Delta T = t_h \frac{Nu.K'}{d_p} \frac{4\pi d_p^2}{4} \Delta T_h \tag{D17}$$

and

$$Q_h = \dot{m}_p C_{pw} \Delta T = \frac{\pi d_p^3}{6} \rho_w C_{pw} \Delta T \tag{D18}$$

Combining equations (D15) and (D16) yields:

$$t_h = \frac{\rho_w \, C_{pw} \, d_p^{\,2}}{3 \, Nu \, K'} \qquad (D19)$$

Therefore, the total heating and evaporating time for the drop

$$t = t_{ev} + t_h \qquad (D20)$$

Thus, the furthest distance a drop can travel in a time t before it reaches equilibrium is given by:

$$S = v_s . t \qquad (D21)$$

where v_s is the velocity of steam.

Example:

<u>Steam</u> $P_u = 12$ bar abs $x_u = 0.952$

$T = 200^{o}C$ $\dot{m}_w = 0.009$

$T_s = 188^{o}C$

<u>Water</u> $T_w = 20^{o}C$

$$\Delta T_{av} = \frac{200 - 188}{2} = 6^{o}C$$

$K'_{av} = 0.6335$ W/m.K

$(C_{pw})_{av} = 4.338$ KJ/kg.K

$\rho_w = 1000$ kg/m^3

$h_{fg} = 1986$ KJ/kg

$Pr = 1.18$

$\dot{m}_w = 0.0088$ kg/sec

$$V_p = 17.7 \text{ m/sec}$$

This is the velocity of the droplet at the spray nozzle exit. The maximum velocity that the drop can possibly have in the flow is the steam velocity (V_s).

$$\dot{m}_s = 0.2282$$

$$V_s = 7.76 \text{ m/sec}$$

$$d_{p1} = 100 \times 10^{-6} \text{ m}$$

$$v_g = 2.4 \times 10^{-6} \text{ m}^2/\text{sec}$$

$$\dot{m}_w = \frac{\pi}{6} (100 \times 10^{-6})^3 \, 1000 \times N$$

i.e. $$N = 17 \times 10^6 \frac{\text{drop}}{\text{sec}}$$

$\Delta\dot{m}$ is calculated to be 27×10^{-3} kg/sec and from equation (D13), $d_{p_2} = 41.2 \times 10^{-6}$ m, therefore evaporation takes place.

From equation (D11) $C_2 = 1.78 \times 10^{-7} \text{ m}^2/\text{sec}$

From equation (D12) $C_3 = 1057.5 \text{ m}^{-0.5}$

Hence from equation (D13) the time required to evaporate the drop (t_{ev}) is: 2.12×10^{-3} sec.

From equation (D7) Nu = 12.6

heating up time $t_h = 1.8 \times 10^{-3}$ sec

therefore, total time $t = 3.93 \times 10^{-3}$ sec

and in that time the drops will have travelled about 30 mm. Therefore it can be seen that thermal equilibrium between the two phases is attained very quickly.

APPENDIX E

CRITICAL TWO-PHASE FLOW EQUATIONS

The change in enthalpy between the gas phase at the upstream and the critical sections is given by:

$$h_u - h^* = Cp\ (T_u - T^*) \qquad (E1)$$

(* = critical condition).

The value of specific heat at constant pressure, C_p, can be written in terms of ratio of specific heats, γ, and specific gas constant, R, i.e.

$$h_u - h^* = \frac{\gamma}{\gamma-1}\ (R\ T_u - RT^*) \qquad (E2)$$

Substituting the value of RT = Pv (equation of state for perfect gas) into equation (E2) and also replacing the value of v by x v_g, will yield:

$$h_u - h^* = \frac{x_u\ v_{gu}\ \gamma}{(\gamma-1)}\ (P_u - P^*)$$

$$= x_u\ v_{gu}\ P_u\ (\frac{\gamma}{\gamma-1}) - x_u\ v_{gu}\ \frac{P^*}{P_u}\ (\frac{\gamma}{\gamma-1})\ P_u \qquad (E3)$$

where $\frac{P^*}{P_u} = (\frac{2}{\gamma+1})^{\frac{\gamma}{\gamma-1}}$ is the critical pressure ratio, therefore, equation (E3) at critical condition, becomes:

$$h_u - h^* = x_u\ v_{gu}\ P_u\ (\frac{\gamma}{\gamma-1})\ [1 - (\frac{2}{\gamma+1})^{\frac{\gamma}{\gamma-1}}]$$

Let $\frac{2}{\gamma+1} = \varepsilon$

i.e.

$$h_u - h^* = x_u\, v_{gu}\, P_u \left(\frac{\gamma}{\gamma-1}\right)\left[1 - \varepsilon^{\frac{\gamma}{\gamma-1}}\right] \qquad \text{(E5)}$$

Volume of mixture (wet steam) can be written as:

$$v_{mix} = x_u\, v_g^* + (1 - x_u)\, v_f \qquad \text{(E6)}$$

From isentropic relation:

$$\frac{P^*}{P_u} = \left(\frac{v_{gu}}{v_g^*}\right)^{\gamma} \qquad \text{(E7)}$$

Substituting a value of $\frac{P^*}{P_u}$ (critical pressure ratio) into equation (E7):

$$\frac{v_{gu}}{v_g^*} = \left[\left(\frac{2}{\gamma+1}\right)^{\frac{\gamma}{\gamma-1}}\right]^{\frac{1}{\gamma}} \qquad \text{(E8)}$$

but $\frac{2}{\gamma+1} = \varepsilon$

$$\text{i.e. } v_g^* = \left(\frac{1}{\varepsilon}\right)^{\frac{1}{\gamma}} v_{gu} \qquad \text{(E9)}$$

Substituting (E9) into (E6):

$$v_{mix} = x_u \left(\frac{1}{\varepsilon}\right)^{\frac{1}{\gamma}} v_{gu} + (1 - x)\, v_f \qquad \text{(E10)}$$

Neglecting initial velocity, fluid velocity at any section is simply

determined by:

$$V = [2\ (h_u - h^*)]^{1/2} \tag{E11}$$

From continuity equation:

$$V = \frac{\dot{m}}{A}\ v_{mix} \tag{E12}$$

Combining equations (E4), (E10), (E11) and (E12) will result in:

$$\frac{\dot{m}_{cr}}{A_e} = \frac{1}{v_{mix}} [2\ x_u\ v_{gu}\ P_u\ (\frac{\gamma}{\gamma-1})(1 - \varepsilon^{\frac{\gamma}{\gamma-1}})]^{1/2} \tag{E13}$$

This is equation (5.1), which is given in Chapter 5, Section 5.2.

APPENDIX F - "DLOG8"

```
  5 TIME=Ø
 1Ø ?&FCØ2=255
 2Ø ?&FCØ3=24Ø
 3Ø S=1Ø
 4Ø DIM A(S)
 5Ø @%=&2Ø21Ø
 6Ø FOR K=1 TO S
 7Ø A(K)=11-K
 8Ø NEXT K
 9Ø INPUT "INPUT NUMBER OF CYCLES";C
 91 DIM SSQ(C,S)
 92 DIM SUM(C,S)
 93 DIM MEAN(C,S)
 94 DIM SSD(C,S)
 95 DIM D(C,S)
 96 DIM Time(C,S)
1ØØ FOR CYCLE=1 TO C
11Ø FOR K=1 TO S
12Ø N=A(K)
13Ø TC=Ø
14Ø N=N-1Ø
15Ø IF N>=Ø THEN 17Ø
16Ø GOTO 19Ø
17Ø TC=TC+1
18Ø GOTO 14Ø
19Ø N=N+1Ø
 2ØØ ?&FCØØ=((TC*16)+N)
 2Ø5 Time(CYCLE,K)=TIME/1ØØ-Time(1,1)
 21Ø GOSUB 1Ø1Ø
 211 SUM(CYCLE,K)=SUM(CYCLE-1,K)+D(CYCLE,K)
 212 MEAN(CYCLE,K)=SUM(CYCLE,K)/CYCLE
 213 SSQ(CYCLE,K)=SSQ(CYCLE-1,K)+D(CYCLE,K)^2
 214 IF CYCLE=1 GOTO 219
 216 X=SSQ(CYCLE,K)-SUM(CYCLE,K)^2/CYCLE
 217 IF X<=Ø GOTO 219
 218 SSD(CYCLE,K)=SQR(X/(CYCLE-1))
 219 PRINT"CHANNEL ";A(K);" READING=";D(CYCLE,K);" TIME=";Time(CYCLE,K)
;" MEAN=";MEAN(CYCLE,K);" STD.DEV.=";SSD(CYCLE,K)
 22Ø NEXT K
 23Ø NEXT CYCLE
 24Ø INPUT "DO YOU REQUIRE A HARD COPY (Y OR N)";A$
 25Ø IF A$<> "Y" THEN 35Ø
 26Ø VDU2
 27Ø PRINT TAB(5);"CHANNEL NO.";TAB(21);"TEMPERATURE";TAB(44);"TIME";TA
B(54);"MEAN TEMP.";TAB(72);"STD.DEV."
 29Ø FOR K=1 TO S
 3ØØ PRINT A(K),D(C,K),Time(C,K),MEAN(C,K),SSD(C,K)
 31Ø NEXT K
>
```

```
 320 PRINT
 340 VDU3
 350 END
1010 ?&FC01=112
1020 t=TIME
1030 test=TIME-t
1040 IF test<36 THEN 1030
1090 ?&FC01=128
1100 ?&FC01=48
1110 P=?&FC01
1120 IF (P AND 1)=0 THEN 1110
1130 ?&FC01=32
1140 P=?&FC01
1150 IF (P AND 1)=0 THEN 1360
1160 ?&FC01=16
1170P=?&FC01
1180 IF (P AND 1)>0 THEN POL$="+"
1190 IF (P AND 1)=0 THEN POL$="-"
1200 ?&FC01=0
1210 D=?&FC01
1220 D1=0
1230 IF (D AND 1)>0 THEN D1=1000
1240 ?&FC01=64
1250 D=?&FC01
1260 D2=(D AND 15)*100
1270 ?&FC01=80
1280 D=?&FC01
1290 D3=(D AND 15)*10
1300 ?&FC01=96
1310 D=?&FC01
1320 D4=(D AND 15)
1325 ?&FC01=112
1330 D(CYCLE,K)=(D1+D2+D3+D4)/10
1340 IF POL$="-" THEN D(CYCLE,K)=D(CYCLE,K)*-1
1350 GOTO 1370
1360 D(CYCLE,K)=10000
1370 RETURN
>
```

APPENDIX G

Calculation of Confined Vortex Temperature and Tangential Velocity

Equation 6.7 is in the form of

$$M = \left(\frac{r}{\gamma p}\frac{dp}{dr}\right)^{1/2}$$

$\frac{dp}{dr}$ was determined by graphical construction

$\gamma = 1.335$ constant

p is measured static pressure

r is radius

i.e. M can be calculated.

Let $\alpha = 1$, i.e. equation 6.3 yields:

$$T_o = T_r$$

One-dimension relation gives:

$$\frac{T_o}{T} = 1 + \frac{\gamma-1}{2} M^2$$

$$\text{i.e. } T = \frac{T_r}{1 + \frac{\gamma-1}{2} M^2}$$

T can be calculated by substituting into this equation the value of Mach number from equation 6.7 and the value of the recorded temperature. The local Prandtl number was determined to enable T to be recalculated as follows:

The recovery factor can be determined by:

$$\alpha = \sqrt[3]{Pr}$$

The new value of α was then used to calculate the average temperature by use of equation 6.3 ($T = \frac{T_r + 273}{\alpha\left(\frac{T_o}{T} - 1\right)} + 1$). A couple of iterations were sufficient to arrive at a value of T.

Now, specific gas, $R = \frac{P}{\rho T}$ and sonic velocity $a = \sqrt{\gamma RT}$, i.e.

$V_\theta = M_t \times a$.

APPENDIX H - "NAVIER4"

```
 10 REM "NAVIER-: " TO FIND TANGENTIAL VELOCITY
 15 @%=&20409
 20 DIM R(10)
 30 R(10)=163
 40 R(9)=147.5
 50 R(8)=131
 60 R(7)=114.5
 70 R(6)=97.5
 80 R(5)=81.5
 90 R(4)=64.5
100 R(3)=49
110 R(2)=33
120 R(1)=17
130 G=1.335
140 g=9.80665
150 FOR K=1 TO 10
160 S=11-K
170 PRINT "STATION NO."S
205 INPUT "RADIAL VELOCITY (m/s)";Vr
206 INPUT "EST. TANGENTIAL VEL. (m/s)";C
207 ANGLE=DEG(ATN(Vr/C))
208 PRINT"EST. FLOW ANGLE ="ANGLE"(deg.)"
210 INPUT "dVr";DVR
220 INPUT "dr";dr
230 DVDR=DVR/dr
240 LHS=((Vr*DVDR)-(C^2)/R(S))*1000/g
250 INPUT "DENSITY (kg./m^3)";p
260 INPUT "DP (bar)";DP
270 INPUT "DR (mm)";DR
280 DPDR=DP/DR
290 PRINT "Vr.dVr/dr-Vt^2/r = -1/p.dP/dr"
300 PRINT "LHS/g ="LHS
305 RHS=(DPDR/p)*100000000
310 PRINT "RHS ="(-RHS/g)
330 Vt=SQR((Vr*DVDR*1000+RHS)*R(S)/1000)
340 PRINT"REVISED TANGENTIAL VELOCITY ="Vt"(m/s)"
350 INPUT "STATIC PRESSURE (bar.abs.)";P
360 RT=P*100000/p
370 A=SQR(G*RT)
380 Mt=Vt/A
390 Mr=Vr/A
393 ANGLE=DEG(ATN(Vr/Vt))
397 PRINT"FLOW ANGLE ="ANGLE"(deg.)"
400 M=SQR(Mt^2+Mr^2)
410 PRINT"TANGENTIAL MACH. NO. ="Mt
420 PRINT"RADIAL MACH. NO. ="Mr
430 PRINT"RESULTANT MACH. NO. ="M
440 ToT=1+(((G-1)*(M^2))/2)
450 INPUT"RECOVERY FACTOR";RF
460 INPUT "TEMPERATURE READING (deg.C)";TR
470 AT=(TR+273)/((RF*(ToT-1))+1)
480 T=AT-273
490 PRINT "STATIC TEMP.(CHECK) ="T"(deg.C)"
492 PRINT
495 NEXT K
500 END
>
```

APPENDIX I

Published Papers

1. Owen, I.
   Motamed-Amini, A.
   "Compressible flow characteristics of a vortex diode operating with superheated steam", presented at the Winter Annual Meeting of ASME, Anaheim, California, December 1986.

2. Motamed-Amini, A.
   Owen, I.
   "The expansion of wet steam through a compressible confined vortex in a fluidic vortex diode". To be published in the International Journal of Multiphase Flow.

3. Wilkinson, J.
   Motamed-Amini, A.
   Owen. I.
   "Compressible and confined vortex flow", submitted to the Jounral of Fluid Mechanics.